

Durham E-Theses

Higgs Bosons and QCD Jets at Two Loops

Athanasios Koukoutsakis

How to cite:

Koukoutsakis, Athanasios (2003) Higgs Bosons and QCD Jets at Two Loops. Doctoral thesis, Durham University.

Use policy

The full-text may be used and/or reproduced, and given to third parties in any format or medium, without prior permission or charge, for personal research or study, educational, or not-for-profit purposes provided that:

- a full bibliographic reference is made to the original source
- a <https://etheses.durham.ac.uk/id/eprint/3652/> is made to the metadata record in Durham E-Theses
- the full-text is not changed in any way

The full-text must not be sold in any format or medium without the formal permission of the copyright holders.

Please consult the [full Durham E-Theses policy](#) for further details.

The copyright of this thesis rests with the author.
No quotation from it should be published without
his prior written consent and information derived
from it should be acknowledged.

Higgs Bosons and QCD Jets at Two Loops

A thesis presented for the degree of
Doctor of Philosophy
by
Athanasios Koukoutsakis

Institute for Particle Physics Phenomenology
Physics Department
University of Durham

April 2003

21 MAY 2003

Abstract

In this thesis we present techniques for the calculation of two-loop integrals contributing to the virtual corrections to physical processes with three on-shell and one off-shell external particles. First, we describe a set of basic tools that simplify the manipulation of complicated two-loop integrals. A technique for deriving helicity amplitudes with use of a set of projectors is demonstrated. Then we present an algorithm, introduced by Laporta, that helps reduce all possible two-loop integrals to a basic set of ‘master integrals’. Subsequently, these master integrals are analytically evaluated by deriving and solving differential equations on the external scales of the process. Two-loop matrix elements and helicity amplitudes are calculated for the physical processes $\gamma^* \rightarrow q\bar{q}g$ and $\mathcal{H} \rightarrow ggg$ respectively. Conventional Dimensional Regularization is used in the evaluation of Feynman diagrams. For both processes, the infrared singular behavior is shown to agree with the one predicted by Catani.

Acknowledgments

I would like to thank my supervisor Professor Nigel Glover for his guidance, support and encouragement throughout my studies in Durham. His dedicated supervision, confidence and inspiration have helped me enhance my knowledge and abilities and led to very successful PhD research.

Also, many thanks go to Lee Garland, for our joint efforts on this work and for numerous conversations and cross-checks of our results. For their collaboration on this research work, I would like to thank Thomas Gehrmann and Ettore Remiddi.

A special mention goes to my friend Babis Anastasiou for his close friendship of the last twelve years and for the great time we have shared. His motivation and assistance have been essential for the outcome of my postgraduate studies.

I am grateful to Jeppe Andersen, Pete Williams and Jon Levell for sharing their computer expertise and to all the people in the CPT for providing a friendly and warm working atmosphere and for tolerating consumption of their CPU times by my running jobs.

I acknowledge the financial support of Durham University. My PhD studies would not have been possible without the Durham studentship.

My very warm feelings go to Katerina for being ο μικρός μου ET's.

Last but not least, I would like to thank my family for their love and support throughout my academic studies. This thesis is dedicated to them.

Declaration

I declare that I have previously submitted no material in this thesis for a degree at this or any other university.

Aspects of chapters 7-8 are based on research carried out in collaboration with L. W. Garland, T. Gehrmann, E. W. N. Glover and E. Remiddi, and published in:

- L. W. Garland, T. Gehrmann, E. W. N. Glover, A. Koukoutsakis and E. Remiddi, “*The two-loop QCD matrix element for $e^+ e^- \rightarrow 3jets$,*” Nucl. Phys. B **627** (2002) 107 [arXiv:hep-ph/0112081].
- L. W. Garland, T. Gehrmann, E. W. N. Glover, A. Koukoutsakis and E. Remiddi, “*Two-loop QCD helicity amplitudes for $e^+ e^- \rightarrow 3jets$,*” Nucl. Phys. B **642** (2002) 227 [arXiv:hep-ph/0206067].

Contents

1	Basic QCD	1
1.1	QCD Lagrangian	1
1.2	Feynman Rules for QCD	4
1.3	Regularization and Renormalization	6
1.3.1	Dimensional Regularization (DR)	8
1.3.2	Renormalization	9
1.3.3	Running Coupling and Renormalization Group Equations	11
1.4	Effective Higgs Lagrangian	13
1.4.1	Feynman Rules for the Effective Lagrangian	15
2	IR Divergences and Matrix Elements	17
2.1	Introduction	17
2.2	Infrared Cancellation:	
	The $\mathcal{H} \rightarrow gg$ decay	18
2.2.1	Notation	18
2.2.2	Tree-Level and LO: No Emissions	18
2.2.3	Virtual Infrared Divergences	20
2.2.4	Real Infrared Divergences	21
2.2.5	Cancellation of Infrared Divergences	25
2.2.6	Infrared Safe Observables	27
2.3	One-Loop Singular Behaviour	29
2.4	Two-Loop Singular Behaviour	31
2.5	Beyond NLO	32

3	Amplitudes For QCD Processes	35
3.1	Introduction	35
3.2	Basic Steps for Helicity Amplitudes and Matrix Element Calculations	38
3.3	The Integral Factory	39
4	Basic Tools For Two-Loop Integrals	41
4.1	Introduction	41
4.2	Tool One: Color Algebra	42
4.2.1	Color in Feynman Diagrams	42
4.2.2	Identities and Rules in Color Algebra	43
4.3	Tool Two: The Auxiliary Integrals	45
4.4	Tool Three: IBP Identities	47
4.4.1	The Integration By Parts (IBP) Method	47
4.4.2	IBP Identities For The Auxiliary Integrals	51
4.5	Tool Four: Master Integrals (MI)	54
4.5.1	The Choice of Master Integrals	54
4.5.2	Planar Master Integrals	55
4.5.3	Non-planar Master Integrals (MI)	57
4.6	Tool Five: Harmonic Polylogarithms	59
4.6.1	Definition of 2DHPL's	59
4.6.2	Useful Properties of 2DHPL's	60
4.6.3	'Minimal' Basis-Set of 2DHPL's	61
4.7	Tool Six: Projectors For Helicity Amplitudes	64
4.7.1	The General Tensor	64
4.7.2	Projectors for the Tensor Coefficients	66
4.7.3	Helicity Amplitudes	67
5	Making Two-Loop Integrals Simpler	69
5.1	Reductions: New Techniques Available	69

5.2	Laporta	70
5.2.1	The Algorithm	70
5.2.2	Laporta Example	74
6	Differential Equations	79
6.1	Introduction	79
6.2	Generating Differential Equations (DE's)	80
6.2.1	Method for Generation of Differential Equations	80
6.2.2	Differential Equations for the General Auxiliary Planar Integral	82
6.3	Solving DE's: The Gehrmann-Remiddi Method	82
6.4	Generating/Solving DE's for the DART ₂ MI	86
7	The $\gamma^* \rightarrow q\bar{q}g$ Two-Loop Matrix Element	94
7.1	Introduction	94
7.2	Notation	96
7.3	Method	99
7.4	The Matrix Element	100
7.4.1	Infrared factorization	101
7.4.2	The finite part	103
8	Two-Loop Helicity Amplitudes for the $\mathcal{H} \rightarrow ggg$ Decay	106
8.1	Introduction	106
8.1.1	Notation	108
8.1.2	The general tensor	110
8.1.3	Projectors for the tensor coefficients	111
8.1.4	The perturbative expansion of the tensor coefficients	112
8.1.5	Ultraviolet renormalization	113
8.1.6	Infrared behaviour of the tensor coefficients	113
8.2	Helicity amplitudes	115
9	Conclusions	118

A	Harmonic Polylogarithms up to weight 3	122
B	Application of the Laporta Algorithm	126
C	Two and Three Body Phase-Space	133
D	Spinor Helicity	134
E	The $\gamma^* \rightarrow q\bar{q}g$ NNLO Matrix Element coefficients	136
F	The $\mathcal{H} \rightarrow ggg$ NNLO Helicity Amplitude coefficients	170

List of Figures

1.1	The Hgg coupling in QCD and the effective Lagrangian theory. . . .	15
2.1	$\mathcal{H} \rightarrow gg$ tree-level diagrams	19
2.2	$\mathcal{H} \rightarrow gg$ one-loop diagrams	20
2.3	$\mathcal{H} \rightarrow ggg$ tree-level diagrams	21
2.4	$\mathcal{H} \rightarrow q\bar{q}g$ tree-level diagrams	22
2.5	Tree-level diagrams that appear as $\mathcal{H} \rightarrow gg$ in the experiments. . . .	22
2.6	Plot of Soft and Collinear Divergences	25
2.7	Single jet inclusive distribution.	34
3.1	General Algorithm For Matrix Elements And Helicity Amplitudes. . .	36
3.2	Integral Factory.	37
4.1	Planar and Non-Planar Auxiliary Diagrams	48
5.1	Laporta Algorithm	72

Preface

The aim of this thesis is to provide an insight into fundamental mechanisms of perturbative Quantum Chromodynamics (QCD), as well as aspects of Higgs physics. More precisely, we perform higher order calculations of matrix elements and helicity amplitudes for processes involving the decay of a massive particle to partons. This thesis is structured in a way that covers all the main building blocks that lead to such calculations.

In the first chapter we present an overview of basic QCD concepts starting with the Lagrangian of the theory and rules for diagrammatically presenting analytic expressions (Feynman rules). Similarly we present the Lagrangian and Feynman rules for the “effective” Higgs-gluon-gluon vertex, an approximation that significantly simplifies calculations. In the same chapter we also describe Dimensional Regularization and Renormalization. The former is a scheme that allows isolation and quantification of divergences (infrared and ultraviolet) that appear in higher order calculations in perturbation theory. Renormalization is a fundamental property of QCD that leads to the cancellation of ultraviolet divergences at each order in the perturbation series. Infrared divergences are treated in the second chapter, where we demonstrate how they can be predicted and how they cancel out for physical observables.

In chapter 3 we illustrate the basic steps leading to a matrix element or helicity amplitude calculation, while in chapter 4 we describe a set of basic tools that can be used toward that direction. Our focus in both chapters is on the calculation of two-loop integrals. An algorithm that allows one to reduce all possible two-loop integrals to a basic set of “master integrals” is introduced in chapter 5. A powerful

method of analytically evaluating those “master integrals” is presented in chapter 6.

All the above tools and techniques are used in chapters 7 and 8 for the calculation of the two-loop corrections to the matrix elements and helicity amplitudes of the decays $\gamma^* \rightarrow q\bar{q}g$ and $\mathcal{H} \rightarrow ggg$ respectively. Finally, in the last chapter we summarize the results of this thesis and give an outlook on future calculations.

Chapter 1

Basic QCD

1.1 QCD Lagrangian

QCD is a non-Abelian gauge theory based on the $SU(N)$ group, with $N=3$ color degrees of freedom. It describes the interactions between spin-1/2 particles (quarks) and spin-1 vector bosons (gluons). The full QCD Lagrangian can be written as the sum of three component parts:

$$\mathcal{L}_{QCD} = \mathcal{L}_{Classical} + \mathcal{L}_{Gauge-Fixing} + \mathcal{L}_{Ghost} .$$

The expression for the classical Lagrangian density is:

$$\mathcal{L}_{Classical} = \sum_f \bar{\psi}_{f,i} (i \not{D} - m_f \delta_{ij}) \psi_{f,j} - \frac{1}{4} F_a^{\mu\nu} F_{\mu\nu}^a . \quad (1.1)$$

Here, i, j run through the number of colors ($N=3$) of $SU(3)$ and a takes values from 1 to $N^2 - 1 = 8$. The index f carried by the quark-fields runs over the quark flavors and \not{D} is the symbolic notation of $\gamma_\mu D^\mu$ with γ_μ being the Dirac matrices that satisfy the Clifford Algebra anti-commutation relation:

$$\{\gamma^\mu, \gamma^\nu\} = 2 g^{\mu\nu} .$$

The gauge covariant derivative D^μ is given by:

$$D_{ij}^\mu = \partial^\mu \delta_{ij} - ig A_a^\mu T_{ij}^a , \quad (1.2)$$

where g is the coupling of the quarks with the gluons and T_{ij}^a are the eight 3×3 hermitian and traceless Gell-Mann matrices that generate the fundamental representation of $SU(3)$. Their commutator defines the $SU(3)$ structure constants f^{abc} :

$$[T^a, T^b] = i f^{abc} T^c .$$

The operator D_μ was constructed so that the covariant derivative of a field transforms just like the field under any local $SU(3)$ transformation $U(x)$:

$$\begin{aligned} \psi_f &\rightarrow U(x) \psi_f , \\ D^\mu &\rightarrow U(x) D^\mu , \end{aligned}$$

with $U(x)$ defined as:

$$U(x) = e^{i T^a \theta_a(x)} .$$

In equation (1.2), A_a^μ are the gluon fields. The field strength tensor $F_{\mu\nu}^a$ that appears in the ‘kinetic’ term of the ‘classical’ Lagrangian in eq. (1.1) can be written in terms of the gluon fields A_a^μ as:

$$F_{\mu\nu}^a = \partial_\mu A_\nu^a - \partial_\nu A_\mu^a - \overbrace{g f^{abc} A_\mu^b A_\nu^c}^{\text{Non-Abelian}} , \quad (1.3)$$

with $F_{\mu\nu}^a$ defined in a way that satisfies the relation:

$$[D_\mu, D_\nu] \psi_f = i g T^a F_{\mu\nu}^a \psi_f .$$

The Non-Abelian term in eq. (1.3) results in the appearance of interaction terms in $\mathcal{L}_{\text{Classical}}$ that contain only gluons (three and four gluon vertices). This is the fundamental difference between QCD and QED. In QED, where the non-Abelian term is absent, the force-carriers (photons) are charge-neutral and therefore there are no multi-photon vertices. However in QCD the force-carriers (gluons) are color-charged allowing for multi-gluon couplings.

Notice that the building of the $\mathcal{L}_{\text{Classical}}$ part of the QCD Lagrangian has been done by following the fundamental principle of gauge invariance, with quark and

gluon fields transforming as:

$$\begin{aligned}\psi_f &\rightarrow U(x) \psi_f , \\ T^a A_\mu^a &\rightarrow U(x) \left(T^a A_\mu^a - \frac{i}{g} U(x)^{-1} \partial_\mu U(x) \right) U(x)^{-1} .\end{aligned}$$

It is trivial to see that while the quark mass term $\bar{\psi}_f m_f \psi_f$ is invariant under local gauge transformations, this is not the case for a possible gluon mass term:

$$\frac{1}{2} m^2 A_\mu A^\mu .$$

because this term obviously violates local gauge invariance.

However the gauge invariance of the Lagrangian of eq. (1.1) prevents us from performing perturbation theory. The problem arises when we try to perform canonical quantization. This is evident in the functional integral of the exponential of the action, which becomes badly divergent, due to the freedom of the gluon fields to transform by a total derivative leaving the Lagrangian invariant. The divergence emerges as we integrate over a continuous infinity of physically equivalent field configurations. It is therefore impossible to define the gluon propagator. To fix the problem we need to find a way to count each physical configuration in the functional integral only once. One way we can achieve this, is by putting a constraint on the freedom of the gluon field A^μ , such as the Lorentz condition:

$$\partial^\mu A_\mu = 0 .$$

This leads to the insertion of a gauge-fixing term in the Lagrangian:

$$\mathcal{L}_{Gauge-Fixing} = -\frac{1}{2\xi} (\partial^\mu A_\mu^a)^2 , \quad (1.4)$$

where the parameter ξ is called the gauge parameter. Because of the gauge fixing term the QCD Lagrangian is no longer gauge invariant. However the physical predictions originating from the Lagrangian ought to be gauge invariant and gauge independent. This means that the value of ξ is not relevant to the physical result. Unless differently stated, for the rest of this thesis it is taken to be $\xi = 1$ in what is called the Feynman gauge.

The gauge fixing term of (1.4) needs to be accompanied by the ghost Lagrangian:

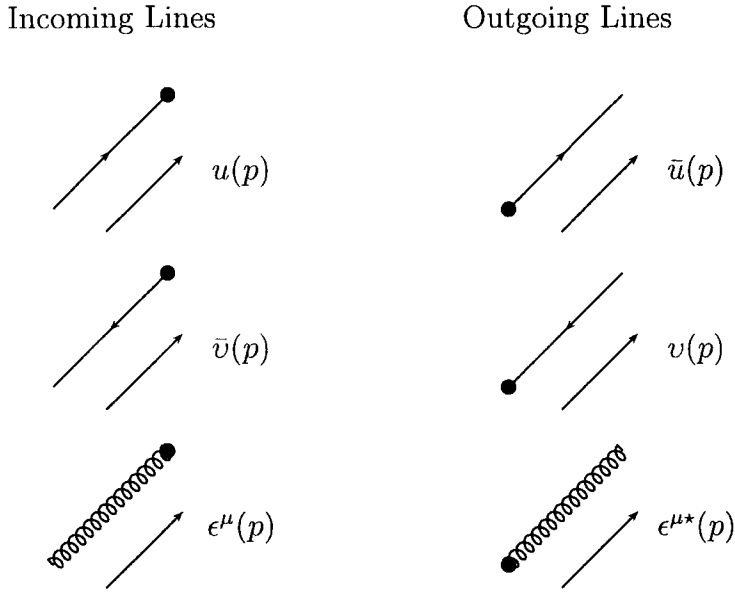
$$\mathcal{L}_{Ghost} = (\partial_\mu n_a^*) (\partial^\mu \delta_{ab} + g f^{abc} A_c^\mu) n_b \quad , \quad (1.5)$$

with n (Fadeev-Popov ghost) being a complex scalar field obeying the Fermi statistics. This term must be added to cancel out the two unphysical polarizations of the gluon field i.e. the time-like and longitudinal degrees of freedom. Therefore, the full Lagrangian for quantum mechanical applications is the sum of equations (1.1), (1.4) and (1.5).

1.2 Feynman Rules for QCD

Within QCD we are interested in providing theoretical predictions for physical observables, such as decay widths (Γ) and cross-sections (σ), involving interactions of the fundamental QCD particles and fields. The measure of these interactions is described by dimensionless quantities called amplitudes (\mathcal{M}). Each amplitude consists of a number of terms containing functions of integrals of the Lagrangian which describes the system. Feynman [1, 2] invented a consistent way of mapping all those terms into easy-to-visualize diagrams. This procedure follows a set of operations called *Feynman rules*. These are rules associating analytic expressions with pieces of diagrams. The product of those pieces gives the value of the diagram which corresponds to a term contributing to the amplitude. In this section we present in brief the Feynman rules for Quantum Chromodynamics. In all Feynman diagrams of this thesis quarks are illustrated with solid straight lines, gluons with spiral coils and ghosts with dashed lines, following the notation of [3]. In consistency with section 1.1, the color indices for gluons and ghosts are denoted with the letters a, b, c, d, e running from $1 \dots (N^2 - 1) = 8$ while for quarks we use i, j who run from $1 \dots N = 3$. The Lorentz indices are designated by the letters μ, ν, ρ, σ , etc.

For the external lines with quarks and gluons we have:



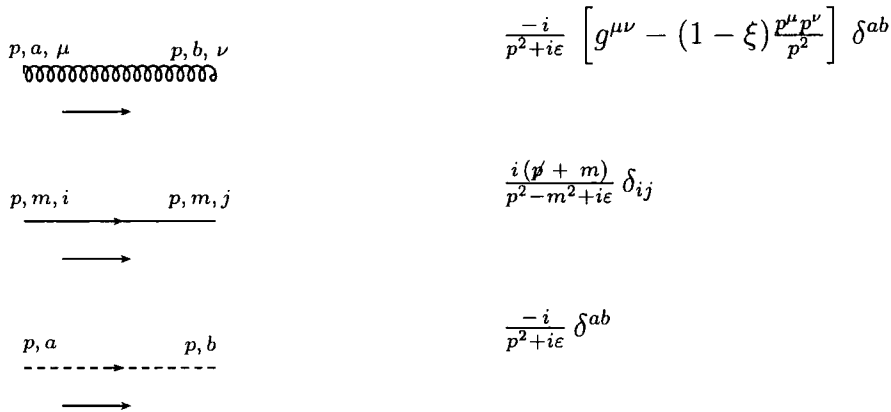
In following chapters we will see that for the calculation of Matrix-Elements one needs the following sums over the fermion spins and gluon polarizations:

$$\sum_{spins} \bar{u}(p) u(p) = \not{p} + m ,$$

$$\sum_{spins} \bar{v}(p) v(p) = \not{p} - m ,$$

$$\sum_{pols} (\epsilon^\mu(p))^* \epsilon^\nu(p) = -g^{\mu\nu} + \frac{(1 - \xi)p^\mu p^\nu}{p^2} .$$

In the Feynman gauge $\xi = 1$ and in the Landau gauge $\xi = 0$. As far as the gluon, quark and ghost propagators are concerned the Feynman rules are:



$$\frac{-i}{p^2 + i\epsilon} \left[g^{\mu\nu} - (1 - \xi) \frac{p^\mu p^\nu}{p^2} \right] \delta^{ab}$$

$$\frac{i(\not{p} + m)}{p^2 - m^2 + i\epsilon} \delta_{ij}$$

$$\frac{-i}{p^2 + i\epsilon} \delta^{ab}$$

Notice that in the denominator of each propagator we have followed the ‘Feynman prescription’ and assigned a positive imaginary part $+i\epsilon$ to guarantee that the

propagation of particles is from earlier to later points in time. We have also given the gluon propagator in a covariant gauge, fixed by the ξ -parameter in line with the analysis of the previous section.

The quark-gluon, ghost-gluon and gluon self-interaction vertices respectively are:

$$\begin{aligned}
 & -i g \gamma^\mu T_{ij}^a \\
 & g p^\mu f^{abc} \\
 & -g f^{abc} \left[(p_1 - p_2)^\rho g^{\mu\nu} + (p_2 - p_3)^\mu g^{\nu\rho} + (p_3 - p_1)^\nu g^{\rho\mu} \right] \\
 & -i g^2 f^{abe} f^{cde} (g^{\nu\sigma} g^{\mu\rho} - g^{\mu\sigma} g^{\nu\rho}) \\
 & -i g^2 f^{ace} f^{bde} (g^{\rho\sigma} g^{\mu\nu} - g^{\mu\sigma} g^{\nu\rho}) \\
 & -i g^2 f^{ade} f^{cbe} (g^{\nu\sigma} g^{\mu\rho} - g^{\rho\sigma} g^{\mu\nu})
 \end{aligned}$$

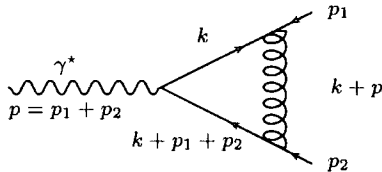
In addition to the previous set of rules one must

- integrate over the loop momentum k_i of each loop with measure $\int \frac{d^D k_i}{(2\pi)^D}$, where D is the dimension,
- multiply with (-1) for every quark or ghost loop,
- multiply by a symmetry factor to take into account permutations of the fields in each diagram.

1.3 Regularization and Renormalization

The Feynman Rules presented in the previous section make the calculation of tree-level diagrams a trivial task. Nevertheless, when one goes to higher orders in pertur-

bation theory loop-integrals appear in the calculation. These integrals can carry divergences originating in the behaviour of the integrand at high and low virtual/loop momenta. Let us now examine how those divergences emerge by studying the behaviour of the integral that corresponds to the following one-loop vertex diagram:



$$\longrightarrow I = \int \frac{d^4 k}{i\pi^2} \frac{f(k^2)}{k^2 (k+p_1)^2 (k+p_1+p_2)^2}$$

There are two types of divergences that can appear in this integral:

- *Ultraviolet Divergences* (UV) are associated with the singularities that appear in the integrals at large loop-momenta. In our example:

$$k \rightarrow \infty \implies I \rightarrow \infty \text{ logarithmically.}$$

- *Infrared Divergences* (IR) are generated when one of the propagators in the loop tends to zero. For our example we have:

$$k \rightarrow \{0, -p_1, -p_1 - p_2\} \implies I \rightarrow \infty, \quad \text{with } p_1^2 = p_2^2 = 0 \quad .$$

Such divergences arise when the propagators are massless as is the case in our example. This occurs in QCD due to the presence of massless gluon and light-quark propagators.

There have been developed several techniques that allow one to surmount the difficulties raised by the existence of such divergences. UV divergences are banished order by order in perturbation theory by a procedure called renormalization, as we will see later in this section. As far as IR divergences are concerned, we will demonstrate in chapter 2 how they cancel at each order for a certain type of physical observables. In the same chapter we will also illustrate a method that enables one to predict the IR structure at one and two loops. In order to demonstrate the appearance and cancellation of both UV and IR divergences one must first separate them from the finite part of the integral. This procedure is called Regularization. The most popular regularization scheme of the last years and the one used throughout this thesis is dimensional regularization due to 't Hooft and Veltman [8–10].

1.3.1 Dimensional Regularization (DR)

In Dimensional Regularization (DR) the Feynman integral is calculated as an analytic function of the space-time dimensionality $D = 4 - 2\epsilon$, with ϵ being a small parameter. Providing that D is treated as a continuous variable, both UV and IR divergences can be quantified in the form of poles in ϵ , i.e. $1/\epsilon^n$, with $n = 1, 2, \dots$. In the limit $D \rightarrow 4$, or equivalently $\epsilon \rightarrow 0$, any observable quantity (cross-section or decay-rate) should be well-defined. The DR method is well explained in references [3], and [6]. To apply DR in an integral one has to go from 4 to D dimensions. After performing the so called Wick rotation to go from the Minkowski to the Euclidian space, one must apply the following modifications:

- In the Feynman rules the measure we use to integrate over each loop-momentum

$$k_i \text{ changes: } \int \frac{d^4 k_i}{(2\pi)^4} \rightarrow \int \frac{d^D k_i}{(2\pi)^D} .$$

- In D dimensions $g^{\mu\nu}$ obeys $g^{\mu\nu} g_{\mu\nu} = D$. The Clifford algebra will also be affected with Dirac matrices being manipulated as a set of $D \times 4 \times 4$ matrices whose contraction identities are modified to:

$$\gamma^\mu \gamma^\nu \gamma_\mu = -(2 - \epsilon) \gamma^\nu , \quad \gamma^\mu \gamma^\nu \gamma^\rho \gamma_\mu = 4g^{\nu\rho} - \epsilon \gamma^\nu \gamma^\rho \quad \dots .$$

- The measure of the phase-space integration of a transition rate over the external momenta will also have to be converted:

$$\int \frac{d^3 p}{2E(2\pi)^3} \cdots (2\pi)^4 \delta(p_i - p_f) \rightarrow \int \frac{d^{D-1} p}{2E(2\pi)^{D-1}} \cdots (2\pi)^D \delta(p_i - p_f) .$$

- Finally, since the action $S = \int d^D x \mathcal{L}$ must remain dimensionless, the terms in the QCD Lagrangian must alter to ensure dimensional coherence. As a consequence, a dimension is imposed on the coupling constant g . The dimensionless coupling constant must be replaced by:

$$g_s \rightarrow \mu^\epsilon g_s . \tag{1.6}$$

As a result the theory has acquired one more scale, μ . Notice that in the limit $D \rightarrow 4$, g has no dimensions.

After the continuation of loop momenta into D dimensions one is still left with some freedom concerning the dimensionality of the momenta of the external particles as well as the number of polarisations for internal and external particles. There are several DR schemes that can be used to deal with this. The calculations of this thesis were carried out using a scheme called Conventional Dimensional Regularization (CDR)¹. Within this scheme, no distinction is made between real and virtual particles and massless quarks are considered to have 2 helicity states while gluons have $D - 2$. For the helicity amplitudes, we use the t'Hooft-Veltman scheme, where the external particle states are 4-dimensional.

1.3.2 Renormalization

So far in this section we have presented a scheme that allows IR and UV divergences to be isolated and quantified. UV divergences cancel order by order in perturbation theory due to a fundamental property of QCD:

QCD is a Renormalizable theory.

“The idea of renormalizable theory is that UV divergences of a field theory are to be cancelled by renormalizations of the parameters of the theory” [6]. In practice one can take the fields and coupling of \mathcal{L}_{QCD} and redefine them with a multiplicative factor. We set:

$$\psi_f^{i,U} \rightarrow Z^{1/2} \psi_f^{i,R} \quad , \quad (1.7)$$

$$A_\mu^{a,U} \rightarrow Z_A^{1/2} A_\mu^{a,R} \quad , \quad (1.8)$$

$$n^{a,U} \rightarrow Z_n^{1/2} n^{a,R} \quad , \quad (1.9)$$

$$g_s^U \rightarrow Z_g g_s^R \quad , \quad (1.10)$$

$$m^U \rightarrow Z_m m^R \quad , \quad (1.11)$$

$$\xi^U \rightarrow Z_A \xi^R \quad , \quad (1.12)$$

¹A variety of regularisation prescriptions within DR can be found in [11,12], whereas in [13] there is a detailed introduction to the DR technique.

where we have used the U and R superscripts to denote the unrenormalized and renormalized quantities respectively. The above redefinition is a simple renaming and will not alter the path integral over the action $S = \int d^D x \mathcal{L}$. This means that the Green's functions and S-matrix elements will remain the same as well as the Feynman rules presented in section 1.2. In a renormalizable theory one can write a UV-divergent Green's function of the unrenormalized fields as the product of a UV-finite renormalized Green's function times a renormalization constant which has absorbed all UV divergence. With proper readjustment, the multiplicative renormalization constants absorb UV divergences at all orders in perturbative QCD, giving physical meaning to the renormalized Green's functions. This enables QCD to make theoretical predictions of finite physical observables such as cross-sections and decay-rates.

Apart from factoring out UV divergences one has the choice of subtracting an arbitrary amount of the finite part. This defines the renormalization scheme used in the calculation. In this thesis we have used the Modified Minimal Subtraction scheme (\overline{MS}), in which we remove the UV poles in $\bar{\epsilon}$ defined as:

$$\frac{1}{\bar{\epsilon}} = (4\pi)^\epsilon e^{-\epsilon\gamma} \frac{1}{\epsilon} \quad \text{with } \gamma \text{ being Euler's constant .}$$

This choice simplifies our calculation because in practice the poles always appear in the combination:

$$\frac{\Gamma(1 + \epsilon)}{\epsilon} (4\pi)^\epsilon = \frac{1}{\epsilon} + \ln(4\pi) - \gamma + \mathcal{O}(\epsilon) .$$

When we performed dimensional regularization we introduced an unphysical mass scale μ to maintain a dimensionless action. This unphysical and arbitrary mass scale is still present in the renormalized fields and couplings. Physical observables do not depend on the renormalization scale. However, there is dependence on μ when the calculation is in fixed-order perturbation theory. Depending on the choice of renormalization scheme and scale μ , one can get different results when predicting the same physical quantity. For the theory to be consistent the expressions of our results must be formally equivalent with each other. This is achievable

due to a set of restrictions imposed on the renormalized fields and couplings. These restrictions have the form of a set of differential equations (*renormalization group equations*) that must be satisfied by the renormalized quantities when varying the renormalization scale. The renormalization group equations are derived by requiring that physical observables are eventually independent of the mass-scale μ .

1.3.3 Running Coupling and Renormalization Group Equations

Using the CDR transformation eq. (1.6) and the renormalization group definitions eq. (1.7) we get a relation between the bare-unrenormalized coupling strength and the renormalized one:

$$\mu_0^\epsilon g_s^U = Z_g \mu^\epsilon g_s^R . \quad (1.13)$$

Taking in mind that:

$$\alpha_s = \frac{g_s^2}{4\pi} ,$$

one can re-write the unrenormalized coupling α_s as:

$$(\mu_0^2)^\epsilon \alpha_s^U = Z_g^2 (\mu^2)^\epsilon \alpha_s^R . \quad (1.14)$$

The value of Z_g has been calculated up to order $(\alpha_s^R)^3$ in perturbation theory. In the \overline{MS} scheme we have:

$$(\mu_0^2)^\epsilon \alpha_s^U S_\epsilon = (\mu^2)^\epsilon \alpha_s^R \left[1 - \frac{\beta_0}{\epsilon} \left(\frac{\alpha_s^R}{2\pi} \right) + \left(\frac{\beta_0^2}{\epsilon^2} - \frac{\beta_1}{2\epsilon} \right) \left(\frac{\alpha_s^R}{2\pi} \right)^2 + \mathcal{O}((\alpha_s^R)^3) \right] , \quad (1.15)$$

where:

$$\begin{aligned} S_\epsilon &= e^{-\epsilon\gamma} (4\pi)^\epsilon , \quad \gamma = \text{Euler constant} , \\ \beta_0 &= \frac{11 C_A - 4 T_R N_f}{6} , \\ \beta_1 &= \frac{17 C_A^2 - 10 C_A T_R N_f - 6 C_f T_R N_f}{6} . \end{aligned} \quad (1.16)$$

Here N_f is the number of active light-quark flavours and C_F , C_A and T_R are the Casimir operators for $SU(N)$ which can be written in terms of the number of colors N as:

$$C_F = \frac{N^2 - 1}{2N}, \quad C_A = N, \quad T_R = \frac{1}{2}. \quad (1.17)$$

The parameters β_0 and β_1 appearing in eq. (1.16) are the first two coefficients of the perturbative expansion of the β function which is defined by the renormalization group equation:

$$\mu^2 \frac{\partial \alpha_s}{\partial \mu^2} \equiv \beta_{(\alpha_s(\mu^2))} = -\beta_0 \alpha_s^2(\mu^2) - \beta_1 \alpha_s^3(\mu^2) - \dots, \quad (1.18)$$

where we have dropped index R from the renormalized α_s^R . The solution of this differential equation yields:

$$\int_{\alpha_s(\mu_0^2)}^{\alpha_s(\mu^2)} \frac{d\alpha}{\beta(\alpha)} = \log \left(\frac{\mu^2}{\mu_0^2} \right), \quad (1.19)$$

where the scale μ_0 expresses a boundary condition. Equation 1.19 defines a new function, the running coupling $\alpha_s(\mu^2)$, providing that we know its value $\alpha_s(\mu_0^2)$ for a certain energy scale μ_0 . If we keep only the first term of the series of the β function, the solution of eq. 1.19 is:

$$\alpha_s(\mu^2) = \frac{\alpha_s(\mu_0^2)}{1 + \alpha_s(\mu_0^2) \beta_0 \log \left(\frac{\mu^2}{\mu_0^2} \right)}. \quad (1.20)$$

Notice that as the scale μ increases, the running coupling $\alpha_s(\mu^2)$ decreases to zero. This is a fundamental property of QCD called *asymptotic freedom*². The significance of this property is evident in the study of physical observables such as decay rates. As we have mentioned earlier, a physical observable should not depend on the unphysical renormalization scale μ . This statement can be expressed through the following renormalization group equation for a decay rate Γ :

$$\frac{d\Gamma}{d\mu^2} = 0. \quad (1.21)$$

²Of course, this statement is valid for $\beta_0 > 0$, which true if in eq. (1.16), the number of light-quark flavours is $N_f \leq \frac{11N}{4T_R} = \frac{33}{2}$ (in the final step we used the number of colors $N = 3$).

As the decay rate is a dimensionless observable, its μ dependence at each order will be a function of the coupling $\alpha_s(\mu^2)$ and the dimensionless ratio s/μ^2 , with s being a squared energy scale on which Γ depends. Eq. (1.21) can therefore be written as:

$$\left[-\frac{\partial}{\partial t} + \beta_{(\alpha_s)} \frac{\partial}{\partial \alpha_s} \right] \Gamma(\alpha_s(\mu^2), e^t) = 0, \quad (1.22)$$

with $t = \log(s/\mu^2)$. It is easy to prove that $\Gamma(\alpha_s(s), 1)$, i.e. $\mu^2 = s$ is a solution of eq. (1.22)³. We can conclude by this that the dimensionless decay rate Γ measured at a large energy s can be expressed as a perturbative series in terms of the strong coupling constant $\alpha_s(s)$:

$$\Gamma = \Gamma(\alpha_s(s), 1) = r_1 \alpha_s(s) + r_2 \alpha_s^2(s) + r_3 \alpha_s^3(s) + \dots \quad (1.23)$$

This perturbative expansion raises a few challenges due to the fact that α_s is a free parameter of QCD and that we need to truncate this series at a point in order to extract a theoretical value for the observable (e.g. decay rate) which will be compared to the one emerging from experimental data. These issues will be addressed in the end of chapter 2.

1.4 Effective Higgs Lagrangian

In section 1.1 we presented the full QCD Lagrangian describing the fundamental interactions between the QCD particles and fields (quarks and gluons). One of the most important unresolved problems of Particle Physics concerns the origin of the particle masses. Within the Standard Model theory, the most accurate and precisely tested theoretical description in the field of Particle Physics, all the particles' masses are generated through a mechanism called electroweak symmetry breaking⁴. In its minimal version, the phenomenological manifestation of this mechanism is an electrically neutral, scalar, zero-spin particle, the Higgs boson, whose mass is an a

³Indeed, $\frac{\partial \Gamma(\alpha_s(s), 1)}{\partial t} = \frac{\partial \alpha_s(s)}{\partial t} \frac{\partial \Gamma(\alpha_s(s), 1)}{\partial \alpha_s(s)} = \beta_{(\alpha_s)} \frac{\partial \Gamma(\alpha_s(s), 1)}{\partial \alpha_s}$.

⁴We will not illustrate this mechanism here. We refer the reader to some of the many books that have been written on the subject like [3, 7].

priori free parameter of the theory. The Higgs boson remains the only still undetected particle of the Standard Model. As a result the search for the Higgs particle is one of the major objectives of present and future colliders like LHC. The most probable range for its mass, as it is predicted by comparing existing experimental data and theoretical estimates, is approximately between 100 and 200 GeV [15]. For this mass range, at LHC, the dominant production mechanism of the Higgs boson will be through gluon fusion [14], at a rate at least five times higher than any other production channel. This accentuates the importance of the theoretical study of the Higgs-gluons interactions. However, the Higgs boson interacts directly with quarks and not with gluons. This interaction can be described by the bare Yukawa Lagrangian,

$$\mathcal{L}_Y = -\frac{H^U}{v} \left(\sum_{q_i} m_{q_i}^U \bar{q}_i^U q_i^U + M_t^U \bar{t}^U t^U \right), \quad (1.24)$$

where v is the Higgs vacuum expectation value related to the Fermi constant by $v = (\sqrt{2}G_F)^{-1/2} = 246 \text{ GeV}$, t is the top quark, q_i are the light quarks and the superscript U symbolizes bare quantities. We have separated the top quark term in \mathcal{L}_Y because, as the Yukawa couplings of the Higgs boson to quarks are proportional to the respective quark masses, the Higgs coupling to gluons ($\mathcal{H}gg$) is essentially generated by the top quark alone, through a top-quark loop. The involvement of two mass scales (M_t , $M_{\mathcal{H}}$) complicates significantly any effort to theoretically describe such interactions. Nevertheless, it has been shown that in the heavy top quark limit, $M_t \rightarrow \infty$, the $\mathcal{H}gg$ coupling becomes independent of the M_t . We can therefore integrate out the top quark field and formulate an effective Lagrangian, \mathcal{L}_{eff} ([16–18]) approximating the Hgg coupling:

$$\mathcal{L}_{eff} = -\frac{H}{4v} C_1^U (G_{\mu\nu}^{\alpha U})^2 = -\frac{H}{4v} C_1 (G_{\mu\nu}^{\alpha'})^2, \quad (1.25)$$

with $G_{\mu\nu}^{\alpha'}$ being the field strength tensor of the gluon. The primes indicate the quantities defined in a light-quark ($n_l = 5$) effective QCD. The dependence on the top quark is restricted to the C_1 coefficient function. We should note here that the second equality in eq. (1.25) is valid because the product $C_1 (G_{\mu\nu}^{\alpha'})^2$ is renormalization group invariant at each order, even though C_1 and $(G_{\mu\nu}^{\alpha'})^2$ separately are not.

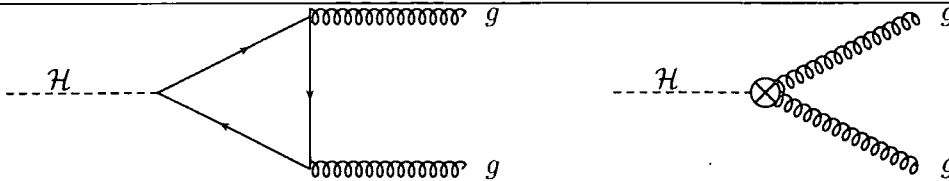


Figure 1.1: The Hgg coupling in full QCD and the effective Lagrangian theory.

C_1 has been calculated up to order $\mathcal{O}(\alpha_s^4)$ in [19]⁵. However, for our purposes we need it only up to order $\mathcal{O}(\alpha_s^3)$ [20, 21],

$$C_1 = -\frac{1}{3} \frac{\alpha_s^{(n_l)}}{\pi} \left\{ 1 + \frac{11}{4} \frac{\alpha_s^{(n_l)}}{\pi} + \left(\frac{\alpha_s^{(n_l)}}{\pi} \right)^2 \left[\frac{2777}{288} + \frac{19}{16} L_{Mt} + n_l \left(-\frac{67}{96} + \frac{1}{3} L_{Mt} \right) \right] + \dots \right\}, \quad (1.26)$$

where $L_{Mt} = \ln(\mu^2/M_t^2)$, $n_l = 5$ is the number of the massless active quark flavors and $\alpha^{(n_l)} \equiv \alpha^{(5)}(\mu^2)$ is the renormalized QCD coupling constant in the $\overline{\text{MS}}$ scheme which can be expressed through $\alpha^{(6)}(\mu^2)$ via the decoupling relation [22],

$$\frac{\alpha_s^{(5)}(\mu)}{\alpha_s^{(6)}(\mu)} = 1 - \frac{\alpha_s^{(6)}(\mu)}{\pi} \left(\frac{1}{6} L_{Mt} \right) + \left(\frac{\alpha_s^{(6)}(\mu)}{\pi} \right)^2 \left(\frac{11}{72} - \frac{11}{24} L_{Mt} + \frac{1}{36} L_{Mt}^2 \right) + \mathcal{O}(\alpha_s^3). \quad (1.27)$$

This approximation works very well under the condition that both the transverse momentum P_τ and the Higgs mass M_H , are smaller than the top quark mass M_t ⁶. The advantage of this method is that it reduces the loops that need to be calculated by one (fig.1.1), simplifying any calculation enormously. Therefore, amplitudes that correspond to two-loop diagrams in the original theory are one-loop diagrams in the effective theory.

1.4.1 Feynman Rules for the Effective Lagrangian

Similarly to the ‘normal’ QCD Lagrangian, the effective Lagrangian generates vertices involving the Higgs boson coupling with two, three or four gluons whose asso-

⁵The calculation involved a large number (657) of three-loop three-point diagrams.

⁶More precisely $M_H < 2M_t$, with $M_t \approx 175$ GeV.

ciated Feynman rules are respectively:

$$\begin{aligned}
 & i C_1 \mathcal{V}_{ab}^{\mu\nu}(p_1, p_2) , \\
 & -C_1 \mathcal{Y}_{abc}^{\mu\nu\rho}(p_1, p_2, p_3) , \\
 & -C_1 g_s^2 \mathcal{X}_{abcd}^{\mu\nu\rho\sigma} ,
 \end{aligned}$$

with

$$\begin{aligned}
 \mathcal{V}_{ab}^{\mu\nu}(p_1, p_2) &= \delta_{ab} (g^{\mu\nu} p_1 \cdot p_2 - p_1^\nu p_2^\mu) , \\
 \mathcal{Y}_{abc}^{\mu\nu\rho}(p_1, p_2, p_3) &= f_{abc} \left((p_1 - p_2)^\rho g^{\mu\nu} + (p_2 - p_3)^\mu g^{\nu\rho} + (p_3 - p_1)^\nu g^{\rho\mu} \right) , \\
 \mathcal{X}_{abcd}^{\mu\nu\rho\sigma} &= f_{abe} f_{cde} (g^{\mu\rho} g^{\nu\sigma} - g^{\mu\sigma} g^{\nu\rho}) + f_{ace} f_{bde} (g^{\mu\nu} g^{\rho\sigma} - g^{\mu\sigma} g^{\nu\rho}) \\
 &\quad + f_{ade} f_{bce} (g^{\mu\nu} g^{\rho\sigma} - g^{\mu\rho} g^{\nu\sigma}) .
 \end{aligned} \tag{1.28}$$

The rest of the propagators, external particles and vertices, that do not entail the effective Higgs coupling, are treated using the standard set of QCD Feynman rules presented in section 1.2.

In section 1.3 we presented techniques that allow one to deal with the appearance of ultraviolet and infrared divergences. A method for canceling UV divergences was also illustrated. In the following chapter we describe a methodology that leads to the cancellation of IR divergences and an independent way of predicting them.

Chapter 2

IR Divergences and Matrix Elements

2.1 Introduction

In section 1.3 we presented a procedure called conventional dimensional regularization (CDR), which allows infrared divergences to be separated from the finite part of an integral and be manifest as poles in ϵ , i.e. $1/\epsilon^n$, $n = 1, 2, \dots$. Apart from the IR divergences generated in loop integrals (*virtual divergences*) there are also divergences arising from real emissions. These can be of two types; *soft divergences* appearing when an on-shell particle radiates a massless low momentum ('soft') particle and remains on-shell and *collinear divergences* arising when the radiating and radiated particles have 'indistinguishable' momentum configurations¹. As we mentioned in section 1.3 all these divergences are eliminated at each order in perturbation series.

In the following subsections we will derive the components needed for the 'total' NLO decay rate of $\mathcal{H} \rightarrow gg$ in the limit $M_t \rightarrow \infty$. In order to calculate the radiative corrections to the $\mathcal{H} \rightarrow gg$ decay we need both the real contributions from the processes $\mathcal{H} \rightarrow ggg$ and $\mathcal{H} \rightarrow gq\bar{q}$, as well as the virtual 1-loop corrections from $\mathcal{H} \rightarrow gg$. Both real and virtual corrections have divergences which are manifest

¹This practically means that the two particles move toward the same direction.

2. IR Divergences and Matrix Elements

as poles in ϵ ($1/\epsilon$ and $1/\epsilon^2$). In 2.2.5 we demonstrate how all these divergences miraculously cancel out. Then we illustrate a formalism developed by Catani [11,12] which can predict the IR pole structure of NLO and NNLO matrix elements. Finally we discuss the need for matrix element and helicity amplitude calculations beyond NLO.

2.2 Infrared Cancellation:

The $\mathcal{H} \rightarrow gg$ decay

2.2.1 Notation

For the general case of the decay of the Higgs boson to particles X , we will use the following notation:

$ \mathcal{M}_{\mathcal{H} \rightarrow X}^{(0)}\rangle$	Tree – level amplitude ,
$ \mathcal{M}_{\mathcal{H} \rightarrow X}^{(1)}\rangle$	One – loop amplitude ,
$ \mathcal{M}_{\mathcal{H} \rightarrow X}^{(2)}\rangle$	Two – loop amplitude ,
$\Gamma_{\mathcal{H} \rightarrow X}^{(0)}$	Tree – level decay rate ,
$\Gamma_{\mathcal{H} \rightarrow X}^{(1)}$	One – loop decay rate ,
$\Gamma_{\mathcal{H} \rightarrow X}^{(2)}$	Two – loop decay rate ,
$\Gamma_{\mathcal{H} \rightarrow X}^{LO}$	Leading order decay rate ,
$\Gamma_{\mathcal{H} \rightarrow X}^{NLO}$	Next – to – leading order decay rate ,
$\Gamma_{\mathcal{H} \rightarrow X}^{NNLO}$	Next – to – next – to – leading order decay rate ,
$d\Phi_{N_X}$	The N_X – body phase space.

(2.1)

2.2.2 Tree-Level and LO: No Emissions

The LO contribution involves only one type of diagram (fig 2.1). The matrix element squared for this process in the $M_t \rightarrow \infty$ limit can be trivially calculated and is well

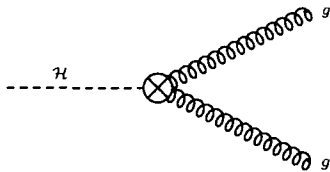


Figure 2.1: Feynman diagram contributing to the $\mathcal{H} \rightarrow gg$ decay at LO. The crossed-dot represents the effective coupling between gluons and the Higgs boson in the infinite top quark mass limit.

known [23] for many years:

$$\sum_{spin,col} \left| \mathcal{M}_{\mathcal{H} \rightarrow gg}^{(0)} \right|^2 = \frac{C_1^2 M_{\mathcal{H}}^4 (N^2 - 1)}{2v^2} (1 - \epsilon) \quad , \quad (2.2)$$

The tree-level differential decay for $\mathcal{H} \rightarrow gg$ is given by:

$$\int d\Gamma_{\mathcal{H} \rightarrow gg}^{(0)} = \int \frac{d\Phi_2}{2M_{\mathcal{H}}} \sum_{spin,col} \left| \mathcal{M}_{\mathcal{H} \rightarrow gg}^{(0)} \right|^2 \quad , \quad (2.3)$$

where $\int d\Phi_2$ is the phase space for two partons in D dimensions. There is also an overall factor $\frac{1}{2M_{\mathcal{H}}}$, accounting for the incoming flux. In order to perform the integration, we use the two-body phase space formula which we have derived in Appendix C, and get:

$$\Gamma_{\mathcal{H} \rightarrow gg}^{(0)} = \frac{C_1^2 M_{\mathcal{H}}^3 (N^2 - 1)}{64\pi v^2} \frac{\Gamma(1 - \epsilon)}{\Gamma(2 - 2\epsilon)} \left(\frac{4\pi}{M_{\mathcal{H}}^2} \right)^\epsilon (1 - \epsilon) \quad . \quad (2.4)$$

In order to get the leading order (LO) term of the decay rate, we keep only the first, order $\mathcal{O}(\alpha(s))$, term of the expression for C_1 (eq. (1.26)):

$$\Gamma_{\mathcal{H} \rightarrow gg}^{LO} = \frac{(\alpha_s)^2 M_{\mathcal{H}}^3 (N^2 - 1)}{576\pi^3 v^2} \frac{\Gamma(1 - \epsilon)}{\Gamma(2 - 2\epsilon)} \left(\frac{4\pi}{M_{\mathcal{H}}^2} \right)^\epsilon (1 - \epsilon) \quad . \quad (2.5)$$

Since we are interested in a NLO calculation, we can keep only the terms up to order $\mathcal{O}((\alpha_s^R)^3)$ of the decay rate $\Gamma_{\mathcal{H} \rightarrow gg}^{(0)}$ (eq. (2.4)). Therefore we renormalize in the \overline{MS} scheme using eq. (1.15) and keep only the first two terms of eq. (1.26) for C_1 . Then eq. (2.4) can be expressed in terms of $\Gamma_{\mathcal{H} \rightarrow gg}^{LO}$ as:

$$\Gamma_{\mathcal{H} \rightarrow gg}^{(0)} = \Gamma_{\mathcal{H} \rightarrow gg}^{LO} \left(1 + \frac{\alpha_s^R}{2\pi} \left(-2\frac{\beta_0}{\epsilon} + \frac{11}{3}N \right) \right) + \mathcal{O}((\alpha_s^R)^4) \quad . \quad (2.6)$$

2. IR Divergences and Matrix Elements

In 4 dimensions ($\epsilon \rightarrow 0$) and for $N = 3$, eq. (2.5) reads:

$$\Gamma_{\mathcal{H} \rightarrow gg}^{LO} = \frac{M_{\mathcal{H}}^3 \alpha_s^2 G_F}{36\sqrt{2}\pi^3} \quad , \quad (2.7)$$

2.2.3 Virtual Infrared Divergences

The contribution to the decay rate coming from virtual graphs involves only two types of diagrams (fig. 2.2)



Figure 2.2: Feynman diagrams contributing to the $\mathcal{H} \rightarrow gg$ decay at NLO in the infinite top quark mass limit

The diagrams of fig. 2.2 that appear in the one-loop amplitude $\mathcal{M}_{\mathcal{H} \rightarrow gg}^{(1)}$ demand the calculation of one-loop integrals of the form:

$$\int \frac{d^D k}{i\pi^{D/2}} \frac{u}{k^2(k+p_1)^2(k+p_1+p_2)^2} \quad , \quad (2.8)$$

where k is the loop momentum, p_1 and p_2 are the external momenta and u is a function of scalar products of k , p_1 and p_2 such as k^2 , $k \cdot p_1$ or $p_1 \cdot p_2$. This type of integral is slightly harder to evaluate. In the following chapters we will demonstrate a methodology that allows one to compute not only one-loop but also two-loop integrals and use them to calculate amplitudes. Here we will just present the result of the interference of the tree level with the one-loop amplitude:

$$\sum_{spin,col} \left\langle \mathcal{M}_{\mathcal{H} \rightarrow gg}^{(0)} | \mathcal{M}_{\mathcal{H} \rightarrow gg}^{(1)} \right\rangle = -(-1)^{-\epsilon} \frac{C_1^2 \alpha_s^2 4\pi}{v^2} N(N^2 - 1) \left(\frac{4\pi}{M_{\mathcal{H}}^2} \right)^{\epsilon-2} \frac{\Gamma(\epsilon)\Gamma(1-\epsilon)^2}{\Gamma(2-2\epsilon)} \left(\frac{1}{\epsilon} - 3 + 2\epsilon + \epsilon^2 \right) \quad (2.9)$$

For reasons that will soon become apparent in subsection 2.2.5 we proceed by integrating $2\mathcal{R}_e \sum_{spin,col} \langle \mathcal{M}_{\mathcal{H} \rightarrow gg}^{(0)} | \mathcal{M}_{\mathcal{H} \rightarrow gg}^{(1)} \rangle$ over the two-body phase space²:

$$\Gamma_{\mathcal{H} \rightarrow gg}^{(1)} = \int \frac{d\Phi_2}{2M_{\mathcal{H}}} 2\mathcal{R}_e \sum_{spin,col} \langle \mathcal{M}_{\mathcal{H} \rightarrow gg}^{(0)} | \mathcal{M}_{\mathcal{H} \rightarrow gg}^{(1)} \rangle . \quad (2.10)$$

The result of the integration up to order $\mathcal{O}(\epsilon)$ is:

$$\Gamma_{\mathcal{H} \rightarrow gg}^{(1)} = \Gamma_{\mathcal{H} \rightarrow gg}^{LO} \frac{\alpha_s e^{-\epsilon\gamma}}{2\pi} \left(\frac{4\pi\mu_0^2}{M_{\mathcal{H}}^2} \right)^\epsilon N \left(-\frac{2}{\epsilon^2} + \frac{7\pi^2}{6} + \mathcal{O}(\epsilon) \right) , \quad (2.11)$$

where we have factored out $\Gamma_{\mathcal{H} \rightarrow gg}^{LO}$. Finally we renormalize in the \overline{MS} scheme by multiplying the above equation with $S_\epsilon^{-1} = e^{\epsilon\gamma}(4\pi)^{-\epsilon}$ and get:

$$\Gamma_{\mathcal{H} \rightarrow gg}^{(1)} = \Gamma_{\mathcal{H} \rightarrow gg}^{LO} \frac{\alpha_s}{2\pi} \left(\frac{\mu^2}{M_{\mathcal{H}}^2} \right)^\epsilon N \left(-\frac{2}{\epsilon^2} + \frac{7\pi^2}{6} + \mathcal{O}(\epsilon) \right) , \quad (2.12)$$

2.2.4 Real Infrared Divergences

We will consider two subprocesses which contribute real emissions to the $\mathcal{H} \rightarrow gg$ decay. The first one involves the emission of a third real gluon in the final state ($\mathcal{H} \rightarrow ggg$), giving diagrams like the ones in fig. 2.3. The second one entails the splitting of one of the two final-state gluons into a quark-antiquark pair ($\mathcal{H} \rightarrow q\bar{q}g$) as shown in fig. 2.4.



Figure 2.3: Feynman diagrams contributing to the tree-level $\mathcal{H} \rightarrow ggg$ decay in the infinite top quark mass limit. One real gluon is emitted.

Both of these processes ‘look’ like the $\mathcal{H} \rightarrow gg$ decay in their collinear and soft limits. For example all three diagrams of fig. 2.5 are phenomenologically indistinguishable.

The squared matrix elements for both contributions are easy to calculate, since they

²The imaginary part was induced by the expansion of $(-1)^{-\epsilon}$.

2. IR Divergences and Matrix Elements

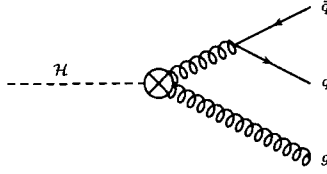


Figure 2.4: Feynman diagram contributing to the tree-level $\mathcal{H} \rightarrow q\bar{q}g$ decay in the infinite top quark mass limit. One gluon splits to a quark-antiquark pair.

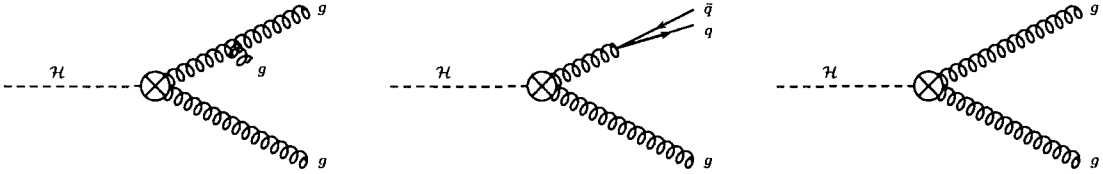


Figure 2.5: Feynman diagrams of decays with soft or collinear emissions that would look like $\mathcal{H} \rightarrow gg$ in the colliders.

do not contain any loop integrals:

$$\sum_{spin,col} \left| \mathcal{M}_{\mathcal{H} \rightarrow ggg}^{(0)} \right|^2 = \frac{C_1^2 \alpha_s^4 \pi}{v^2} N(N^2 - 1) \times \left[\frac{M_{\mathcal{H}}^8 + s_{12}^4 + s_{23}^4 + s_{13}^4}{s_{12}s_{23}s_{13}} (1 - 2\epsilon) + \frac{\epsilon (M_{\mathcal{H}}^4 + s_{12}^2 + s_{23}^2 + s_{13}^2)^2}{2 s_{12}s_{23}s_{13}} \right], \quad (2.13)$$

$$\sum_{spin,col} \left| \mathcal{M}_{\mathcal{H} \rightarrow q\bar{q}g}^{(0)} \right|^2 = \frac{C_1^2 \alpha_s^4 \pi}{v^2} N_f (N^2 - 1) \frac{s_{23}^2 + s_{13}^2 - \epsilon (s_{23} + s_{13})^2}{s_{12}}, \quad (2.14)$$

where $s_{ij} = (p_i + p_j)^2$. The decay rate of each of the two contributions is given schematically by:

$$\int d\Gamma_{\mathcal{H} \rightarrow ggg}^{(0)} = \int \frac{d\Phi_3}{2M_{\mathcal{H}}} \sum_{spin,col} \left| \mathcal{M}_{\mathcal{H} \rightarrow ggg}^{(0)} \right|^2, \quad (2.15)$$

and

$$\int d\Gamma_{\mathcal{H} \rightarrow q\bar{q}g}^{(0)} = \int \frac{d\Phi_3}{2M_{\mathcal{H}}} \sum_{spin,col} \left| \mathcal{M}_{\mathcal{H} \rightarrow q\bar{q}g}^{(0)} \right|^2. \quad (2.16)$$

where the integration is over the three-body phase-space $d\Phi_3$ which we have calculated in Appendix C. However this integration is not trivial. We will demonstrate

how it works for eqs. (2.15) and (2.16). We make the change of variables:

$$s_{12} \rightarrow y_{12}M_{\mathcal{H}}^2, \quad s_{13} \rightarrow y_{13}M_{\mathcal{H}}^2 \quad \text{and} \quad s_{23} \rightarrow y_{23}M_{\mathcal{H}}^2, \quad (2.17)$$

with $0 \leq y_{ij} \leq 1$. From the momentum conservation formula: $s_{12} + s_{13} + s_{23} = M_{\mathcal{H}}^2$ one can get:

$$y_{12} + y_{13} + y_{23} = 1 \quad . \quad (2.18)$$

As the momenta of the outgoing partons are p_i^μ , we have $p_i^0 = E_i$. Using the definition of the invariant scales $s_{ij} = (p_i + p_j)^2$ we get:

$$y_{ij} = \frac{(p_i + p_j)^2}{M_{\mathcal{H}}^2} = \frac{2E_i E_j}{M_{\mathcal{H}}^2} (1 - \cos \theta_{ij}) \quad . \quad (2.19)$$

With the change of variables (2.17) equation (2.15) becomes:

$$\begin{aligned} \int d\Gamma_{\mathcal{H} \rightarrow ggg}^{(0)} &\sim \int dy_{12} dy_{13} dy_{23} \delta(1 - y_{12} - y_{13} - y_{23}) \\ &\times \left[\frac{1 + y_{12}^4 + y_{13}^4 + y_{23}^4}{y_{12}^{1+\epsilon} y_{13}^{1+\epsilon} y_{23}^{1+\epsilon}} (1 - 2\epsilon) + \frac{\epsilon (1 + y_{12} + y_{13} + y_{23})^2}{2 y_{12}^{1+\epsilon} y_{13}^{1+\epsilon} y_{23}^{1+\epsilon}} \right], \end{aligned} \quad (2.20)$$

while equation (2.16) reads:

$$\begin{aligned} \int d\Gamma_{\mathcal{H} \rightarrow q\bar{q}g}^{(0)} &\sim \int dy_{12} dy_{13} dy_{23} \delta(1 - y_{12} - y_{13} - y_{23}) \\ &\times \left[\frac{y_{13}^2 + y_{23}^2 - \epsilon(y_{13} + y_{23})^2}{y_{12}^{1+\epsilon} y_{13}^\epsilon y_{23}^\epsilon} \right]. \end{aligned} \quad (2.21)$$

If we had worked in 4 dimensions the integrands of (2.20) and (2.21) would be respectively:

$$\frac{1 + y_{12}^4 + y_{13}^4 + y_{23}^4}{y_{12} y_{13} y_{23}}, \quad (2.22)$$

$$\frac{y_{13}^2 + y_{23}^2}{y_{12}}, \quad (2.23)$$

and there would be singularities for certain values of the integration parameters. The first integrand (2.22) will provide the decay rate $\Gamma_{\mathcal{H} \rightarrow ggg}^{(0)}$ with *collinear* singularities

2. IR Divergences and Matrix Elements

for:

$$\begin{aligned}
y_{12} \rightarrow 0 &\xrightarrow{eq.(2.19)} \theta_{12} \rightarrow 0 \text{ (partons 1 and 2 are collinear)} \quad \text{or} \\
y_{13} \rightarrow 0 &\xrightarrow{eq.(2.19)} \theta_{13} \rightarrow 0 \text{ (partons 1 and 3 are collinear)} \quad \text{or} \\
y_{23} \rightarrow 0 &\xrightarrow{eq.(2.19)} \theta_{23} \rightarrow 0 \text{ (partons 2 and 3 are collinear)} \quad .
\end{aligned} \tag{2.24}$$

On top of that, from the energy constraint of eq. (2.18) we get another type of singularities, *soft*, which arise as:

$$\begin{aligned}
y_{12} \rightarrow 1 &\xrightarrow{eq.(2.18)} y_{13} \text{ and } y_{23} \rightarrow 0 \implies \text{parton 3 is soft} , \\
y_{13} \rightarrow 1 &\xrightarrow{eq.(2.18)} y_{12} \text{ and } y_{23} \rightarrow 0 \implies \text{parton 2 is soft} , \\
y_{23} \rightarrow 1 &\xrightarrow{eq.(2.18)} y_{12} \text{ and } y_{13} \rightarrow 0 \implies \text{parton 1 is soft} .
\end{aligned} \tag{2.25}$$

Similarly, for the $\Gamma_{\mathcal{H} \rightarrow q\bar{q}g}^{(0)}$ transition rate we can see that the integrand (2.23) will produce only *collinear* singularities, as:

$$y_{12} \rightarrow 0 \xrightarrow{eq.(2.19)} \theta_{12} \rightarrow 0 \text{ (partons 1 and 2 are collinear)} \quad , \tag{2.26}$$

where partons 1 and 2 correspond to the quark-antiquark pair. All the above singularities are schematically depicted in figure 2.6. Both *soft* and *collinear* singularities become evident as poles in ϵ in D dimensions, after CDR is applied. Performing the integrations in the way demonstrated in Appendix C one gets:

$$\Gamma_{\mathcal{H} \rightarrow ggg}^{(0)} = \Gamma_{\mathcal{H} \rightarrow gg}^{LO} \frac{\alpha_s e^{-\epsilon\gamma}}{2\pi} \left(\frac{4\pi\mu_0^2}{M_{\mathcal{H}}^2} \right)^\epsilon N \left(\frac{2}{\epsilon^2} + \frac{11}{3\epsilon} + \frac{73}{6} - \frac{7\pi^2}{6} + \mathcal{O}(\epsilon) \right), \tag{2.27}$$

$$\Gamma_{\mathcal{H} \rightarrow q\bar{q}g}^{(0)} = \Gamma_{\mathcal{H} \rightarrow gg}^{LO} \frac{\alpha_s e^{-\epsilon\gamma}}{2\pi} \left(\frac{4\pi\mu_0^2}{M_{\mathcal{H}}^2} \right)^\epsilon N_f \left(-\frac{2}{3\epsilon} - \frac{7}{3} + \mathcal{O}(\epsilon) \right). \tag{2.28}$$

Eventually, in the \overline{MS} scheme the real emission contributions to the $\mathcal{H} \rightarrow gg$ decay become:

$$\Gamma_{\mathcal{H} \rightarrow ggg}^{(0)} = \Gamma_{\mathcal{H} \rightarrow gg}^{LO} \frac{\alpha_s}{2\pi} \left(\frac{\mu^2}{M_{\mathcal{H}}^2} \right)^\epsilon N \left(\frac{2}{\epsilon^2} + \frac{11}{3\epsilon} + \frac{73}{6} - \frac{7\pi^2}{6} + \mathcal{O}(\epsilon) \right), \tag{2.29}$$

$$\Gamma_{\mathcal{H} \rightarrow q\bar{q}g}^{(0)} = \Gamma_{\mathcal{H} \rightarrow gg}^{LO} \frac{\alpha_s}{2\pi} \left(\frac{\mu^2}{M_{\mathcal{H}}^2} \right)^\epsilon N_f \left(-\frac{2}{3\epsilon} - \frac{7}{3} + \mathcal{O}(\epsilon) \right). \tag{2.30}$$

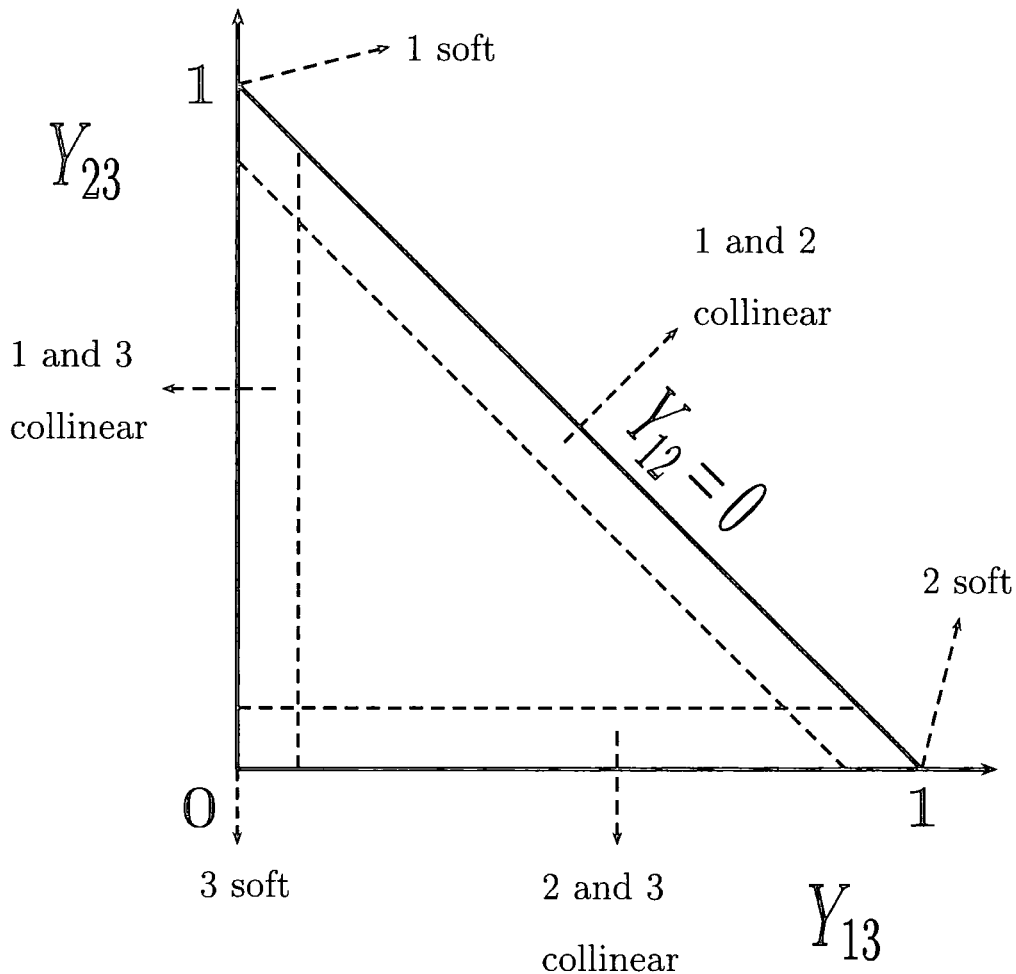


Figure 2.6: This plot represents the physical configuration of the partons for limiting behaviour within the allowed triangle.

2.2.5 Cancellation of Infrared Divergences

In the previous subsections we calculated all the pieces we need for a total NLO decay rate. Let us now see how all those pieces fit together. In perturbation theory the renormalized amplitude $|\mathcal{M}_{\mathcal{H} \rightarrow gg}\rangle$ can be expanded as:

$$|\mathcal{M}_{\mathcal{H} \rightarrow gg}\rangle = |\mathcal{M}_{\mathcal{H} \rightarrow gg}^{(0)}\rangle + |\mathcal{M}_{\mathcal{H} \rightarrow gg}^{(1)}\rangle + \mathcal{O}(\alpha_s^3) . \quad (2.31)$$

2. IR Divergences and Matrix Elements

Thus the squared matrix element and the decay rate at NLO read:

$$|\mathcal{M}_{\mathcal{H} \rightarrow gg}|^2 = \left| \mathcal{M}_{\mathcal{H} \rightarrow gg}^{(0)} \right|^2 + 2\mathcal{R}_e \left\langle \mathcal{M}_{\mathcal{H} \rightarrow gg}^{(0)} \middle| \mathcal{M}_{\mathcal{H} \rightarrow gg}^{(1)} \right\rangle, \quad (2.32)$$

$$\begin{aligned} \Gamma_{\mathcal{H} \rightarrow gg} &= \int \frac{d\Phi_3}{2M_{\mathcal{H}}} \sum_{spin,col} \left(\left| \mathcal{M}_{\mathcal{H} \rightarrow gg}^{(0)} \right|^2 + 2\mathcal{R}_e \sum_{spin,col} \left\langle \mathcal{M}_{\mathcal{H} \rightarrow gg}^{(0)} \middle| \mathcal{M}_{\mathcal{H} \rightarrow gg}^{(1)} \right\rangle \right) \\ &= \Gamma_{\mathcal{H} \rightarrow gg}^{(0)} + \Gamma_{\mathcal{H} \rightarrow gg}^{(1)}. \end{aligned} \quad (2.33)$$

Notice, however, that eq. (2.33) contains the term $\Gamma_{\mathcal{H} \rightarrow gg}^{(1)}$, which is divergent as it is evident in eq. (2.12). In order to cancel out the divergences we need to add contributions from the emission of a real soft or collinear gluon ($\Gamma_{\mathcal{H} \rightarrow ggg}$) and from the splitting of a gluon to a collinear quark-antiquark pair ($\Gamma_{\mathcal{H} \rightarrow q\bar{q}g}$). Eq. (2.33) becomes:

$$\Gamma_{\mathcal{H} \rightarrow gg}(\alpha_s^R) = \Gamma_{\mathcal{H} \rightarrow gg}^{(0)}(\alpha_s^R) + \Gamma_{\mathcal{H} \rightarrow gg}^{(1)}(\alpha_s^R) + \Gamma_{\mathcal{H} \rightarrow ggg}^{(0)}(\alpha_s^R) + \Gamma_{\mathcal{H} \rightarrow q\bar{q}g}^{(0)}(\alpha_s^R). \quad (2.34)$$

At this point we have included the upper index R on the coupling to show that all the decay rates are renormalized. Notice that for the rest of this section we fix the renormalization scale to $M_{\mathcal{H}}^2$. Subsequently the total NLO decay rate, all contributions included becomes:

$$\Gamma_{\mathcal{H} \rightarrow gg}^{NLO} = \underbrace{\Gamma_{\mathcal{H} \rightarrow gg}^{LO}}_{finite \mathcal{O}(\alpha_s^2)} + \overbrace{\left(\Gamma_{\mathcal{H} \rightarrow gg}^{(1)} + \Gamma_{\mathcal{H} \rightarrow ggg}^{(0)} + \Gamma_{\mathcal{H} \rightarrow q\bar{q}g}^{(0)} + \frac{\alpha_s^R}{2\pi} \left(-2\frac{\beta_0}{\epsilon} + \frac{11}{3}N \right) \Gamma_{\mathcal{H} \rightarrow gg}^{LO} \right)}^{finite \mathcal{O}(\alpha_s^3)}. \quad (2.35)$$

The coefficient of $\mathcal{O}(\alpha_s^3)$ is finite because the IR divergences of the decay width for the production of two gluons³,

$$\Gamma_{\mathcal{H} \rightarrow gg}^{(1) \text{ sing}} + \left(-2\frac{\beta_0}{\epsilon} \right) \frac{\alpha_s^R}{2\pi} \Gamma_{\mathcal{H} \rightarrow gg}^{LO} = \Gamma_{\mathcal{H} \rightarrow gg}^{LO} \frac{\alpha_s^R}{2\pi} \left[-N\frac{2}{\epsilon^2} - \frac{11N - 2N_f}{3} \frac{1}{\epsilon} \right], \quad (2.36)$$

are canceled out by soft and collinear divergences for the three-particle contribution:

$$\Gamma_{\mathcal{H} \rightarrow ggg}^{(0) \text{ sing}} + \Gamma_{\mathcal{H} \rightarrow q\bar{q}g}^{(0) \text{ sing}} = \Gamma_{\mathcal{H} \rightarrow gg}^{LO} \frac{\alpha_s^R}{2\pi} \left[N\frac{2}{\epsilon^2} + \frac{11N - 2N_f}{3} \frac{1}{\epsilon} \right], \quad (2.37)$$

³The superscript *sing* (singular) on the decay widths in equations (2.36) and (2.37) means that we have considered only the singular part of these widths.

2. IR Divergences and Matrix Elements

Substituting equations (2.12), (2.29) and (2.30) in eq. (2.35) we finally derive the desirable finite total NLO decay rate for the Higgs decay to two gluons, which normalised to the LO rate, can be written as⁴:

$$\Gamma_{\mathcal{H} \rightarrow gg}^{NLO} = \Gamma_{\mathcal{H} \rightarrow gg}^{LO} \left[1 + \frac{\alpha_s^R}{2\pi} \left(\frac{95}{6} N - \frac{7}{3} N_f \right) \right] , \quad (2.38)$$

with the scale of the coupling constant fixed at $M_{\mathcal{H}}^2$. We are now able to calculate the effect of the NLO term on the decay rate. If we use $N_f = 5$ and $N = 3$, the NLO corrections to the decay rate read:

$$\frac{\delta\Gamma}{\Gamma} = 62.73\% , \quad (2.39)$$

where we have used a value of α_s of about 0.11. This result is in complete agreement with the rate presented in [24]. It is evident from the above result that the NLO corrections to the decay rate of the Higgs to two gluons is extremely large, being of order more than 60% of the Born term. Such large corrections made the calculation of even higher order terms in the perturbative series essential. The NNLO calculation of the $\mathcal{H} \rightarrow gg$ decay rate in the infinite top-mass limit has been published by Chetyrkin, Kniehl and Steinhauser in [19]. Their result added an extra 21% correction on the LO decay width.

2.2.6 Infrared Safe Observables

In the previous subsection we demonstrated (eq. 2.38) that at least up to next-to-leading order in perturbation theory, the inclusive total decay rate of the Higgs boson to two gluons is an infrared safe quantity, whereas the exclusive gluon-gluon final state with no emissions is not. The question here is how those divergences emerge and why they cancel out so nicely when we come to calculate physical observables.

In subsection 2.2.3 we explained that the calculation of one-loop integrals (created when a *virtual* gluon is emitted by one external particle and absorbed by another) induces infrared divergences, at the limit where the loop momentum goes to zero. Within dimensional regularization these divergences are manifest as poles

⁴The substitution $\beta_0 = \frac{11N-2N_f}{6}$ was made.

2. IR Divergences and Matrix Elements

in ϵ . To cancel these *virtual* divergences we need to add degenerate states that are due to the emission of one extra *indistinguishable* particle. Real emission creates two types of degenerate states: *soft* and *collinear*. The former may appear if the theory under consideration includes a massless spin-1 field like a gluon in QCD, when the emitted particle's 4-momentum⁵ $\rightarrow 0$. There is an indefinite number of emitted soft gluons that can accompany physical observables with partons in the final state. Infrared collinear divergences emerge when a (massless) gluon is emitted collinear to a massless quark, so that the two become indistinguishable. However collinear divergences can appear even when the quark masses are not vanishing, because of the gluon's ability to couple with itself (triple-gluon vertex) and split into two collinear indistinguishable gluons. In the example of the Higgs decay to two gluons, soft divergences emerge when one soft gluon is emitted in the process $\mathcal{H} \rightarrow ggg$ and collinear divergences emerge when a final-state gluon emits another gluon toward the 'same' direction ($\mathcal{H} \rightarrow ggg$) or when a final-state gluon splits into a quark-antiquark pair moving 'almost' collinearly ($\mathcal{H} \rightarrow q\bar{q}g$). Assuming that quarks and gluons fragment collinearly to hadrons, we can deduce that when the emitted gluon is collinear or soft, the two-jet structure of the lowest order is maintained at higher powers of α_s . Therefore phenomenologically the singular behaviour arises only when the configuration of the three final-state partons is such that we can experimentally identify only a 'two-jet event' and not a 'three-jet' one⁶.

Several schemes have been devised to regularize infrared divergences⁷. The one we have used for our example is the dimensional regularization scheme. Within this scheme IR divergences show up as poles in $\epsilon = 2 - D/2$. Notice that we have already used dimensional regularization to regularize the ultraviolet (UV) divergence, going from 4 to $D = 4 - 2\epsilon$ dimensions.

Having explained how IR divergences appear, we need to investigate the mechanism that leads to their cancellation. Essentially, this mechanism is explained by

⁵Or D -momentum in D dimensions.

⁶This is where the introduction of a *jet measure* is essential. In [5] one can find an insightful approach in this area.

⁷For a detailed account we refer the reader to basic QCD text books such as [3], [4] or [5].

the Bloch-Nordsieck theorem: “Use of degenerate states, which can be constructed by associating soft and collinear massless particles with the external final-state lines, leads to infrared-safe physical cross-sections and transition rates” ([25], [26]). The Bloch-Nordsieck theorem applies in the Higgs decay of our example, but breaks down in other QCD processes, where initial-state soft and collinear IR divergences must be taken into account as is suggested by the Kinoshita-Lee-Nauenberg theorem: “In a theory with massless fields, transition rates are free of the infrared (soft and collinear) divergence if the summation over the initial and final degenerate states is carried out” ([27], [28]).

2.3 One-Loop Singular Behaviour

We consider the QCD amplitude $|\mathcal{M}_m \rangle$, that has m external partons (quarks or gluons) with momenta $p_1 \dots p_m$ and an arbitrary number of color-free particles, such as the Z or the Higgs boson. The perturbative expansion of the amplitude $|\mathcal{M}_m \rangle^8$ in the \overline{MS} scheme can be written as:

$$|\mathcal{M} \rangle = \left(\frac{\alpha_s}{2\pi} \right)^\rho \left[|\mathcal{M}^{(0)} \rangle + \left(\frac{\alpha_s}{2\pi} \right) |\mathcal{M}^{(1)} \rangle + \left(\frac{\alpha_s}{2\pi} \right)^2 |\mathcal{M}^{(2)} \rangle + \mathcal{O}(\alpha_s^3) \right] \quad , \quad (2.40)$$

where ρ is a half integer ($\rho = 0, 1/2, 1, 3/2, \dots$), that depends on the process. We should note that all amplitudes in eq. (2.40) are renormalized. The sub-amplitude $|\mathcal{M}^{(1)} \rangle$ has singularities which within CDR are expressed as single and double poles in ϵ ($1/\epsilon$ and $1/\epsilon^2$). In [11, 12], Catani and Seymour proposed that these singularities can be separated from the finite part $|\mathcal{M}^{(1)fin} \rangle$ with the formula:

$$|\mathcal{M}^{(1)} \rangle = \mathbf{I}^{(1)}(\epsilon) |\mathcal{M}^{(0)} \rangle + |\mathcal{M}^{(1)fin} \rangle \quad . \quad (2.41)$$

In eq. (2.41) all one-loop singularities are absorbed in the universal factor $\mathbf{I}^{(1)}(\epsilon)$ which acts on the lowest-level amplitude $|\mathcal{M}^{(0)} \rangle$. Both $\mathbf{I}^{(1)}$ and $\mathbf{I}^{(2)}$, that we will introduce in the following section, have a finite part which is not uniquely defined. This creates an ambiguity in the definition of amplitude $|\mathcal{M}^{(1)fin} \rangle$. The general

⁸From now on we will drop index m from the amplitude.

structure of $\mathbf{I}^{(1)}(\epsilon)$ with respect to the color charges of the m partons is chosen to be:

$$\mathbf{I}^{(1)}(\epsilon) = \frac{1}{2} \frac{e^{-\epsilon\gamma}}{\Gamma(1-\epsilon)} \sum_i \frac{1}{\mathbf{T}_i^2} \mathcal{V}_i^{sing}(\epsilon) \sum_{j \neq i} \mathbf{T}_i \mathbf{T}_j \left(\frac{\mu^2 e^{-i\lambda_{ij}\pi}}{2p_i \cdot p_j} \right)^\epsilon, \quad (2.42)$$

with i, j running from 1 to m while $\lambda_{ij} = +1$ if i and j are both incoming or outgoing and $\lambda_{ij} = 0$ otherwise. Notice that all singularities are encapsulated in $\mathcal{V}_i^{sing}(\epsilon)$ as single and double ϵ poles:

$$\mathcal{V}_i^{sing}(\epsilon) = \mathbf{T}_i^2 \frac{1}{\epsilon^2} + \gamma_i \frac{1}{\epsilon}. \quad (2.43)$$

We can see that $\mathcal{V}_i^{sing}(\epsilon)$ depends only on the parton flavor. For quarks, antiquarks and gluons the coefficients \mathbf{T}_i^2 and γ_i are:

$$\begin{aligned} \mathbf{T}_q^2 = \mathbf{T}_{\bar{q}}^2 = C_F, \quad \mathbf{T}_g^2 = C_A \\ \gamma_q = \gamma_{\bar{q}} = \frac{3}{2} C_F, \quad \gamma_g = \frac{11}{6} C_A - \frac{2}{3} T_R N_f = \beta_0 \end{aligned} \quad (2.44)$$

Let us now apply the Catani formalism to the example of the Higgs decay to two gluons that we studied in the previous section. From eq. (2.42) one can trivially derive the color charge operator $\mathbf{I}^{(1)}(\epsilon)$, for $\mathcal{H} \rightarrow gg$:

$$\mathbf{I}_{\mathcal{H} \rightarrow gg}^{(1)}(\epsilon) = -\frac{e^{\epsilon\gamma}}{\Gamma(1-\epsilon)} \left(\frac{-\mu^2}{s_{12}} \right)^\epsilon \left[N \frac{1}{\epsilon^2} + \beta_0 \frac{1}{\epsilon} \right], \quad (2.45)$$

where $s_{12} = (p_1 + p_2)^2 = 2p_1 \cdot p_2$ is the Mandelstam variable. Here, p_i are the momenta of the external particles, i.e. the two gluons. From momentum conservation one gets: $s_{12} = M_{\mathcal{H}}^2$. If we use $\mathbf{I}_{\mathcal{H} \rightarrow gg}^{(1)}(\epsilon)$ in equation (2.41) we can derive the singular part of the interference of the tree-level with the one-loop amplitude:

$$\left\langle \mathcal{M}_{\mathcal{H} \rightarrow gg}^{(0)} \mid \mathcal{M}_{\mathcal{H} \rightarrow gg}^{(1) \text{ sing}} \right\rangle = \left\langle \mathcal{M}_{\mathcal{H} \rightarrow gg}^{(0)} \mid \mathbf{I}_{\mathcal{H} \rightarrow gg}^{(1)}(\epsilon) \mid \mathcal{M}_{\mathcal{H} \rightarrow gg}^{(0)} \right\rangle. \quad (2.46)$$

Subsequently one can easily derive the one-loop part of the decay $\mathcal{H} \rightarrow gg$ that contains all the infrared singularities at this order of α_s :

$$\Gamma_{\mathcal{H} \rightarrow gg}^{(1) \text{ sing}} = \Gamma_{\mathcal{H} \rightarrow gg}^{LO} \frac{\alpha_s}{2\pi} \left(\frac{\mu^2}{M_{\mathcal{H}}^2} \right)^\epsilon \left[N \frac{2}{\epsilon^2} + \frac{11N - 2N_f}{3} \frac{1}{\epsilon} \right]. \quad (2.47)$$

The above equation fully predicts⁹ the singularities of the decay rate of the Higgs boson to two gluons (with no radiation) at order α_s^3 , calculated in equation (2.36).

⁹After fixing the renormalization scale to $M_{\mathcal{H}}^2$.

2.4 Two-Loop Singular Behaviour

At two-loops the singular structure of the amplitudes becomes more complicated as the poles in ϵ become even deeper of order $\mathcal{O}(\epsilon^{-4})$. A formula analogous to eq. (2.41) was proposed by Catani for the two-loop case:

$$|\mathcal{M}^{(2)}\rangle = \mathbf{I}^{(1)}(\epsilon)|\mathcal{M}^{(1)}\rangle + \mathbf{I}^{(2)}(\epsilon)|\mathcal{M}^{(0)}\rangle + |\mathcal{M}^{(2)fin}\rangle, \quad (2.48)$$

where $\mathcal{M}^{(2)fin}$ is finite as $\epsilon \rightarrow 0$. In contrast to the one-loop case, here the singularities lie in two distinct terms. The first is in the ‘product’ of the color charge operator $\mathbf{I}^{(1)}(\epsilon)$, which carries $\mathcal{O}(\epsilon^{-2})$ poles, with the one-loop amplitude, which also carries $\mathcal{O}(\epsilon^{-2})$ poles, giving poles with a maximum degree of ϵ^{-4} . The second contribution emerges as the result of acting on the lowest-order amplitude with a new charge operator $\mathbf{I}^{(2)}(\epsilon)$, which contains poles of order up to $\mathcal{O}(\epsilon^{-4})$ and is given by:

$$\begin{aligned} \mathbf{I}^{(2)}(\epsilon) = & -\frac{1}{2} \mathbf{I}^{(1)}(\epsilon) \left(\mathbf{I}^{(1)}(\epsilon) + \frac{2\beta_0}{\epsilon} \right) \\ & + e^{-\epsilon\gamma} \frac{\Gamma(1-2\epsilon)}{\Gamma(1-\epsilon)} \left(\frac{\beta_0}{\epsilon} + K \right) \mathbf{I}^{(1)}(2\epsilon) \\ & + \mathbf{H}^{(2)}, \end{aligned} \quad (2.49)$$

with

$$K = \left(\frac{67}{18} - \frac{\pi^2}{6} \right) C_A - \frac{10}{9} T_R N_f. \quad (2.50)$$

The first two lines of eq. (2.49) contain all dependence on poles of order $1/\epsilon^4$, $1/\epsilon^3$ and $1/\epsilon^2$ as well as part of the $1/\epsilon$ poles. The term in the third line contains only single poles:

$$\mathbf{H}^{(2)} = \mathcal{O}(\epsilon^{-1}). \quad (2.51)$$

$\mathbf{H}^{(2)}$, that contains the remaining single pole dependence, is not a universal factor. It is process and renormalization scheme dependent and comprises of constants like C_A , C_F , ζ_3 and π^2 . The origins of the above formulae, that were first proposed in [12], were presented in [29]. It was shown that the exponentiation of single and double poles at each order in perturbation theory, can be derived from the factorization

properties of hard-scattering amplitudes. This allows one to assemble these poles in terms of universal functions which are associated with incoming and outgoing partons, leading to the prediction of the complete pole structure for multi-loop amplitudes.

To conclude, eq. (2.48), predicts the singular structure of the two-loop amplitude by providing all the 4th, 3rd and 2nd order ϵ -poles. In order to get the full structure of the $1/\epsilon$ poles together with the finite part, we need to calculate explicitly the Feynman diagrams that contribute to the two-loop amplitude. In chapters 7 and 8 we provide the factor $\mathbf{H}^{(2)}$ and the finite piece for the processes $\gamma^* \rightarrow q\bar{q}g$ and $\mathcal{H} \rightarrow ggg$ respectively.

2.5 Beyond NLO

In the end of section 2.2.5 we showed that for the $\mathcal{H} \rightarrow gg$ decay, the NLO and NNLO terms added significant corrections to the LO decay width. In this section we will study the reasons calling for higher order calculations if we want to increase our accuracy in the determination of observables and theory constants such as the strong coupling α_s . It was shown in section 1.3 that an observable can be written as a perturbative expansion depending on the renormalization scale μ^2 :

$$\Gamma = \Gamma(\alpha_{s(\mu^2)}, s/\mu^2) = r_1(s/\mu^2)\alpha_{s(\mu^2)} + r_2(s/\mu^2)\alpha_{s(\mu^2)}^2 + r_3(s/\mu^2)\alpha_{s(\mu^2)}^3 + \dots ,$$

or more generally:

$$\Gamma \sim \sum_{i=1}^{\infty} r_i \alpha_{s(\mu^2)}^i . \quad (2.52)$$

However, whenever we want to make a theoretical prediction, we have to truncate the series, keeping only the terms which are lower than a certain order N ,

$$\Gamma \sim \sum_{i=1}^N r_i \alpha_{s(\mu^2)}^i + \overbrace{\sum_{i=N+1}^{\infty} r_i \alpha_{s(\mu^2)}^i}^{\text{dropped}} , \quad (2.53)$$

which, substituted in eq. (1.22) leaves a residual dependence on μ of order $\mathcal{O}\left(\alpha_s^{N+1}(\mu^2)\right)$:

$$\frac{d}{d\ln(\mu^2)} \sum_{i=1}^N r_i \alpha_s^i(\mu^2) = \mathcal{O}\left(\alpha_s^{N+1}(\mu^2)\right). \quad (2.54)$$

The number of terms we can include is restricted by the increasing difficulty at higher orders. Omission of those terms induces a systematic error in our calculation, which results in uncertainty in the determination of QCD parameters such as α_s . Thus, the higher the order, the smaller the omitted part and the error.

In addition the truncation of the series makes the theoretical predictions more sensitive to the dependence on the renormalization scale μ . It turns out that this sensitivity reduces as we go to higher orders in perturbation series. In order to see how this works we will consider the rate for the single jet production in $p\bar{p}$ collisions. The NNLO perturbative expansion for a system with energy S is:

$$\frac{d\sigma}{dS} = \alpha_{s(S)}^2 A + \alpha_{s(S)}^3 B + \alpha_{s(S)}^4 C, \quad (2.55)$$

which, using the renormalization group equation at NNLO:

$$\alpha_{s(S)} = \alpha_{s(\mu^2)} + \beta_0 L_S \alpha_{s(\mu^2)}^2 + (\beta_1 L_S + \beta_0^2 (L_S)^2) \alpha_{s(\mu^2)}^3, \quad (2.56)$$

becomes:

$$\begin{aligned} \frac{d\sigma}{dS} &= \alpha_{s(\mu^2)}^2 A \\ &+ \alpha_{s(\mu^2)}^3 (B + 2\beta_0 L_S A) \\ &+ \alpha_{s(\mu^2)}^4 (C + 3\beta_0 L_S B + (3\beta_0^2 L_S^2 + 2\beta_1 L_S) A), \end{aligned} \quad (2.57)$$

with $L_S = \ln(\mu^2/S)$. Notice that if one differentiates eq. (2.57) with respect to $\ln(\mu^2)$ and substitutes the renormalization group equation (1.18), the result is of order $\mathcal{O}\left(\alpha_{s(\mu^2)}^5\right)$, in accordance with eq. (2.54). The coefficients A and B are the known LO and NLO components while the NNLO coefficient C has not been calculated yet. In figure 2.7 the renormalization scale dependence (within a factor of two of the jet energy S) of the LO, NLO and NNLO terms is given [30, 31], for jets with transverse energy $S = 100$ GeV. Despite the fact that the contribution from

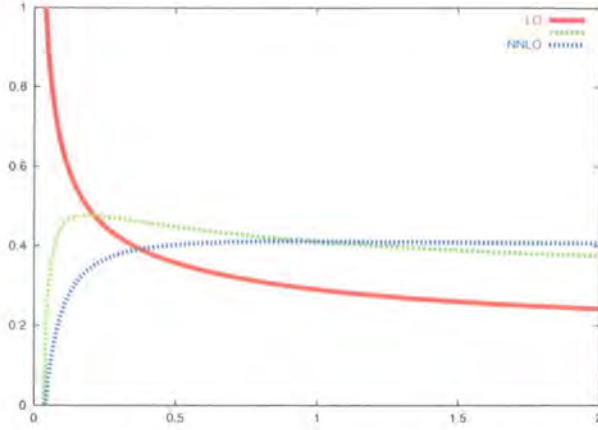


Figure 2.7: Single jet inclusive distribution at $S = 100$ GeV and $0.1 < |\eta| < 0.7$ at $\sqrt{s} = 1800$ GeV at LO , NLO and NNLO . The same pdf's and α_s are used throughout.

the unknown coefficient C has not been taken into account, it is evident that the renormalization scale dependence is significantly reduced as we include higher terms in the perturbative expansion.¹⁰

The above example shows that the NLO accuracy at which most theoretical predictions are performed today, despite the generally good agreement with data, entails a significant dependence on the renormalization scale μ . Future colliders (LHC) with high precision data will lead to experimental errors smaller than the theoretical ones, calling for improvement in theoretical predictions. This could be achieved if NNLO corrections were included in calculations. A set of motivation factors for NNLO calculations, in addition to the ones mentioned in this section, can be found in [30,31].

¹⁰The uncertainty reduces from 20% at LO to 9% at NLO and about 1% at NNLO.

Chapter 3

Amplitudes For QCD Processes

3.1 Introduction

In previous chapters we identified an imperative requirement for estimating the size of NNLO corrections affecting physical observables such as cross-sections or decay widths. A primary task toward the achievement of this goal is the calculation of two-loop helicity amplitudes and matrix elements. The main objective of this PhD has been the calculation of NNLO matrix elements (ME) and helicity amplitudes (HA 's) for physical processes which involve four external particles, one of which is off-shell. The cornerstone of this calculation has been the cumbersome task of evaluating two-loop integrals. In section 3.2 we outline step-by-step the scheme we applied in order to accomplish this project, from using QGRAF [32] to generate all possible diagrams, to calculating the squared ME or HA 's of a process. Due to the significance of the two-loop integrals, a separate section (3.3) is used to present the stages involved in their analytic evaluation. A diagrammatic illustration of all the basic steps can be found in figures 3.1 and 3.2.

**GENERAL ALGORITHM FOR:
MATRIX ELEMENTS & HELICITY AMPLITUDES**

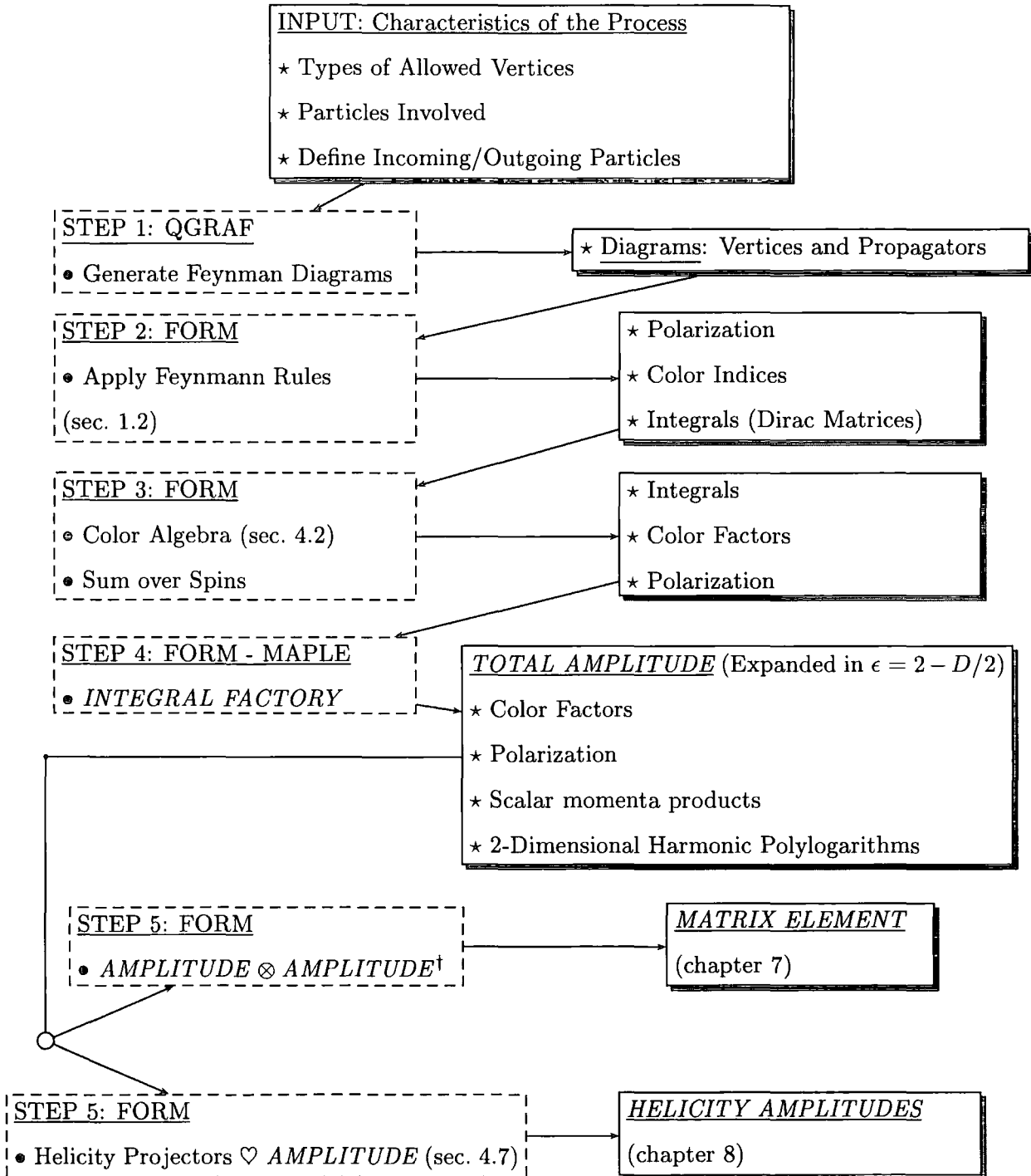


Figure 3.1: The dashed boxes on the left represent the program used to apply the bullet-point procedures and the shadowed boxes on the right represent the output of the previous dashed box process and the input to the following one.

INTEGRAL FACTORY

INPUT= Integrals of the type:

$$\mathcal{J} = \int \frac{d^D k}{i\pi^{d/2}} \int \frac{d^D l}{i\pi^{d/2}} \frac{(k)^\nu (k)^\mu (l)^\sigma}{k^2 (k+p_1+p_2+p_3)^2 l^2 (l+p_1+p_2+p_3)^2 (k-l)^2}$$

STEP 1: FORM

- Translate to Auxiliary Integral Representation (sec. 4.3)

★ Integrals written in the form:

$$\mathcal{J}(D, \{1, 1, 1, -4, 1, 0, 1, 1, 1\}, s_{12}, s_{23}, s_{123})$$

STEP 2: MAPLE - FORM

- Use Laporta Algorithm (sec. 5.2)
- Master Integrals (sec. 4.5)

★ Integrals in terms of MI's:

$$\begin{aligned} \mathcal{J}(D, \{1, 1, \dots, 1\}, s_{12}, s_{23}, s_{123}) = \\ a \cdot \text{Pbox}_1(s_{12}, s_{23}, s_{123}) + \dots \\ + f \cdot \text{Dart}_2(s_{12}, s_{123}) + g \cdot \text{Suns}(s_{123}) \end{aligned}$$

STEP 3: MAPLE - FORM

- Derive-Solve Differential Equations for the Master Integrals (chapter. 6)
- expansion of MI's in ϵ , in terms of 2-D Harmonic Polylogarithms (sec.4.6):

$$\begin{aligned} \text{Dart}_2(s_{12}, s_{123}) = \frac{1}{\epsilon^4} a + \dots + \\ \frac{1}{\epsilon^2} b \text{H}(1, 0; X) + \dots + \epsilon^2 c \text{H}(1, 1, 1, 0; X) + \dots \end{aligned}$$

★ Integrals, expanded in ϵ , in terms of 2-D HPL:

$$\begin{aligned} \mathcal{J}(D, \{1, 1, \dots, 1\}, s_{12}, s_{23}, s_{123}) = \\ \frac{1}{\epsilon^4} a + \dots + \frac{1}{\epsilon^2} b \text{H}(1, 0; X) + \dots + \\ \epsilon^2 c \text{H}(1, 1, 1, 0; X) + \dots \end{aligned}$$

Figure 3.2: Integral Factory.

3.2 Basic Steps for Helicity Amplitudes and Matrix Element Calculations

Step 1 \diamond QGRAF: Generate the Feynman Diagrams

The first step in a ME or HA calculation is the generation of the Feynman diagrams contributing to the process. In processes involving a large number of Feynman diagrams this can be a painstaking task. For this purpose we used QGRAF [32]. QGRAF is a computer program for automatic generation of symbolic descriptions of Feynman diagrams in quantum field theories. It does not perform any kind of field theoretic calculation. The user mainly provides information about the external particles, the propagators, the number of loops and the types of vertices, and sets features such as the desired output style. This determines the output which consists of a list of diagrams, labeled in a combinatorial style, accompanied by their symmetry factor.

Step 2-3 \diamond FORM: Feynman Rules - Color Algebra

After completion of Step 1 we are left with a set of diagrams written in terms of propagators and vertices. First, we apply the Feynman rules for the Lagrangian of the process under consideration (see for example sections 1.2 and 1.4.1). Subsequently, color algebra (sec. 4.2) is performed to sum over the color factors. This part is totally implemented in FORM [34], a program for symbolic manipulation, specialized to handle very large algebraic expressions in an efficient way.

Step 4 \diamond MAPLE [33] - FORM: Integral Factory

The integrals that descended from Step 3 are calculated in terms two dimensional harmonic polylogarithms (2DHPL). The process of calculating two-loop integrals is outlined in the following section. Finally we derive an expression for the amplitude expanded in $\epsilon = 2 - D/2$ and written in terms of 2DHPL's, color factors, scalar momenta products (Mandelstam variables and squared masses) and polarization factors.

Step 5 \diamond FORM: Matrix Elements or Helicity Amplitudes

At this stage one has two options, depending on whether we are interested in cal-

culating a matrix element or helicity amplitudes. In the first case the two-loop (one-loop) amplitude is contracted with the tree-level (one-loop) amplitude and then summation over the colors and spins is performed. The gluon polarizations are summed over using an axial gauge to ensure that the polarization states are physical:

$$\sum_{spins} \epsilon_i^\mu(n_i) (\epsilon_i^\nu(p_i))^* = -g^{\mu\nu} + \frac{n_i^\mu p_i^\nu + n_i^\nu p_i^\mu}{n_i \cdot p_i} \quad (3.1)$$

Our final result is expressed as a series in $\epsilon = 2 - D/2$ poles, whose coefficients contain the number of colors and quark flavors as well as functions (2DHPL's) of the system's scales.

If helicity amplitudes are required, then one can use a helicity projectors' method, described in detail in section 4.7. Acting on the general tensorial form of the amplitude with a set of projectors it is possible to derive the coefficients of the tensor structures that comprise HA's. The result is an ϵ expansion in terms of color factors and functions (2DHPL) of the scales appearing in the process.

3.3 The Integral Factory

After application of the Feynman rules in the QGRAF output, two-loop integrals of the form

$$\mathcal{J} = \int \frac{d^D k}{i\pi^{d/2}} \int \frac{d^D l}{i\pi^{d/2}} \frac{(k)^\nu (k)^\mu (l)^\sigma}{k^2 (k + p_1 + p_2 + p_3)^2 l^2 (l + p_1 + p_2 + p_3)^2 (k - l)^2},$$

make their appearance. These integrals are translated to the auxiliary integral representation (presented in section 4.3), which allows them to be written in a more compact notation, for example:

$$\begin{aligned} \mathcal{J}(D, \{1, 1, 1, -4, 1, 0, 1, 1, 1\}, s_{12}, s_{23}, s_{123}) & \quad \text{or} \\ \mathcal{J}(D, \{1, 1, 1, -1, 1, 0, 1, 1, 2\}, s_{12}, s_{23}, s_{123}) & \quad . \end{aligned}$$

This notation is preferred because it is more compatible with programs of symbolic manipulation like FORM and MAPLE [33]. A system of relations between all the

integrals of the process is derived and solved (see chapter 5), allowing them to be written in terms of a basis set of few ‘master’ integrals (MI) with nice names like:

$$\begin{aligned} \mathcal{J}(D, \{0, 0, 0, 1, 1, 0, 0, 0, 1\}, s_{12}, s_{23}, s_{123}) &= \text{Suns}(s_{123}) , \\ \mathcal{J}(D, \{1, 0, 1, 0, 0, 0, 0, 1, 1\}, s_{12}, s_{23}, s_{123}) &= \text{Dart}_2(s_{12}, s_{123}) , \\ \mathcal{J}(D, \{1, 1, 1, -4, 1, 0, 1, 1, 1\}, s_{12}, s_{23}, s_{123}) &= a \text{Pbox}_1(s_{12}, s_{23}, s_{123}) + \dots \\ &\quad + f \text{Dart}_2(s_{12}, s_{123}) + g \text{Suns}(s_{123}) . \end{aligned}$$

The final but not trivial task is the calculation of the master integrals. Of the several methods that have been employed toward this direction the one that achieved the most, calculating the most difficult integrals, was the differential equations method (by Gehrmann and Remiddi [42, 43]) presented in chapter 6. Differential equations on the external scales for the master integrals were derived and solved, enabling us to write the MI and consequently all possible integrals, as expansions in ϵ with coefficients functions (2DHPL) of the system’s scalars. For example:

$$\text{Dart}_2(s_{12}, s_{123}) = \frac{1}{\epsilon^4} a + \dots + \frac{1}{\epsilon^2} b \text{H}(1, 0; X) + \dots + \epsilon^2 c \text{H}(1, 1, 1, 0; X) + \dots ,$$

where the factors a , b , c , \dots and X depend on s_{12} and s_{123} .

In the rest of this thesis we will describe in detail the basic steps we have outlined in this short chapter. In figures 3.1 and 3.2, apart from the basic steps involved in ME and HA calculations, we have also illustrated the specific section where each stage of the calculation is treated.

Chapter 4

Basic Tools For Two-Loop Integrals

4.1 Introduction

In the previous chapter we illustrated the basic steps involved in a helicity amplitude or matrix element two-loop calculation. In each step we face challenges that need to overcome. However, we have some really powerful tools in our disposal, that have been developed during the last few years. First of all there is the color algebra which is used to deal with the color factors appearing in Feynman rules. Next there are the auxiliary integrals, a formalism that allows one to write complicated tensor integrals in a compact computer-friendly notation. The third tool, the integration by parts method, is probably the most effective technique for the simplification of tensor integrals to a basic set of irreducible Master Integrals (tool four). The calculation of those Master Integrals is not a trivial task though. A usual way of expressing them is through expansions in $\epsilon = 2 - D/2$ in terms of functions of the system's scales. The family of functions used in the calculations throughout this PhD are the Harmonic Polylogarithms (tool five). The sixth and final tool is a method for extracting helicity amplitudes from the total amplitude by acting with a set of projectors.

4.2 Tool One: Color Algebra

4.2.1 Color in Feynman Diagrams

In chapter 2 we calculated squared tree-level amplitudes involving diagrams like the ones in fig.(2.2.2), (2.2.4) or (2.2.4). We also calculated the interference of tree-level with one-loop amplitudes which contained diagrams like the one in fig.(2.2.3). As one can see in the QCD Feynman rules (section 1.2) as well as in the equivalent rules for the effective Lagrangian (section 1.4.1), all the above diagrams include SU(N) color factors. Isolating these factors for each diagram we get:

(a) For the gluon, quark and ghost propagators:

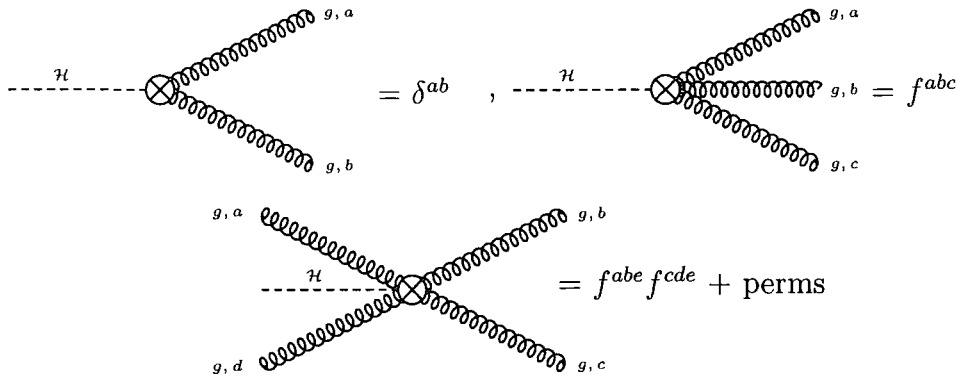
$$g \overset{a}{\text{-----}} \overset{b}{\text{-----}} = \delta^{ab} \quad , \quad \overset{i}{\text{-----}} \overset{j}{\text{-----}} = \delta_{ij} \quad , \quad \overset{a}{\text{-----}} \overset{b}{\text{-----}} = \delta^{ab} .$$

(b) For the gluon-gluon, gluon-quark and gluon-ghost vertices:

The diagrams show the color factors for various vertices:

- Gluon-gluon vertex:** A vertex with three incoming gluon lines (curly) labeled g, c , g, a , and g, b . The color factor is f^{abc} .
- Gluon-gluon vertex (antisymmetric):** A vertex with three incoming gluon lines (curly) labeled g, d , g, a , and g, b . The color factor is $f^{abe} f^{cde} + \text{perms}$.
- Gluon-quark vertex:** A vertex with one incoming gluon line (curly) labeled g, a and two outgoing quark lines (straight) labeled i and j . The color factor is T_{ij}^a .
- Gluon-ghost vertex:** A vertex with one incoming gluon line (curly) labeled g, a and two outgoing ghost lines (dashed) labeled c and b . The color factor is f^{abc} .

(c) For the Higgs-gluon vertices:

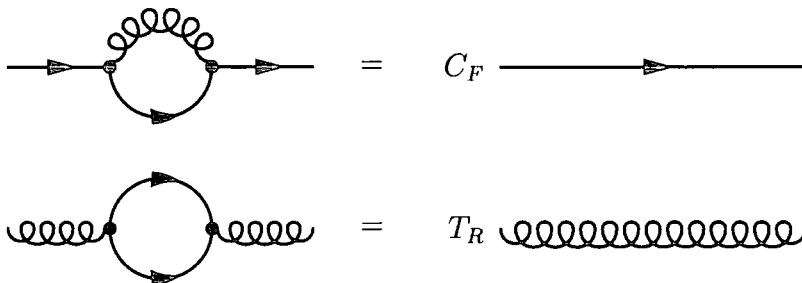


As we have seen in section 1.1, T_{ij}^a are the generators of the fundamental representation of the SU(N) group and f^{abc} are the generators of the adjoint representation. In all cases the color indices a, b, c, d and e run from $1 \dots N^2 - 1$, which is the total number of different gluon colors and indices i, j run from $1 \dots N$ which is the total number of different quark colors.

4.2.2 Identities and Rules in Color Algebra

There are a few rules and identities that can help us reduce the amount of color algebra involved in the calculation of a squared matrix element.

(a) One very useful concept is that of the Casimir color charges¹ of SU(N). They are defined as the products of generators ($T \cdot T$ or $f \cdot f$), where only one index of each generator is free and the rest are fixed. Diagrammatically the Casimir operators for the fundamental representation can be given as:



¹They are called charges in analogy with the electromagnetic charge.

while for the adjoint representation we have:

$$\text{Gluon loop with two external lines} = C_A \text{Gluon line}$$

with

$$C_F = \frac{N^2 - 1}{2N} ,$$

$$C_A = N ,$$

$$T_R = \frac{1}{2} .$$

(b) A most valuable tool in color algebra is Fierz identity [35], which gives the most general product for the fundamental representation:

$$\sum_a T_{ij}^a T_{kl}^a = T_R \left(\delta_{il} \delta_{jk} - \frac{1}{N} \delta_{ij} \delta_{kl} \right) ,$$

$$\text{Diagrammatic Fierz identity} = T_R \left(\text{Horizontal exchange} - \frac{1}{N} \text{Vertical exchange} \right) . \quad (4.1)$$

(c) In any Lie Algebra one can apply the Jacobi identity in the adjoint representation, $f^{ade} f^{bcd} + f^{bde} f^{cad} + f^{cde} f^{abd} = 0$, and the commutation relation in the fundamental representation, $f^{abc} T_{ij}^a = T_{ik}^b T_{kj}^c - T_{ik}^c T_{kj}^b$, which respectively take the graphic forms:

$$\text{Diagrammatic Jacobi identity} = \text{Diagrammatic commutation relation} \quad (4.2)$$

(d) Finally there are relationships when we sum over the number of colors:

$$\begin{aligned}
\delta_{ij}\delta_{ji} &= \delta_{ii} = N , \\
\delta^{ab}\delta^{ba} &= \delta^{aa} = N^2 - 1 , \\
T_{ii}^a &= \text{tr}[T^a] = 0 , \\
f^{abb} &= 0 .
\end{aligned}
\tag{4.3}$$

The identities presented in this subsection are sufficient in order to simplify all Color Algebra.

4.3 Tool Two: The Auxiliary Integrals

All possible planar and non-planar, scalar and tensor, two-loop integrals that appear in the physical processes, where one external particle is off-shell and three are on-shell, can be written in terms of only three auxiliary integrals². The auxiliary planar ($2\mathcal{D}$) and non-planar ($3\mathcal{D}$) integrals in D dimensions³ are (figure 4.1):

$$\begin{aligned}
\mathcal{J}_{2\mathcal{D}}(D, \nu_{\{1,2,3,4,5,6,7,8,9\}}, s_{12}, s_{23}, s_{123}) &= \\
&\int \frac{d^D k}{i\pi^{d/2}} \int \frac{d^D l}{i\pi^{d/2}} \frac{1}{A_1^{\nu_1} A_2^{\nu_2} A_3^{\nu_3} A_4^{\nu_4} A_5^{\nu_5} A_6^{\nu_6} A_7^{\nu_7} A_8^{\nu_8} A_9^{\nu_9}}
\end{aligned}
\tag{4.4}$$

$$\begin{aligned}
\mathcal{J}_{3\mathcal{D}_{out}}(D, \nu_{\{1,2,3,4,5,6,11,8,9\}}, s_{12}, s_{23}, s_{123}) &= \\
&\int \frac{d^D k}{i\pi^{d/2}} \int \frac{d^D l}{i\pi^{d/2}} \frac{1}{A_1^{\nu_1} A_2^{\nu_2} A_3^{\nu_3} A_4^{\nu_4} A_5^{\nu_5} A_6^{\nu_6} A_{11}^{\nu_{11}} A_8^{\nu_8} A_9^{\nu_9}}
\end{aligned}
\tag{4.5}$$

²In the case of all four external particles being on-shell, there are only two auxiliary integrals, since the two non-planar ($3\mathcal{D}$) integrals are related by momentum relabeling.

³Note: Do not confuse the dimension of the integrals, which is D for all three auxiliary integrals, with the indices $2\mathcal{D}$ and $3\mathcal{D}$ that appear in their names. The latter are used in order to visualize the difference between planar and non-planar diagrams.

$$\mathcal{J}_{3\mathcal{D}_{in}}(D, \nu_{\{1,2,3,10,5,6,7,8,9\}}, s_{12}, s_{23}, s_{123}) = \int \frac{d^D k}{i\pi^{d/2}} \int \frac{d^D l}{i\pi^{d/2}} \frac{1}{A_1^{\nu_1} A_2^{\nu_2} A_3^{\nu_3} A_{10}^{\nu_{10}} A_5^{\nu_5} A_6^{\nu_6} A_7^{\nu_7} A_8^{\nu_8} A_9^{\nu_9}} \quad (4.6)$$

Where:

$$\begin{aligned} A_1 &= k^2 & A_5 &= l^2 & A_9 &= (k-l)^2 \\ A_2 &= (k+p_1)^2 & A_6 &= (l+p_1)^2 & A_{10} &= (k-l-p_1-p_2-p_3)^2 \\ A_3 &= (k+p_1+p_2)^2 & A_7 &= (l+p_1+p_2)^2 & A_{11} &= (k-l+p_2)^2 \\ A_4 &= (k+p_1+p_2+p_3)^2 & A_8 &= (l+p_1+p_2+p_3)^2 & & \end{aligned} \quad (4.7)$$

For the on-shell case considered here $p_1^2 = p_2^2 = p_3^2 = 0$, $(p_i + p_j)^2 = s_{ij}$ and $(p_1 + p_2 + p_3)^2 = s_{123}$. Note that both non-planar auxiliary diagrams ($\mathcal{J}_{3\mathcal{D}_{out}}$ and $\mathcal{J}_{3\mathcal{D}_{in}}$) have eight propagators in common with the planar auxiliary integral ($\mathcal{J}_{2\mathcal{D}}$). The only difference is the interchange $A_7 \rightarrow A_{11}$ in order to go from $\mathcal{J}_{2\mathcal{D}}$ to $\mathcal{J}_{3\mathcal{D}_{out}}$ and $A_4 \rightarrow A_{10}$ in order to go from $\mathcal{J}_{2\mathcal{D}}$ to $\mathcal{J}_{3\mathcal{D}_{in}}$.

It is very important to stress here that the three auxiliary integrals *do not* correspond to real diagrams. Real two-loop diagrams with three external independent momenta can have only up to seven propagators. As we can see in equations (4.4), (4.5), (4.6) and (4.7), each auxiliary integral has nine linearly independent propagators. This number of propagators is the minimum we need in order to be able to express the nine scalar products⁴ that can appear in the numerators of the integrals, in terms of a predetermined set of propagators. This method turns out to be a lot more convenient for the representation of tensor integrals. For example, the planar

⁴For diagrams with two loop momenta (k and l) and three independent external momenta (p_1 , p_2 and p_3), there are nine combinations of scalar products: $k \cdot k$, $k \cdot p_1$, $k \cdot p_2$, $k \cdot p_3$, $l \cdot l$, $l \cdot p_1$, $l \cdot p_2$, $l \cdot p_3$ and $k \cdot l$

tensor integral:

$$\int \frac{d^D k}{i\pi^{d/2}} \int \frac{d^D l}{i\pi^{d/2}} \frac{l \cdot p_2}{[(k)^2]^2 [(k+p_1)^2]^2 [(l+p_1+p_2)^2]^1 [(l+p_1+p_2+p_3)^2]^3 [(k-l)^2]^2} , \quad (4.8)$$

can be written as:

$$\int \frac{d^D k}{i\pi^{d/2}} \int \frac{d^D l}{i\pi^{d/2}} \frac{(l+p_1+p_2)^2 - (l+p_1)^2 - 2p_1 \cdot p_2}{[(k)^2]^2 [(k+p_1)^2]^2 [(l+p_1+p_2)^2]^1 [(l+p_1+p_2+p_3)^2]^3 [(k-l)^2]^2} . \quad (4.9)$$

Substituting eq.(4.7) and expanding we get:

$$\int \frac{d^D k}{i\pi^{d/2}} \int \frac{d^D l}{i\pi^{d/2}} \left[\frac{A_7}{A_1^2 A_2^2 A_7^1 A_8^3 A_9^2} - \frac{A_6}{A_1^2 A_2^2 A_7^1 A_8^3 A_9^2} - \frac{s_{12}}{A_1^2 A_2^2 A_7^1 A_8^3 A_9^2} \right] . \quad (4.10)$$

Using the definition of eq.(4.4) we can finally write the tensor integral (eq. 4.8) as:

$$\begin{aligned} & \mathcal{J}_{2D}(D, \{2, 2, 0, 0, 0, 0, 0, 3, 2\}, s_{12}, s_{23}, s_{123}) - \\ & \mathcal{J}_{2D}(D, \{2, 2, 0, 0, 0, -1, 1, 3, 2\}, s_{12}, s_{23}, s_{123}) - \\ & s_{12} \times \mathcal{J}_{2D}(D, \{2, 2, 0, 0, 0, 0, 0, 1, 3, 2\}, s_{12}, s_{23}, s_{123}) . \end{aligned} \quad (4.11)$$

This notation is a lot more convenient for our purposes, since it makes our results more compact and it is easier to manipulate in computer programmes.

4.4 Tool Three: IBP Identities

4.4.1 The Integration By Parts (IBP) Method

The IBP method [8, 36, 37] is based on the following identity for an m -loop n -propagator integral :

$$\int \frac{d^D k_1}{i\pi^{d/2}} \cdots \int \frac{d^D k_m}{i\pi^{d/2}} \frac{\partial}{\partial k_i^\mu} \frac{u^\mu}{A_1^{\nu_1} \cdots A_n^{\nu_n}} = 0 , \quad (4.12)$$

where $i = 1 \dots m$ and u^μ is any linear combination of the loop and the external momenta. This identity is valid because we can impose that the integral of the total

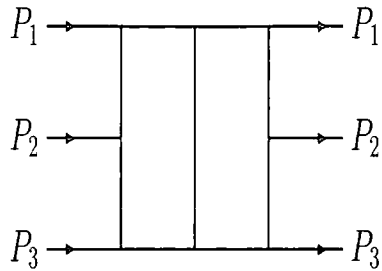
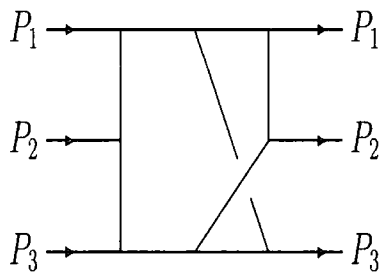
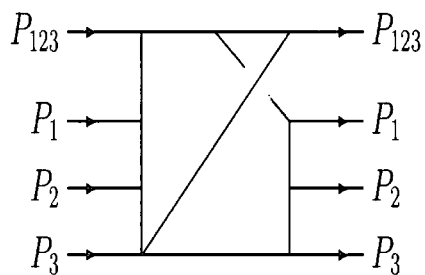
$2\mathcal{D}$ Auxiliary $3\mathcal{D}_{out}$ Auxiliary $3\mathcal{D}_{in}$ Auxiliary

Figure 4.1: The planar ($2\mathcal{D}$) and two non-planar ($3\mathcal{D}$) auxiliary diagrams. All nine possible dot-products involving the loop momenta and the external particle momenta are mapped onto the nine propagators.

derivative vanishes (there is no contribution coming from the surface). This can be considered as a consequence of translational invariance of dimensionally regularized integrals in momentum space.

To take a simple example consider the following two-loop scalar diagram:



which corresponds to the integral:

$$\mathcal{J} = \int \frac{d^D k}{i\pi^{d/2}} \int \frac{d^D l}{i\pi^{d/2}} \frac{1}{A_1 A_4 A_5 A_8 A_9}, \quad (4.13)$$

where the A_i 's are those defined in eq. (4.7) and the corresponding ν_i 's are taken to be equal to one.

Applying the identity :

$$\mathcal{J} = \int \frac{d^D k}{i\pi^{d/2}} \int \frac{d^D l}{i\pi^{d/2}} \frac{\partial}{\partial k^\mu} \frac{(k-l)^\mu}{k^2(k+p_1+p_2+p_3)^2 l^2 (l+p_1+p_2+p_3)^2 (k-l)^2} = 0, \quad (4.14)$$

and the identity:

$$2(a+b)(a+c) = (a+b)^2 + (a+c)^2 - (b-c)^2, \quad (4.15)$$

we get the equation:

$$\begin{aligned} (D-4) \int \frac{d^D k}{i\pi^{d/2}} \int \frac{d^D l}{i\pi^{d/2}} \frac{1}{k^2(k+p_1+p_2+p_3)^2 l^2 (l+p_1+p_2+p_3)^2 (k-l)^2} = \\ + \int \frac{d^D k}{i\pi^{d/2}} \int \frac{d^D l}{i\pi^{d/2}} \frac{1}{(k^2)^2 (k+p_1+p_2+p_3)^2 l^2 (l+p_1+p_2+p_3)^2} \\ - \int \frac{d^D k}{i\pi^{d/2}} \int \frac{d^D l}{i\pi^{d/2}} \frac{1}{(k^2)^2 (k+p_1+p_2+p_3)^2 (l+p_1+p_2+p_3)^2 (k-l)^2} \\ + \int \frac{d^D k}{i\pi^{d/2}} \int \frac{d^D l}{i\pi^{d/2}} \frac{1}{k^2 ((k+p_1+p_2+p_3)^2)^2 l^2 (l+p_1+p_2+p_3)^2} \\ - \int \frac{d^D k}{i\pi^{d/2}} \int \frac{d^D l}{i\pi^{d/2}} \frac{1}{k^2 ((k+p_1+p_2+p_3)^2)^2 l^2 (k-l)^2}. \end{aligned} \quad (4.16)$$

The integrals on the right hand side have come from cancellations of squared combinations of momenta in the numerator and the denominator. Every such cancellation is equivalent to the shrinking (pinching) of the corresponding line to a point. This

can easily be seen in the pictorial form of the above equation :

$$\begin{aligned}
 (D - 4) \rightarrow \text{circle with vertical line} &= + \text{circle with vertical line and top dot} - \text{circle with vertical line and top cross} \\
 &+ \text{circle with vertical line and bottom dot} - \text{circle with vertical line and bottom cross}
 \end{aligned}
 \tag{4.17}$$

A cross on the line represents a pinching, while a dot an additional power of the relevant propagator in the denominator, i.e. $\nu_i \rightarrow \nu_i + 1$. Therefore eq. (4.17) becomes:

$$\begin{aligned}
 (D - 4) \rightarrow \text{circle with vertical line} &= + \text{two circles with top dot} - \text{circle with top dot and self-energy} \\
 &+ \text{two circles with bottom dot} - \text{circle with bottom dot and self-energy}
 \end{aligned}
 \tag{4.18}$$

In the general case the IBP gives integrals with raised and lowered powers of the propagators. This will be represented with the shorthand notation \mathbf{i}^+ , for raising and \mathbf{i}^- , for lowering propagator \mathbf{i} :

$$\nu_i \mathbf{i}^+ \mathcal{J}(D, \dots, \nu_i, \dots) = \nu_i \mathcal{J}(D, \dots, \nu_i + 1, \dots) , \tag{4.19}$$

$$\mathbf{i}^- \mathcal{J}(D, \dots, \nu_i, \dots) = \mathcal{J}(D, \dots, \nu_i - 1, \dots) . \tag{4.20}$$

Each raising operator is always accompanied by a factor of ν_i so that it is impossible to raise the power of the propagator if it is not already present, i.e $\nu_i \neq 0$. In this notation, our example equation for the propagators defined in eq. (4.12) becomes:

$$(D - 4)\mathcal{J} = +\mathbf{1}^+\mathbf{9}^- \mathcal{J} - \mathbf{1}^+\mathbf{5}^- \mathcal{J} + \mathbf{4}^+\mathbf{9}^- \mathcal{J} - \mathbf{4}^+\mathbf{8}^- \mathcal{J} . \tag{4.21}$$

4.4.2 IBP Identities For The Auxiliary Integrals

Applying the IBP method to the planar auxiliary integral $\mathcal{J}_{2\mathcal{D}}$ (eq. 4.4) we get the following ten identities:

$$\begin{aligned} s_{12}\nu_1\mathbf{1}^+\mathcal{J}_{2\mathcal{D}} &= -(D - \nu_1 - \nu_2 - 2\nu_3 - \nu_4 - \nu_9)\mathcal{J}_{2\mathcal{D}} \\ &+ ((\nu_1\mathbf{1}^+ + \nu_2\mathbf{2}^+ + \nu_4\mathbf{4}^+)\mathbf{3}^- + \nu_9\mathbf{9}^+(\mathbf{3}^- - \mathbf{7}^-))\mathcal{J}_{2\mathcal{D}} \end{aligned} \quad (4.22)$$

$$\begin{aligned} (s_{23}\nu_2\mathbf{2}^+ + s_{123}\nu_1\mathbf{1}^+)\mathcal{J}_{2\mathcal{D}} &= -(D - \nu_1 - \nu_2 - \nu_3 - 2\nu_4 - \nu_9)\mathcal{J}_{2\mathcal{D}} \\ &+ ((\nu_1\mathbf{1}^+ + \nu_2\mathbf{2}^+ + \nu_3\mathbf{3}^+)\mathbf{4}^- + \nu_9\mathbf{9}^+(\mathbf{4}^- - \mathbf{8}^-))\mathcal{J}_{2\mathcal{D}} \end{aligned} \quad (4.23)$$

$$\begin{aligned} (s_{12}\nu_3\mathbf{3}^+ + s_{123}\nu_4\mathbf{4}^+)\mathcal{J}_{2\mathcal{D}} &= -(D - 2\nu_1 - \nu_2 - \nu_3 - \nu_4 - \nu_9)\mathcal{J}_{2\mathcal{D}} \\ &+ ((\nu_2\mathbf{2}^+ + \nu_3\mathbf{3}^+ + \nu_4\mathbf{4}^+)\mathbf{1}^- + \nu_9\mathbf{9}^+(\mathbf{1}^- - \mathbf{5}^-))\mathcal{J}_{2\mathcal{D}} \end{aligned} \quad (4.24)$$

$$\begin{aligned} s_{23}\nu_4\mathbf{4}^+\mathcal{J}_{2\mathcal{D}} &= -(D - \nu_1 - 2\nu_2 - \nu_3 - \nu_4 - \nu_9)\mathcal{J}_{2\mathcal{D}} \\ &+ ((\nu_1\mathbf{1}^+ + \nu_3\mathbf{3}^+ + \nu_4\mathbf{4}^+)\mathbf{2}^- + \nu_9\mathbf{9}^+(\mathbf{2}^- - \mathbf{6}^-))\mathcal{J}_{2\mathcal{D}} \end{aligned} \quad (4.25)$$

$$\begin{aligned} s_{12}\nu_5\mathbf{5}^+\mathcal{J}_{2\mathcal{D}} &= -(D - \nu_5 - \nu_6 - 2\nu_7 - \nu_8 - \nu_9)\mathcal{J}_{2\mathcal{D}} \\ &+ ((\nu_5\mathbf{5}^+ + \nu_6\mathbf{6}^+ + \nu_8\mathbf{8}^+)\mathbf{7}^- + \nu_9\mathbf{9}^+(\mathbf{7}^- - \mathbf{3}^-))\mathcal{J}_{2\mathcal{D}} \end{aligned} \quad (4.26)$$

$$\begin{aligned} (s_{23}\nu_6\mathbf{6}^+ + s_{123}\nu_5\mathbf{5}^+)\mathcal{J}_{2\mathcal{D}} &= -(D - \nu_5 - \nu_6 - \nu_7 - 2\nu_8 - \nu_9)\mathcal{J}_{2\mathcal{D}} \\ &+ ((\nu_5\mathbf{5}^+ + \nu_6\mathbf{6}^+ + \nu_7\mathbf{7}^+)\mathbf{8}^- + \nu_9\mathbf{9}^+(\mathbf{8}^- - \mathbf{4}^-))\mathcal{J}_{2\mathcal{D}} \end{aligned} \quad (4.27)$$

$$\begin{aligned} (s_{12}\nu_7\mathbf{7}^+ + s_{123}\nu_8\mathbf{8}^+)\mathcal{J}_{2\mathcal{D}} &= -(D - 2\nu_5 - \nu_6 - \nu_7 - \nu_8 - \nu_9)\mathcal{J}_{2\mathcal{D}} \\ &+ ((\nu_6\mathbf{6}^+ + \nu_7\mathbf{7}^+ + \nu_8\mathbf{8}^+)\mathbf{5}^- + \nu_9\mathbf{9}^+(\mathbf{5}^- - \mathbf{1}^-))\mathcal{J}_{2\mathcal{D}} \end{aligned} \quad (4.28)$$

$$\begin{aligned} s_{23}\nu_8\mathbf{8}^+\mathcal{J}_{2\mathcal{D}} &= -(D - \nu_5 - 2\nu_6 - \nu_7 - \nu_8 - \nu_9)\mathcal{J}_{2\mathcal{D}} \\ &+ ((\nu_5\mathbf{5}^+ + \nu_7\mathbf{7}^+ + \nu_8\mathbf{8}^+)\mathbf{6}^- + \nu_9\mathbf{9}^+(\mathbf{6}^- - \mathbf{2}^-))\mathcal{J}_{2\mathcal{D}} \end{aligned} \quad (4.29)$$

$$\begin{aligned} (D - \nu_5 - \nu_6 - \nu_7 - \nu_8 - 2\nu_9)\mathcal{J}_{2\mathcal{D}} &= (\nu_5\mathbf{5}^+(\mathbf{9}^- - \mathbf{1}^-) + \nu_6\mathbf{6}^+(\mathbf{9}^- - \mathbf{2}^-) \\ &+ \nu_7\mathbf{7}^+(\mathbf{9}^- - \mathbf{3}^-) + \nu_8\mathbf{8}^+(\mathbf{9}^- - \mathbf{4}^-))\mathcal{J}_{2\mathcal{D}} \end{aligned} \quad (4.30)$$

$$\begin{aligned} (D - \nu_1 - \nu_2 - \nu_3 - \nu_4 - 2\nu_9)\mathcal{J}_{2\mathcal{D}} &= (\nu_1\mathbf{1}^+(\mathbf{9}^- - \mathbf{5}^-) + \nu_2\mathbf{2}^+(\mathbf{9}^- - \mathbf{6}^-) \\ &+ \nu_3\mathbf{3}^+(\mathbf{9}^- - \mathbf{7}^-) + \nu_4\mathbf{4}^+(\mathbf{9}^- - \mathbf{8}^-))\mathcal{J}_{2\mathcal{D}} \end{aligned} \quad (4.31)$$

where $s_{12} = (p_1 + p_2)^2$, $s_{23} = (p_2 + p_3)^2$ and $s_{123} = (p_1 + p_2 + p_3)^2$.

These are the ten basic independent identities that we need in order to reduce all the possible two-loop planar scalar functions to the master integrals which are listed in the next subsection. There are ten such identities because for three independent external momenta p_i and two loop momenta, k and l , we differentiate once over k^μ

and once over l^μ i.e. ten times in total. We must emphasise the fact that the only independent momentum scales present in the problem are: s_{12}, s_{23} and s_{123} .

Similarly for the non-planar auxiliary integral $\mathcal{J}_{3\mathcal{D}_{out}}$ of eq. (4.5) we get the following set of IBP identities:

$$-8^+\nu_8 s_{123} + (8^+\nu_8 + 7^+\nu_7) s_{12} - 8^+3^-\nu_8 + (-5^-\nu_9 + 1^-\nu_9) 9^+ + 8^+1^-\nu_8 + (-6^+\nu_6 - 7^+\nu_7 - 8^+\nu_8) 5^- + D - 2\nu_5 - \nu_6 - \nu_8 + 8^+4^-\nu_8 - \nu_7 - \nu_9 = 0 \quad (4.32)$$

$$(8^+\nu_8 + 4^+\nu_4) s_{123} + (3^+\nu_3 - 8^+\nu_8) s_{12} + (-1^-\nu_9 + 5^-\nu_9) 9^+ + (-2^+\nu_2 - 3^+\nu_3 - 8^+\nu_8 - 4^+\nu_4) 1^- + (3^-\nu_8 - 4^-\nu_8 - 9^-\nu_8 + 5^-\nu_8) 8^+ + D - 2\nu_1 - \nu_2 - \nu_3 - \nu_4 - \nu_9 = 0 \quad (4.33)$$

$$(8^+\nu_8 + 4^+\nu_4) s_{23} + (-2^-\nu_9 + 6^-\nu_9) 9^+ + (-3^+\nu_3 - 1^+\nu_1 - 8^+\nu_8 - 4^+\nu_4) 2^- + (3^-\nu_8 - 9^-\nu_8 + 6^-\nu_8 - 4^-\nu_8) 8^+ + D - \nu_1 - 2\nu_2 - \nu_9 - \nu_3 - \nu_4 = 0 \quad (4.34)$$

$$-8^+\nu_8 s_{23} + (-3^-\nu_8 + 2^-\nu_8 + 4^-\nu_8) 8^+ + (-7^+\nu_7 - 8^+\nu_8 - 5^+\nu_5) 6^- + (-6^-\nu_9 + 2^-\nu_9) 9^+ + D - \nu_5 - \nu_8 - 2\nu_6 - \nu_9 - \nu_7 = 0 \quad (4.35)$$

$$-5^+\nu_5 s_{123} + 5^+\nu_5 s_{12} - 6^+\nu_6 s_{23} + (-3^-\nu_5 + 1^-\nu_5 - 8^-\nu_5 + 4^-\nu_5) 5^+ + (-9^+\nu_9 - 6^+\nu_6 - 7^+\nu_7) 8^- + (4^-\nu_6 - 3^-\nu_6 + 2^-\nu_6) 6^+ + 7^+4^-\nu_7 + D - \nu_5 - \nu_6 - \nu_9 - \nu_7 - 2\nu_8 = 0 \quad (4.36)$$

$$1^+\nu_1 s_{12} + (8^+\nu_8 + 9^+\nu_9) 7^- + (-1^+\nu_1 - 2^+\nu_2 - 9^+\nu_9 - 4^+\nu_4) 3^- + (-4^-\nu_8 - 9^-\nu_8) 8^+ + D - \nu_1 - 2\nu_3 - \nu_9 - \nu_4 - \nu_2 = 0 \quad (4.37)$$

$$5^+\nu_5 s_{12} + (-5^+\nu_5 - 8^+\nu_8 - 6^+\nu_6 - 9^+\nu_9) 7^- + 8^+4^-\nu_8 + 9^+3^-\nu_9 + D - \nu_5 - 2\nu_7 - \nu_8 - \nu_6 - \nu_9 = 0 \quad (4.38)$$

$$1^+\nu_1 s_{123} + 2^+\nu_2 s_{23} + (8^+\nu_8 + 9^+\nu_9) 7^- + (-1^+\nu_1 - 2^+\nu_2 - 8^+\nu_8 - 3^+\nu_3) 4^- + (-8^-\nu_9 - 3^-\nu_9) 9^+ + D - \nu_1 - 2\nu_4 - \nu_3 - \nu_2 - \nu_8 = 0 \quad (4.39)$$

$$(3^+\nu_3 + 4^+\nu_4) 7^- + (-8^-\nu_4 - 3^-\nu_4) 4^+ + 6^-2^+\nu_2 + (-9^-\nu_1 + 5^-\nu_1) 1^+ + (-2^+\nu_2 - 3^+\nu_3 - 8^+\nu_8) 9^- + D - \nu_1 - \nu_3 - \nu_2 - \nu_8 - 2\nu_9 = 0 \quad (4.40)$$

$$(-9^-\nu_5 + 1^-\nu_5) 5^+ + 7^+3^-\nu_7 + (-8^+\nu_8 - 7^+\nu_7 - 6^+\nu_6) 9^- + 6^+2^-\nu_6 + D - \nu_6 - \nu_5 - \nu_7 - 2\nu_9 - \nu_8 = 0 \quad (4.41)$$

Note that all the operators of the above equations act upon the auxiliary integral

$\mathcal{J}_{3\mathcal{D}_{out}}$ which we omitted for simplicity.

Finally for the non-planar auxiliary integral $\mathcal{J}_{3\mathcal{D}_{in}}$ of eq. (4.6) the ten IBP identities read:

$$(8^+\nu_8 + 4^+\nu_4) s_{123} + 7^+\nu_7 s_{12} + (-5^-\nu_9 + 1^-\nu_9) 9^+ + (-8^-\nu_4 + 1^-\nu_4 - 9^-\nu_4) 4^+ + (-6^+\nu_6 - 7^+\nu_7 - 8^+\nu_8) 5^- + D - 2\nu_5 - \nu_6 - \nu_8 - \nu_7 - \nu_9 = 0 \quad (4.42)$$

$$3^+\nu_3 s_{12} + (-1^-\nu_9 + 5^-\nu_9) 9^+ + (-2^+\nu_2 - 3^+\nu_3) 1^- + (-1^-\nu_4 + 8^-\nu_4) 4^+ + D - 2\nu_1 - \nu_9 - \nu_2 - \nu_3 - \nu_4 = 0 \quad (4.43)$$

$$(\nu_4 s_{123} - \nu_4 s_{23}) 4^+ + (-2^-\nu_9 + 6^-\nu_9) 9^+ + (-3^+\nu_3 - 4^+\nu_4 - 1^+\nu_1) 2^- + (6^-\nu_4 - 5^-\nu_4 + 8^-\nu_4) 4^+ + D - \nu_1 - \nu_4 - 2\nu_2 - \nu_3 - \nu_9 = 0 \quad (4.44)$$

$$(8^+\nu_8 + 4^+\nu_4) s_{23} + (-6^-\nu_9 + 2^-\nu_9) 9^+ + (-5^+\nu_5 - 7^+\nu_7 - 4^+\nu_4 - 8^+\nu_8) 6^- + (-9^-\nu_4 + 2^-\nu_4 + 5^-\nu_4 - 8^-\nu_4) 4^+ + D - 2\nu_6 - \nu_5 - \nu_9 - \nu_7 - \nu_8 = 0 \quad (4.45)$$

$$(-4^+\nu_4 + 5^+\nu_5) s_{12} + (-4^+\nu_4 - 6^+\nu_6 - 8^+\nu_8 - 9^+\nu_9) 7^- + (4^+\nu_4 + 9^+\nu_9) 3^- - 7^- 5^+\nu_5 + (-9^-\nu_4 + 5^-\nu_4 - 8^-\nu_4) 4^+ + D - \nu_9 - \nu_6 - 2\nu_7 - \nu_8 - \nu_5 = 0 \quad (4.46)$$

$$(4^+\nu_4 + 1^+\nu_1) s_{12} + (4^+\nu_4 + 9^+\nu_9) 7^- + (-1^+\nu_1 - 2^+\nu_2 - 9^+\nu_9 - 4^+\nu_4) 3^- + 4^+\nu_4 s_{123} + (-5^-\nu_4 + 8^-\nu_4) 4^+ + D - \nu_1 - \nu_4 - \nu_2 - 2\nu_3 - \nu_9 = 0 \quad (4.47)$$

$$(5^+\nu_5 + 9^+\nu_9) s_{123} + 6^+\nu_6 s_{23} + (1^-\nu_9 - 4^-\nu_9 - 5^-\nu_9) 9^+ + (-8^-\nu_4 + 1^-\nu_4) 4^+ + (-6^+\nu_6 - 7^+\nu_7 - 5^+\nu_5) 8^- + D - \nu_5 - \nu_4 - \nu_6 - \nu_7 - 2\nu_8 = 0 \quad (4.48)$$

$$(3^+\nu_3 + 2^+\nu_2 + 9^+\nu_9) s_{123} + 3^+\nu_3 s_{12} - 2^+\nu_2 s_{23} - 9^+ 4^-\nu_9 + (6^-\nu_2 - 5^-\nu_2 - 4^-\nu_2 + 8^-\nu_2) 2^+ + (-4^-\nu_3 - 5^-\nu_3 + 8^-\nu_3 + 7^-\nu_3) 3^+ + (-4^-\nu_1 + 8^-\nu_1) 1^+ + D - \nu_1 - \nu_3 - \nu_9 - \nu_2 - 2\nu_4 = 0 \quad (4.49)$$

$$4^+\nu_4 s_{123} + (-9^-\nu_2 + 6^-\nu_2) 2^+ + (7^-\nu_3 - 9^-\nu_3) 3^+ + (-9^-\nu_1 + 5^-\nu_1) 1^+ - 9^- 4^+\nu_4 + D - \nu_2 - \nu_1 - \nu_3 - \nu_4 - 2\nu_9 = 0 \quad (4.50)$$

$$(8^+\nu_8 + 4^+\nu_4) s_{123} + (-9^-\nu_5 + 1^-\nu_5) 5^+ + 7^+ 3^-\nu_7 + (-6^+\nu_6 - 4^+\nu_4 - 7^+\nu_7) 9^- + 6^+ 2^-\nu_6 + (-5^-\nu_8 + 1^-\nu_8 - 4^-\nu_8) 8^+ + D - \nu_5 - \nu_4 - \nu_7 - \nu_6 - 2\nu_9 = 0 \quad (4.51)$$

Note that like in the case of the previous non-planar identities, all the operators of the above equations act upon the auxiliary integral $\mathcal{J}_{3\mathcal{D}_{in}}$ which we omitted for simplicity.

Comparing the above identities of the non-planar auxiliary integrals with the identities of the planar auxiliary integral, we notice that the symmetries that are so evident in the planar case, disappear in the non-planar cases. One can easily understand why this happens by observing the diagrams that represent those integrals in figure (4.3).

4.5 Tool Four: Master Integrals (MI)

As we have already mentioned, our aim is to find a general way⁵ to express, all possible complicated integrals that appear in the physical processes, in terms of a basic set of simpler integrals (Master Integrals). The Master Integrals (MI) can then be analytically calculated as we will demonstrate in Chapter 6. In the following subsections we justify our choice of MI and list the set of planar and non-planar Master Integrals relevant for $1 \rightarrow 3$ or $2 \rightarrow 2$ scattering processes with massless propagators and one off-shell leg.

4.5.1 The Choice of Master Integrals

The choice of Master Integrals in each topology (if there are any) is not unique. It turns out that the most convenient option is the scalar integral of each topology with units in all propagator powers. However, in some cases it is not possible to write all the integrals of the topology in terms of only one MI. The choice of a second MI is required. As we show in the following two subsections, the second MI of the same topology is usually chosen to be a first rank tensor integral, with unit powers of the propagators, or a scalar integral with the power of one propagator equal to two (2) and the rest of the powers equal to one (1). In some of the reduction methods of complicated integrals to Master Integrals, which we will present in the following chapters, we chose the MI's for each topology, while in other methods, the MI's are chosen by the computer algorithm according to a set of predefined priorities.

⁵See Chapter 5

The reduction of all possible planar and non-planar two-loop integrals that appear in physical processes with three external particles on-shell and one external particle off-shell, leads to a set of only 24 Master Integrals that belong to 19 different topologies. There are 16 planar MI's (14 topologies) and 8 non-planar MI's (5 topologies).

4.5.2 Planar Master Integrals

The planar Master Integrals can be two three or four point functions with three to seven propagators and they can depend on one, two or three momentum scales.

There is only one MI with three propagators:

$$\text{Sunrise}(s_{12}) = \begin{array}{c} p_{12} \\ \rightarrow \text{---} \bigcirc \text{---} \end{array} .$$

At four propagators there are five MI's. One of them is a two-point function:

$$\text{Glass}(s_{12}) = \begin{array}{c} p_{12} \\ \rightarrow \bigcirc \text{---} \bigcirc \text{---} \end{array} .$$

The remaining four-propagator MI's are three-point functions. There is one topology with one external leg off-shell:

$$\text{Dart}_1(s_{12}) = \begin{array}{c} p_{12} \quad \rightarrow p_1 \\ \rightarrow \bigcirc \text{---} \bigcirc \text{---} \\ \quad \quad \quad \rightarrow p_2 \end{array}$$

and three topologies with two external legs off-shell:

$$\begin{aligned} \text{Dart}_2(s_{12}, s_{123}) &= \begin{array}{c} p_{123} \quad \rightarrow p_{12} \\ \rightarrow \bigcirc \text{---} \bigcirc \text{---} \\ \quad \quad \quad \rightarrow p_3 \end{array} , & (4.52) \\ \text{Dart}_2(s_{123}, s_{23}) &= \begin{array}{c} p_{123} \quad \rightarrow p_1 \\ \rightarrow \bigcirc \text{---} \bigcirc \text{---} \\ \quad \quad \quad \rightarrow p_{23} \\ \quad \quad \quad p_3 \end{array} , \\ \text{Tglass}(s_{12}, s_{123}) &= \begin{array}{c} p_{123} \quad \rightarrow p_{12} \\ \rightarrow \bigcirc \text{---} \bigcirc \text{---} \end{array} . \end{aligned}$$

Here the second MI of the topology is a first rank tensor. The number two (2) in left loop of the diagram that corresponds to Pbox₂ defines the numerator of the tensor MI. This is evident in the auxiliary integral representation of eq. (4.53):

$$\begin{aligned} \text{Pbox}_1(s_{23}, s_{13}, s_{123}) &= \mathcal{J}_{2\mathcal{D}}(D, \{1, 1, 1, 0, 1, 0, 1, 1, 1\}, s_{12}, s_{23}, s_{123}) , \\ \text{Pbox}_2(s_{23}, s_{13}, s_{123}) &= \mathcal{J}_{2\mathcal{D}}(D, \{1, 1, 1, 0, 1, -1, 1, 1, 1\}, s_{12}, s_{23}, s_{123}) . \end{aligned} \quad (4.54)$$

4.5.3 Non-planar Master Integrals (MI)

All integrals that can be produced from the non-planar Feynman diagrams can be reduced to the Master Integrals of the previous section, plus some extra six and seven propagator non-planar Master Integrals⁶.

Apart from the planar MI, the two different types of non-planar integrals that can be produced from the two types of non-planar auxiliary integrals have the following six-propagator Master Integrals in common:

$$\begin{aligned} \text{Ebox}_1(s_{12}, s_{13}, s_{123}) &= \begin{array}{c} p_{123} \rightarrow \text{---} \text{---} \text{---} \rightarrow p_2 \\ \diagdown \quad \diagup \\ \text{---} \quad \text{---} \\ \diagup \quad \diagdown \\ p_3 \leftarrow \text{---} \text{---} \text{---} \rightarrow p_1 \end{array} , \\ \text{Ebox}_2(s_{12}, s_{13}, s_{123}) &= \begin{array}{c} p_{123} \rightarrow \text{---} \text{---} \text{---} \rightarrow p_2 \\ \diagdown \quad \diagup \\ \text{---} \quad \text{---} \\ \diagup \quad \diagdown \\ p_3 \leftarrow \text{---} \text{---} \text{---} \rightarrow p_1 \end{array} . \end{aligned}$$

Note that both MI's belong to the same topology. The only difference is that the second MI, Ebox₂, is a tensor integral, as can be seen in the auxiliary integral representation:

$$\begin{aligned} \text{Ebox}_1(s_{12}, s_{13}, s_{123}) &= \mathcal{J}_{3\mathcal{D}_{out}}(D, 1, 0, 0, 1, 1, 1, 1, 0, 1, s_{12}, s_{23}, s_{123}) , \\ \text{Ebox}_2(s_{12}, s_{13}, s_{123}) &= \mathcal{J}_{3\mathcal{D}_{out}}(D, 1, 0, 0, 1, 1, 1, 1, -1, 1, s_{12}, s_{23}, s_{123}) . \end{aligned}$$

There are some master integrals that appear only in the reduction of the $\mathcal{J}_{3\mathcal{D}_{out}}$

⁶There are no non-planar MI's with less than six propagators because, in the case of integrals with five propagators or less, there is always an appropriate momentum-shift that can 'translate' them to planar MI's.

non-planar auxiliary diagram. One of them is a six-propagator, one-scale, three-point function:

$$\text{Xtri}_1(s_{12}) = \begin{array}{c} \text{---} p_{12} \text{---} \\ \diagup \quad \diagdown \\ \text{---} p_1 \text{---} \\ \diagdown \quad \diagup \\ \text{---} p_2 \text{---} \end{array} .$$

The other two MI's have seven propagators:

$$\begin{array}{l} \text{Xbmo}_1(s_{12}, s_{13}, s_{123}) = \begin{array}{c} p_{123} \text{---} \text{---} p_2 \\ | \quad \diagdown \quad \diagup \\ p_3 \text{---} \text{---} p_1 \end{array} , \\ \text{Xbmo}_2(s_{12}, s_{13}, s_{123}) = \begin{array}{c} p_{123} \text{---} \text{---} p_2 \\ | \quad \diagdown \quad \diagup \\ p_3 \text{---} \text{---} p_1 \end{array} (2) , \end{array}$$

where

$$\begin{aligned} \text{Xbmo}_1(s_{12}, s_{13}, s_{123}) &= \mathcal{J}_{3\mathcal{D}_{out}}(D, 1, 0, 1, 1, 1, 1, 1, 0, 1, s_{12}, s_{23}, s_{123}) , \\ \text{Xbmo}_2(s_{12}, s_{13}, s_{123}) &= \mathcal{J}_{3\mathcal{D}_{out}}(D, 1, 0, 1, 1, 1, 1, 1, -1, 1, s_{12}, s_{23}, s_{123}) . \end{aligned}$$

Here we have once more the case of a topology with two MI's.

The reduction of the diagrams that are represented by the other non-planar auxiliary diagram, $\mathcal{J}_{3\mathcal{D}_{in}}$, leads to three extra MI's. One is a six-propagator, two-scale, three-point function:

$$\text{Xtri}_2(s_{123}, s_{12}) = \begin{array}{c} p_{123} \text{---} \text{---} p_{12} \\ \diagup \quad \diagdown \\ \text{---} p_3 \text{---} \end{array} ,$$

and two are seven-propagator integrals, a scalar and a tensor integral, that belong to the same topology:

$$\begin{array}{l} \text{Xbmi}_1(s_{12}, s_{13}, s_{123}) = \begin{array}{c} p_{123} \text{---} \text{---} p_2 \\ | \quad \diagdown \quad \diagup \\ p_3 \text{---} \text{---} p_1 \end{array} , \\ \text{Xbmi}_2(s_{12}, s_{13}, s_{123}) = \begin{array}{c} p_{123} \text{---} \text{---} p_2 \\ | \quad \diagdown \quad \diagup \\ p_3 \text{---} \text{---} p_1 \end{array} (3) . \end{array}$$

4.6 Tool Five: Harmonic Polylogarithms

In [42] the solutions of the differential equations for two-loop four-point functions with one off-shell leg were expressed in terms of Hypergeometric functions. However, this formalism is not so convenient for practical applications, where expansions around $\epsilon = 0$ are required. This obstacle was overcome with the introduction of 1-dimensional and 2-dimensional Harmonic polylogarithms. One-dimensional Harmonic polylogarithms (HPL) were introduced in [39] as generalisation of Nielsen's polylogarithms [40, 41]. They were later generalised to two-dimensional Harmonic polylogarithms in [43]. Since the HPL's are just a subclass of the 2DHPL's, we will not consider them separately here.

4.6.1 Definition of 2DHPL's

The 2DHPL's were introduced as the most appropriate functions for solving differential equations on the Master Integrals. In the in-homogeneous terms of the X^7 DE's, for the two scale MI's like $\text{Dart}_2(X, s_{123})$, one can find denominators of one scale:

$$\begin{aligned} f(1; X) &\equiv \frac{1}{1-X}, \\ f(0; X) &\equiv \frac{1}{X}. \end{aligned}$$

This is evident in the very simple X differential equation for the MI Dart_2 :

$$\begin{aligned} \frac{\partial \text{Dart}_2(X, s_{123})}{\partial X} &= \frac{\epsilon}{1-X} \text{Dart}_2(X, s_{123}) \\ &\quad - \frac{(-2 + 3\epsilon)}{s_{123}(1-X)X} \text{Suns}(X \cdot s_{123}), \end{aligned} \tag{4.55}$$

⁷For simplicity, as we will see in chapter 6, we prefer to differentiate over a new variable $X = s_{12}/s_{123}$.

where one can easily identify $f(1; X)$ and $f(0; X)$. Equivalently, in the more complicated X DE' s, for three scale MI' s, one can also find denominators of two scales⁸:

$$\begin{aligned} f(1 - Y; X) &\equiv \frac{1}{1 - X - Y}, \\ f(Y; X) &\equiv \frac{1}{X + Y}. \end{aligned}$$

Based on that, the 2DHPL $H(\vec{m}_w; X)$, is described as a function of a w -dimensional vector \vec{m}_w and its argument X . w is called the weight of H .

For $w = 1$ the 2DHPL's are defined as:

$$H(a_1; X) \equiv \int_0^X dX' f(a_1; X'),$$

or equivalently:

$$\frac{\partial}{\partial X} H(a_1; X) = f(a_1; X) \quad \text{with} \quad a_1 = 1, 0, Y, 1 - Y. \quad (4.56)$$

For weight $w > 1$ the 2DHPL's are defined as:

$$H(a_1, \vec{b}_{w-1}; X) \equiv \int_0^X dX' f(a_1; X') H(\vec{b}_{w-1}; X'),$$

or equivalently:

$$\frac{\partial}{\partial X} H(a_1, \vec{b}_{w-1}; X) = f(a_1; X) H(\vec{b}_{w-1}; X) \quad \text{with} \quad a_1 = 1, 0, Y, 1 - Y. \quad (4.57)$$

4.6.2 Useful Properties of 2DHPL's

Property 1

2DHPL's fulfil an algebra that allows one to write the product of two 2DHPL's, of the same argument X and weights w_1 and w_2 respectively, as the sum of 2DHPL's, each with argument X and weight $w = w_1 + w_2$:

$$H(\vec{a}_{w_1}; X) H(\vec{b}_{w_2}; X) = \sum_{\vec{c}_w = \vec{a}_{w_1} \uplus \vec{b}_{w_2}} H(\vec{c}_w; X), \quad (4.58)$$

⁸As previously, for simplicity we have defined the variables $X = s_{12}/s_{123}$ and $Y = s_{23}/s_{123}$.

where $\vec{a}_{w_1} \uplus \vec{b}_{w_2}$, represents all permutations of the elements of \vec{a}_{w_1} and \vec{b}_{w_2} , in which their relative orders are preserved.

For example, at $w_1 = 2, \vec{a}_{w_1} = (k, l)$ and $w_2 = 3, \vec{b}_{w_2} = (r, s, t)$, one has:

$$\begin{aligned} \mathrm{H}(k, l; X)\mathrm{H}(r, s, t; X) &= \mathrm{H}(k, l, r, s, t; X) + \mathrm{H}(k, r, l, s, t; X) \\ &+ \mathrm{H}(k, r, s, l, t; X) + \mathrm{H}(k, r, s, t, l; X) \\ &+ \mathrm{H}(r, k, l, s, t; X) + \mathrm{H}(r, k, s, l, t; X) \\ &+ \mathrm{H}(r, s, k, l, t; X) + \mathrm{H}(r, k, s, t, l; X) \\ &+ \mathrm{H}(r, s, k, t, l; X) + \mathrm{H}(r, s, t, k, l; X) , \end{aligned}$$

Property 2

2DHPL's, of any weight $w = q > 1$, satisfy the Integration By Parts identities:

$$\begin{aligned} \mathrm{H}(m_1 \cdots m_q; X) &= \int_0^x dX' f(m_1; X')\mathrm{H}(m_2, \cdots, m_q; X') \\ &= \mathrm{H}(m_1; X)\mathrm{H}(m_2, \cdots, m_q; X) \\ &- \int_0^x dX' \mathrm{H}(m_1; X')f(m_2; X')\mathrm{H}(m_3, \cdots, m_q; X') \\ &= \mathrm{H}(m_1; X)\mathrm{H}(m_2, \cdots, m_q; X) - \mathrm{H}(m_2, m_1; X)\mathrm{H}(m_3, \cdots, m_q; X) \\ &+ \mathrm{H}(m_3, m_2, m_1; X)\mathrm{H}(m_4, \cdots, m_q; X) - \cdots - (-1)^p \mathrm{H}(m_q, \cdots, m_1; X) . \end{aligned} \tag{4.59}$$

4.6.3 ‘Minimal’ Basis-Set of 2DHPL’s

The set of all possible ‘product’ identities (4.58) and Integration By Parts relations (4.59), can be used in order to express as many as possible of the 2DHPL’s of weight w and certain ‘not-preferred’ indices, in terms of:

- (i) a ‘Minimal’ set of 2DHPL’s of the same weight and certain ‘preferred’ indices, and
- (ii) products of 2DHPL’s of lower weight (these are also part of the ‘Minimal’ set for their weight).

The ‘Minimal’ set of 2DHPL’s up to weight 3, expressed in terms of Nielsen’s polylogarithms [43], can be found in Appendix A. Here we present this base:

$w = 1$:

$$\begin{aligned}
 & H(0; X) , \\
 & H(1; X) , \\
 & H(1 - Y; X) , \\
 & H(Y; X) .
 \end{aligned} \tag{4.60}$$

$w = 2$:

$$\begin{aligned}
 & H(0, 1; X) , \\
 & H(0, 1 - Y; X) , \\
 & H(0, Y; X) , \\
 & H(1, 1 - Y; X) , \\
 & H(1, Y; X) , \\
 & H(1 - Y, Y; X) .
 \end{aligned} \tag{4.61}$$

and $w = 3$:

$$\begin{array}{ll}
 H(0, 0, 1; X) , & H(0, Y, 1 - Y; X) , \\
 H(0, 1, 1; X) , & H(0, Y, Y; X) , \\
 H(0, 0, 1 - Y; X) , & H(1, 1 - Y, 1 - Y; X) , \\
 H(0, 0, Y; X) , & H(1, 1 - Y, Y; X) , \\
 H(0, 1, 1 - Y; X) , & H(1, Y, 1 - Y; X) , \\
 H(0, 1, Y; X) , & H(1, Y, Y; X) , \\
 H(0, 1 - Y, 1; X) , & H(1 - Y, 1, 1; X) , \\
 H(0, 1 - Y, 1 - Y; X) , & H(1 - Y, Y, Y; X) , \\
 H(0, 1 - Y, Y; X) , & H(Y, 1, 1; X) , \\
 H(0, Y, 1; X) , & H(Y, 1 - Y, 1 - Y; X) .
 \end{array} \tag{4.62}$$

Let us now demonstrate how the reduction to a ‘Minimal’ basis takes place. As an example, $H(1 - Y, 1, 0; X)$ can be written in terms of our ‘Minimal’ base, just

with use of the IBP identity (4.59) for $H(0, 1, 1 - Y; X)$, giving:

$$H(1 - Y, 1, 0; X) = H(1 - Y; X)H(1, 0; X) - H(1, 1 - Y; X)H(0; X) + H(0, 1, 1 - Y; X).$$

The only 2DHPL which is not part of the ‘Minimal’ set is $H(1, 0; X)$, whose calculation is straight forward by application of the ‘product’ identity for $H(1; X)$ and $H(0; X)$:

$$H(1, 0; X) = -H(0, 1; X) + H(1; X)H(0; X),$$

which could be expressed in terms of logarithms and dilogarithms as:

$$H(1, 0; X) = -\text{Li}_2(X) - \ln(1 - X)\ln(X) = \text{Li}_2(1 - X) - \frac{\pi^2}{6}.$$

In summary one can construct table 4.1, where *full basis* is the set of all possible 2DHPL’s with a certain weight, *irreducible set* is the set that remains after trivial relations arising from the definition of each 2DHPL, and finally the *Minimal set* is the basis of 2DHPL’s that remains after use of ‘product’ identities and IBP relations.

Weight	Full basis	Irreducible set	Minimal set
1	4	4	4
2	16	9	6
3	64	36	20

Table 4.1: Sizes of the various bases

As we have already mentioned the 2DHPL’s were used in [43] to express all planar and non-planar master integrals. All 2DHPL’s that appear in the divergent parts of the planar master integrals have weight ≤ 3 and can be related to the more commonly known Nielsen generalized polylogarithms [40, 41] of suitable arguments (see appendix A). The functions of weight 4 appearing in the finite parts of the master integrals can all be represented, by the very definition (eq. 4.57), as one-dimensional integrals over 2DHPL’s of weight 3, hence of Nielsen’s generalized polylogarithms of suitable arguments according to the above remark. Numerical routines providing an evaluation of 2DHPL’s [87, 88] are available.

4.7 Tool Six: Projectors For Helicity Amplitudes

In this section we present a D -dimensional projection method which can be employed at all orders in perturbation theory to extract helicity amplitudes. Using this approach helicity amplitudes were calculated in [46,47] (two-loops). The technique involves analysis of the tensorial structure of the amplitude and subsequent derivation of projectors, which acting on the amplitude can isolate the coefficients of certain tensor structures. The decay of the Higgs boson to a gluon pair is used here as a pedagogical example to demonstrate the major stages of a helicity amplitude calculation. In chapter 8 the same method is used to produce the NNLO helicity amplitudes for the Higgs decay to three gluons.

4.7.1 The General Tensor

We will consider the production of a pair of gluons in a Higgs decay,

$$\mathcal{H}(p_3) \longrightarrow g(p_1) + g(p_2) . \quad (4.63)$$

where the invariant scales satisfy

$$s_{12} = (p_1 + p_2)^2 = M_{\mathcal{H}}^2 \quad (4.64)$$

We can also define the dimensionless invariant

$$x = s_{12}/M_{\mathcal{H}}^2 . \quad (4.65)$$

The hadron current may be perturbatively decomposed as,

$$H_{\mu\nu}(g_1; g_2) = C_1 \left(H_{\mu\nu}^{(0)}(g_1; g_2) + \left(\frac{\alpha_s}{2\pi}\right) H_{\mu\nu}^{(1)}(g_1; g_2) + \left(\frac{\alpha_s}{2\pi}\right)^2 H_{\mu\nu}^{(2)}(g_1; g_2) + \mathcal{O}(\alpha_s^3) \right), \quad (4.66)$$

where α_s denotes the QCD coupling constant at the renormalization scale μ , and the $H_{\mu\nu}^{(i)}$ are the i -loop contributions to the renormalized amplitude. Renormalization of ultraviolet divergences is performed in the $\overline{\text{MS}}$ scheme.

4. Basic Tools For Two-Loop Integrals

The most general tensor structure for the hadron current $H_{\mu\nu}(g_1; g_2)$, contracted with the polarizations of the external gluons is

$$\begin{aligned}
 H_{\mu\nu}(g_1; g_2)\epsilon_1^\mu\epsilon_2^\nu &= \sum_{i,j=1}^2 A_{ij} p_i \cdot \epsilon_1 p_j \cdot \epsilon_2 + B \epsilon_1 \cdot \epsilon_2 \\
 &= A_{11} p_1 \cdot \epsilon_1 p_1 \cdot \epsilon_2 + A_{22} p_2 \cdot \epsilon_1 p_2 \cdot \epsilon_2 \\
 &\quad + A_{12} p_1 \cdot \epsilon_1 p_2 \cdot \epsilon_2 + A_{21} p_2 \cdot \epsilon_1 p_1 \cdot \epsilon_2 + B \epsilon_1 \cdot \epsilon_2 \\
 &= A_{21} p_2 \cdot \epsilon_1 p_1 \cdot \epsilon_2 + B \epsilon_1 \cdot \epsilon_2 ,
 \end{aligned} \tag{4.67}$$

where the constraints $p_1 \cdot \epsilon_1 = 0$ and $p_2 \cdot \epsilon_2 = 0$, due to the transversality condition have been applied. The tensor must satisfy the QCD Ward identity when the gluon polarization vectors ϵ_1 and ϵ_2 are replaced with the respective gluon momentum,

$$\begin{aligned}
 (\epsilon_1 \rightarrow p_1) &\longrightarrow H_{\mu\nu}(g_1; g_2)p_1^\mu\epsilon_2^\nu = 0 , \\
 (\epsilon_2 \rightarrow p_2) &\longrightarrow H_{\mu\nu}(g_1; g_2)\epsilon_1^\mu p_2^\nu = 0 .
 \end{aligned} \tag{4.68}$$

These two constraints are actually linearly dependent and yield one relation amongst the two distinct tensor structures of eq. (4.67):

$$B = -p_1 \cdot p_2 A_{21} . \tag{4.69}$$

Applying this identity in eq. (4.67) gives the gauge invariant form of the tensor,

$$H_{\mu\nu}(g_1; g_2)\epsilon_1^\mu\epsilon_2^\nu = A_{21}T_{21} , \text{ or } H_{\mu\nu}(g_1; g_2) = A_{21} (p_{1\nu}p_{2\mu} - p_1 \cdot p_2 g_{\mu\nu}) , \tag{4.70}$$

where A_{21} is a gauge independent function and the tensor structure T_{21} is given by,

$$T_{21} = p_2 \cdot \epsilon_1 p_1 \cdot \epsilon_2 - p_1 \cdot p_2 \epsilon_1 \cdot \epsilon_2 . \tag{4.71}$$

It should be noted that in the case of a more complicated process (i.e. more external particles) one would have to solve a system of equations like eq. (4.69) in order to derive the minimum basis set of independent coefficients (i.e. B , A_{21} etc.). It turns out [47] that the number of the components of the basis set equals the number of the independent helicity amplitudes.

4. Basic Tools For Two-Loop Integrals

4.7.2 Projectors for the Tensor Coefficients

The coefficient A_{ij} may be easily extracted from a Feynman diagram calculation using projectors such that:

$$\sum_{\text{spins}} \mathcal{P}(A_{XY}) H_{\mu\nu}(g_1; g_2) \epsilon_1^\mu \epsilon_2^\nu = A_{XY}. \quad (4.72)$$

We can write the tensor structure T_{21} and its complex conjugate T_{21}^\dagger as:

$$T_{21} = \epsilon_1^\mu \epsilon_2^\nu T_{21\mu\nu}, \quad T_{21}^\dagger = \epsilon_{1\rho}^* \epsilon_{2\sigma}^* T_{21}^{\rho\sigma\dagger}, \quad (4.73)$$

with

$$\begin{aligned} T_{21\mu\nu} &= p_{1\nu} p_{2\mu} - p_1 \cdot p_2 g_{\mu\nu}, \\ T_{21}^{\rho\sigma} &= p_1^\sigma p_2^\rho - p_1 \cdot p_2 g^{\rho\sigma}. \end{aligned} \quad (4.74)$$

We proceed by acting on both sides of eq. (4.70) with T_{21}^\dagger and solving for A_{12} :

$$\sum_{\text{spins}} T_{21}^\dagger H_{\mu\nu}(g_1; g_2) \epsilon_1^\mu \epsilon_2^\nu = \sum_{\text{spins}} T_{21}^\dagger T_{21} A_{21}. \quad (4.75)$$

Comparing equations (4.72) and (4.75) we can identify projector $\mathcal{P}(A_{21})$ as:

$$\mathcal{P}(A_{21}) = \frac{T_{21}^\dagger}{\sum_{\text{spins}} T_{21}^\dagger T_{21}}, \quad (4.76)$$

which, using spinor algebra⁹ yields:

$$\mathcal{P}(A_{21}) = \frac{4}{s_{12}^2 (D-2)} T_{21}^\dagger. \quad (4.77)$$

At this point, it should be stressed that things would be more complicated if the general tensor depended on more than one tensor structures. In such a case, one would have to solve a system with respect to the coefficients (A 's, B 's etc.) and then identify the coefficients of the general amplitude in each equation as the projector for the respective coefficient.

⁹Appendix D

4. Basic Tools For Two-Loop Integrals

4.7.3 Helicity Amplitudes

Let us now summarize what we have accomplished so far. Starting from the most general tensor structure for the hadron current $H_{\mu\nu}(g_1; g_2)$ and applying certain constraints, we have managed to write it in terms of a known tensor structure (T_{21}) and an unknown gauge independent function (A_{21}) The unrenormalised coefficient A_{21} has perturbative expansion of the form:

$$A_{21}^U = C_1 \left[A_{21}^{U(0)} + \left(\frac{\alpha_s}{2\pi} \right) A_{21}^{U(1)} + \left(\frac{\alpha_s}{2\pi} \right)^2 A_{21}^{U(2)} + \mathcal{O}(\alpha_s^3) \right], \quad (4.78)$$

where the dependence on s_{12} is implicit. At order i each of the $A_{21}^{U(i)}$ can be calculated by acting with the general all-order projector $\mathcal{P}(A_{21})$ on the i^{th} order hadron current $H_{\mu\nu}^{(i)}(g_1; g_2)$ of eq. (4.66):

$$\sum_{\text{spins}} \mathcal{P}(A_{21}) H_{\mu\nu}^{(i)}(g_1; g_2) \epsilon_1^\mu \epsilon_2^\nu = A_{21}^{U(i)}. \quad (4.79)$$

At tree level it is trivial to calculate the $H_{\mu\nu}^{(0)}(g_1; g_2)$ amplitude from the Feynmann diagrams:

$$H_{\mu\nu}^{(0)}(g_1; g_2) = -i p_2^\mu p_1^\nu \delta^{\alpha\beta} + i p_1 \cdot p_2 g^{\mu\nu} \delta^{\alpha\beta}. \quad (4.80)$$

Substituting eqs. (4.80, 4.76) in eq. (4.79) and applying the algebra of Appendix D one can derive $A_{21}^{(0)}$:

$$A_{21}^{(0)} = -i \delta^{\alpha\beta}. \quad (4.81)$$

The general form of the renormalized helicity amplitude $|\mathcal{M}^{\lambda_1 \lambda_2}\rangle$ for the process $\mathcal{H}(p_3) \longrightarrow g(p_1, \lambda_1) + g(p_2, \lambda_2)$ can be written as:

$$|\mathcal{M}^{\lambda_1 \lambda_2}\rangle = \epsilon_1^\mu(\lambda_1) \epsilon_2^\nu(\lambda_2) H_{\mu\nu}(g_1; g_2), \quad (4.82)$$

where the $\lambda_i = \pm$ denote the helicity. At tree level one can use the general form for $H_{\mu\nu}^{(0)}(g_1; g_2)$ as it is given in eq. (4.70), modified for the lowest order:

$$H_{\mu\nu}^{(0)}(g_1; g_2) = A_{21}^{(0)} (p_{1\nu} p_{2\mu} - p_1 \cdot p_2 g_{\mu\nu}). \quad (4.83)$$

4. Basic Tools For Two-Loop Integrals

At this point 4-dimensional helicity techniques can be employed - corresponding to treating the external particle states as physical - the t'Hooft-Veltman scheme. The two non-zero helicity amplitudes are $++$ and $--$. The former can be obtained by substituting eqs. (4.83, 4.81) in eq. (4.82)¹⁰:

$$|\mathcal{M}^{(0)++}\rangle = \frac{i}{2} C_1 [p_1 p_2]^2 \delta^{\alpha\beta}, \quad (4.84)$$

while the parity conjugate amplitude $--$ can be attained with reversal of the square for triangle brackets:

$$|\mathcal{M}^{(0)--}\rangle = \frac{i}{2} C_1 \langle p_1 p_2 \rangle^2 \delta^{\alpha\beta}. \quad (4.85)$$

The two remaining helicity configurations $+-$ and $-+$ are zero.

Similarly one can derive helicity amplitudes for all orders in perturbation theory as the tensorial structures T_{XY} are independent of the order of calculation. As a result the relation between the helicity amplitude and the tensorial coefficients remains unchangeable at any order.

¹⁰See Appendix D.

Chapter 5

Making Two-Loop Integrals Simpler

5.1 Reductions: New Techniques Available

Within the last few years new techniques were developed for the reduction of all possible tensor integrals appearing in a two-loop calculation to a basic set of Master Integrals (MI's). Two of those techniques are based on the integration by parts (IBP) method. In the first one [48], each tensor integral is translated (through its Schwinger parametric form) into a sum of scalar integrals in higher dimensions ($D \rightarrow D + 2n$) and powers of propagators. Using recursive relations that were derived applying the IBP for each topology separately, one can turn those integrals into MI's (still at higher dimensions). Then the high dimensions ($D + 2n$) MI's are given in terms of MI's in D using a method called dimensional shift. Gehrmann and Remiddi [42] have introduced another way of reducing arbitrary tensor integrals to MI's by solving a system of equations. This system is produced by deriving the IBP equations for all the members of a set of seed-integrals. The seed-integrals are mainly defined by the topology and rank of the highest tensor integrals. These techniques were primarily applied successfully to the calculation of two-loop integrals with four on-shell external legs [49–52]. The next more challenging task at two-loops was the calculation of two-loop integrals with three external on-shell and one off-

shell legs. Deriving individual recursive relations for each topology, apart from being a non-trivial task due to the increased number of hard topologies, proved to require computer speed and capacity beyond our current limits. A more general and systematic way was demanded. The solution came in [38], where Laporta introduced an algorithm that enables one to meet all the difficulties arising in two-loop integral reductions.

5.2 Laporta

In an influential paper [38], Laporta introduced an algorithm suitable for the reduction of complicated scalar and tensor integrals, to a simple set of Master Integrals (MI's). What the algorithm does is to solve a system of equations in a systematic way. The MI's are chosen by the algorithm itself as the result of a set of priorities that we impose.

5.2.1 The Algorithm

The general form of the Laporta algorithm can be presented schematically in figure 5.1. The numbers correspond to the steps we will see in the main part of the algorithm. The input to the Laporta algorithm is:

INPUT : [*DenSet*], [*MaxDen*], [*MaxNum*], [*SolutionSet*].

Let us study one-by-one the input terms. First of all, *DenSet* is the set of denominators, which is defined as the set of propagators raised to a positive power in the denominator of the integral. The possible set of numerators is the set of propagators of the Auxiliary Integral that have zero or negative powers of propagators in the denominator of the integral. In the Auxiliary Integral notation $\mathcal{J}(\nu_1, \nu_2, \dots, \nu_9)$, the denominators are the propagators which correspond to positive ν_i 's and the numerators are the propagators which correspond to zero or negative ν_i 's. With this in mind, we define *Md* for an integral as:

$$Md = \sum_i (\nu_i - 1) \quad , \quad (5.1)$$

with i running through all the positive ν_i 's. and Mp as:

$$Mp = \sum_i (\nu_i) \quad , \quad (5.2)$$

with i running through all the zero or negative ν_i 's. $MaxDen$ and $MaxNum$ are then defined as the more positive value for Md and the more negative value for Mp respectively, that we allow for our 'Seed' integrals. We note that a 'Seed' is the integral on which we act to generate the Integration By Parts identities. In most cases we set $MaxDen$ and $MaxNum$ to be equal respectively to the Md and Mp values of the integral we want to calculate. However, sometimes the system we want to solve does not close to the simplest possible form and we have to use higher values for $MaxDen$ and $MaxNum$ in order to produce more equations and hopefully solve the system in the optimum way. $SolutionSet$ is the set of solutions (equations between integrals), that we have already stored from previous uses of the algorithm. This set is empty, $\{\}$, when we first apply the algorithm.

THE MAIN ALGORITHM

Before we present the main algorithm that is implemented in MAPLE, let us define Nk as the number of loops (1 for one-loop and 2 for two-loop integrals) and Nd as the number of denominators (or the number of propagators in $DenSet$) of the integral we are interested in calculating. All integrals appearing in the calculation, as the result of the IBP identities, which have number of denominators $n = Nk$, are set to zero automatically.

1. Using the denominators of the given integral, generate all combinations of the $n = Nk + 1$ to $n = Nd$ denominators and put them in a set called *SetOfAllIntegrals*. Express the denominators in the auxiliary integral form with unit powers in the position of every denominator and zero powers in the rest of the positions.
2. Let $n = Nk + 1$.
3. Take all combinations with n denominators that are members of *SetOfAllIntegrals* and put them in a set named *SetWithnDen*.

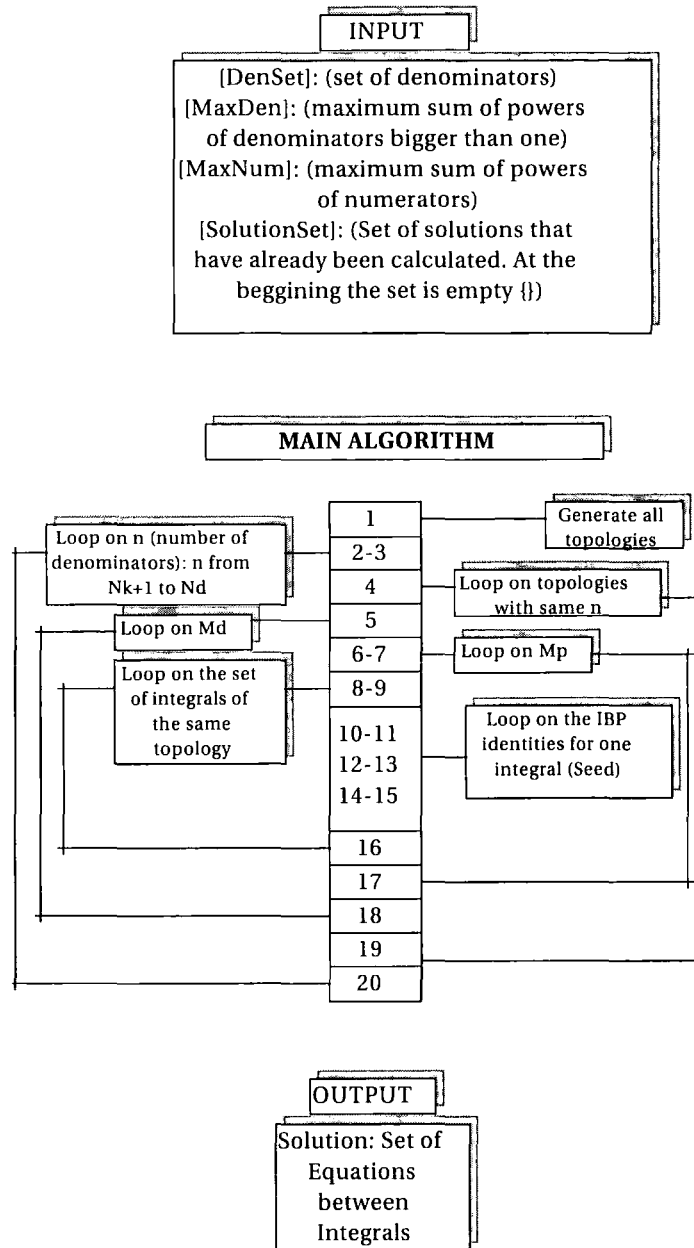


Figure 5.1: The input, main part and output of the Laporta algorithm. The numbers correspond to the steps as they appear in the main text of this subsection (5.2.1).

4. Select the first topology = $Topo$.
5. Let $Md = 0$.
6. Let $Mp = 0$.
7. For $Topo$ (fixed position of propagators) take all possible combinations in which the sum of the powers of the n denominators is $Md + n$ and the sum of the of the powers of the numerators is Mp . Put all the combinations in a set named $SetOfOneTopo$.
8. Take the 1st member of $SetOfOneTopo$ and name it $SeedIntegral$.
9. Generate the 10 IBP equations for the $SeedIntegral$ and put them in a set named $SeedIBPSet$.
10. Take the 1st equation of $SeedIBPSet$ and name it $Equat$.
11. Substitute all the members of $SolutionSet$ in $Equat$.
12. If $Equat$ is linearly independent of the other members of $SolutionSet$ then $Equat = [\text{solve } Equat \text{ in terms of the integral with the highest priority}]$, else Go To step (15).
13. Substitute $Equat$ in the $SolutionSet$.
14. $SolutionSet = SolutionSet \text{ union } Equat$.
15. END LOOP on $SeedIBPSet$. [Take the next member of $SeedIBPSet$, name it $Equat$ and Go To step (11)][else continue]
16. END LOOP on $SetOfOneTopo$. [Take next member of $SetOfOneTopo$, name it $SeedIntegral$ and Go To step (9)][else continue]
17. END LOOP on Mp . [if $Mp < MaxNum$ then Let $Mp = Mp + 1$ and Go To step (7)][else continue]

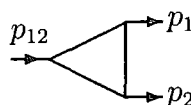
18. END LOOP on Md . [if $Md < MaxDen$ then Let $Md = Md + 1$ and Go To step (6)][else continue]
19. END LOOP on topologies. [Select next member of $SetWithnProps$, name it Topo and Go To step (5)][else continue]
20. END LOOP on n . [If $n \leq Nd$ then Let $n = n + 1$ and Go To step (3)][else Go To *OUTPUT*]

OUTPUT: [*SolutionSet*]

This completes the algorithm. The only aspect that we have not covered so far, is the priorities we use to select the ‘highest priority integral’ of the equations. As we have seen, each integral has a certain n (number of denominators), Md and Mp (see definitions eq (5.1) and eq (5.2)). Of all the integrals appearing in a relation, we first choose the ones with the highest n and put them in a set. Then from this set we pick out the integrals with the highest Md and from these ones the integrals with the most negative Mp . If in our final set there are more than one integrals with the same n , Md and Mp , then we can proceed in two ways. We can either set even more restrictive priorities concerning the position of the highest negative or highest positive power of the propagators, as Laporta proposes in his paper [38], or choose the integral with the simplest and better-factorised coefficient. This choice seems to work better since, when solving for the integral of the highest priority, we divide the entire expression with its coefficient.

5.2.2 Laporta Example

In order to demonstrate how the method works in practice, we present a very simple example. The integral we are interested in simplifying is the one-loop vertex diagram:



$$(5.3)$$

In terms of the notation initiated in subsection 5.2.1 this vertex integral can be written as $\mathcal{J}_{2D}(1, 1, 1, 0, s_{12})$. We must note that, since we are dealing with a

one-loop diagram, our Auxiliary Integral has only four propagators, the first four ($[A_1, A_2, A_3, A_4]$) of the two-loop planar Auxiliary Integral of eq (4.7). In our example A_1, A_2 and A_3 are the denominators and A_4 is the numerator. Therefore the input to the algorithm will be:

$$\begin{aligned}
 INPUT : \quad & [DenSet = [A_1, A_2, A_3] \\
 & MaxDen = 0 \\
 & MaxNum = 0 \\
 & SolutionSet = \{\} \} .
 \end{aligned} \tag{5.4}$$

The values of $MaxDen$ and $MaxNum$ were calculated, using the definitions of Md and Mp for the integral we want to calculate ($\mathcal{J}_{2D}(1, 1, 1, 0, s_{12})$):

$$\begin{aligned}
 MaxDen &= \sum_{i=1}^3 (\nu_i - 1) = (1 - 1) + (1 - 1) + (1 - 1) = 0 , \\
 MaxNum &= \sum_{i=4}^4 (\nu_i) = 0 .
 \end{aligned} \tag{5.5}$$

If at the end of the algorithm, $\mathcal{J}_{2D}(1, 1, 1, 0, s_{12})$ is not solved for in the $SolutionSet$, we will have to re-run the algorithm using a more negative $MaxNum$ or a more positive $MaxDen$. The denominator set $DenSet$ was chosen to be $[A_1, A_2, A_3]$ because the three positive propagators of $\mathcal{J}_{2D}(1, 1, 1, 0, s_{12})$ are A_1, A_2 and A_3 . In the rest of this section we will skip the invariant scale s_{12} from the notation of the integral, i.e. $\mathcal{J}_{2D}(\nu_1, \nu_2, \nu_3, \nu_4, s_{12}) = J(\nu_1, \nu_2, \nu_3, \nu_4)$.

THE MAIN ALGORITHM

First we generate all possible combinations (within our $DenSet$) of integrals with n number of denominators, where n runs from $Nk + 1 = 1 + 1 = 2$ to $Nd = 3$. For $n = 3$ we have the original (input) integral $[A_1, A_2, A_3]$ and for $n = 2$ there are three combinations of propagators: $[A_1, A_2]$, $[A_1, A_3]$ and $[A_2, A_3]$. We notice straight away that integrals with denominators $[A_1, A_2]$ and $[A_2, A_3]$ vanish in CDR, since the square of the incoming momenta in both cases is zero. Their relevant diagrams would be:

$$\begin{array}{c}
 \begin{array}{ccc}
 \begin{array}{c} p_1 \\ \rightarrow \end{array} \text{---} \bigcirc \text{---} & \text{and} & \begin{array}{c} p_2 \\ \rightarrow \end{array} \text{---} \bigcirc \text{---} \\
 \end{array}
 \end{array} . \tag{5.6}$$

Integrals with only one propagator vanish as well. They correspond to this type of diagram:

$$\text{Diagram: a circle with an incoming arrow from the left and an outgoing arrow to the right.} \quad (5.7)$$

Therefore in the rest of the algorithm we set them equal to zero in advance. This way we save time and space in the computer program. The two topologies that survive in our example are the triangle integral with denominators $[A_1, A_2, A_3]$ and the bubble integral with denominators $[A_1, A_3]$, which correspond to the following diagrams respectively:

$$\text{Diagram: a triangle with an incoming arrow from the left labeled } p_{12} \text{ and two outgoing arrows labeled } p_1 \text{ and } p_2. \quad \text{and} \quad \text{Diagram: a circle with an incoming arrow from the left labeled } p_{12} \text{ and an outgoing arrow to the right.} \quad (5.8)$$

We put those integrals in a set:

$$\text{SetOfAllIntegrals} = \{[A_1, A_2, A_3], [A_1, A_3]\} . \quad (5.9)$$

Next we start the loop on n^1 .

1. $n = 2$ From the *SetOfAllIntegrals* eq (5.9) we take all the integrals with $n = 2$ and put them in a new set. Thus we get:

$$\text{SetWithnDen} = \{[A_1, A_3]\} . \quad (5.10)$$

After performing steps 4... 18 of the *Main Algorithm* we derive the following *SolutionSet*:

$$\begin{aligned} \text{SolutionSet} = & \\ & \{J(1, 0, 2, 0) = -\frac{(d-3)}{s_{12}} J(1, 0, 1, 0), \\ & J(1, -1, 2, 0) = -J(2, -1, 1, 0) + (d-2)J(1, 0, 1, 0), \\ & J(2, 0, 1, 0) = -\frac{(d-3)}{s_{12}} J(1, 0, 1, 0), \\ & J(1, 0, 2, -1) = -\frac{(-s_{12}d + 2s_{12} + s_{123}d - 3s_{123})}{s_{12}} J(1, 0, 1, 0) \\ & -J(2, 0, 1, -1)\} . \end{aligned} \quad (5.11)$$

¹A more detailed version of this example is illustrated in Appendix B.

2. $n = 3$ From the *SetOfAllIntegrals* eq. (5.9) we take all the integrals with $n = 3$ and put them in a new set getting:

$$\text{SetWithnDen} = \{[A_1, A_2, A_3]\} . \quad (5.12)$$

Once more, we recursively apply steps 4...18 and get our final *SolutionSet*:

$$\begin{aligned} \text{SolutionSet} = & \\ \{ & J(1, 1, 2, 0) = 2 \frac{(d-3)}{s_{12}^2} J(1, 0, 1, 0), \\ & J(1, 1, 1, 0) = -2 \frac{(d-3)}{s_{12}(d-4)} J(1, 0, 1, 0), \\ & J(2, 1, 1, 0) = 2 \frac{(d-3)}{s_{12}^2} J(1, 0, 1, 0), \\ & J(1, 0, 2, 0) = -\frac{(d-3)}{s_{12}} J(1, 0, 1, 0), \\ & J(1, -1, 2, 0) = -J(2, -1, 1, 0) + (d-2)J(1, 0, 1, 0), \\ & J(2, 0, 1, 0) = -\frac{(d-3)}{s_{12}} J(1, 0, 1, 0), \\ & J(1, 0, 2, -1) = -\frac{(-s_{12}d + 2s_{12} + s_{123}d - 3s_{123})}{s_{12}} J(1, 0, 1, 0) \\ & -J(2, 0, 1, -1), \\ & J(1, 1, 2, -1) = +2 \frac{(d-3)(-s_{12}d + s_{123}d - 4s_{123} + 3s_{12})}{s_{12}^2(d-4)} J(1, 0, 1, 0) \\ & -J(1, 2, 1, -1) - J(2, 1, 1, -1) \\ & +s_{23}J(1, 2, 1, 0)\} . \end{aligned} \quad (5.13)$$

At this point all the recursive loops terminate and our output is what is left in the *SolutionSet*. Therefore:

$$\text{OUTPUT} = \text{SolutionSet} . \quad (5.14)$$

The second equation of the *SolutionSet* eq (5.13) is the one that gives the integral ($J(1, 1, 1, 0)$) we wanted in terms of other simpler integrals, in this case a two

propagator bubble diagram ($J(1, 0, 1, 0)$):

$$\begin{aligned}
 J(1, 1, 1, 0) &= -2 \frac{(d-3)}{s_{12}(d-4)} J(1, 0, 1, 0), \\
 \begin{array}{c} \text{Diagram 1: A triangle with an incoming line from the left labeled } p_{12} \text{ and two outgoing lines to the right labeled } p_1 \text{ and } p_2. \end{array} &= -2 \frac{(d-3)}{s_{12}(d-4)} \begin{array}{c} \text{Diagram 2: A circle with an incoming line from the left labeled } p_{12} \text{ and an outgoing line to the right.} \end{array}.
 \end{aligned}
 \tag{5.15}$$

Note that apart from the integral we were interested in, we found relations that simplify a number of other integrals. In two-loop physical processes, the calculation of the seven-propagator integrals with the Laporta algorithm, results in the calculation of all needed integrals with less number of propagators. This is a highly welcome bonus, since it reduces significantly the number of times we have to apply the algorithm.

Chapter 6

Differential Equations

6.1 Introduction

In chapter 5 we presented an algorithm that, by solving a big set of Integration By Parts (IBP) identities, allows all possible integrals, which can appear in an actual calculation, to be written in terms of a small number of Master Integrals (MI). Use of these identities, however, can not reduce the Master Integrals any further (after all, this is the definition of a Master Integral). Thus MI's have to be computed using a different method. Several methods have been successfully used toward the calculation of two-loop MI's, such as for example, the Negative Dimensions approach [53] and the Mellin Barnes method [54, 55]. In both methods, analytic computation of MI's, involves some form of explicit integration over the loop momenta. The differential equations method, which will be presented in detail throughout this chapter, is a method for the analytic calculation of MI's without application of any loop momenta integrations. The method was first presented by Kotikov [56], as a method of relating loop integrals with internal massive propagators, to loop integrals with massless internal propagators. Kotikov used differential equations on the internal masses. The method was embroidered in [57, 58], where differential equations on the external momenta were derived and solved. First applications appeared in [59]. Finally, in a series of papers Gehrmann and Remiddi [42, 43], derived and solved differential equations on the external scales of all, two and three scale, two-loop

Master Integrals, with massless propagators, for the off-shell case. As we have already pointed out in this thesis, this is the set of Master Integrals that we need for two-loop calculations of the physical processes $H \rightarrow ggg$, $H \rightarrow gq\bar{q}$ and $\gamma^* \rightarrow gq\bar{q}$. In section 6.2 we demonstrate how differential equations on the external scales are derived and in section 6.3 we explain the basic techniques for solving them. The method is displayed in detail using the MI Dart₂ (eq. 4.52) as an example.

6.2 Generating Differential Equations (DE's)

6.2.1 Method for Generation of Differential Equations

Our aim is to derive differential equations in the external scales for the Master Integrals. In the case of four-point functions with three external legs on-shell, one external leg off-shell and massless propagators, there are only three independent scales (s_{12}, s_{13}, s_{23}), resulting in three differential equations.

As it is not possible to differentiate straight away with respect to external scales, we can use relation:

$$\frac{\partial}{\partial p_i^\mu} = \sum_j 2(p_{i\mu} + p_{j\mu}) \frac{\partial}{\partial s_{ij}}, \quad (6.1)$$

to express derivatives in the invariant scales $s_{ij} = (p_i + p_j)^2$, in terms of derivatives in the external momenta p_1, p_2, p_3 :

$$s_{12} \frac{\partial}{\partial s_{12}} = \frac{1}{2} \left(+p_1^\mu \frac{\partial}{\partial p_1^\mu} + p_2^\mu \frac{\partial}{\partial p_2^\mu} - p_3^\mu \frac{\partial}{\partial p_3^\mu} \right), \quad (6.2)$$

$$s_{23} \frac{\partial}{\partial s_{23}} = \frac{1}{2} \left(-p_1^\mu \frac{\partial}{\partial p_1^\mu} + p_2^\mu \frac{\partial}{\partial p_2^\mu} + p_3^\mu \frac{\partial}{\partial p_3^\mu} \right), \quad (6.3)$$

$$s_{13} \frac{\partial}{\partial s_{13}} = \frac{1}{2} \left(+p_1^\mu \frac{\partial}{\partial p_1^\mu} - p_2^\mu \frac{\partial}{\partial p_2^\mu} + p_3^\mu \frac{\partial}{\partial p_3^\mu} \right). \quad (6.4)$$

Acting with the right hand side of these equations on a MI and interchanging derivation and integration, one would produce a relationship which contains a set of integrals similar to the ones derived from the IBP identities.

Suppose now that we have an integral $\mathcal{J}_{t,r,s}(s_{12}, s_{23}, s_{13}, D)$ where:

$$r = Md, \quad s = Mp, \quad t = Nd, \quad (6.5)$$

with Mp , Md defined in equations (5.1), (5.2) and Nd is the number of propagators in the denominator of integral $\mathcal{J}_{t,r,s}$.

Equations (6.2), (6.3) and (6.4), when applied on $\mathcal{J}_{t,r,s}(s_{12}, s_{23}, s_{13}, D)$, are not linearly independent, but are related through the scaling identity:

$$\mathcal{J}_{t,r,s}(s_{12}, s_{23}, s_{13}, D) = \lambda^{-\alpha(D,r,s)} \mathcal{J}_{t,r,s}(\lambda^2 s_{12}, \lambda^2 s_{23}, \lambda^2 s_{13}, D), \quad (6.6)$$

which is the result of the properties of integral $\mathcal{J}_{t,r,s}$ under rescaling of all external momenta:

$$\left. \begin{array}{l} p_1^\mu \longrightarrow \lambda p_1^\mu \\ p_2^\mu \longrightarrow \lambda p_2^\mu \\ p_3^\mu \longrightarrow \lambda p_3^\mu \end{array} \right\} \longrightarrow \begin{array}{l} s_{12} \longrightarrow \lambda^2 s_{12}, \\ s_{23} \longrightarrow \lambda^2 s_{23}, \\ s_{13} \longrightarrow \lambda^2 s_{13}. \end{array} \quad (6.7)$$

$\alpha(D, r, s)$ is the mass dimension of the integral and, for an m -loop integral in D space-time dimensions, is given by:

$$\alpha(D, r, s) = mD + 2s - 2r, \quad (6.8)$$

where r and s were defined in eq (6.5). Thus the scaling equation reads:

$$\left(-\frac{\alpha}{2} + s_{12} \frac{\partial}{\partial s_{12}} + s_{23} \frac{\partial}{\partial s_{23}} + s_{13} \frac{\partial}{\partial s_{13}} \right) \mathcal{J}_{t,r,s}(s_{12}, s_{23}, s_{13}, D) = 0. \quad (6.9)$$

In practice, we are principally interested in obtaining the differential equation with respect to scale $M^2 = s_{123} = (p_1 + p_2 + p_3)^2$. Therefore, we change to a new set of variables, namely: $M^2 = s_{123} = s_{12} + s_{23} + s_{13}$, $S = s_{12}$ and $T = s_{23}$. Consequently, the set of differential equations becomes:

$$\begin{aligned} \frac{\partial}{\partial S} &= \frac{\partial}{\partial s_{12}} - \frac{\partial}{\partial s_{13}}, \\ \frac{\partial}{\partial T} &= \frac{\partial}{\partial s_{23}} - \frac{\partial}{\partial s_{13}}, \\ \frac{\partial}{\partial M^2} &= \frac{\partial}{\partial s_{13}}. \end{aligned} \quad (6.10)$$

6.2.2 Differential Equations for the General Auxiliary Planar Integral

Applying eq. (6.10) on the General Auxiliary Planar Integral (eq. 4.4) we get the following set of differential equations:

$$\begin{aligned}
\frac{\partial}{\partial s_{123}} &= \frac{1}{s_{123}-s_{12}-s_{23}} \left(\mathbf{8}^+ \mathbf{7}^- \nu_8 + \mathbf{1}^+ \mathbf{2}^- \nu_1 + \mathbf{5}^+ \mathbf{6}^- \nu_5 + \mathbf{4}^+ \mathbf{3}^- \nu_4 + \nu_2 + \nu_3 - D + \nu_9 + \nu_6 + \nu_7 \right) \\
\frac{\partial}{\partial s_{23}} &= \frac{1}{s_{23}} \left(-\mathbf{1}^+ \mathbf{2}^- \nu_1 - \mathbf{5}^+ \mathbf{6}^- \nu_5 - \nu_2 - \nu_3 + D - \nu_9 - \nu_4 - \nu_6 - \nu_7 - \nu_8 \right) \\
&\quad - \frac{1}{s_{123}-s_{12}-s_{23}} \left(\mathbf{8}^+ \mathbf{7}^- \nu_8 + \mathbf{1}^+ \mathbf{2}^- \nu_1 + \mathbf{5}^+ \mathbf{6}^- \nu_5 + \mathbf{4}^+ \mathbf{3}^- \nu_4 + \nu_2 + \nu_3 - D + \nu_9 + \nu_6 + \nu_7 \right) \\
\frac{\partial}{\partial s_{12}} &= \frac{1}{s_{12}} \left(-\mathbf{8}^+ \mathbf{7}^- \nu_8 - \mathbf{4}^+ \mathbf{3}^- \nu_4 - \nu_1 - \nu_2 - \nu_3 + D - \nu_9 - \nu_5 - \nu_6 - \nu_7 \right) \\
&\quad - \frac{1}{s_{123}-s_{12}-s_{23}} \left(\mathbf{8}^+ \mathbf{7}^- \nu_8 + \mathbf{1}^+ \mathbf{2}^- \nu_1 + \mathbf{5}^+ \mathbf{6}^- \nu_5 + \mathbf{4}^+ \mathbf{3}^- \nu_4 + \nu_2 + \nu_3 - D + \nu_9 + \nu_6 + \nu_7 \right)
\end{aligned} \tag{6.11}$$

where we have used the ten IBP identities (eq. 4.22) to simplify the format of the equations. One can trivially see, without having to perform reductions to MI, that eq. (6.11) satisfy the scaling equation (6.9). We get similar forms of differential equations if we apply eq. (6.10) on the General Non-Planar Auxiliary Integrals eqs. (4.5 and 4.6).

The righthand side of eqs. (6.11) consists of the Master Integral we are interested in calculating, and of integrals of the form: $\mathbf{5}^+ \mathbf{6}^-$, $\mathbf{8}^+ \mathbf{7}^-$, $\mathbf{4}^+ \mathbf{3}^-$ and $\mathbf{1}^+ \mathbf{2}^-$. With use of the algorithm of section 5.2.1, we can turn these integrals into MI's of the same topology, or topologies with less propagators, whose analytic expansions in ϵ have already been calculated.

6.3 Solving DE's: The Gehrmann-Remiddi Method

In the previous section we demonstrated one method of producing differential equations in the external momenta. In this section we will present the techniques used by Gehrmann and Remiddi in [43] when they solved differential equations for all MI's, with two or three scales, that could appear in the reduction of planar and non-planar

four-point functions with one external leg off-shell. All Master Integrals were written as Laurent series around $\epsilon = 0$, in terms of one and two dimensional Harmonic Polylogarithms (HPL and 2DHPL), and the external invariant scales: s_{12}, s_{23} and s_{123} .

Notice, however, that not every Master Integral (MI) depends on all three invariant scales, but on certain one or two scale combinations. There are some MI's which depend on only one scale:

$$\begin{aligned}
 \text{Sunrise}(s_{12}) &= \text{Diagram 1} , \\
 \text{Glass}(s_{12}) &= \text{Diagram 2} , \\
 \text{Dart}_1(s_{12}) &= \text{Diagram 3} , \\
 \text{Xtri}_1(s_{12}) &= \text{Diagram 4} .
 \end{aligned}$$

The only non-trivial differential equations these integrals satisfy are homogeneous equations in s_{12} , thus they can not be calculated using the differential equations method. Nevertheless, computing these MI's is a relatively simple task, that can be performed using Feynman parameters [60,61]. Integrals that depend on two or three external invariant scales, fulfill one or two in-homogeneous differential equations respectively, on top of the homogeneous re-scaling one. Therefore all these MI's can be solved using the Gehrmann-Remiddi method. In the rest of this section we will demonstrate, in brief, the basic steps involved in solving differential equations as they were initiated in [43].

First we obtain the set of differential equations in the external scales and express it in terms of the variables: $s_{123} = s_{12} + s_{23} + s_{13}$, $X = s_{12}/s_{123}$ and $Y = s_{23}/s_{123}$. We end up having a homogeneous equation in s_{123} , which is the re-scaling equation, and two in-homogeneous equations in X and Y . In the latter, the coefficient of the homogeneous term and the entire in-homogeneous term (the known sub-topologies and their coefficients) are expanded as a series in ϵ . The Master Integral under consideration can be written as the sum of terms, each equal to a pre-factor times a

combination of HPL's and 2DHPL's multiplied by simple coefficients. Thus we use the following ansatz:

$$\sum_i \mathcal{R}_i(Y, X, s_{123}, \epsilon) \mathcal{H}_i(Y, X, \epsilon) \quad , \quad (6.12)$$

where $\mathcal{R}_i(Y, X, s_{123}, \epsilon)$ is the pre-factor (a rational function of X and Y multiplied by a normalization factor) and $\mathcal{H}_i(Y, X, \epsilon)$ is a Laurent series in ϵ :

$$\mathcal{H}_i(Y, X, \epsilon) = \frac{\epsilon^p}{\epsilon^4} \sum_{n=0}^4 \epsilon^n \left(T_n(Y) + \sum_{j=1}^n \sum_{m_j \in V_j(Y)} T_{n, \vec{m}_j}(Y) H(\vec{m}_j; X) \right). \quad (6.13)$$

When a topology has only one MI then there is only one pre-factor $\mathcal{R}(Y, X, s_{123}, \epsilon)$ and there is no need for the sum in (6.12). When a topology has two MI's then there are only two terms in the sum (6.12) for each MI¹. Let us now study in detail the components of this formula (6.13). $H(\vec{m}_j; X)$ are 2DHPL's of weight determined by the order of the Laurent series. Coefficients $T_n(Y), T_{n, \vec{m}_j}(Y)$, which can contain ordinary HPL's and depend only on Y , are left to be calculated. The deepest allowed pole of the series is taken to be $1/\epsilon^4$, as it was predicted by Catani in [12]. However, some of the MI's may have superficial degree of divergence smaller than 4. This cannot be known before hand, therefore p is used to include this possibility. $V_j(Y)$ is a set with members all possible permutations of j elements from the set $(0, 1, Y, 1 - Y)$, depending only on scale Y . This set comprises all possible indices for 2DHPL's of weight j . When the MI under consideration depends only on one scale, then the V_j 's do not depend on Y and are j -dimensional permutations of $(0, 1)$.

To summarize, what remains to be calculated are the coefficients $T_n(Y), T_{n, \vec{m}_j}(Y)$ and the pre-factors $\mathcal{R}_i(Y, X, s_{123}, \epsilon)$. Determination of factors $\mathcal{R}_i(Y, X, s_{123}, \epsilon)$ can be carried out from the homogeneous part of the differential equations in X and Y , by inserting in them only the leading singularity term ($n = 0$) of $\mathcal{H}_i(Y, X, \epsilon)$. Having determined pre-factors $\mathcal{R}_i(Y, X, s_{123}, \epsilon)$, we substitute the ansatz (6.12), in the DE in X , getting an X differential equation for the Laurent series $\mathcal{H}_i(Y, X, \epsilon)$. Consequently, we substitute 6.13 in the DE to end up with a relation that has X

¹For this to happen the two MI's must be appropriately chosen as will be explained later in this section.

derivatives of 2DHPL. However, by definition the weight 1 and weight j 2DHPL's satisfy the following relations respectively:

$$\begin{aligned} \frac{d}{dX}H(m; X) &= f(m, X) , \\ \frac{d}{dX}H\left(m, \vec{m}_{j-1}; X\right) &= f(m, X)H\left(\vec{m}_{j-1}; X\right) , \end{aligned} \quad (6.14)$$

where $f(m, X)$ are the X -dependent factors:

$1/X, 1/(1-X), 1/(Y+X)$ and $1/(1-Y-X)$,

present in the DE. Thus, all derivatives disappear and we are left with a purely algebraic equation. If in this equation we group the coefficients of $1/X, 1/(1-X), 1/(Y+X)$ and $1/(1-Y-X)$ and use the linear independence of the base of $H\left(\vec{m}_j; X\right)$, we can derive a linear system of equations from which one can determine all the wanted $T_{n, \vec{m}_j}(Y)$. The factors $T_n(Y)$ can not be calculated from this system because they do not multiply any X -dependent factors in eq. 6.13. These terms are evaluated by calculating the MI's at a boundary condition.

In the case of planar MI's², one can use their property of being regular in the entire kinematic plane, apart from the two branch points $X = 0$ and $Y = 0$. As a result, any of the denominators $(1-X), (Y+X)$ and $(1-Y-X)$ of the homogeneous part of the DE can be used to calculate a boundary condition at $X = 1, X = -Y$ and $X = 1 - Y$ respectively. This can be achieved by multiplying the DE with one of these factors, that appears in the homogeneous part, and taking the X limit where that factor vanishes. This will 'kill' all terms, including all derivatives, apart from the ones that had the multiplying factor in the denominator and we will end up calculating the MI, at this kinematic point, in terms of its sub-topologies.

When the topology has two MI's, one has to derive DE's in X and Y for both integrals, which now have two terms each in the ansatz (6.12). Therefore one needs to calculate two pre-factors $\mathcal{R}_i(Y, X, s_{123}, \epsilon)$ for each MI. This can be achieved by choosing the Master Integrals in a way that the equations de-couple when one expands the coefficients of the homogeneous part of the DE, and takes the lowest

²The case of boundary conditions for the non planar MI's is more complicated and will not be presented here.

If we apply equations (6.16), (6.17) and (6.18) on integral $J(1, 0, 0, 1, 0, 0, 1, 0, 1)$, we get:

$$\begin{aligned}
\frac{\partial J(1, 0, 0, 1, 0, 0, 1, 0, 1)}{\partial s_{123}} &= \frac{J(2, -1, 0, 1, 0, 0, 1, 0, 1)}{s_{123} - s_{12} - s_{23}} + \\
&\quad \frac{J(1, 0, -1, 2, 0, 0, 1, 0, 1)}{s_{123} - s_{12} - s_{23}} + \frac{(2 - \mathcal{D}) J(1, 0, 0, 1, 0, 0, 1, 0, 1)}{s_{123} - s_{12} - s_{23}}, \\
\frac{\partial J(1, 0, 0, 1, 0, 0, 1, 0, 1)}{\partial s_{23}} &= -\frac{J(2, -1, 0, 1, 0, 0, 1, 0, 1)}{s_{123} - s_{12} - s_{23}} - \\
&\quad \frac{J(1, 0, -1, 2, 0, 0, 1, 0, 1)}{s_{123} - s_{12} - s_{23}} - \frac{(2 - \mathcal{D}) J(1, 0, 0, 1, 0, 0, 1, 0, 1)}{s_{123} - s_{12} - s_{23}} - \\
&\quad \frac{J(2, -1, 0, 1, 0, 0, 1, 0, 1)}{s_{23}} - \frac{(3 - \mathcal{D}) J(1, 0, 0, 1, 0, 0, 1, 0, 1)}{s_{23}}, \\
\frac{\partial J(1, 0, 0, 1, 0, 0, 1, 0, 1)}{\partial s_{12}} &= -\frac{J(2, -1, 0, 1, 0, 0, 1, 0, 1)}{s_{123} - s_{12} - s_{23}} - \\
&\quad \frac{J(1, 0, -1, 2, 0, 0, 1, 0, 1)}{s_{123} - s_{12} - s_{23}} - \frac{(2 - \mathcal{D}) J(1, 0, 0, 1, 0, 0, 1, 0, 1)}{s_{123} - s_{12} - s_{23}} - \\
&\quad \frac{J(1, 0, -1, 2, 0, 0, 1, 0, 1)}{s_{12}} - \frac{(3 - \mathcal{D}) J(1, 0, 0, 1, 0, 0, 1, 0, 1)}{s_{12}}.
\end{aligned} \tag{6.19}$$

All the integrals on the right-hand side can be written in terms of Master Integrals with use of the Laporta reduction algorithm presented in subsection 5.2.1. Subsequently, the three differential equations take the form:

$$\begin{aligned}
\frac{\partial J(1, 0, 0, 1, 0, 0, 1, 0, 1)}{\partial s_{123}} &= \frac{1}{2} \frac{(-4 + D)(2s_{123} - s_{12})}{s_{123}(s_{123} - s_{12})} J(1, 0, 0, 1, 0, 0, 1, 0, 1) \\
&\quad - \frac{1}{2} \frac{(-8 + 3D)}{s_{123}(s_{123} - s_{12})} J(1, 0, 0, 0, 0, 0, 1, 0, 1), \tag{6.20}
\end{aligned}$$

$$\frac{\partial J(1, 0, 0, 1, 0, 0, 1, 0, 1)}{\partial s_{23}} = 0, \tag{6.21}$$

$$\begin{aligned}
\frac{\partial J(1, 0, 0, 1, 0, 0, 1, 0, 1)}{\partial s_{12}} &= -\frac{1}{2} \frac{(-4 + D)}{s_{123} - s_{12}} J(1, 0, 0, 1, 0, 0, 1, 0, 1) + \\
&\quad \frac{1}{2} \frac{(-8 + 3D)}{(s_{123} - s_{12})s_{12}} J(1, 0, 0, 0, 0, 0, 1, 0, 1). \tag{6.22}
\end{aligned}$$

We should note here, that equations (6.20), (6.21) and (6.22), have no dependence on scale s_{23} . This could be expected, as in eq. (6.15) we see that Dart₂ depends only on scales s_{12} and s_{123} . In this example, we will solve the differential equation on scale s_{12} (eq. 6.22). It is more convenient for our purposes to perform the substitution:

$s_{12} \rightarrow X s_{123}$. This way, our result will depend on s_{123} and on ratio $X \left(= \frac{s_{12}}{s_{123}} \right)$.

Written in terms of X equation (6.22) takes the form:

$$\begin{aligned} \frac{\partial \text{Dart}_2(X, s_{123})}{\partial X} &= -\frac{\epsilon}{-1+X} \text{Dart}_2(X, s_{123}) \\ &\quad + \frac{(-2+3\epsilon)}{s_{123}(-1+X)X} \text{Suns}(X s_{123}) , \\ \frac{\partial \text{Dart}_2(X, s_{123})}{\partial s_{123}} &= -\frac{\epsilon(-2+X)}{s_{123}(-1+X)} \text{Dart}_2(X, s_{123}) \\ &\quad - \frac{(-2+3\epsilon)}{s_{123}^2(-1+X)} \text{Suns}(X s_{123}) , \end{aligned} \quad (6.23)$$

where we have also trivially substituted:

$$\begin{aligned} D &= 4 - 2\epsilon , \\ J(1, 0, 0, 0, 0, 0, 1, 0, 1) &= \text{Suns}(s_{12}) , \\ J(1, 0, 0, 1, 0, 0, 1, 0, 1) &= \text{Dart}_2(s_{12}, s_{123}) . \end{aligned} \quad (6.24)$$

It is straight forward to see that the above equations (6.23) satisfy the scaling equation (6.9).

What we need to know before hand.

According to the methodology presented in subsection (6.3), in order to solve a differential equation, we need the ϵ expansion of the ‘pinching’ Master Integrals (here the $\text{Suns}(X s_{123})$):

$$\begin{aligned} \text{Suns}(X s_{123}) &= \text{FAC}(\epsilon) (-X s_{123})^{1-2\epsilon} \left[-\frac{1}{4} \epsilon^{-1} - \frac{13}{8} - \frac{115}{16} \epsilon - \right. \\ &\quad \left. \left(\frac{865}{32} - \frac{3}{2} \zeta(3) \right) \epsilon^2 - \left(\frac{5971}{64} - \frac{39}{4} \zeta(3) - \frac{\pi^4}{40} \right) \epsilon^3 + \mathcal{O}(\epsilon^4) \right] . \end{aligned} \quad (6.25)$$

The factor FAC that appears in eq. (6.25) is given by:

$$\begin{aligned} \text{FAC}(\epsilon) &= \left(\frac{\text{SE}(\epsilon)}{16\pi^2} \right)^2 , \quad \text{with} \\ \text{SE}(\epsilon) &= \frac{(4\pi)^\epsilon \Gamma(1+\epsilon) (\Gamma(1-\epsilon))^2}{\Gamma(1-2\epsilon)} . \end{aligned} \quad (6.26)$$

In addition an initial condition is required, which, in our case, is the ϵ expansion of the Master Integral we are interested in, at the limit $X = 0$. It is easy to see,

comparing the diagrams which correspond to Master Integrals in subsection 4.5.2, that in the limit $X = 0$:

$$\text{Dart}_2(s_{12}, s_{123}) \xrightarrow{X \rightarrow 0} \text{Dart}_1(s_{123}) ,$$

with:

$$\begin{aligned} \text{Dart}_1(s_{123}) = & \text{FAC}(\epsilon) (-s_{123})^{-2\epsilon} \left[-\frac{1}{2}\epsilon^{-2} - \frac{5}{2}\epsilon^{-1} - \frac{19}{2} - \frac{\pi^2}{6} - \right. \\ & \left. \left(\frac{65}{2} + \frac{5}{6}\pi^2 - 2\zeta(3) \right) \epsilon - \left(\frac{211}{2} + \frac{19}{6}\pi^2 - 10\zeta(3) \right) \epsilon^2 + \mathcal{O}(\epsilon^3) \right] \end{aligned} \quad (6.27)$$

Solving the differential equation.

First we calculate the pre-factor $\mathcal{R}_i(X, s_{123}, \epsilon)$, as demonstrated in section 6.3, from the homogeneous part of the differential equation (6.23),

$$\frac{\partial \text{Dart}_2(X, s_{123})}{\partial X} = \frac{\epsilon}{1-X} \text{Dart}_2(X, s_{123}) \quad (6.28)$$

and get (using the initial condition from the expansion of Dart_1 : $\mathcal{R}_i(0, s_{123}, \epsilon) = \text{FAC}(\epsilon) (-s_{123})^{-2\epsilon}$ (eq. 6.27)):

$$\mathcal{R}(X, s_{123}, \epsilon) = \text{FAC}(\epsilon) (-s_{123})^{-2\epsilon} . \quad (6.29)$$

Note that there is only one pre-factor $\mathcal{R}(X, s_{123}, \epsilon)$, since the topology has only one master integral. Next we define $\mathcal{H}(X, \epsilon)$ as a Laurent series in ϵ , with coefficients of ϵ written as the sum of 2DHPL's. In our example, p of eq. (6.13) is 2, from the requirement that the order of the Laurent series of the in-homogeneous term of the differential equation (6.23), matches the Laurent series of the master integral. For the deepest pole in the series we get:

$$\begin{aligned} -\epsilon \text{Dart}_2(X, s_{123}) &= \text{Suns}(X \cdot s_{123}) \Rightarrow \\ \frac{\epsilon^p}{\epsilon^4} &= \frac{1}{\epsilon^1} \Rightarrow \\ p &= 2 \end{aligned} \quad (6.30)$$

\mathcal{V}_j is the set of all possible indices for 2DHPL's of weight j (j -dimensional vectors made from all possible combinations of the set: $(0, 1)$). Here, we must stress that, in this example, \mathcal{V}_j has no dependence on a massive scale, as the differential equations depend on only two and not three massive scales. Therefore, for example:

$$\begin{aligned}\mathcal{V}_1 &= \{(0), (1)\}, \\ \mathcal{V}_2 &= \{(0, 0), (0, 1), (1, 0), (1, 1)\}, \\ &\dots\end{aligned}$$

The expression for $\mathcal{H}(X, \epsilon)$ (eq. 6.13), becomes:

$$\begin{aligned}\mathcal{H}(X, \epsilon) &= \frac{1}{\epsilon^2} \{ \epsilon^0 T_0 \\ &+ \epsilon^1 [T_1 + T_{1,(0)} \mathbf{H}(0; X) + T_{1,(1)} \mathbf{H}(1; X)] \\ &+ \epsilon^2 [T_2 + T_{2,(0)} \mathbf{H}(0; X) + T_{2,(1)} \mathbf{H}(1; X) + T_{2,(0,0)} \mathbf{H}(0, 0; X) \\ &+ T_{2,(0,1)} \mathbf{H}(0, 1; X) + T_{2,(1,0)} \mathbf{H}(1, 0; X) + T_{2,(1,1)} \mathbf{H}(1, 1; X)] \\ &+ \epsilon^3 [T_3 + T_{3,(0)} \mathbf{H}(0; X) + T_{3,(1)} \mathbf{H}(1; X) + T_{3,(0,0)} \mathbf{H}(0, 0; X) \\ &+ T_{3,(0,1)} \mathbf{H}(0, 1; X) + T_{3,(1,0)} \mathbf{H}(1, 0; X) + T_{3,(1,1)} \mathbf{H}(1, 1; X) \\ &+ T_{3,(0,0,0)} \mathbf{H}(0, 0, 0; X) + T_{3,(1,0,0)} \mathbf{H}(1, 0, 0; X) \\ &+ \dots + T_{3,(1,1,1)} \mathbf{H}(1, 1, 1; X)] \\ &+ \epsilon^4 [T_4 + T_{4,(0)} \mathbf{H}(0; X) + \dots + T_{4,(1,1,1,1)} \mathbf{H}(1, 1, 1, 1; X)] \} .\end{aligned}\tag{6.31}$$

The final step of the calculation is concentrated on the evaluation of the coefficients T_{n, \vec{m}_j} . The terms T_0, T_1, T_2, T_3 and T_4 , which are by definition not multiplied by any

X -dependent functions, correspond to the boundary conditions of equation (6.27):

$$\begin{aligned}
 T_0 &= -\frac{1}{2}, \\
 T_1 &= -\frac{5}{2}, \\
 T_2 &= -\frac{19}{2} - \frac{\pi^2}{6}, \\
 T_3 &= -\left(\frac{65}{2} + \frac{5}{6}\pi^2 - 2\zeta(3)\right), \\
 T_4 &= -\left(\frac{211}{2} + \frac{19}{6}\pi^2 - 10\zeta(3)\right).
 \end{aligned}
 \tag{6.32}$$

Inserting the right-hand side of equation (6.31) in the differential equation (6.23) and using the identities (eq. 6.14) that lie in the definition of the 2DHPL we get a purely algebraic equation, which, after substituting T_0, T_1, T_2, T_3 and T_4 from (eq. 6.32), becomes (up to the finite term, $\mathcal{O}(\epsilon^0)$):

$$\begin{aligned}
 0 &= \frac{1}{\epsilon} \left[-\frac{1}{(-1+X)X} T_{1,(0)} + \frac{1}{(-1+X)} T_{1,(0)} - \frac{1}{(-1+X)} T_{1,(1)} \right] + \\
 &H(0; X) \left\{ -\frac{1}{(-1+X)X} T_{2,(0,0)} + \frac{1}{(-1+X)} T_{2,(0,0)} - \frac{1}{(-1+X)} T_{2,(1,0)} \right. \\
 &\quad \left. - \frac{1}{(-1+X)} + \frac{1}{(-1+X)} T_{1,(0)} \right\} + \\
 &H(1; X) \left\{ -\frac{1}{(-1+X)X} T_{2,(0,1)} + \frac{1}{(-1+X)} T_{2,(0,1)} + \right. \\
 &\quad \left. \frac{1}{(-1+X)} T_{1,(1)} - \frac{1}{(-1+X)} T_{2,(1,1)} \right\} + \\
 &2 \frac{\ln(-M)}{(-1+X)} T_{1,(1)} + \frac{1}{(-1+X)} T_{2,(0)} - \frac{1}{(-1+X)} T_{2,(1)} + \\
 &2 \frac{\ln(-M)}{(-1+X)X} T_{1,(0)} - \frac{1}{(-1+X)X} T_{2,(0)} - 2 \frac{\ln(-M)}{(-1+X)} T_{1,(0)} \\
 &+ \mathcal{O}(\epsilon^1).
 \end{aligned}
 \tag{6.33}$$

All we have to do now is create a system of equations by, first grouping the different powers of ϵ , 2DHPL and then the inverse powers of X and $(-1+X)$. Thus from the

coefficient of $1/\epsilon$ we get two equations:

$$\begin{aligned} 0 &= T_{1,(0)} , \\ 0 &= T_{1,(1)} - T_{1,(0)} , \end{aligned} \tag{6.34}$$

and from the coefficients of $H(0; X)$ and $H(1; X)$:

$$\begin{aligned} 0 &= T_{2,(0,0)} , \\ 0 &= T_{2,(0,0)} - T_{2,(1,0)} - 1 + T_{1,(0)} , \\ 0 &= T_{2,(0,1)} , \\ 0 &= T_{2,(0,1)} + T_{1,(1)} - T_{2,(1,1)} , \end{aligned} \tag{6.35}$$

respectively. The relations derived from the rest of equation (6.33) up to $\mathcal{O}(\epsilon^0)$ are linearly dependent with equations (6.34) and (6.35). Solving this system we get:

$$\begin{aligned} T_{1,(0)} &= 0 , & T_{2,(1,0)} &= -1 , \\ T_{1,(1)} &= 0 , & T_{2,(0,1)} &= 0 , \\ T_{2,(0,0)} &= 0 , & T_{2,(1,1)} &= 0 . \end{aligned} \tag{6.36}$$

If in equation (6.33), we take all orders in ϵ , up to $\mathcal{O}(\epsilon^2)$ and solve the system for the coefficients T_{n,\vec{m}_j} , we get:

$$\begin{aligned}
T_{3,(1)} &= -\frac{\pi^2}{6}, & T_{4,(1,1)} &= -\frac{\pi^2}{6}, \\
T_{3,(1,0)} &= -5, & T_{4,(1,0,0)} &= +10, \\
T_{3,(1,0,0)} &= +2, & T_{4,(1,1,0)} &= -5, \\
T_{3,(1,1,0)} &= -1, & T_{4,(1,0,0,0)} &= -4, \\
T_{4,(1)} &= -\frac{5\pi^2}{6} - \zeta(3), & T_{4,(1,1,0,0)} &= +2, \\
T_{4,(1,0)} &= -19, & T_{4,(1,1,1,0)} &= -1.
\end{aligned} \tag{6.37}$$

The rest of the T_{n,\vec{m}_j} 's are zero. This result is in complete accordance with reference [43].

Chapter 7

The $\gamma^* \rightarrow q\bar{q}g$ Two-Loop Matrix Element

7.1 Introduction

Among jet observables, the three-jet production rate in electron–positron annihilation plays an outstanding role. The initial experimental observation of three-jet events at PETRA [62], in agreement with the theoretical prediction [63], provided first evidence for the gluon, and thus strong support for the theory of Quantum Chromodynamics (QCD). Subsequently the three-jet rate and related event shape observables were used for the precise determination of the QCD coupling constant α_s (see [64] for a review). Especially at LEP, three-jet observables were measured to a very high precision and the error on the extraction of α_s from these data is dominated by the uncertainty inherent in the theoretical next-to-leading order (NLO) calculation [44, 65–68] of the jet observables. The planned TESLA [69] linear e^+e^- collider will allow precision QCD studies at even higher energies than at LEP. Given the projected luminosity of TESLA, one again expects the experimental errors to be well below the uncertainty of the NLO calculation.

Related to $e^+e^- \rightarrow 3$ jets by crossing symmetry are $(2 + 1)$ -jet production in deep inelastic ep scattering and vector-boson-plus-jet production at hadron colliders. The experimental data from HERA on $ep \rightarrow (2 + 1)$ jets and related event shape

observables have already reached a level of precision demanding predictions beyond the present NLO accuracy; a further improvement on these data is expected soon from the HERA high luminosity programme. Similarly, vector-boson production at large transverse momentum is a classic test of QCD in hadron–hadron collisions and demands the theoretical prediction to be as precise as possible. In this case, it is also an important background in searches for new physics at the Tevatron and the LHC.

Besides its phenomenological importance, the three-jet rate has also served as a theoretical testing ground for the development of new techniques for higher order calculations in QCD: both the subtraction [65] and the phase-space slicing [66] methods for the extraction of infrared singularities from NLO real radiation processes were developed in the context of the first three-jet calculations. The systematic formulation of phase-space slicing [44] as well as the dipole subtraction [68] method were also first demonstrated for three-jet observables, before being applied to other processes. It is very likely that similar techniques at higher orders will first be developed in the context of jet production in e^+e^- annihilation, which in contrast to hadron–hadron collisions or electron–proton scattering does not pose the additional difficulty of the regularization of initial state singularities.

The calculation of next-to-next-to-leading order (NNLO), i.e. $\mathcal{O}(\alpha_s^3)$, corrections to the three-jet rate in e^+e^- annihilation has been considered as a highly important project for a long time [70]. In terms of matrix elements, it requires the computation of three contributions: the tree level $\gamma^* \rightarrow 5$ partons amplitudes [71–73], the one-loop corrections to the $\gamma^* \rightarrow 4$ partons amplitudes [74–77], and the two-loop (as well as the one-loop times one-loop) corrections to the $\gamma^* \rightarrow 3$ partons matrix elements. While the former two contributions have been known for some time already, the two-loop amplitudes have presented an obstacle that prevented further progress on this calculation up to now.

This calculation has now become tractable owing to various technical developments over the last three years. In particular, the systematic application of the methods presented in chapters 4 and 5 allowed the large number of Feynman in-

tegrals appearing in two-loop four-point matrix elements to be reduced to a small number of so-called master integrals (MI). The master integrals relevant in the context of the present work are massless four-point functions with three legs on-shell and one leg off-shell. Using the technique illustrated in chapter 6, the complete set of these integrals was computed in [43]. Earlier partial results had been presented in [85, 86].

In this chapter, we present the $\mathcal{O}(\alpha_s^3)$ corrections to the $\gamma^* \rightarrow q\bar{q}g$ matrix element [45]. At this order, two combinations of amplitudes contribute: the interference of two-loop and tree amplitudes and the self-interference of the one-loop amplitude. We work in conventional dimensional regularization [8–10], with $D = 4 - 2\epsilon$ space-time dimensions, where all external particles are D -dimensional. Ultraviolet renormalization is performed in the $\overline{\text{MS}}$ scheme. The infrared pole structure of the two-loop corrections to the $\gamma^* \rightarrow q\bar{q}g$ matrix element was predicted by Catani [12], using an infrared factorization formula. We confirm Catani's prediction with our explicit calculation, and we use the formalism introduced in [12] to present the infrared poles and the finite parts of the $\gamma^* \rightarrow q\bar{q}g$ matrix elements in a compact form.

The chapter is structured as follows. In Section 7.2, we define the notation and kinematics as they were used in [45]. Section 7.3 briefly summarizes the method we used to express the NNLO squared matrix element for $\gamma^* \rightarrow q\bar{q}g$ as a series in $\epsilon = 2 - D/2$. The result for the two-loop QCD contribution to the $\gamma^* \rightarrow q\bar{q}g$ matrix element, decomposed into infrared-divergent and infrared-finite parts according to the prescription derived in [12], is given in Section 7.4.

7.2 Notation

We consider the decay of a virtual photon into a quark–antiquark–gluon system:

$$\gamma^*(q) \longrightarrow q(p_1) + \bar{q}(p_2) + g(p_3). \quad (7.1)$$

The kinematics of this process is fully described by the invariants:

$$s_{12} = (p_1 + p_2)^2, \quad s_{13} = (p_1 + p_3)^2, \quad s_{23} = (p_2 + p_3)^2, \quad (7.2)$$

which fulfill:

$$q^2 = s_{12} + s_{13} + s_{23} \equiv s_{123}. \quad (7.3)$$

It is convenient to define the dimensionless invariants:

$$x = s_{12}/s_{123}, \quad y = s_{13}/s_{123}, \quad z = s_{23}/s_{123}, \quad (7.4)$$

with $x + y + z = 1$.

Our calculation is performed in conventional dimensional regularization [8–10] with $D = 4 - 2\epsilon$, and all external particle states are taken to be D -dimensional. Renormalization of ultraviolet divergences is performed in the $\overline{\text{MS}}$ scheme. The renormalized amplitude can be written as:

$$|\mathcal{M}\rangle = \sqrt{4\pi\alpha}e_q\sqrt{4\pi\alpha_s} \left[|\mathcal{M}^{(0)}\rangle + \left(\frac{\alpha_s}{2\pi}\right) |\mathcal{M}^{(1)}\rangle + \left(\frac{\alpha_s}{2\pi}\right)^2 |\mathcal{M}^{(2)}\rangle + \mathcal{O}(\alpha_s^3) \right], \quad (7.5)$$

where α denotes the electromagnetic coupling constant, e_q the quark charge, α_s the QCD coupling constant at the renormalization scale μ , and the $|\mathcal{M}^{(i)}\rangle$ are the i -loop contributions to the renormalized amplitude. They are vectors in colour space. The renormalized amplitudes are obtained as

$$\begin{aligned} |\mathcal{M}^{(0)}\rangle &= |\mathcal{M}^{(0),\text{un}}\rangle, \\ |\mathcal{M}^{(1)}\rangle &= S_\epsilon^{-1} |\mathcal{M}^{(1),\text{un}}\rangle - \frac{\beta_0}{2\epsilon} |\mathcal{M}^{(0),\text{un}}\rangle, \\ |\mathcal{M}^{(2)}\rangle &= S_\epsilon^{-2} |\mathcal{M}^{(2),\text{un}}\rangle - \frac{3\beta_0}{2\epsilon} S_\epsilon^{-1} |\mathcal{M}^{(1),\text{un}}\rangle - \left(\frac{\beta_1}{4\epsilon} - \frac{3\beta_0^2}{8\epsilon^2} \right) |\mathcal{M}^{(0),\text{un}}\rangle, \end{aligned} \quad (7.6)$$

where S_ϵ , β_0 and β_1 where defined in equation 1.16.

The squared amplitude, summed over spins, colours and quark flavours, is denoted by:

$$\langle \mathcal{M} | \mathcal{M} \rangle = \sum |\mathcal{M}(\gamma^* \rightarrow q\bar{q}g)|^2 = \mathcal{T}(x, y, z). \quad (7.7)$$

The perturbative expansion of $\mathcal{T}(x, y, z)$ at renormalization scale $\mu^2 = q^2 = s_{123}$

reads:

$$\begin{aligned} \mathcal{T}(x, y, z) = & 16\pi^2\alpha \sum_q e_q^2 \alpha_s(q^2) \left[\mathcal{T}^{(2)}(x, y, z) + \left(\frac{\alpha_s(q^2)}{2\pi} \right) \mathcal{T}^{(4)}(x, y, z) \right. \\ & \left. + \left(\frac{\alpha_s(q^2)}{2\pi} \right)^2 \mathcal{T}^{(6)}(x, y, z) + \mathcal{O}(\alpha_s^3(q^2)) \right], \end{aligned} \quad (7.8)$$

where:

$$\mathcal{T}^{(2)}(x, y, z) = \langle \mathcal{M}^{(0)} | \mathcal{M}^{(0)} \rangle = 4V(1-\epsilon) \left[(1-\epsilon) \left(\frac{y}{z} + \frac{z}{y} \right) + \frac{2(1-y-z) - 2\epsilon yz}{yz} \right] \quad (7.9)$$

$$\mathcal{T}^{(4)}(x, y, z) = \langle \mathcal{M}^{(0)} | \mathcal{M}^{(1)} \rangle + \langle \mathcal{M}^{(1)} | \mathcal{M}^{(0)} \rangle, \quad (7.10)$$

$$\mathcal{T}^{(6)}(x, y, z) = \langle \mathcal{M}^{(1)} | \mathcal{M}^{(1)} \rangle + \langle \mathcal{M}^{(0)} | \mathcal{M}^{(2)} \rangle + \langle \mathcal{M}^{(2)} | \mathcal{M}^{(0)} \rangle, \quad (7.11)$$

where $V = N^2 - 1$, with N the number of colours. $\mathcal{T}^{(4)}(x, y, z)$ was first derived in [65, 66]; we quote an explicit expression for it in Section 7.4.1. In the following, we present the contribution to $\mathcal{T}^{(6)}(x, y, z)$ from the interference of two-loop and tree diagrams:

$$\mathcal{T}^{(6, [2 \times 0])}(x, y, z) = \langle \mathcal{M}^{(0)} | \mathcal{M}^{(2)} \rangle + \langle \mathcal{M}^{(2)} | \mathcal{M}^{(0)} \rangle, \quad (7.12)$$

as well as the one-loop self-interference:

$$\mathcal{T}^{(6, [1 \times 1])}(x, y, z) = \langle \mathcal{M}^{(1)} | \mathcal{M}^{(1)} \rangle. \quad (7.13)$$

At the same order in α_s , one finds also a contribution to three-jet final states from the self-interference of the $\gamma^* \rightarrow ggg$ amplitude. The matrix element for this process does not contain infrared or ultraviolet divergences; it was computed long ago and can be found in [89, 90].

For the remainder of this chapter we will set the renormalization scale $\mu^2 = q^2$. The full scale dependence of the perturbative expansion is given by:

$$\begin{aligned} \mathcal{T}(x, y, z) = & 16\pi^2\alpha \sum_q e_q^2 \alpha_s(\mu^2) \left\{ \mathcal{T}^{(2)}(x, y, z) \right. \\ & + \left(\frac{\alpha_s(\mu^2)}{2\pi} \right) \left[\mathcal{T}^{(4)}(x, y, z) + \beta_0 \mathcal{T}^{(2)}(x, y, z) \ln \left(\frac{\mu^2}{q^2} \right) \right] \\ & + \left(\frac{\alpha_s(\mu^2)}{2\pi} \right)^2 \left[\mathcal{T}^{(6)}(x, y, z) + \left(2\beta_0 \mathcal{T}^{(4)}(x, y, z) + \beta_1 \mathcal{T}^{(2)}(x, y, z) \right) \ln \left(\frac{\mu^2}{q^2} \right) \right. \\ & \left. \left. + \beta_0^2 \mathcal{T}^{(2)}(x, y, z) \ln^2 \left(\frac{\mu^2}{q^2} \right) \right] + \mathcal{O}(\alpha_s^3) \right\}. \end{aligned} \quad (7.14)$$

7.3 Method

The Feynman diagrams contributing to the i -loop amplitude $|\mathcal{M}^{(i)}\rangle$ ($i = 0, 1, 2$) were all generated using QGRAF [32] according to the first step of the methodology presented in chapter 3. There are two diagrams at tree-level, 13 diagrams at one loop and 229 diagrams at two loops. We then project $|\mathcal{M}^{(2)}\rangle$ by $\langle\mathcal{M}^{(0)}|$ and $|\mathcal{M}^{(1)}\rangle$ by $\langle\mathcal{M}^{(1)}|$, and perform the summation over colours and spins using the computer algebra programs MAPLE [33] and FORM3 [34]. When summing over the polarizations of the external gluon and off-shell photon, we use the Feynman gauge:

$$\sum_{\text{spins}} \epsilon_i^\mu \epsilon_i^{\nu*} = -g^{\mu\nu}. \quad (7.15)$$

This is valid because the gluon always couples to a conserved fermionic current, which selects only the physical degrees of polarization. The use of an axial gauge polarization sum to project out the transverse polarizations (eq. 3.1) is therefore not needed.

The one-loop self-interference contribution $\mathcal{T}^{(6,[1\times 1])}$ is computed by reducing all tensorial loop integrals according to the standard Passarino–Veltman procedure [91] to scalar one-loop two-point, three-point and four-point integrals. It has been known for a long time that those three-point integrals can be further reduced to linear combinations of two-point integrals using integration-by-parts identities. After this reduction, $\mathcal{T}^{(6,[1\times 1])}$ is expressed as a bilinear combination of only two integrals: the one-loop box and the one-loop bubble, which are listed in appendix of [45].

The computation of $\mathcal{T}^{(6,[2\times 0])}$ is by far less straightforward. The methodology applied and the tools used to express $\mathcal{T}^{(6,[2\times 0])}$ in terms of master integrals (MI) was discussed in chapters 3, 4 and 5. The two-loop MI's relevant to the $\gamma^* \rightarrow q\bar{q}g$ matrix element are two-loop four-point functions with one leg off-shell. These functions were all computed in [43] in the framework of dimensional regularization with $D = 4 - 2\epsilon$ space-time dimensions. The differential equations method, presented in chapter 6, was used for this purpose. The results of [43] take the form of a Laurent series in ϵ , starting at ϵ^{-4} , with coefficients containing two-dimensional harmonic polylogarithms [39]. All master integrals in [43] were given for one particular config-

uration of the external momenta. They were expressed in a form where the argument of the 2DHPL's was always y , while z appeared in the index vector of the 2DHPL's. In [43] there was a separation in the notation referring to HPL's and 2DHPL's. The symbol 'H' remained only for the HPL's while the symbol 'G' was used for the 2DHPL's. For simplicity, in the rest of this thesis we will express both HPL's and 2DHPL's with the symbol 'H'.

Each master integral can occur in six kinematic configurations (corresponding to the permutations of (p_1, p_2, p_3)). To avoid hidden zeros (arising from cancellations occurring in the combinations of 2DHPL's with different arguments and different variables in the index vector), we express the master integrals for all kinematic configurations in a unique form, which is the same as in [43]: the argument of the 2DHPL's is always y , the variable in their index vector is z , which appears also as argument of the HPL's.

The master integrals in [43] were derived in the kinematical situation of a (space-like) $1 \rightarrow 3$ decay, which corresponds to the $\gamma^* \rightarrow q\bar{q}g$, such that the only analytic continuation of them required here is the expansion of the overall factor in the time-like region:

$$\text{Re}(-1)^{-2\epsilon} = 1 - 2\pi^2\epsilon^2 + 2/3\pi^4\epsilon^4 + \mathcal{O}(\epsilon^6). \quad (7.16)$$

The analytic continuation of the master integrals to other kinematical regions is discussed in the appendix of [43].

7.4 The Matrix Element

We further decompose the renormalized one- and two-loop contributions to $\mathcal{T}^{(6)}$ as a sum of two terms:

$$\mathcal{T}^{(6,[i \times j])}(x, y, z) = \mathcal{Poles}^{(i \times j)}(x, y, z) + \mathcal{Finite}^{(i \times j)}(x, y, z). \quad (7.17)$$

\mathcal{Poles} contains infrared singularities that will be analytically cancelled by those occurring in radiative processes of the same order (ultraviolet divergences are removed by renormalization). \mathcal{Finite} is the renormalized remainder, which is finite as $\epsilon \rightarrow 0$.

In this section we first give explicit expressions for the infrared pole structure using the procedure advocated by Catani [12] and then give the analytic results for the finite remainders. For simplicity we set the renormalization scale $\mu^2 = s_{123}$ and restore the renormalization scale dependence using Eq. (7.14).

7.4.1 Infrared factorization

Catani [12] has shown how to organize the infrared pole structure of the two-loop contributions renormalized in the $\overline{\text{MS}}$ scheme in terms of the tree and renormalized one-loop amplitudes, $|\mathcal{M}^{(0)}\rangle$ and $|\mathcal{M}^{(1)}\rangle$ respectively, as:

$$\begin{aligned} \mathcal{Poles}^{(2\times 0)} = 2\Re \left[& -\frac{1}{2} \langle \mathcal{M}^{(0)} | \mathbf{I}^{(1)}(\epsilon) \mathbf{I}^{(1)}(\epsilon) | \mathcal{M}^{(0)} \rangle - \frac{\beta_0}{\epsilon} \langle \mathcal{M}^{(0)} | \mathbf{I}^{(1)}(\epsilon) | \mathcal{M}^{(0)} \rangle \right. \\ & + \langle \mathcal{M}^{(0)} | \mathbf{I}^{(1)}(\epsilon) | \mathcal{M}^{(1)} \rangle \\ & + e^{-\epsilon\gamma} \frac{\Gamma(1-2\epsilon)}{\Gamma(1-\epsilon)} \left(\frac{\beta_0}{\epsilon} + K \right) \langle \mathcal{M}^{(0)} | \mathbf{I}^{(1)}(2\epsilon) | \mathcal{M}^{(0)} \rangle \\ & \left. + \langle \mathcal{M}^{(0)} | \mathbf{H}^{(2)}(\epsilon) | \mathcal{M}^{(0)} \rangle \right] \end{aligned} \quad (7.18)$$

and

$$\mathcal{Poles}^{(1\times 1)} = \Re \left[2 \langle \mathcal{M}^{(1)} | \mathbf{I}^{(1)}(\epsilon) | \mathcal{M}^{(0)} \rangle - \langle \mathcal{M}^{(0)} | \mathbf{I}^{(1)\dagger}(\epsilon) \mathbf{I}^{(1)}(\epsilon) | \mathcal{M}^{(0)} \rangle \right], \quad (7.19)$$

where the constant K is defined in eq. (2.50). It should be noted that, in this prescription, part of the finite terms in $\mathcal{T}^{(6, [i\times j])}$ are accounted for by the $\mathcal{O}(\epsilon^0)$ expansion of $\mathcal{Poles}^{(i\times j)}$.

For this particular process, there is only one colour structure present at tree level which, in terms of the gluon colour a and the quark and antiquark colours i and j , is simply \mathbf{T}_{ij}^a . Adding higher loops does not introduce additional colour structures, and the amplitudes are therefore vectors in a one-dimensional space. Similarly, the infrared singularity operator $\mathbf{I}^{(1)}(\epsilon)$ is a 1×1 matrix in the colour space and is given by:

$$\mathbf{I}^{(1)}(\epsilon) = -\frac{e^{\epsilon\gamma}}{2\Gamma(1-\epsilon)} \left[N \left(\frac{1}{\epsilon^2} + \frac{3}{4\epsilon} + \frac{\beta_0}{2N\epsilon} \right) (\mathbf{S}_{13} + \mathbf{S}_{23}) - \frac{1}{N} \left(\frac{1}{\epsilon^2} + \frac{3}{2\epsilon} \right) \mathbf{S}_{12} \right], \quad (7.20)$$



where (since we have set $\mu^2 = s_{123}$):

$$\mathbf{S}_{ij} = \left(-\frac{s_{123}}{s_{ij}} \right)^\epsilon. \quad (7.21)$$

Note that on expanding \mathbf{S}_{ij} , imaginary parts are generated, the sign of which is fixed by the small imaginary part $+i0$ of s_{ij} . Other combinations such as $\langle \mathcal{M}^{(0)} | \mathbf{I}^{(1)\dagger}(\epsilon) \rangle$ are obtained by using the hermitian conjugate operator $\mathbf{I}^{(1)\dagger}(\epsilon)$, where the only practical change is that the sign of the imaginary part of \mathbf{S} is reversed. The origin of the various terms in Eq. (7.20) is straightforward. Each parton pair ij in the event forms a radiating antenna of scale s_{ij} . Terms proportional to \mathbf{S}_{ij} are cancelled by real radiation emitted from leg i and absorbed by leg j . The soft singularities $\mathcal{O}(1/\epsilon^2)$ are independent of the identity of the participating partons and are universal. However, the collinear singularities depend on the identities of the participating partons. For each quark we find a contribution of $3/(4\epsilon)$ and for each gluon we find a contribution of $\beta_0/(2\epsilon)$ coming from the integral over the collinear splitting function.

Finally, the last term of Eq. (7.18) that involves $\mathbf{H}^{(2)}(\epsilon)$ produces only a single pole in ϵ and is given by:

$$\langle \mathcal{M}^{(0)} | \mathbf{H}^{(2)}(\epsilon) | \mathcal{M}^{(0)} \rangle = \frac{e^{\epsilon\gamma}}{4\epsilon\Gamma(1-\epsilon)} H^{(2)} \langle \mathcal{M}^{(0)} | \mathcal{M}^{(0)} \rangle, \quad (7.22)$$

where the constant $H^{(2)}$ is renormalization-scheme-dependent. As with the single pole parts of $\mathbf{I}^{(1)}(\epsilon)$, the process-dependent $H^{(2)}$ can be constructed by counting the number of radiating partons present in the event. In our case, there is a quark-antiquark pair and a gluon present in the final state, so that:

$$H^{(2)} = 2H_q^{(2)} + H_g^{(2)} \quad (7.23)$$

where in the $\overline{\text{MS}}$ scheme:

$$H_g^{(2)} = \left(\frac{1}{2}\zeta_3 + \frac{5}{12} + \frac{11\pi^2}{144} \right) N^2 + \frac{5}{27} N_F^2 + \left(-\frac{\pi^2}{72} - \frac{89}{108} \right) N N_F - \frac{N_F}{4N}, \quad (7.24)$$

$$H_q^{(2)} = \left(\frac{7}{4}\zeta_3 + \frac{409}{864} - \frac{11\pi^2}{96} \right) N^2 + \left(-\frac{1}{4}\zeta_3 - \frac{41}{108} - \frac{\pi^2}{96} \right) + \left(-\frac{3}{2}\zeta_3 - \frac{3}{32} + \frac{\pi^2}{8} \right) \frac{1}{N^2} + \left(\frac{\pi^2}{48} - \frac{25}{216} \right) \frac{(N^2 - 1)N_F}{N}, \quad (7.25)$$

so that:

$$\begin{aligned}
H^{(2)} = & \left(4\zeta_3 + \frac{589}{432} - \frac{11\pi^2}{72}\right) N^2 + \left(-\frac{1}{2}\zeta_3 - \frac{41}{54} - \frac{\pi^2}{48}\right) + \left(-3\zeta_3 - \frac{3}{16} + \frac{\pi^2}{4}\right) \frac{1}{N^2} \\
& + \left(-\frac{19}{18} + \frac{\pi^2}{36}\right) NN_F + \left(-\frac{1}{54} - \frac{\pi^2}{24}\right) \frac{N_F}{N} + \frac{5}{27} N_F^2.
\end{aligned} \tag{7.26}$$

The factors $H_q^{(2)}$ and $H_g^{(2)}$ are directly related to those found in gluon–gluon scattering [81], quark–quark scattering [79] and quark–gluon scattering [80] (which each involve four partons) as well as in the quark form factor [60, 92–94]. We also note that (on purely dimensional grounds) one might expect terms of the type \mathbf{S}_{ij}^2 to be present in $H^{(2)}$. Of course such terms are $1 + \mathcal{O}(\epsilon)$ and therefore leave the pole part unchanged and only modify the finite remainder. At present it is not known how to systematically include these effects.

The renormalized interference of tree and one-loop amplitudes also appears in eq. (7.18). This can be written to all orders in ϵ using the relation:

$$\langle \mathcal{M}^{(0)} | \mathcal{M}^{(1)} \rangle = S_\epsilon^{-1} \langle \mathcal{M}^{(0),un} | \mathcal{M}^{(1),un} \rangle - \frac{\beta_0}{2\epsilon} \langle \mathcal{M}^{(0),un} | \mathcal{M}^{(0),un} \rangle, \tag{7.27}$$

where:

$$\langle \mathcal{M}^{(0),un} | \mathcal{M}^{(1),un} \rangle = V \left(N f_1(y, z) + \frac{1}{N} f_2(y, z) + (y \leftrightarrow z) \right). \tag{7.28}$$

The functions $f_1(y, z)$ and $f_2(y, z)$, presented in appendix E, can be written in terms of the one-loop bubble integral and the one-loop box integral in $D = 6 - 2\epsilon$ dimensions, Box^6 . As mentioned before, explicit formulae for the bubble and box integrals are given in the appendix of [45]. The square of the Born amplitude is given in eq. (7.9).

7.4.2 The finite part

The finite remainders of the one- and two-loop contributions to $\mathcal{T}^{(6)}$ can be decomposed according to their colour structure and to their dependence on the number of quark flavours N_F . In the two-loop contribution, one finds moreover a term proportional to the charge-weighted sum of the quark flavours $N_{F,\gamma}$; this equals, in the

case of purely electromagnetic interactions:

$$N_{F,\gamma} = \frac{\left(\sum_q e_q\right)^2}{\sum_q e_q^2}. \quad (7.29)$$

This term originates from diagrams containing a closed quark loop coupling to the virtual photon and which first appear at the two-loop level.

The tree-level combination of invariants:

$$T = \frac{y}{z} + \frac{z}{y} + \frac{2}{yz} - \frac{2}{y} - \frac{2}{z} \quad (7.30)$$

frequently occurs in the finite part. We therefore extracted this combination by expressing $1/(yz)$ by T according to the above equation.

Two-loop contribution to $\mathcal{T}^{(6)}$

The finite remainder of the interference of the two-loop amplitude with the tree-level amplitude is decomposed as:

$$\begin{aligned} \mathcal{F}inite^{(2\times 0)}(x, y, z) = & V \left[N^2 (A_{20}(y, z) + A_{20}(z, y)) + (B_{20}(y, z) + B_{20}(z, y)) \right. \\ & + \frac{1}{N^2} (C_{20}(y, z) + C_{20}(z, y)) + NN_F (D_{20}(y, z) + D_{20}(z, y)) \\ & + \frac{N_F}{N} (E_{20}(y, z) + E_{20}(z, y)) + N_F^2 (F_{20}(y, z) + F_{20}(z, y)) \\ & \left. + N_{F,\gamma} \left(\frac{4}{N} - N \right) (G_{20}(y, z) + G_{20}(z, y)) \right], \quad (7.31) \end{aligned}$$

where the coefficients $A_{20}(y, z), B_{20}(y, z), \dots, G_{20}(y, z)$ appear in appendix E.

One-loop contribution to $\mathcal{T}^{(6)}$

The finite remainder of the self-interference of the one-loop amplitude is decomposed as:

$$\begin{aligned} \mathcal{F}inite^{(1\times 1)}(x, y, z) = & V \left[N^2 (A_{11}(y, z) + A_{11}(z, y)) + (B_{11}(y, z) + B_{11}(z, y)) \right. \\ & + \frac{1}{N^2} (C_{11}(y, z) + C_{11}(z, y)) + NN_F (D_{11}(y, z) + D_{11}(z, y)) \\ & \left. + \frac{N_F}{N} (E_{11}(y, z) + E_{11}(z, y)) + N_F^2 (F_{11}(y, z) + F_{11}(z, y)) \right]. \quad (7.32) \end{aligned}$$

The coefficients $A_{11}(y, z), B_{11}(y, z), \dots, F_{11}(y, z)$ are presented in the appendix of [45].

Chapter 8

Two-Loop Helicity Amplitudes for the $\mathcal{H} \rightarrow ggg$ Decay

8.1 Introduction

Within the SM, the Higgs Boson is the only particle remaining to be discovered. Its importance is great because of the fundamental part the Higgs plays in the Electroweak Symmetry Breaking, the spontaneous mechanism that explains the generation of the masses of the fermions and the weak gauge bosons. Although the vacuum expectation value of the Higgs field is very well defined (of order 246 GeV), its mass remains a free parameter that can be constrained but not predicted by the theory.

The detection of the Higgs boson in the major electron and hadron accelerators has been a very challenging, but unsuccessful, task during the last few years. After the termination of the LEP program, the efforts for the discovery of the Higgs are concentrated on the hadron colliders at CERN Large Hadron Collider (LHC) and Tevatron Run II. The data from the e^+e^- collider LEP have set a lower limit of ~ 113 GeV [111] for the Higgs mass. A global fit with electroweak precision data predicts a maximum limit of around 200 GeV [112] with 95% certainty.

If the Higgs mass is below ~ 700 GeV, the dominant mechanism for Higgs production in the hadron colliders will be the gluon fusion providing $\sim 65\%$ of the total cross section at Tevatron [113]. The gluon fusion will be most important at LHC

due to the high machine luminosity which will enable the measurement of the rare, of $\mathcal{O}(10^{-3})$, $\mathcal{H} \rightarrow \gamma\gamma$ decay, despite the large QCD background from processes like $gg \rightarrow \gamma\gamma$, $q\bar{q} \rightarrow \gamma\gamma$, as well as misidentified photons from π^0 decay and jet fragmentation.

At leading order (LO) the Higgs coupling to the two gluons is mediated through a quark loop. Since the Higgs coupling to the quarks is proportional to the quark masses, the dominant contribution is generated from the top quark. The next to leading order (NLO) corrections have also been calculated and are significantly big ($>60\%$). As we mentioned in section 1.4, in the heavy top quark limit, $M_t \rightarrow \infty$, we can integrate out the top mass (M_t) and formulate an effective Lagrangian \mathcal{L}_{eff} for the $\mathcal{H}gg$ coupling. In this limit the evaluation of the LO and NLO contributions was completed along time ago [114]. Recently the NNLO, two-loop virtual corrections were calculated [115].

At the same time, other, less inclusive mechanisms of gluon fusion, have been studied and in [116] the transverse momentum spectrum of the Higgs boson was considered. Despite the fact that the channel $pp \rightarrow \mathcal{H} + jet \rightarrow \gamma\gamma + jet$ has a cross section much smaller than the inclusive channel $pp \rightarrow \mathcal{H} + X \rightarrow \gamma\gamma + X$, the former presents some significant advantages as far as the background is concerned. First of all, the photons that are produced by the Higgs decay are more energetic in the case of a Higgs with large transverse momentum and second, the jet itself produces a signal that can significantly suppress the QCD background. In fact, at LO the Signal/Background ratio is approximately $\sim 1/15$ for the inclusive $pp \rightarrow \gamma\gamma$ process and $\sim 1/2$ or $1/3$ for the $pp \rightarrow \gamma\gamma + jet$ reaction in [117].

The three QCD processes contributing to the reaction $pp \rightarrow \gamma\gamma + jet$ are:

$$gg \rightarrow \mathcal{H} + g, \quad gq \rightarrow \mathcal{H} + q, \quad q\bar{q} \rightarrow \mathcal{H} + g. \quad (8.1)$$

Numerically, it was calculated [117] that the contribution of the gq channel is about 12% of the main gg production signal, while the contribution of the $q\bar{q}$ production channel is negligible. The helicity amplitudes for the processes (8.1) can be given by analytic continuation of the $\mathcal{H} \rightarrow ggg$ and $\mathcal{H} \rightarrow q\bar{q}g$ helicity amplitudes.

The relevant LO helicity amplitudes and matrix elements of the processes $\mathcal{H} \rightarrow ggg$ and $\mathcal{H} \rightarrow gq\bar{q}$ were calculated analytically both in the $M_t \rightarrow \infty$ limit and with full M_t dependence [116]. The one-loop virtual contributions at $M_t \rightarrow \infty$ were provided somewhat later [118], but a two-loop calculation has not been done yet.

In the limit $M_t \rightarrow \infty$ a full NNLO calculation requires the computation of the helicity amplitudes of three contributions: (i) the ‘tree_{eff}’ $\mathcal{H} \rightarrow 5$ partons amplitudes, (ii) the ‘one-loop_{eff}’ corrections to the $\mathcal{H} \rightarrow 4$ partons amplitudes and (iii) the ‘two-loop_{eff}’ (as well as the ‘one-loop_{eff}’ times ‘one-loop_{eff}’) corrections to the $\mathcal{H} \rightarrow ggg$ and $\mathcal{H} \rightarrow gq\bar{q}$ helicity amplitudes. Although the one-loop five-point integrals with one external leg off-shell that appear in (ii) are known, the computation of the amplitudes has not been done yet. The two-loop four-point integrals with one external leg off-shell that appear in (iii) were until recently a major obstacle in any NNLO calculation in which they are involved. This calculation has now become tractable owing to various technical developments over the last two years, some of which were presented in previous chapters.

In this chapter, we present the $\mathcal{O}(\alpha_s^3)$ corrections to the $\mathcal{H} \rightarrow ggg$ helicity amplitudes in the $M_t \rightarrow \infty$ limit. At this order, two combinations of amplitudes contribute: the interference of ‘two-loop_{eff}’ and ‘tree_{eff}’ amplitudes and the self-interference of the ‘one-loop_{eff}’ amplitude. Ultraviolet renormalization is performed in the $\overline{\text{MS}}$ scheme. The infrared pole structure of the two-loop corrections to the $\mathcal{H} \rightarrow ggg$ helicity amplitudes have been predicted by Catani [12], using an infrared factorization formula. We confirm Catani’s prediction with our explicit calculation, and we use the formalism introduced in [12] to present the infrared poles and the finite parts of the $\mathcal{H} \rightarrow ggg$ helicity amplitudes in a compact form.

8.1.1 Notation

We consider the decay of the Higgs boson to three gluons:

$$\mathcal{H}(p_4) \longrightarrow g_1(p_1) + g_2(p_2) + g_3(p_3) . \quad (8.1)$$

As we have seen in previous chapters it is convenient to define by the invariants:

$$s_{12} = (p_1 + p_2)^2, \quad s_{13} = (p_1 + p_3)^2, \quad s_{23} = (p_2 + p_3)^2, \quad (8.2)$$

which fulfill:

$$p_4^2 = s_{12} + s_{13} + s_{23} \equiv s_{123}, \quad (8.3)$$

as well as the dimensionless invariants:

$$x = s_{12}/s_{123}, \quad y = s_{13}/s_{123}, \quad z = s_{23}/s_{123}, \quad (8.4)$$

which satisfy $x + y + z = 1$.

The renormalized amplitude $|\mathcal{M}\rangle$ can be written as:

$$|\mathcal{M}\rangle = S_{\mu\nu\rho}(g_1; g_2; g_3) \epsilon_1^\mu \epsilon_2^\nu \epsilon_3^\rho, \quad (8.5)$$

while the hadron current may be perturbatively decomposed as:

$$\begin{aligned} S_{\mu\nu\rho}(g_1; g_2; g_3) = & C_1 \sqrt{4\pi\alpha_s} f^{abc} \left[S_{\mu\nu\rho}^{(0)}(g_1; g_2; g_3) + \left(\frac{\alpha_s}{2\pi}\right) S_{\mu\nu\rho}^{(1)}(g_1; g_2; g_3) \right. \\ & \left. + \left(\frac{\alpha_s}{2\pi}\right)^2 S_{\mu\nu\rho}^{(2)}(g_1; g_2; g_3) + \mathcal{O}(\alpha_s^3) \right], \end{aligned} \quad (8.6)$$

where α_s is the QCD coupling constant at the renormalization scale μ , and the $S_{\mu\nu\rho}^{(i)}$ are the i -loop contributions to the renormalized amplitude. C_1 was defined in eq. 1.26. Renormalization of ultraviolet divergences is performed in the $\overline{\text{MS}}$ scheme.

8.1.2 The general tensor

The most general tensor structure for the hadron current $S_{\mu\nu\rho}(g_1; g_2; g_3)$ is:

$$\begin{aligned}
S_{\mu\nu\rho}(g_1; g_2; g_3)\epsilon_1^\mu\epsilon_2^\nu\epsilon_3^\rho &= \sum_{i,j,k=1}^3 A_{ijk} p_i \cdot \epsilon_1 p_j \cdot \epsilon_2 p_k \cdot \epsilon_3 + \sum_{i=1}^3 B_i p_i \cdot \epsilon_1 \epsilon_2 \cdot \epsilon_3 \\
&+ \sum_{i=1}^3 C_i p_i \cdot \epsilon_2 \epsilon_1 \cdot \epsilon_3 + \sum_{i=1}^3 D_i p_i \cdot \epsilon_3 \epsilon_1 \cdot \epsilon_2 \\
&= A_{211} p_2 \cdot \epsilon_1 p_1 \cdot \epsilon_2 p_1 \cdot \epsilon_3 + A_{212} p_2 \cdot \epsilon_1 p_1 \cdot \epsilon_2 p_2 \cdot \epsilon_3 + A_{231} p_2 \cdot \epsilon_1 p_3 \cdot \epsilon_2 p_1 \cdot \epsilon_3 \\
&+ A_{232} p_2 \cdot \epsilon_1 p_3 \cdot \epsilon_2 p_2 \cdot \epsilon_3 + A_{311} p_3 \cdot \epsilon_1 p_1 \cdot \epsilon_2 p_1 \cdot \epsilon_3 + A_{312} p_3 \cdot \epsilon_1 p_1 \cdot \epsilon_2 p_2 \cdot \epsilon_3 \\
&+ A_{331} p_3 \cdot \epsilon_1 p_3 \cdot \epsilon_2 p_1 \cdot \epsilon_3 + A_{332} p_3 \cdot \epsilon_1 p_3 \cdot \epsilon_2 p_2 \cdot \epsilon_3 \\
&+ B_2 \epsilon_2 \cdot \epsilon_3 p_2 \cdot \epsilon_1 + B_3 \epsilon_2 \cdot \epsilon_3 p_3 \cdot \epsilon_1 \\
&+ C_1 \epsilon_1 \cdot \epsilon_3 p_1 \cdot \epsilon_2 + C_3 \epsilon_1 \cdot \epsilon_3 p_3 \cdot \epsilon_2 \\
&+ D_1 \epsilon_1 \cdot \epsilon_2 p_1 \cdot \epsilon_3 + D_2 \epsilon_1 \cdot \epsilon_2 p_2 \cdot \epsilon_3, \tag{8.7}
\end{aligned}$$

where the constraints $p_1 \cdot \epsilon_1 = 0$, $p_2 \cdot \epsilon_2 = 0$ and $p_3 \cdot \epsilon_3 = 0$ have been applied. The tensor must satisfy the QCD Ward identity when the gluon polarization vectors ϵ_1 , ϵ_2 and ϵ_3 are replaced with the respective gluon momentum:

$$\begin{aligned}
(\epsilon_1 \rightarrow p_1) \rightarrow S_{\mu\nu\rho}(g_1; g_2; g_3)p_1^\mu\epsilon_2^\nu\epsilon_3^\rho &= 0, \\
(\epsilon_2 \rightarrow p_2) \rightarrow S_{\mu\nu\rho}(g_1; g_2; g_3)\epsilon_1^\mu p_2^\nu\epsilon_3^\rho &= 0, \\
(\epsilon_3 \rightarrow p_3) \rightarrow S_{\mu\nu\rho}(g_1; g_2; g_3)\epsilon_1^\mu\epsilon_2^\nu p_3^\rho &= 0. \tag{8.8}
\end{aligned}$$

These constraints yield relations amongst the 14 distinct tensor structures and applying these identities give the gauge invariant form of the tensor:

$$S_{\mu\nu\rho}(g_1; g_2; g_3)\epsilon_1^\mu\epsilon_2^\nu\epsilon_3^\rho = A_{211}T_{211} + A_{311}T_{311} + A_{232}T_{232} + A_{312}T_{312}, \tag{8.9}$$

where A_{ijk} are gauge independent functions and the tensor structures T_{ijk} are given by:

$$\begin{aligned}
T_{232} &= p_2 \cdot \epsilon_1 p_3 \cdot \epsilon_2 p_2 \cdot \epsilon_3 - \frac{1}{2} \epsilon_2 \cdot \epsilon_3 p_2 \cdot \epsilon_1 s_{23} - \frac{p_3 \cdot \epsilon_1 p_3 \cdot \epsilon_2 p_2 \cdot \epsilon_3 s_{12}}{s_{13}} + \frac{1}{2} \frac{\epsilon_2 \cdot \epsilon_3 p_3 \cdot \epsilon_1 s_{23} s_{12}}{s_{13}}, \\
T_{211} &= p_2 \cdot \epsilon_1 p_1 \cdot \epsilon_2 p_1 \cdot \epsilon_3 - \frac{1}{2} \epsilon_1 \cdot \epsilon_2 p_1 \cdot \epsilon_3 s_{12} - \frac{p_2 \cdot \epsilon_1 p_1 \cdot \epsilon_2 p_2 \cdot \epsilon_3 s_{13}}{s_{23}} + \frac{1}{2} \frac{\epsilon_1 \cdot \epsilon_2 p_2 \cdot \epsilon_3 s_{13} s_{12}}{s_{23}}, \\
T_{311} &= p_3 \cdot \epsilon_1 p_1 \cdot \epsilon_2 p_1 \cdot \epsilon_3 - \frac{1}{2} \epsilon_1 \cdot \epsilon_3 p_1 \cdot \epsilon_2 s_{13} - \frac{p_3 \cdot \epsilon_1 p_3 \cdot \epsilon_2 p_1 \cdot \epsilon_3 s_{12}}{s_{23}} + \frac{1}{2} \frac{\epsilon_1 \cdot \epsilon_3 p_3 \cdot \epsilon_2 s_{13} s_{12}}{s_{23}}, \\
T_{312} &= p_3 \cdot \epsilon_1 p_1 \cdot \epsilon_2 p_2 \cdot \epsilon_3 - p_2 \cdot \epsilon_1 p_3 \cdot \epsilon_2 p_1 \cdot \epsilon_3 + \frac{1}{2} \epsilon_1 \cdot \epsilon_3 p_3 \cdot \epsilon_2 s_{12} + \frac{1}{2} \epsilon_1 \cdot \epsilon_2 p_1 \cdot \epsilon_3 s_{23} \\
&\quad - \frac{1}{2} \epsilon_1 \cdot \epsilon_3 p_1 \cdot \epsilon_2 s_{23} + \frac{1}{2} \epsilon_2 \cdot \epsilon_3 p_2 \cdot \epsilon_1 s_{13} - \frac{1}{2} \epsilon_1 \cdot \epsilon_2 p_2 \cdot \epsilon_3 s_{13} - \frac{1}{2} \epsilon_2 \cdot \epsilon_3 p_3 \cdot \epsilon_1 s_{12}. \quad (8.10)
\end{aligned}$$

The coefficients are functions of the invariants s_{12} , s_{23} and s_{13} and are further related by symmetry under the interchange of the three gluons:

$$\begin{aligned}
A_{211}(s_{12}, s_{13}, s_{23}) &= -A_{311}(s_{13}, s_{12}, s_{23}), \\
A_{232}(s_{12}, s_{13}, s_{23}) &= -A_{311}(s_{12}, s_{23}, s_{13}). \quad (8.11)
\end{aligned}$$

8.1.3 Projectors for the tensor coefficients

The coefficients A_{ijk} may be easily extracted from a Feynman diagram calculation using projectors such that:

$$\sum_{\text{spins}} \mathcal{P}(A_{ijk}) S_{\mu\nu\rho}(g_1; g_2; g_3) \epsilon_1^\mu \epsilon_2^\nu \epsilon_3^\rho = A_{ijk}. \quad (8.12)$$

The explicit forms for the four projectors are,

$$\begin{aligned}
\mathcal{P}(A_{311}) &= -\frac{(D-4)}{s_{12} s_{23} s_{13} (D-3)} T_{232}^\dagger - \frac{s_{23} (D-4)}{s_{13}^2 s_{12}^2 (D-3)} T_{211}^\dagger \\
&\quad + \frac{s_{23} D}{s_{12} s_{13}^3 (D-3)} T_{311}^\dagger - \frac{(D-2)}{s_{13}^2 s_{12} (D-3)} T_{312}^\dagger, \\
\mathcal{P}(A_{232}) &= \frac{s_{13} D}{s_{12} s_{23}^3 (D-3)} T_{232}^\dagger + \frac{(D-4)}{s_{23} s_{12}^2 (D-3)} T_{211}^\dagger \\
&\quad - \frac{(D-4)}{s_{12} s_{23} s_{13} (D-3)} T_{311}^\dagger + \frac{(D-2)}{s_{23}^2 s_{12} (D-3)} T_{312}^\dagger, \\
\mathcal{P}(A_{312}) &= \frac{(D-2)}{s_{23}^2 s_{12} (D-3)} T_{232}^\dagger + \frac{(D-2)}{s_{13} s_{12}^2 (D-3)} T_{211}^\dagger \\
&\quad - \frac{(D-2)}{s_{13}^2 s_{12} (D-3)} T_{311}^\dagger + \frac{D}{s_{12} s_{23} s_{13} (D-3)} T_{312}^\dagger, \\
\mathcal{P}(A_{211}) &= \frac{(D-4)}{s_{23} s_{12}^2 (D-3)} T_{232}^\dagger + \frac{s_{23} D}{s_{13} s_{12}^3 (D-3)} T_{211}^\dagger \\
&\quad - \frac{s_{23} (D-4)}{s_{13}^2 s_{12}^2 (D-3)} T_{311}^\dagger + \frac{(D-2)}{s_{13} s_{12}^2 (D-3)} T_{312}^\dagger.
\end{aligned} \tag{8.13}$$

8.1.4 The perturbative expansion of the tensor coefficients

Each of the unrenormalized coefficients A_{ijk} have perturbative expansions of the form:

$$A_{ijk}^U = C_1^U \sqrt{4\pi\alpha_s^U} f^{abc} \left[A_{ijk}^{(0),U} + \left(\frac{\alpha_s^U}{2\pi} \right) A_{ijk}^{(1),U} + \left(\frac{\alpha_s^U}{2\pi} \right)^2 A_{ijk}^{(2),U} + \mathcal{O}((\alpha_s^U)^3) \right]. \tag{8.14}$$

At tree-level:

$$\begin{aligned}
A_{211}^{(0)} &= \frac{2}{s_{13}}, \\
A_{311}^{(0)} &= -\frac{2}{s_{12}}, \\
A_{232}^{(0)} &= \frac{2}{s_{12}}, \\
A_{312}^{(0)} &= -\frac{2}{s_{12}} - \frac{2}{s_{23}} - \frac{2}{s_{13}},
\end{aligned} \tag{8.15}$$

where a, b, c are the adjoint color indices for the gluon.

The unrenormalized one and two-loop coefficients $A_{ijk}^{(1),U}$ and $A_{ijk}^{(2),U}$ were obtained analytically using the methodology and tools described in previous chapters. The ϵ -expanded coefficients in terms of HPL's and 2DHPL's, can be obtained in FORM format from the author of this thesis.

8.1.5 Ultraviolet renormalization

The renormalization of the matrix element is carried out by replacing the bare coupling α^U with the renormalized coupling $\alpha_s \equiv \alpha_s(\mu^2)$, evaluated at the renormalization scale μ^2 :

$$\alpha^U \mu_0^{2\epsilon} S_\epsilon = \alpha_s \mu^{2\epsilon} \left[1 - \frac{\beta_0}{\epsilon} \left(\frac{\alpha_s}{2\pi} \right) + \left(\frac{\beta_0^2}{\epsilon^2} - \frac{\beta_1}{2\epsilon} \right) \left(\frac{\alpha_s}{2\pi} \right)^2 + \mathcal{O}(\alpha_s^3) \right], \quad (8.16)$$

where S_ϵ , β_0 and β_1 were defined in section 1.3.3. The renormalization relation for the effective coupling C_1 is given in [119] as:

$$C_1^U = C_1 \left[1 - \frac{\beta_0}{\epsilon} \left(\frac{\alpha_s}{2\pi} \right) + \left(\frac{\beta_0^2}{\epsilon^2} - \frac{\beta_1}{\epsilon} \right) \left(\frac{\alpha_s}{2\pi} \right)^2 + \mathcal{O}(\alpha_s^3) \right]. \quad (8.17)$$

We denote the i -loop contribution to the unrenormalized coefficients by $A_{ijk}^{(i),U}$, using the same normalization as for the decomposition of the renormalized amplitude (8.6).

The renormalized coefficients are then obtained as:

$$\begin{aligned} A_{ijk}^{(0)} &= A_{ijk}^{(0),U}, \\ A_{ijk}^{(1)} &= S_\epsilon^{-1} A_{ijk}^{(1),U} - \frac{3\beta_0}{2\epsilon} A_{ijk}^{(0),U}, \\ A_{ijk}^{(2)} &= S_\epsilon^{-2} A_{ijk}^{(2),U} - \frac{5\beta_0}{2\epsilon} S_\epsilon^{-1} A_{ijk}^{(1),U} - \left(\frac{5\beta_1}{4\epsilon} - \frac{15\beta_0^2}{8\epsilon^2} \right) A_{ijk}^{(0),U}. \end{aligned} \quad (8.18)$$

8.1.6 Infrared behaviour of the tensor coefficients

The amplitudes contain infrared singularities that will be analytically canceled by those occurring in radiative processes of the same order (ultraviolet divergences are removed by renormalization). Catani [11] has shown how to organize the infrared pole structure of the one- and two-loop contributions renormalized in the $\overline{\text{MS}}$ scheme

in terms of the tree and renormalized one-loop amplitudes. The same procedure applies to the tensor coefficients. In particular, the infrared behaviour of the one-loop coefficients is given by:

$$A_{ijk}^{(1)} = \mathbf{I}^{(1)}(\epsilon) A_{ijk}^{(0)} + A_{ijk}^{(1),finite}, \quad (8.19)$$

while the two-loop singularity structure is:

$$\begin{aligned} A_{ijk}^{(2)} = & \left(-\frac{1}{2} \mathbf{I}^{(1)}(\epsilon) \mathbf{I}^{(1)}(\epsilon) - \frac{\beta_0}{\epsilon} \mathbf{I}^{(1)}(\epsilon) \right. \\ & \left. + e^{-\epsilon\gamma} \frac{\Gamma(1-2\epsilon)}{\Gamma(1-\epsilon)} \left(\frac{\beta_0}{\epsilon} + K \right) \mathbf{I}^{(1)}(2\epsilon) + \mathbf{H}^{(2)}(\epsilon) \right) A_{ijk}^{(0)} \\ & + \mathbf{I}^{(1)}(\epsilon) A_{ijk}^{(1)} + A_{ijk}^{(2),finite}, \end{aligned} \quad (8.20)$$

where the constant K is:

$$K = \left(\frac{67}{18} - \frac{\pi^2}{6} \right) C_A - \frac{10}{9} T_R N_F. \quad (8.21)$$

The finite remainders $A_{ijk}^{(i),finite}$ remain to be calculated.

For this particular process, there is only one color structure present at tree level which, in terms of the gluon colors a, b and c , is simply f^{abc} . Adding higher loops does not introduce additional color structures, and the amplitudes are therefore vectors in a one-dimensional space. Similarly, the infrared singularity operator $\mathbf{I}^{(1)}(\epsilon)$ is given by:

$$\mathbf{I}^{(1)}(\epsilon) = -\frac{e^{\epsilon\gamma}}{2\Gamma(1-\epsilon)} \left(\frac{N}{\epsilon^2} + \frac{\beta_0}{\epsilon} \right) (\mathbf{S}_{13} + \mathbf{S}_{23} + \mathbf{S}_{12}), \quad (8.22)$$

where (since we have set $\mu^2 = s_{123}$):

$$\mathbf{S}_{ij} = \left(-\frac{s_{123}}{s_{ij}} \right)^\epsilon. \quad (8.23)$$

Note that on expanding \mathbf{S}_{ij} , imaginary parts are generated, the sign of which is fixed by the small imaginary part $+i0$ of s_{ij} .

Finally, the last term of Eq. (8.20) that involves $\mathbf{H}^{(2)}(\epsilon)$ produces only a single pole in ϵ and is given by:

$$\mathbf{H}^{(2)}(\epsilon) = \frac{e^{\epsilon\gamma}}{4\epsilon\Gamma(1-\epsilon)} \mathbf{H}^{(2)}, \quad (8.24)$$

where the constant $H^{(2)}$ is renormalization-scheme-dependent. As with the single pole parts of $\mathbf{I}^{(1)}(\epsilon)$, the process-dependent $H^{(2)}$ can be constructed by counting the number of radiating partons present in the event. In our case, there are three gluons present in the final state, so that:

$$H^{(2)} = 3H_g^{(2)} \quad (8.25)$$

where in the $\overline{\text{MS}}$ scheme:

$$H_g^{(2)} = \left(\frac{1}{2}\zeta_3 + \frac{5}{12} + \frac{11\pi^2}{144} \right) N^2 + \frac{5}{27} N_F^2 + \left(-\frac{\pi^2}{72} - \frac{89}{108} \right) NN_F - \frac{N_F}{4N} . \quad (8.26)$$

The factor $H_g^{(2)}$ is directly related to the one found in gluon–gluon scattering [81] and quark–gluon scattering [80] (which each involve four partons).

8.2 Helicity amplitudes

The general form of the renormalized helicity amplitude $|\mathcal{M}^{\lambda_1\lambda_2\lambda_3}\rangle$ for the decay: $\mathcal{H}(p_4) \rightarrow g_1(p_1, \lambda_1) + g_2(p_2, \lambda_2) + g_3(p_3, \lambda_3)$ can be written as:

$$|\mathcal{M}^{\lambda_1\lambda_2\lambda_3}\rangle = S_{\mu\nu\rho}(g_1; g_2; g_3)\epsilon_1^\mu(\lambda_1)\epsilon_2^\nu(\lambda_2)\epsilon_3^\rho(\lambda_3), \quad (8.27)$$

where the $\lambda_i = \pm$ denote helicity. A convenient method to evaluate helicity amplitudes is in terms of Weyl spinors, which is described briefly in Appendix D and in detail in [123]. Using the spinor calculus of Appendix D and substituting eq. (8.10) in eq. (8.9) we can express the helicity amplitudes, in terms of spinor products. It turns out that the only two independent helicity amplitudes are $+++$ and $++-$. Explicitly, we find,

$$\begin{aligned} |\mathcal{M}^{+++}\rangle &= \alpha \frac{1}{\sqrt{2}} [p_1 p_2] [p_2 p_3] [p_1 p_3] \\ |\mathcal{M}^{++-}\rangle &= \beta \frac{1}{\sqrt{2}} \frac{[p_1 p_2]^3}{[p_2 p_3] [p_1 p_3]} \end{aligned} \quad (8.28)$$

The other helicity amplitudes are obtained from $|\mathcal{M}^{+++}\rangle$ and $|\mathcal{M}^{++-}\rangle$ by the usual parity and charge conjugation relations, while the coefficients α and β are written

in terms of the tensor coefficients,

$$\begin{aligned}\alpha &= \frac{1}{2} \left(\frac{s_{12}}{s_{23}} A_{211} + \frac{s_{23}}{s_{13}} A_{232} - \frac{s_{13}}{s_{23}} A_{311} - 2A_{312} \right), \\ \beta &= \frac{s_{13}}{2} A_{211}.\end{aligned}$$

As with the tensor coefficients, the helicity amplitude coefficients α and β are vectors in color space and have perturbative expansions,

$$\Omega = C_1 \sqrt{4\pi\alpha_s} f^{abc} \left[\Omega^{(0)} + \left(\frac{\alpha_s}{2\pi} \right) \Omega^{(1)} + \left(\frac{\alpha_s}{2\pi} \right)^2 \Omega^{(2)} + \mathcal{O}(\alpha_s^3) \right],$$

for $\Omega = \alpha, \beta$. The ultraviolet and infrared properties of the helicity coefficients match with those of the tensor coefficients,

$$\begin{aligned}\Omega^{(0)} &= \Omega^{(0),U}, \\ \Omega^{(1)} &= S_\epsilon^{-1} \Omega^{(1),U} - \frac{3\beta_0}{2\epsilon} \Omega^{(0),U}, \\ \Omega^{(2)} &= S_\epsilon^{-2} \Omega^{(2),U} - \frac{5\beta_0}{2\epsilon} S_\epsilon^{-1} \Omega^{(1),U} - \left(\frac{5\beta_1}{4\epsilon} - \frac{15\beta_0^2}{8\epsilon^2} \right) \Omega^{(0),U},\end{aligned}\quad (8.29)$$

and,

$$\begin{aligned}\Omega^{(1)} &= \mathbf{I}^{(1)}(\epsilon) \Omega^{(0)} + \Omega^{(1),finite}, \\ \Omega^{(2)} &= \left(-\frac{1}{2} \mathbf{I}^{(1)}(\epsilon) \mathbf{I}^{(1)}(\epsilon) - \frac{\beta_0}{\epsilon} \mathbf{I}^{(1)}(\epsilon) + e^{-\epsilon\gamma} \frac{\Gamma(1-2\epsilon)}{\Gamma(1-\epsilon)} \left(\frac{\beta_0}{\epsilon} + K \right) \mathbf{I}^{(1)}(2\epsilon) + \mathbf{H}^{(2)}(\epsilon) \right) \Omega^{(0)} \\ &\quad + \mathbf{I}^{(1)}(\epsilon) \Omega^{(1)} + \Omega^{(2),finite},\end{aligned}\quad (8.30)$$

where $\mathbf{I}^{(1)}(\epsilon)$ and $\mathbf{H}^{(2)}(\epsilon)$ are defined in eqs 8.22 and 8.25 respectively.

At leading order, one can use the values of $A_{ijk}^{(0)}$, given in eq. (8.15), to get:

$$\alpha^{(0)} = \frac{(s_{12} + s_{23} + s_{13})^2}{s_{12}s_{23}s_{13}} = \frac{M_{\mathcal{H}}^4}{s_{12}s_{23}s_{13}} \quad \text{and} \quad \beta^{(0)} = 1. \quad (8.31)$$

The renormalized next-to-leading order helicity amplitude coefficients can be straightforwardly obtained to all orders in ϵ from the tensor coefficients $A_{ijk}^{(1)}$. For practical purposes they are needed through to $\mathcal{O}(\epsilon^2)$ in evaluating the one-loop self-interference and the infrared divergent one-loop contribution to the two-loop amplitude, while only the finite piece is needed for the one-loop self-interference. They can be decomposed according to their color structure as follows:

$$\Omega^{(1),finite} = f^{abc} \left(N A_\Omega^{(1)} + N_F B_\Omega^{(1)} \right), \quad (8.32)$$

8. Two-Loop Helicity Amplitudes for the $\mathcal{H} \rightarrow ggg$ Decay

The finite two-loop remainder is obtained by subtracting the predicted infrared structure (expanded through to $\mathcal{O}(\epsilon^0)$) from the renormalized helicity coefficient. We further decompose the finite remainder according to the color casimirs as follows,

$$\Omega^{(2),finite} = f^{abc} \left(N^2 A_{\Omega}^{(2)} + \frac{N_F}{N} B_{\Omega}^{(2)} + N N_F C_{\Omega}^{(2)} + N_F^2 D_{\Omega}^{(2)} \right), \quad (8.33)$$

All one-loop coefficients $A_{\Omega}^{(1)}$, $B_{\Omega}^{(1)}$ and two-loop coefficients $A_{\alpha}^{(2)}$, $B_{\alpha}^{(2)}$, $C_{\alpha}^{(2)}$ and $D_{\alpha}^{(2)}$ are given in appendix F, while coefficients $A_{\beta}^{(2)}$, $B_{\beta}^{(2)}$, $C_{\beta}^{(2)}$ and $D_{\beta}^{(2)}$ can be obtained in FORM format from the author.

Chapter 9

Conclusions

The main purpose of this thesis has been the calculation of two-loop matrix elements and helicity amplitudes, for physical processes that involve three on-shell and one off-shell particles. Two-loop calculations, which are the most challenging component in the evaluation of NNLO contributions to physical processes, have only recently become tractable due to the appearance of new calculation tools. Accuracy at NNLO can enhance the theoretical knowledge and understanding, as well as our predictive abilities in conjunction with the high precision experimental data that are expected from LHC.

In the first chapter, we gave a short description of the QCD Lagrangian and the Feynman rules that can be derived from it. The fundamental mechanisms of regularization and renormalization are also explained. Finally, we presented the effective Higgs Lagrangian, a limit of the full theory that significantly simplifies calculations involving the Higgs–gluon interaction.

Infrared divergences are discussed in the second chapter. Using the example of the $\mathcal{H} \rightarrow gg$ decay, we explain how IR divergences appear and cancel out when it comes to the calculation of physical observables. In addition, a method for the prediction of IR divergences, initiated by Catani [11, 12], is presented and used to verify the results of our example calculation. In the third chapter we draw an outline of the basic steps involved in the calculation of two-loop QCD amplitudes. Emphasis is given to the computation of two-loop integrals.

9. Conclusions

The fourth chapter contains a detailed presentation of all the basic tools needed for our purposes. Four of those tools, the auxiliary integral representation, the integration by parts identities (IBP), the master integrals (MI) and the two dimensional harmonic polylogarithms ('2DHPL), can be used in order to find expansions in $\epsilon = 2 - D/2$ for all possible two-loop integrals that can appear in the calculations presented in this thesis.

In chapter 5, we introduce a very powerful algorithm, influenced by a paper from Laporta [38], that enables one to produce and solve a system of equations containing relationships between integrals. The solution of the system gives all required integrals in terms of a small basic set of master integrals (MI). A method for the calculation of those master integrals, due to Gehrmann and Remiddi [42,43], is presented in chapter 6. For each master integral it is possible to derive and solve a differential equation on the external scales of the problem. As a result each master integral can be written as an ϵ expansion in terms of two-dimensional harmonic polylogarithms.

In chapter 7, we have derived analytic formulae for the two-loop virtual corrections to the process $\gamma^* \rightarrow q\bar{q}g$, which arise from the interference of the two-loop with the tree amplitude and from the self-interference of the one-loop amplitude. Together with the contribution from the self-interference of the one-loop amplitudes for $\gamma^* \rightarrow ggg$ [89, 90], these form the full $\mathcal{O}(\alpha_s^3)$ corrections to the three-parton subprocess contribution to $e^+e^- \rightarrow 3$ jets at NNLO.

It must also be kept in mind that these virtual corrections form only part of a full NNLO calculation, which also has to include the one-loop corrections to $\gamma^* \rightarrow 4$ partons [74–77] where one of the partons becomes collinear or soft, as well as the tree-level $\gamma^* \rightarrow 5$ partons processes [71–73] with two soft or collinear partons. Only after summing all these contributions (and including terms from the renormalization of parton distributions for processes with partons in the initial state), do the infrared divergent terms cancel among one another. The factorization properties of both the one-loop, one-unresolved-parton contribution [95–100] and the tree-level, two-unresolved-parton contributions [101–104] have been studied, but a systematic

9. Conclusions

procedure for isolating the infrared singularities has not been established. Although this is still an open and highly non-trivial issue, significant progress is anticipated in the near future.

The remaining finite terms must then be combined into a numerical program implementing the experimental definition of jet observables and event-shape variables. A first calculation involving the above features was presented for the case of photon-plus-one-jet final states in electron-positron annihilation in [105, 106], thus demonstrating the feasibility of this type of calculations. A prerequisite for such a numerical program is a stable and efficient next-to-leading order four-jet program, where the infrared singularities for the one-loop $\gamma^* \rightarrow 4$ partons are combined with the tree-level $\gamma^* \rightarrow 5$ parton with one parton unresolved. Four such programs currently exist [107–110], each of which could be used as a starting point for a full $\mathcal{O}(\alpha_s^3)$ NNLO three-jet program.

In chapter 8, we have derived analytic formulae for the helicity amplitudes of the NNLO virtual corrections to the Higgs decay $\mathcal{H} \rightarrow ggg$, which are required for the interference of the two-loop with the tree amplitude and for the self-interference of the one-loop amplitude. The amplitudes were calculated in the infinite top-mass limit, $M_t \rightarrow \infty$, with use of the effective $\mathcal{H}gg$ coupling. Together with the contribution from the same set of amplitudes for the decay $\mathcal{H} \rightarrow q\bar{q}g$, these form the full virtual NNLO corrections to the three-parton subprocess contribution to $\mathcal{H} \rightarrow 3$ jets at NNLO. Note that for a full NNLO calculation one must also compute the ‘one-loop_{eff}’ corrections to the $\mathcal{H} \rightarrow 4$ partons and the tree-level corrections to the $\mathcal{H} \rightarrow 5$ partons.

Similar results can in principle be obtained for the non-inclusive Higgs production in hadron-hadron collisions, $pp \rightarrow \mathcal{H} + jet$, where the dominant contributions come from the processes $gg \rightarrow g + \mathcal{H}$ and $qg \rightarrow q + \mathcal{H}$. However, the complexity of the cut structure of the non-planar graphs together with the rather different domains of convergence of the one- and two-dimensional harmonic polylogarithms makes this a non-trivial task, and we defer this to a future project [120].

To summarize, in this thesis we present, with more or less detail, a basic set of

9. Conclusions

powerful techniques that can be used in the calculation of two-loop matrix elements and helicity amplitudes. We also describe how we applied those techniques in the calculation of the matrix elements of the process $\gamma^* \rightarrow q\bar{q}g$ and for the calculation of the helicity amplitudes for the Higgs decay $\mathcal{H} \rightarrow ggg$. Matrix elements and helicity amplitudes for the former were published in [45] and [46] respectively, while processes involving the Higgs with three partons at NNLO, will be examined in future work.

Appendix A

Harmonic Polylogarithms up to weight 3

$w = 1$:

$$\begin{aligned} \mathrm{H}(0; X) &= \ln X , \\ \mathrm{H}(1; X) &= -\ln(1 - X) , \\ \mathrm{H}(1 - Y; X) &= -\ln\left(1 - \frac{X}{1 - Y}\right) , \\ \mathrm{H}(Y; X) &= \ln\left(\frac{X + Y}{Y}\right) . \end{aligned} \tag{A.1}$$

$w = 2$:

$$\begin{aligned} \mathrm{H}(0, 1; X) &= \mathrm{Li}_2(X) , \\ \mathrm{H}(0, 1 - Y; X) &= \mathrm{Li}_2\left(\frac{X}{1 - Y}\right) , \\ \mathrm{H}(0, Y; X) &= -\mathrm{Li}_2\left(-\frac{X}{Y}\right) , \\ \mathrm{H}(1, 1 - Y; X) &= \frac{1}{2} \ln^2(1 - X) - \ln(1 - X) \ln(1 - Y) + \mathrm{Li}_2\left(\frac{Y}{1 - X}\right) - \mathrm{Li}_2(Y) , \\ \mathrm{H}(1, Y; X) &= -\ln\left(\frac{1 - X}{1 + Y}\right) \ln\left(\frac{X + Y}{Y}\right) + \mathrm{Li}_2\left(\frac{Y}{1 + Y}\right) - \mathrm{Li}_2\left(\frac{X + Y}{1 + Y}\right) , \\ \mathrm{H}(1 - Y, Y; X) &= -\ln(1 - X - Y) \ln\left(\frac{X + Y}{Y}\right) + \mathrm{Li}_2(Y) - \mathrm{Li}_2(X + Y) . \end{aligned} \tag{A.2}$$

A. Harmonic Polylogarithms up to weight 3

and $w = 3$:

$$H(0, 0, 1; X) = \text{Li}_3(X) ,$$

$$H(0, 1, 1; X) = S_{1,2}(X) ,$$

$$H(0, 0, 1 - Y; X) = \text{Li}_3\left(\frac{X}{1 - Y}\right) ,$$

$$H(0, 0, Y; X) = -\text{Li}_3\left(-\frac{X}{Y}\right) ,$$

$$\begin{aligned} H(0, 1, 1 - Y; X) = & \text{Li}_3\left(\frac{-X}{1 - X - Y}\right) + \text{Li}_3\left(\frac{-Y}{1 - X - Y}\right) - \text{Li}_3\left(\frac{-XY}{1 - X - Y}\right) \\ & + \text{Li}_3(X) - \text{Li}_3\left(\frac{-Y}{1 - Y}\right) - \ln\left(1 - \frac{X}{1 - Y}\right) \text{Li}_2(Y) \\ & - \ln\left(1 - \frac{X}{1 - Y}\right) \text{Li}_2(X) - \frac{1}{6} \ln^3(1 - X - Y) + \frac{1}{6} \ln^3(1 - Y) , \end{aligned}$$

$$\begin{aligned} H(0, 1, Y; X) = & \text{Li}_3\left(\frac{X(1 + Y)}{X + Y}\right) - \text{Li}_3\left(\frac{X}{X + Y}\right) - \text{Li}_3\left(\frac{X + Y}{1 + Y}\right) + \text{Li}_3\left(\frac{Y}{1 + Y}\right) \\ & - \text{Li}_3(X) + \ln\left(\frac{X + Y}{Y}\right) \text{Li}_2\left(\frac{Y}{1 + Y}\right) + \ln\left(\frac{X + Y}{Y}\right) \text{Li}_2(X) \\ & - \ln Y \ln(1 + Y) \ln\left(\frac{X + Y}{Y}\right) + \frac{1}{2} \ln(1 + Y) \ln^2(X + Y) \\ & - \frac{1}{2} \ln(1 + Y) \ln^2 Y , \end{aligned}$$

$$\begin{aligned} H(0, 1 - Y, 1; X) = & S_{1,2}(X) - \text{Li}_3\left(\frac{XY}{(1 - X)(1 - Y)}\right) + \text{Li}_3\left(\frac{X}{1 - Y}\right) + \text{Li}_3\left(\frac{Y}{1 - X}\right) \\ & - \text{Li}_3(X) - \text{Li}_3(Y) - \ln(1 - X) \text{Li}_2\left(\frac{X}{1 - Y}\right) + \ln(1 - X) \text{Li}_2(X) \\ & + \ln(1 - X) \text{Li}_2(Y) + \frac{1}{2} \ln(1 - Y) \ln^2(1 - X) , \end{aligned}$$

$$H(0, 1 - Y, 1 - Y; X) = S_{1,2}\left(\frac{X}{1 - Y}\right) ,$$

$$\begin{aligned} H(0, 1 - Y, Y; X) = & \text{Li}_3\left(\frac{X}{(1 - Y)(X + Y)}\right) - \text{Li}_3\left(\frac{X}{1 - Y}\right) - \text{Li}_3\left(\frac{X}{X + Y}\right) \\ & - \text{Li}_3(X + Y) + \text{Li}_3(Y) + \ln\left(\frac{X + Y}{Y}\right) \text{Li}_2(Y) \\ & + \ln\left(\frac{X + Y}{Y}\right) \text{Li}_2\left(\frac{X}{1 - Y}\right) - \frac{1}{2} \ln(1 - Y) \ln^2\left(\frac{X + Y}{Y}\right) , \end{aligned}$$

$$\begin{aligned} H(0, Y, 1; X) = & -S_{1,2}(X) + \text{Li}_3\left(-\frac{X(1 + Y)}{Y(1 - X)}\right) - \text{Li}_3\left(-\frac{X}{Y}\right) - \text{Li}_3\left(\frac{1 - X}{1 + Y}\right) \\ & + \text{Li}_3\left(\frac{1}{1 + Y}\right) + \text{Li}_3(X) + \ln(1 - X) \text{Li}_2\left(-\frac{X}{Y}\right) \\ & + \ln(1 - X) \text{Li}_2\left(\frac{1}{1 + Y}\right) - \ln(1 - X) \text{Li}_2(X) + \frac{1}{2} \ln\left(\frac{1 + Y}{Y}\right) \ln^2(1 - X) \\ & - \frac{1}{6} \ln^3(1 - X) , \end{aligned}$$

A. Harmonic Polylogarithms up to weight 3

$$\begin{aligned}
 H(0, Y, 1 - Y; X) = & S_{1,2} \left(\frac{X}{(1 - Y)(X + Y)} \right) - S_{1,2} \left(\frac{X}{1 - Y} \right) - S_{1,2} \left(\frac{X}{X + Y} \right) \\
 & + S_{1,2}(X + Y) - S_{1,2}(Y) - \text{Li}_3 \left(\frac{X}{(1 - Y)(X + Y)} \right) \\
 & + \text{Li}_3 \left(\frac{X}{X + Y} \right) + \ln \left(\frac{(1 - Y)(X + Y)}{Y} \right) (\text{Li}_2(X + Y) - \text{Li}_2(Y)) \\
 & - \ln \left(\frac{X + Y}{Y} \right) \text{Li}_2 \left(\frac{X}{1 - Y} \right) + \ln(1 - Y) \ln^2 \left(\frac{X + Y}{Y} \right) \\
 & + \frac{1}{2} \ln^2(1 - Y) \ln \left(\frac{X + Y}{Y} \right) + \text{Li}_3 \left(\frac{X}{1 - Y} \right),
 \end{aligned}$$

$$H(0, Y, Y; X) = S_{1,2} \left(-\frac{X}{Y} \right),$$

$$\begin{aligned}
 H(1, 1 - Y, 1 - Y; X) = & -\frac{1}{2} \ln \left(\frac{1 - X}{Y} \right) \ln^2 \left(\frac{1 - X - Y}{1 - Y} \right) \\
 & - \ln \left(\frac{1 - X - Y}{1 - Y} \right) \text{Li}_2 \left(1 - \frac{1 - X}{Y} \right) \\
 & - \text{Li}_3 \left(1 - \frac{1}{Y} \right) + \text{Li}_3 \left(1 - \frac{1 - X}{Y} \right),
 \end{aligned}$$

$$\begin{aligned}
 H(1, 1 - Y, Y; X) = & 2S_{1,2}(X) - 2\text{Li}_3 \left(\frac{Y}{X + Y} \right) + \text{Li}_3 \left(\frac{Y}{(1 - X)(X + Y)} \right) \\
 & - \text{Li}_3 \left(\frac{Y}{1 - X} \right) + \text{Li}_3 \left(-\frac{1}{Y} \right) + \ln \left(\frac{X + Y}{Y(1 - X)} \right) \text{Li}_2 \left(\frac{1}{1 + Y} \right) \\
 & + \text{Li}_3 \left(\frac{Y(1 - X)}{X + Y} \right) - \text{Li}_3 \left(-\frac{1 - X}{X + Y} \right) - \text{Li}_3(X + Y) \\
 & + 2\text{Li}_3(Y) + \ln \left(\frac{X + Y}{Y} \right) \text{Li}_2 \left(\frac{Y}{1 - X} \right) \\
 & - \ln(1 - X) \text{Li}_2(Y) + 2\ln(1 - X) \text{Li}_2(X) + \ln X \ln^2(1 - X) \\
 & - \frac{1}{2} \ln Y \ln^2 \left(\frac{1 - X}{1 + Y} \right) - \ln Y \ln(1 + Y) \ln \left(\frac{X + Y}{Y} \right) \\
 & - \frac{1}{2} \ln(1 - X) \ln^2(X + Y) + \frac{1}{2} \ln \left(\frac{X + Y}{1 - X} \right) \ln^2(1 + Y) \\
 & + \frac{1}{6} \ln^3(X + Y) - \frac{1}{6} \ln^3 Y,
 \end{aligned}$$

A. Harmonic Polylogarithms up to weight 3

$$\begin{aligned}
 H(1, Y, 1 - Y; X) &= S_{1,2} \left(\frac{Y(X+Y)}{1-X} \right) - S_{1,2} \left(\frac{Y}{1-X} \right) - S_{1,2}(X+Y) - S_{1,2}(Y^2) \\
 &+ 2S_{1,2}(Y) + \text{Li}_3 \left(\frac{1-X}{1+Y} \right) - \text{Li}_3 \left(\frac{1}{1+Y} \right) \\
 &+ \ln(1+Y) \text{Li}_2 \left(\frac{Y}{1-X} \right) \\
 &- \ln(1+Y) \text{Li}_2(Y) + \ln \left(\frac{1-Y^2}{1-X} \right) \text{Li}_2 \left(\frac{1-X}{1+Y} \right) \\
 &- \ln(1-Y^2) \text{Li}_2 \left(\frac{1}{1+Y} \right) + \ln \left(\frac{1+Y}{1-X} \right) \text{Li}_2(X+Y) \\
 &- \ln \left(\frac{1+Y}{1-X} \right) \text{Li}_2(Y) + \ln Y \ln(1-X) \ln(1-Y) \\
 &+ \frac{1}{2} \ln^2(1-X) \ln \left(\frac{1+Y}{X+Y} \right) + \ln(1-X) \ln(1+Y) \ln \left(\frac{X+Y}{1-Y} \right) \\
 &- \frac{1}{2} \ln(1-X) \ln^2(1+Y) - \frac{1}{2} \ln^2(1+Y) \ln \left(\frac{X+Y}{Y} \right), \\
 H(1, Y, Y; X) &= -\frac{1}{2} \ln \left(\frac{1-X}{1+Y} \right) \ln^2 \left(\frac{X+Y}{Y} \right) - \ln \left(\frac{X+Y}{Y} \right) \text{Li}_2 \left(\frac{X+Y}{1+Y} \right) \\
 &- \text{Li}_3 \left(\frac{Y}{1+Y} \right) + \text{Li}_3 \left(\frac{X+Y}{1+Y} \right), \\
 H(1-Y, 1, 1; X) &= \frac{1}{2} \ln^2 Y \ln(1-Y) - \frac{1}{2} \ln^2 Y \ln(1-X-Y) + \ln Y \text{Li}_2 \left(1 - \frac{1-X}{Y} \right) \\
 &- \ln Y \text{Li}_2 \left(1 - \frac{1}{Y} \right) - S_{1,2} \left(1 - \frac{1-X}{Y} \right) + S_{1,2} \left(1 - \frac{1}{Y} \right), \\
 H(1-Y, Y, Y; X) &= -\frac{1}{2} \ln(1-X-Y) \ln^2 \left(\frac{X+Y}{Y} \right) \\
 &- \ln \left(\frac{X+Y}{Y} \right) \text{Li}_2(X+Y) \\
 &- \text{Li}_3(Y) + \text{Li}_3(X+Y), \\
 H(Y, 1, 1; X) &= \frac{1}{2} \ln^2(1-X) \ln \left(\frac{X+Y}{1+Y} \right) \\
 &+ \ln(1-X) \text{Li}_2 \left(\frac{1-X}{1+Y} \right) \\
 &+ \text{Li}_3 \left(\frac{1}{1+Y} \right) - \text{Li}_3 \left(\frac{1-X}{1+Y} \right), \\
 H(Y, 1-Y, 1-Y; X) &= \frac{1}{2} \ln(X+Y) \ln^2 \left(\frac{1-X-Y}{1-Y} \right) \\
 &+ \ln \left(\frac{1-X-Y}{1-Y} \right) \text{Li}_2(1-X-Y) \\
 &+ \text{Li}_3(1-Y) - \text{Li}_3(1-X-Y). \tag{A.3}
 \end{aligned}$$

Appendix B

Application of the Laporta Algorithm

We want to calculate the integral $J(1, 1, 1, 0)$. The input to the algorithm is:

$$\begin{aligned} \text{INPUT : } \quad & [DenSet = [A_1, A_2, A_3]] \\ & MaxDen = 0 \\ & MaxNum = 0 \\ & SolutionSet = \{\} \end{aligned} \tag{B.1}$$

We also find:

$Nk = 2$ and $Nd = 3$ The non-trivial topologies are:

$$SetOfAllIntegrals = \{[A_1, A_2, A_3], [A_1, A_3]\} \tag{B.2}$$

Next we start the loop on n

1. $n = 2$ From the *SetOfAllIntegrals* eq (B.2) we take all the integrals with $n = 2$ and put them in a new set. Thus we get:

$$SetWithnDen = \{[A_1, A_3]\} \tag{B.3}$$

The following steps should be performed for all the indets of *SetWithnDen*.

In this example there is only one topology:

$$Topo = \{[A_1, A_3]\} \tag{B.4}$$

B. Application of the Laporta Algorithm

Now we start the loops on Md (from 0 to $MaxDen$) and Mp (from 0 to $MaxNum$). In our case, both $Maxed$ and $MaxNum$ are set to be zero in the *INPUT* (B.1). Therefore we only have to take $Md = 0$ and $Mp = 0$. For our topology (*Topo*) we need to take all possible combinations, written in the auxiliary integral form, in which the sum of the powers of the $n = 2$ denominators is $Md + n = 2$ and the sum of the powers of numerators is $Mp = 0$. All combinations are put in a set:

$$SetOfOneTopo = \{J(1, 0, 1, 0)\} \quad (B.5)$$

The following steps would be applied to all the indets of *SetOfOneTopo*. Once more in our simple example we have only one indet:

$$Seed = \{J(1, 0, 1, 0)\} \quad (B.6)$$

First we generate the four IBP relations for our *Seed*:

$$\begin{aligned} SeedIBPSet = \{ & 0 = (D - 3) J(1, 0, 1, 0) + s_{12} J(1, 0, 2, 0) \\ & 0 = (D - 2) J(1, 0, 1, 0) - J(1, -1, 2, 0) \\ & \quad - J(2, -1, 1, 0) \\ & 0 = (D - 3) J(1, 0, 1, 0) + s_{12} J(2, 0, 1, 0) \\ & 0 = (D - 2) J(1, 0, 1, 0) - J(1, 0, 2, -1) \\ & \quad - J(2, 0, 1, -1) + s_{123} J(2, 0, 1, 0) \} \end{aligned} \quad (B.7)$$

Next we start a loop on the above IBP equations.

- (a) **1st IBP identity** We take the first of the four equations of the *SeedIBPSet* eq. (B.7) and substitute all the equations of the *SolutionSet* in it. We then solve for the integral of the maximum priority getting:

$$Equat : \quad J(1, 0, 2, 0) = -\frac{(d-3)}{s_{12}} J(1, 0, 1, 0) \quad (B.8)$$

B. Application of the Laporta Algorithm

If eq. (B.8) is linearly independent from all the equations in the *SolutionSet*, we “back-substitute” *Equat* in the *SolutionSet* and then put it in the *SolutionSet*:

$$SolutionSet = \left\{ J(1, 0, 2, 0) = -\frac{(D-3)}{s_{12}} J(1, 0, 1, 0) \right\} \quad (B.9)$$

(b) **2nd IBP identity** We take second of the four equations of the *SeedIBPSet* eq. (B.7) and substitute all the equations of the *SolutionSet* in it. We then solve for the integral of the maximum priority getting:

$$\begin{aligned} Equat : \quad J(1, -1, 2, 0) &= J(1, 0, 1, 0) D - 2J(1, 0, 1, 0) \\ &\quad - J(2, -1, 1, 0) \end{aligned} \quad (B.10)$$

Since eq. (B.10) is linearly independent from all the equations in the *SolutionSet*, we “back-substitute” *Equat* in the *SolutionSet* and then put it in the *SolutionSet*:

$$\begin{aligned} SolutionSet = \\ \left\{ J(1, 0, 2, 0) = -\frac{(D-3)}{s_{12}} J(1, 0, 1, 0), \right. \\ \left. J(1, -1, 2, 0) = -J(2, -1, 1, 0) + (D-2)J(1, 0, 1, 0) \right\} \end{aligned} \quad (B.11)$$

(c) **3rd . . . 4th IBP identities** Working similarly for the third and fourth IBP

B. Application of the Laporta Algorithm

equations of eq. (B.7) we get the following *SolutionSet*:

$$\begin{aligned}
 \text{SolutionSet} = & \\
 \{J(1, 0, 2, 0) = & -\frac{(D-3)}{s_{12}}J(1, 0, 1, 0), \\
 J(1, -1, 2, 0) = & -J(2, -1, 1, 0) + (D-2)J(1, 0, 1, 0), \\
 J(2, 0, 1, 0) = & -\frac{(D-3)}{s_{12}}J(1, 0, 1, 0), \\
 J(1, 0, 2, -1) = & -\frac{(-s_{12}D + 2s_{12} + s_{123}D - 3s_{123})}{s_{12}}J(1, 0, 1, 0) \\
 & -J(2, 0, 1, -1)\}
 \end{aligned} \tag{B.12}$$

2. $n = 3$ From the *SetOfAllIntegrals* eq. (B.2) we take all the integrals with $n = 3$ and put them in a new set. Thus we get:

$$\text{SetWithnDen} = \{[A_1, A_2, A_3]\} \tag{B.13}$$

There is only one topology in the *SetWithnDen*:

$$\text{Topo} = \{[A_1, A_2, A_3]\} \tag{B.14}$$

Now we start the loops on Md (from 0 to $MaxDen$) and Mp (from 0 to $MaxNum$). As we have already shown, we only have to take $Md = 0$ and $Mp = 0$. For the $\text{Topo} = \{[A_1, A_2, A_3]\}$, all possible combinations, written in the auxiliary integral form, in which the sum of the powers of the $n = 3$ denominators is $Md + n = 3$ and the sum of the powers of numerators is $Mp = 0$ are:

$$\text{SetOfOneTopo} = \{J(1, 1, 1, 0)\} \tag{B.15}$$

The following steps would be applied to all the indets of *SetOfOneTopo*. Once more in our simple example the *SetOfOneTopo* has only one indet:

$$\text{Seed} = \{J(1, 1, 1, 0)\} \tag{B.16}$$

B. Application of the Laporta Algorithm

Initially we generate the four IBP relations for our *Seed*:

$$\begin{aligned}
 \text{SeedIBPSet} = \{ & 0 = (D - 4)J(1, 1, 1, 0) + s_{12}J(1, 1, 2, 0) \\
 & 0 = (D - 4)J(1, 1, 1, 0) - J(1, 0, 2, 0) \\
 & \quad - J(2, 0, 1, 0) \\
 & 0 = (D - 4)J(1, 1, 1, 0) + s_{12}J(2, 1, 1, 0) \\
 & 0 = (D - 3)J(1, 1, 1, 0) - J(1, 1, 2, -1) \\
 & \quad + s_{123}J(2, 1, 1, 0) + s_{23}J(1, 2, 1, 0) \\
 & \quad - J(1, 2, 1, -1) - J(2, 1, 1, -1)\}
 \end{aligned} \tag{B.17}$$

Next we start a loop on the above IBP equations eq. (B.17)

- (a) **1st IBP identity** We take the first of the four equations of the *SeedIBPSet* eq. (B.17) and substitute all the equations of the *SolutionSet* in it. We then solve for the integral of the maximum priority getting:

$$\text{Equat : } J(1, 1, 2, 0) = -\frac{(D - 4)}{s_{12}}J(1, 1, 1, 0) \tag{B.18}$$

If eq. (B.18) is linearly independent from all the equations in the *SolutionSet*, we “back-substitute” *Equat* in the *SolutionSet* and then put it in the *SolutionSet*:

$$\begin{aligned}
 \text{SolutionSet} = & \\
 \{ & J(1, 0, 2, 0) = -\frac{(D - 3)}{s_{12}}J(1, 0, 1, 0), \\
 & J(1, -1, 2, 0) = -J(2, -1, 1, 0) + (D - 2)J(1, 0, 1, 0), \\
 & J(2, 0, 1, 0) = -\frac{(D - 3)}{s_{12}}J(1, 0, 1, 0), \\
 & J(1, 0, 2, -1) = -\frac{(-s_{12}D + 2s_{12} + s_{123}D - 3s_{123})}{s_{12}}J(1, 0, 1, 0) \\
 & \quad - J(2, 0, 1, -1), \\
 & J(1, 1, 2, 0) = -\frac{(D - 4)}{s_{12}}J(1, 1, 1, 0)\}
 \end{aligned} \tag{B.19}$$

B. Application of the Laporta Algorithm

(b) **2nd IBP identity** We take the second of the four equations of the *SeedIBPSet* eq. (B.17) and substitute all the equations of the *SolutionSet* in it. We then solve for the integral of the maximum priority getting:

$$\text{Equat : } J(1, 1, 1, 0) = -2 \frac{(D-3)}{s_{12}(D-4)} J(1, 0, 1, 0) \quad (\text{B.20})$$

Since eq. (B.20) is linearly independent from all the equations in the *SolutionSet*, we “back-substitute” *Equat* in the *SolutionSet* and then put it in the *SolutionSet*:

$$\begin{aligned} \text{SolutionSet} = \\ J(1, 1, 2, 0) &= 2 \frac{(D-3)}{s_{12}^2} J(1, 0, 1, 0), \\ J(1, 1, 1, 0) &= -2 \frac{(D-3)}{s_{12}(D-4)} J(1, 0, 1, 0), \\ J(1, 0, 2, 0) &= -\frac{(D-3)}{s_{12}} J(1, 0, 1, 0), \\ J(1, -1, 2, 0) &= -J(2, -1, 1, 0) + (D-2)J(1, 0, 1, 0), \\ J(2, 0, 1, 0) &= -\frac{(D-3)}{s_{12}} J(1, 0, 1, 0), \\ J(1, 0, 2, -1) &= -\frac{(-s_{12}D + 2s_{12} + s_{123}D - 3s_{123})}{s_{12}} J(1, 0, 1, 0) \\ &- J(2, 0, 1, -1) \end{aligned} \quad (\text{B.21})$$

(c) **3rd ... 4th IBP identities** Working similarly for the third and fourth IBP

B. Application of the Laporta Algorithm

equations of eq. (B.17) we get the following *SolutionSet*:

$$\begin{aligned}
 & \text{SolutionSet} = \\
 & \{ J(1, 1, 2, 0) = 2 \frac{(D-3)}{s_{12}^2} J(1, 0, 1, 0), \\
 & J(1, 1, 1, 0) = -2 \frac{(D-3)}{s_{12}(D-4)} J(1, 0, 1, 0), \\
 & J(2, 1, 1, 0) = 2 \frac{(D-3)}{s_{12}^2} J(1, 0, 1, 0), \\
 & J(1, 0, 2, 0) = -\frac{(D-3)}{s_{12}} J(1, 0, 1, 0), \\
 & J(1, -1, 2, 0) = -J(2, -1, 1, 0) + (D-2)J(1, 0, 1, 0), \\
 & J(2, 0, 1, 0) = -\frac{(D-3)}{s_{12}} J(1, 0, 1, 0), \\
 & J(1, 0, 2, -1) = -\frac{(-s_{12}D + 2s_{12} + s_{123}D - 3s_{123})}{s_{12}} J(1, 0, 1, 0) \\
 & -J(2, 0, 1, -1), \\
 & J(1, 1, 2, -1) = +2 \frac{(D-3)(-s_{12}D + s_{123}D - 4s_{123} + 3s_{12})}{s_{12}^2(D-4)} J(1, 0, 1, 0) \\
 & -J(1, 2, 1, -1) - J(2, 1, 1, -1) \\
 & +s_{23}J(1, 2, 1, 0) \} \tag{B.22}
 \end{aligned}$$

At this point all the recursive loops terminate and our output is what is left in the *SolutionSet*. Therefore:

$$\text{OUTPUT} = \text{SolutionSet} \tag{B.23}$$

The second equation of the *SolutionSet* eq (5.13) is the one that gives as the integral ($J(1, 1, 1, 0)$) we wanted to express in terms of other simpler integrals, in this case a two propagator bubble diagram ($J(1, 0, 1, 0)$):

$$\begin{aligned}
 J(1, 1, 1, 0) &= -2 \frac{(D-3)}{s_{12}(D-4)} J(1, 0, 1, 0), \\
 \begin{array}{c} \text{Diagram 1: A triangle with an incoming line from the left labeled } p_{12} \text{ and two outgoing lines to the right labeled } p_1 \text{ and } p_2. \end{array} &= -2 \frac{(D-3)}{s_{12}(D-4)} \begin{array}{c} \text{Diagram 2: A circle with an incoming line from the left labeled } p_{12} \text{ and an outgoing line to the right.} \end{array}
 \end{aligned} \tag{B.24}$$

Appendix C

Two and Three Body Phase-Space

The phase-space in D -dimensions for r particles can be written as:

$$PS_r^D = (2\pi)^{D-r(D-1)} R_r^D, \quad (\text{C.1})$$

where:

$$R_r^D = \int \prod_{i=1}^r \frac{d^{D-1}p_i}{2E_i} \delta^D \left(p_0^2 - \sum_{1 \leq i < j \leq r} s_{ij} \right). \quad (\text{C.2})$$

Two-Body Phase-Space

Applying the above formulas for the case of two final state particles we get the two-body phase-space:

$$PS_2^D = \frac{1}{8\pi} \frac{\Gamma(1-\epsilon)}{\Gamma(2-2\epsilon)} \left(\frac{4\pi}{M^2} \right)^\epsilon \int dy_{12} \delta(y_{12} - 1), \quad (\text{C.3})$$

with y_{ij} defined as:

$$y_{ij} = s_{ij} M^2 \quad (\text{C.4})$$

Three-Body Phase-Space

Similarly when the three-body phase-space reads:

$$PS_3^D = \frac{1}{128\pi^3} \frac{1}{\Gamma(2-2\epsilon)} \left(\frac{4\pi}{M^2} \right)^{2\epsilon} M^2 \cdot \int dy_{12} dy_{23} dy_{13} [y_{12} y_{23} y_{13}]^{-\epsilon} \delta(y_{12} + y_{23} + y_{13} - 1). \quad (\text{C.5})$$

Appendix D

Spinor Helicity

Tree-level and loop QCD amplitudes can be decomposed to partial helicity amplitudes using the spinor helicity formalism [121,122]. Each amplitude can be expressed in terms of spinors in a Weyl basis. This is achieved by introducing a set of kinematic objects, spinor products, which reflect the amplitude's collinear behavior. For a massless particle of momentum k and helicity $\lambda = \pm 1$ one can write:

$$|k^\pm\rangle = \frac{1}{2}(1 \pm \gamma_5)u(k) = \frac{1}{2}(1 \mp \gamma_5)v(k), \quad (\text{D.1})$$

$$\langle k^\pm| = \bar{u}(k)\frac{1}{2}(1 \mp \gamma_5) = \bar{v}(k)\frac{1}{2}(1 \pm \gamma_5). \quad (\text{D.2})$$

The second equality of equations (D.1) and (D.2) is valid because positive and negative energy solutions of the massless Dirac equation can be chosen to be equal to each other. The above spinors can be used to represent polarization vectors for massless vector bosons. Therefore, the polarization vector of a gluon with momentum k reads:

$$\epsilon_\mu^\pm(k; q) = \frac{\langle q^\pm | \gamma_\mu | k^\pm \rangle}{\sqrt{2}\langle q^\mp | k^\pm \rangle}, \quad (\text{D.3})$$

where q is a reference momentum that satisfies $q^2 = 0$ and $q \cdot k \neq 0$, which drops out in final gauge invariant amplitudes. Each helicity amplitude can be expressed in terms of the following spinor inner products:

$$\begin{aligned} \langle k^- | l^+ \rangle &\equiv \langle kl \rangle, \\ \langle k^+ | l^- \rangle &\equiv [kl], \end{aligned} \quad (\text{D.4})$$

D. Spinor Helicity

where $[kl]$ was defined through the identity:

$$\langle kl \rangle [lk] = 2k \cdot l = s_{kl}. \quad (\text{D.5})$$

Significant simplifications in the final results can be achieved with use of spinor identities:

- antisymmetry:

$$\begin{aligned} \langle kl \rangle &= -\langle lk \rangle, \\ [kl] &= -[lk], \\ \langle kk \rangle &= [kk] = 0, \end{aligned} \quad (\text{D.6})$$

- the Gordon identity:

$$\langle k^\pm | \gamma^\mu | k^\pm \rangle = 2k^\mu, \quad |k^\pm \rangle \langle k^\pm| = \frac{1}{2}(1 \pm \gamma_5) \not{k}, \quad (\text{D.7})$$

- the Fierz rearrangement:

$$\langle k^+ | \gamma^\mu | l^+ \rangle \langle m^+ | \gamma_\mu | n^+ \rangle = 2 [kl] \langle mn \rangle, \quad (\text{D.8})$$

- the charge conjugation of current:

$$\langle k^+ | \gamma^\mu | l^+ \rangle = \langle l^- | \gamma^\mu | k^- \rangle, \quad (\text{D.9})$$

- and the Schouten identity:

$$\langle kl \rangle \langle mn \rangle = \langle km \rangle \langle ln \rangle + \langle kn \rangle \langle lm \rangle \quad (\text{D.10})$$

In this thesis we are interested in the helicity amplitudes of the $\mathcal{H} \rightarrow ggg$ decay, in which all particles except the Higgs boson are on-shell. The above set of identities are sufficient for this purpose. In [123] one can find a more detailed presentation of the spinor-product formalism.

Appendix E

The $\gamma^* \rightarrow q\bar{q}g$ NNLO Matrix

Element coefficients

In this appendix we give the coefficients $f_1(y, z)$ and $f_2(y, z)$ of equation 7.28 and coefficients $A_{20}(y, z), B_{20}(y, z), \dots, G_{20}(y, z)$ of equation 7.31:

$$\begin{aligned}
 f_1(y, z) = & \frac{1}{yz} \left((-3 + \epsilon + 2\epsilon^2) \text{Bub}(s_{123}) + \left(-\frac{4}{\epsilon} + 12 - 8\epsilon \right) \text{Bub}(ys_{123}) \right) \\
 & + \frac{y}{z} \left(\left(-\frac{2}{\epsilon} + 8 - 10\epsilon + 3\epsilon^2 + \epsilon^3 \right) \text{Bub}(zs_{123}) + (-3 + 4\epsilon + \epsilon^2 - 2\epsilon^3) \text{Bub}(s_{123}) \right) \\
 & + \left(-\frac{2}{\epsilon} + 8 - 10\epsilon + 4\epsilon^2 \right) \text{Bub}(ys_{123}) \\
 & + \frac{1}{z} \left(\left(\frac{4}{\epsilon} - 12 + 9\epsilon - \epsilon^2 \right) \text{Bub}(zs_{123}) + (6 - 2\epsilon - 4\epsilon^2) \text{Bub}(s_{123}) \right) \\
 & + \left(\frac{4}{\epsilon} - 12 + 8\epsilon \right) \text{Bub}(ys_{123}) \\
 & + \frac{y}{(1-z)^2} (1-\epsilon) \left(\text{Bub}(zs_{123}) - \text{Bub}(s_{123}) \right) \\
 & + \frac{y}{(1-z)} \left((3 - 5\epsilon + 2\epsilon^3) \text{Bub}(zs_{123}) + (-3 + 4\epsilon + \epsilon^2 - 2\epsilon^3) \text{Bub}(s_{123}) \right) \\
 & + \frac{1}{(1-z)} (4 - 3\epsilon - 3\epsilon^2 - 2\epsilon^3) \left(\text{Bub}(s_{123}) - \text{Bub}(zs_{123}) \right) \\
 & + (4 - 9\epsilon + 6\epsilon^2 - \epsilon^3) \text{Bub}(zs_{123}) \\
 & + s_{123} \text{Box}^6(y s_{123}, z s_{123}, s_{123}) (1 - 2\epsilon) \left(\frac{1}{z} 8(-1 + \epsilon) + \frac{y^2}{z} (-2 + 4\epsilon - 2\epsilon^2) \right. \\
 & \left. + \frac{y}{z} (6 - 8\epsilon + 2\epsilon^2) + z(-2 + 2\epsilon - 8\epsilon^2) + (4 - 3\epsilon + 3\epsilon^2) + \frac{1}{yz} 2(1 - \epsilon) \right), \tag{E.1}
 \end{aligned}$$

$$\begin{aligned}
f_2(y, z) = & \frac{1}{yz} \left((3 - \epsilon - 2\epsilon^2) \text{Bub}(s_{123}) + \left(\frac{2}{\epsilon} - 6 + 4\epsilon \right) \text{Bub}((1 - y - z)s_{123}) \right) \\
& + \frac{y}{z} \left(-\epsilon^2(1 - \epsilon) \text{Bub}(zs_{123}) + (3 - 4\epsilon - \epsilon^2 + 2\epsilon^3) \text{Bub}(s_{123}) \right) \\
& + \left(\frac{2}{\epsilon} - 8 + 10\epsilon - 4\epsilon^2 \right) \text{Bub}((1 - y - z)s_{123}) \\
& + \frac{1}{z} \left(\epsilon(1 - \epsilon) \text{Bub}(zs_{123}) + (-6 + 2\epsilon + 4\epsilon^2) \text{Bub}(s_{123}) \right) \\
& + \left(-\frac{4}{\epsilon} + 12 - 8\epsilon \right) \text{Bub}((1 - y - z)s_{123}) \\
& + \frac{1}{(y+z)^2} 2 \left(\text{Bub}((1 - y - z)s_{123}) - \text{Bub}(s_{123}) \right) \\
& + \frac{1}{(y+z)} 2\epsilon \left(\text{Bub}(s_{123}) - 2\text{Bub}((1 - y - z)s_{123}) \right) \\
& + \frac{y}{(1-z)^2} (1 - \epsilon) \left(\text{Bub}(s_{123}) - \text{Bub}(zs_{123}) \right) \\
& + \frac{y}{(1-z)} \left((3 - 4\epsilon - \epsilon^2 + 2\epsilon^3) \text{Bub}(s_{123}) + (-3 + 5\epsilon - 2\epsilon^3) \text{Bub}(zs_{123}) \right) \\
& + \frac{1}{(1-z)} (2 + \epsilon - 5\epsilon^2 - 2\epsilon^3) \left(\text{Bub}(zs_{123}) - \text{Bub}(s_{123}) \right) \\
& + (2 - 7\epsilon + 2\epsilon^2 + 3\epsilon^3) \text{Bub}(zs_{123}) + (-4 + 10\epsilon - 4\epsilon^2) \text{Bub}((1 - y - z)s_{123}) \\
& + s_{123} \text{Box}^6((1 - y - z)s_{123}, zs_{123}, s_{123}) (1 - 2\epsilon) \left((8 - 4\epsilon) - \frac{(1 - y)}{z} 4(1 - \epsilon) \right) \\
& + (y + z)(-4 + 4\epsilon - 6\epsilon^2 - 2\epsilon^3) + \frac{y^2}{z} (-2 + 4\epsilon - 2\epsilon^2). \tag{E.2}
\end{aligned}$$

The above expressions are written in terms of the one-loop MI's Bub and Box⁶. Expansions in ϵ for both MI's can be found in the appendix of [45].

$$\begin{aligned}
 A_{20}(y, z) = & \frac{z}{12y} [2\pi^2 + 6\pi^2 H(0; z) - 12\pi^2 H(1; y) - 72\zeta_3 + 8H(0; z) - 36H(0; z)H(1, 0; y) - 36H(0, 1, 0; z) \\
 & + 39H(1, 0; z) + 39H(1, 0; y) + 72H(1, 1, 0; y)] + \frac{1}{2y(y+z)} [17H(1, 0; z) + 17H(1, 0; y)] \\
 & + \frac{1}{36y} [-12\pi^2 - 24\pi^2 H(0; z) + 48\pi^2 H(1; y) + 288\zeta_3 + 457 - 84H(0; z) - 36H(0; z)H(0; y) \\
 & + 144H(0; z)H(1, 0; y) + 144H(0, 1, 0; z) - 306H(1, 0; z) - 192H(0; y) - 234H(1, 0; y) \\
 & - 288H(1, 1, 0; y)] + \frac{z}{36(1-y)^2} [-\pi^2 + 6\pi^2 H(0; z) + 6\pi^2 H(1; z) - 6\pi^2 H(2; y) + 18\pi^2 H(0; y) \\
 & - 12\pi^2 H(1; y) + 36\zeta_3 - 36H(0; z)H(2, 0; y) + 60H(0; z)H(0; y) \\
 & + 72H(0; z)H(0, 0; y) + 36H(0, 1, 0; z) - 36H(1, 0; z)H(2; y) + 36H(1, 0; z)H(0; y) \\
 & + 36H(1, 1, 0; z) + 36H(2, 1, 0; y) - 355H(0; y) + 270H(0, 0; y) - 108H(0, 1, 0; y) + 6H(1, 0; y) \\
 & - 72H(1, 0, 0; y) + 72H(1, 1, 0; y)] + \frac{z}{36(1-y)} [-33\pi^2 + 18\pi^2 H(0; z) + 18\pi^2 H(1; z) \\
 & - 18\pi^2 H(2; y) + 54\pi^2 H(0; y) - 36\pi^2 H(1; y) + 108\zeta_3 - 277 + 60H(0; z) - 108H(0; z)H(2, 0; y) \\
 & + 216H(0; z)H(0; y) + 216H(0; z)H(0, 0; y) + 108H(0, 1, 0; z) + 36H(1, 0; z) \\
 & + 108H(1, 0; z)H(0; y) + 108H(1, 1, 0; z) + 108H(2, 1, 0; y) - 615H(0; y) + 594H(0, 0; y) \\
 & - 324H(0, 1, 0; y) + 198H(1, 0; y) - 216H(1, 0, 0; y) + 216H(1, 1, 0; y) - 108H(1, 0; z)H(2; y)] \\
 & + \frac{z}{(y+z)^3} \left[\frac{11\pi^2}{2} H(1; z) - \frac{11\pi^2}{2} H(2; y) - 33H(0; z)H(2, 0; y) - 33H(0, 1, 0; z) - 33H(1, 0; z) \right. \\
 & \left. - 33H(1, 0; z)H(2; y) + 33H(1, 0; z)H(0; y) + 33H(1, 1, 0; z) + 33H(2, 1, 0; y) \right. \\
 & \left. + 33H(0, 1, 0; y) - 33H(1, 0; y) \right] + \frac{z}{2(y+z)^2} \left[-11\pi^2 - \frac{22\pi^2}{3} H(1; z) \right. \\
 & \left. + \frac{22\pi^2}{3} H(2; y) + 33H(0; z) + 44H(0; z)H(2, 0; y) - 66H(0; z)H(0; y) + 44H(0, 1, 0; z) \right. \\
 & \left. - 22H(1, 0; z) + 44H(1, 0; z)H(2; y) - 44H(1, 0; z)H(0; y) - 44H(1, 1, 0; z) - 44H(2, 1, 0; y) \right. \\
 & \left. - 33H(0; y) - 44H(0, 1, 0; y) + 110H(1, 0; y) \right] + \frac{z}{2(y+z)} \left[\frac{11\pi^2}{6} - 11H(0; z) + 11H(0; z)H(0; y) \right. \\
 & \left. + 11H(1, 0; z) + 11H(0; y) - 11H(1, 0; y) \right] + \frac{z^2}{(y+z)^4} \left[-\frac{11\pi^2}{2} H(1; z) + \frac{11\pi^2}{2} H(2; y) \right. \\
 & \left. + 33H(0; z)H(2, 0; y) + 33H(0, 1, 0; z) + 33H(1, 0; z)H(2; y) - 33H(1, 0; z)H(0; y) \right. \\
 & \left. - 33H(1, 1, 0; z) - 33H(2, 1, 0; y) - 33H(0, 1, 0; y) \right] \\
 & + \frac{z^2}{(y+z)^3} \left[\frac{11\pi^2}{2} + \frac{11\pi^2}{3} H(1; z) - \frac{11\pi^2}{3} H(2; y) \right. \\
 & \left. - 22H(0; z)H(2, 0; y) + 33H(0; z)H(0; y) - 22H(0, 1, 0; z) + 33H(1, 0; z) - 22H(1, 0; z)H(2; y) \right. \\
 & \left. + 22H(1, 0; z)H(0; y) + 22H(1, 1, 0; z) + 22H(2, 1, 0; y) + 22H(0, 1, 0; y) - 33H(1, 0; y) \right]
 \end{aligned}$$

E. The $\gamma^* \rightarrow q\bar{q}g$ NNLO Matrix Element coefficients

$$\begin{aligned}
& +\frac{z^2}{2(y+z)^2} \left[-\frac{11\pi^2}{6} - 11H(0; z)H(0; y) - 11H(1, 0; z) + 11H(1, 0; y) \right] \\
& +\frac{1}{18(1-y)} \left[+23\pi^2 - 12\pi^2H(0; z) - 12\pi^2H(1; z) + 12\pi^2H(2; y) \right. \\
& -36\pi^2H(0; y) + 24\pi^2H(1; y) - 72\zeta_3 + 72H(1, 0; z)H(2; y) + 216H(0, 1, 0; y) \\
& -120H(0; z)H(0; y) - 144H(0; z)H(0, 0; y) - 72H(0, 1, 0; z) - 18H(1, 0; z) \\
& -72H(1, 0; z)H(0; y) - 72H(1, 1, 0; z) - 72H(2, 1, 0; y) + 515H(0; y) - 432H(0, 0; y) \\
& \left. -138H(1, 0; y) + 144H(1, 0, 0; y) - 144H(1, 1, 0; y) + 72H(0; z)H(2, 0; y) \right] \\
& +\frac{1}{(y+z)^2} \left[-\frac{7\pi^2}{3}H(1; z) + \frac{7\pi^2}{3}H(2; y) - 14H(1, 1, 0; z) \right. \\
& +14H(0; z)H(2, 0; y) + 14H(0, 1, 0; z) + 14H(1, 0; z)H(2; y) - 14H(1, 0; z)H(0; y) \\
& \left. -14H(2, 1, 0; y) - 14H(0, 1, 0; y) \right] +\frac{1}{4(y+z)} \left[\frac{28\pi^2}{3} + \frac{14\pi^2}{3}H(1; z) - \frac{14\pi^2}{3}H(2; y) - 22 \right. \\
& +11H(0; z) - 28H(0; z)H(2, 0; y) + 56H(0; z)H(0; y) - 28H(0, 1, 0; z) + 56H(1, 0; z) \\
& -28H(1, 0; z)H(2; y) + 28H(1, 0; z)H(0; y) + 28H(1, 1, 0; z) + 28H(2, 1, 0; y) + 11H(0; y) \\
& \left. +28H(0, 1, 0; y) - 56H(1, 0; y) \right] +\frac{T\pi^2}{216} \left[-1045 + 147H(0; z) + 36H(0; z)H(2; y) \right. \\
& -36H(0; z)H(1; y) + 72H(0, 1; z) + 54H(1; z) + 72H(1; z)H(2; y) - 72H(1; z)H(3; y) \\
& -36H(1; z)H(1; y) + 72H(1, 0; z) + 36H(1, 1; z) - 186H(2; y) + 36H(2, 0; y) - 72H(2, 1; y) \\
& +72H(3, 2; y) - 72H(0, 2; y) + 147H(0; y) - 72H(0, 1; y) + 36H(1, 2; y) + 132H(1; y) \\
& \left. -108H(1, 0; y) + 72H(1, 1; y) + 108H(0; z)H(0; y) \right] \\
& +\frac{T}{216} \left[-\frac{99931}{12} + \frac{132\pi^4}{5} + 4776\zeta_3 - 216\zeta_3H(0; z) + 1080\zeta_3H(1; z) \right. \\
& -864\zeta_3H(2; y) - 216\zeta_3H(0; y) - 216\zeta_3H(1; y) + 304H(0; z) - 1116H(0; z)H(2, 0; y) \\
& -216H(0; z)H(2, 1, 0; y) + 432H(0; z)H(3, 2, 0; y) - 432H(0; z)H(0, 2, 0; y) \\
& -144H(0; z)H(0; y) + 1512H(0; z)H(0, 0; y) - 216H(0; z)H(0, 1, 0; y) \\
& -36H(0; z)H(1, 0; y) - 432H(0; z)H(1, 0, 0; y) + 1920H(0, 0; z) + 1512H(0, 0; z)H(0; y) \\
& +432H(0, 0; z)H(0, 0; y) + 864H(0, 0, 1, 0; z) + 1008H(0, 1, 0; z) - 216H(0, 1, 0; z)H(2; y) \\
& +432H(0, 1, 0; z)H(3; y) + 216H(0, 1, 0; z)H(0; y) - 216H(0, 1, 0; z)H(1; y) \\
& \left. -1095H(1, 0; z) - 1116H(1, 0; z)H(2; y) + 216H(1, 0; z)H(2, 0; y) + 432H(1, 0; z)H(3, 2; y) \right]
\end{aligned}$$

$$\begin{aligned}
&+216H(0; z)H(1, 2, 0; y) + 432H(0, 1, 1, 0; z) + 432H(1, 0, 0; z)H(0; y) \\
&-432H(1, 0; z)H(3, 0; y) - 432H(1, 0; z)H(0, 2; y) + 1152H(1, 0; z)H(0; y) \\
&+216H(1, 0; z)H(1, 2; y) - 216H(1, 0; z)H(1, 0; y) + 1512H(1, 0, 0; z) \\
&+864H(1, 0, 1, 0; z) + 324H(1, 1, 0; z) + 432H(1, 1, 0; z)H(2; y) - 432H(1, 1, 0; z)H(3; y) \\
&-216H(1, 1, 0; z)H(1; y) + 432H(1, 1, 0, 0; z) + 216H(1, 1, 1, 0; z) + 216H(2, 0, 1, 0; y) \\
&+1116H(2, 1, 0; y) + 432H(2, 1, 1, 0; y) - 432H(3, 2, 1, 0; y) - 432H(3, 0, 1, 0; y) \\
&+432H(0, 2, 1, 0; y) + 304H(0; y) + 1920H(0, 0; y) - 432H(0, 0, 1, 0; y) - 1008H(0, 1, 0; y) \\
&+432H(0, 1, 1, 0; y) - 216H(1, 2, 1, 0; y) + 1095H(1, 0; y) - 1512H(1, 0, 0; y) \\
&-792H(1, 1, 0; y) + 432H(1, 1, 0, 0; y) - 432H(1, 1, 1, 0; y) + 648H(1, 0, 1, 0; y)] \\
&+\frac{1}{2}\left[-\frac{7\pi^2}{3} + 1 - 14H(0; z)H(0; y) \right. \\
&\left. -14H(1, 0; z) + 14H(1, 0; y)\right] , \tag{E.3}
\end{aligned}$$

$$B_{20}(y, z) =$$

$$\begin{aligned}
&\frac{z}{y^2}\left[-3H(0; z)H(2; y) - 3H(1; z)H(3; y) + 3H(3, 2; y)\right] + \frac{z^2}{y^2}\left[H(0; z)H(2; y) \right. \\
&+H(1; z)H(3; y) - H(3, 2; y)] + \frac{1}{y^2}\left[2H(0; z)H(2; y) + 2H(1; z)H(3; y) - 2H(3, 2; y)\right] \\
&+\frac{z\pi^2}{18y}\left[3H(0; z) - 24H(0; z)H(2; y) + 21H(1; z) - 12H(1; z)H(2; y) + 12H(2, 2; y) \right. \\
&+H(2; y) + 12H(2, 1; y) + 6H(0, 2; y) + 36H(1; y)] + \frac{z}{9y}\left[-27\zeta_3 - 90\zeta_3H(2; y) \right. \\
&-36H(0; z) - 84H(0; z)H(2, 2; y) + 18H(0; z)H(2, 2, 0; y) \\
&+18H(0; z)H(2, 3, 2; y) + 152H(0; z)H(2; y) - 57H(0; z)H(2, 0; y) \\
&+36H(0; z)H(3, 2, 2; y) + 78H(0; z)H(3, 2; y) - 18H(0; z)H(3, 0, 2; y) \\
&-18H(0; z)H(0, 2, 2; y) - 3H(0; z)H(0, 2; y) + 36H(0; z)H(0, 2, 0; y) \\
&+18H(0; z)H(0, 3, 2; y) + 54H(0; z)H(1, 0; y) - 18H(0, 0; z)H(2, 2; y) \\
&-36H(0, 0; z)H(2; y) - 18H(0, 0; z)H(2, 0; y) - 18H(0, 0; z)H(0, 2; y) \\
&-9H(0, 0, 1; z) + 54H(0, 0, 1; z)H(2; y) - 72H(0, 0, 1; z)H(3; y) - 9H(0, 1; z) \\
&+54H(0, 1; z)H(2, 3; y) + 9H(0, 1; z)H(2; y) - 18H(0, 1; z)H(2, 0; y) \\
&-108H(0, 1; z)H(3, 3; y) + 6H(0, 1; z)H(3; y) + 18H(0, 1; z)H(3, 0; y) \\
&-36H(0, 1; z)H(0, 3; y) + 9H(0, 1, 0; z) - 36H(0, 1, 0; z)H(2; y) \\
&+18H(0, 1, 0; z)H(3; y) + 18H(0, 1; z)H(0, 2; y)
\end{aligned}$$

E. The $\gamma^* \rightarrow q\bar{q}g$ NNLO Matrix Element coefficients

$$\begin{aligned}
& +72H(1; z)H(2, 3, 3; y) - 75H(1; z)H(2, 3; y) - 18H(1; z)H(2, 3, 0; y) \\
& -18H(1; z)H(2, 0, 3; y) + 36H(1; z)H(3, 2, 3; y) - 84H(1; z)H(3, 2; y) \\
& +36H(1; z)H(3, 3, 2; y) - 108H(1; z)H(3, 3, 3; y) + 84H(1; z)H(3, 3; y) \\
& +36H(1; z)H(3, 3, 0; y) + 143H(1; z)H(3; y) + 24H(1; z)H(3, 0; y) - 18H(1; z)H(0, 3, 2; y) \\
& -18H(1; z)H(0, 3, 3; y) - 3H(1; z)H(0, 3; y) + 36H(1; z)H(0, 3, 0; y) + 9H(1; z)H(0; y) \\
& +27H(1; z)H(1, 0; y) + 36H(1, 0; z)H(2, 2; y) - 18H(1, 0; z)H(2, 3; y) \\
& +57H(1, 0; z)H(2; y) - 18H(1, 0; z)H(2, 0; y) - 18H(1, 0; z)H(3, 2; y) \\
& -78H(1, 0; z)H(3; y) + 36H(1, 0; z)H(0, 2; y) - 18H(1, 0; z)H(0, 3; y) - 18H(1, 0, 0; z)H(2; y) \\
& -36H(1, 0, 1; z) - 18H(1, 0, 1; z)H(2; y) - 36H(1, 1; z)H(3, 3; y) + 84H(1, 1; z)H(3; y) \\
& +18H(1, 1; z)H(0, 3; y) - 18H(1, 1, 0; z) - 54H(1, 1, 0; z)H(2; y) + 18H(1, 1, 0; z)H(3; y) \\
& -18H(2, 2, 1, 0; y) + 75H(2, 3, 2; y) + 18H(2, 3, 2, 0; y) \\
& -72H(2, 3, 3, 2; y) + 18H(2, 3, 0, 2; y) + 18H(2, 0, 3, 2; y) - 9H(2, 0; y) \\
& +18H(2, 0, 1, 0; y) + 54H(2, 1, 0; y) - 36H(2, 1, 1, 0; y) + 84H(3, 2, 2; y) \\
& -36H(3, 2, 3, 2; y) - 143H(3, 2; y) - 24H(3, 2, 0; y) + 18H(3, 2, 1, 0; y) \\
& -36H(3, 3, 2, 2; y) - 84H(3, 3, 2; y) - 36H(3, 3, 2, 0; y) \\
& +108H(3, 3, 3, 2; y) - 36H(3, 3, 0, 2; y) - 24H(3, 0, 2; y) + 18H(3, 0, 1, 0; y) \\
& -9H(0, 2; y) + 18H(0, 3, 2, 2; y) + 3H(0, 3, 2; y) - 36H(0, 3, 2, 0; y) \\
& +18H(0, 3, 3, 2; y) - 36H(0, 3, 0, 2; y) + 27H(0, 1, 0; y) - 27H(1, 2, 0; y) \\
& -27H(1, 0, 2; y) + 9H(1, 0; y) - 108H(1, 1, 0; y)] + \frac{z^2}{y} [2H(0; z)H(2; y) + 2H(1; z)H(3; y) \\
& -2H(3, 2; y)] + \frac{1}{y(y+z)} [2H(0; z)H(2; y) + 6H(0; z)H(3, 2; y) - 6H(0; z)H(0, 2; y) \\
& -2H(0, 1; z) - 6H(0, 1; z)H(3; y) + 6H(1; z)H(3, 0; y) - 6H(1; z)H(0, 3; y) + 2H(1; z)H(0; y) \\
& +6H(1, 0; z)H(2; y) - 6H(1, 0; z)H(3; y) - 6H(1, 1, 0; z) - 2H(2, 0; y) + 6H(2, 1, 0; y) \\
& -6H(3, 2, 0; y) - 6H(3, 0, 2; y) - 2H(0, 2; y) + 6H(0, 3, 2; y) + 6H(0, 1, 0; y) \\
& +2H(1, 0; y)] + \frac{\pi^2}{9y} [-3 + 3H(0; z) + 24H(0; z)H(2; y) - 15H(1; z) + 12H(1; z)H(2; y) \\
& -12H(2, 2; y) - 7H(2; y) - 12H(2, 1; y) - 6H(0, 2; y) - 24H(1; y)] + \frac{1}{9y} \left[\frac{45}{2} H(1; z) \right]
\end{aligned}$$

E. The $\gamma^* \rightarrow q\bar{q}g$ NNLO Matrix Element coefficients

$$\begin{aligned}
& -\frac{45}{2}H(2; y) - 54\zeta_3 + 180\zeta_3 H(2; y) + 139 + 57H(0; z) + 132H(0; z)H(2, 2; y) \\
& - 36H(0; z)H(2, 2, 0; y) - 36H(0; z)H(2, 3, 2; y) - 250H(0; z)H(2; y) \\
& + 96H(0; z)H(2, 0; y) - 72H(0; z)H(3, 2, 2; y) - 210H(0; z)H(3, 2; y) \\
& + 36H(0; z)H(3, 0, 2; y) + 36H(0; z)H(0, 2, 2; y) + 96H(0; z)H(0, 2; y) \\
& - 72H(0; z)H(0, 2, 0; y) - 36H(0; z)H(0, 3, 2; y) - 72H(0; z)H(1, 0; y) \\
& + 36H(0, 0; z)H(2, 2; y) + 144H(0, 0; z)H(2; y) + 36H(0, 0; z)H(2, 0; y) \\
& + 36H(0, 0; z)H(0, 2; y) - 108H(0, 0, 1; z)H(2; y) + 144H(0, 0, 1; z)H(3; y) \\
& - 9H(0; z)H(0; y) + 72H(0, 1, 0; z)H(2; y) \\
& - 18H(0, 0, 1; z) + 36H(0, 1; z) + 72H(0, 1; z)H(0, 3; y) \\
& - 108H(0, 1; z)H(2, 3; y) + 36H(0, 1; z)H(2, 0; y) + 216H(0, 1; z)H(3, 3; y) \\
& + 42H(0, 1; z)H(3; y) - 36H(0, 1; z)H(3, 0; y) - 36H(0, 1; z)H(0, 2; y) \\
& + 18H(0, 1, 0; z) - 36H(0, 1, 0; z)H(3; y) - 144H(1; z)H(2, 3, 3; y) \\
& + 132H(1; z)H(2, 3; y) + 36H(1; z)H(2, 3, 0; y) + 36H(1; z)H(2, 0, 3; y) \\
& - 72H(1; z)H(3, 2, 3; y) + 132H(1; z)H(3, 2; y) - 72H(1; z)H(3, 3, 2; y) \\
& + 216H(1; z)H(3, 3, 3; y) - 168H(1; z)H(3, 3; y) - 72H(1; z)H(3, 3, 0; y) \\
& - 214H(1; z)H(3; y) - 30H(1; z)H(3, 0; y) + 36H(1; z)H(0, 3, 2; y) \\
& + 96H(1; z)H(0, 3; y) - 72H(1; z)H(0, 3, 0; y) - 27H(1; z)H(0; y) - 18H(1, 0; z) \\
& - 18H(1; z)H(1, 0; y) + 36H(1; z)H(0, 3, 3; y) \\
& - 72H(1, 0; z)H(2, 2; y) + 36H(1, 0; z)H(2, 3; y) - 168H(1, 0; z)H(2; y) \\
& + 36H(1, 0; z)H(2, 0; y) + 36H(1, 0; z)H(3, 2; y) + 210H(1, 0; z)H(3; y) \\
& - 72H(1, 0; z)H(0, 2; y) + 36H(1, 0; z)H(0, 3; y) + 36H(1, 0, 0; z)H(2; y) \\
& - 36H(1, 1; z)H(0, 3; y) + 36H(1, 0, 1; z) + 72H(1, 1, 0; z) \\
& + 36H(1, 0, 1; z)H(2; y) + 72H(1, 1; z)H(3, 3; y) - 132H(1, 1; z)H(3; y) \\
& + 108H(1, 1, 0; z)H(2; y) - 36H(1, 1, 0; z)H(3; y) + 36H(2, 2, 1, 0; y) \\
& - 132H(2, 3, 2; y) - 36H(2, 3, 2, 0; y) + 144H(2, 3, 3, 2; y) \\
& - 36H(2, 3, 0, 2; y) - 36H(2, 0, 3, 2; y) + 27H(2, 0; y) - 36H(2, 0, 1, 0; y) \\
& - 108H(2, 1, 0; y) + 72H(2, 1, 1, 0; y) - 132H(3, 2, 2; y) + 72H(3, 2, 3, 2; y) \\
& + 214H(3, 2; y) + 30H(3, 2, 0; y) - 36H(3, 2, 1, 0; y) + 72H(3, 3, 2, 2; y) \\
& + 168H(3, 3, 2; y) + 72H(3, 3, 2, 0; y) - 216H(3, 3, 3, 2; y)
\end{aligned}$$

E. The $\gamma^* \rightarrow q\bar{q}g$ NNLO Matrix Element coefficients

$$\begin{aligned}
& +72H(3, 3, 0, 2; y) + 30H(3, 0, 2; y) - 36H(3, 0, 1, 0; y) + 27H(0, 2; y) \\
& - 36H(0, 3, 2, 2; y) - 96H(0, 3, 2; y) + 72H(0, 3, 2, 0; y) - 36H(0, 3, 3, 2; y) \\
& + 72H(0, 3, 0, 2; y) - 48H(0; y) - 54H(0, 1, 0; y) + 18H(1, 2, 0; y) + 18H(1, 0, 2; y) \\
& - 18H(1, 0; y) + 144H(1, 1, 0; y) \Big] + \frac{z}{9(1-y)^2} \Big[-11\pi^2 \\
& - \frac{27\pi^2}{2}H(0; z) - \frac{27\pi^2}{2}H(1; z) + \frac{27\pi^2}{2}H(2; y) \\
& - 6\pi^2H(0; y) + 6\pi^2H(1; y) + 225\zeta_3 + \frac{81}{2}H(1; z)H(0; y) - \frac{81}{2}H(2, 0; y) - \frac{81}{2}H(0, 2; y) \\
& + 9H(0; z)H(2, 0; y) - 72H(0; z)H(0, 2; y) + 12H(0; z)H(0; y) - 9H(0; z)H(0, 0; y) \\
& - 81H(1; z)H(2, 3; y) + 81H(0, 0, 1; z) - 36H(1, 0; z) \\
& + 36H(0, 1; z) - 81H(0, 1; z)H(2; y) - 9H(0, 1; z)H(0; y) - 81H(0, 1, 0; z) \\
& + 36H(1; z)H(3; y) - 81H(1; z)H(0, 3; y) + 27H(1; z)H(0, 0; y) + 81H(1, 0; z)H(2; y) \\
& - 9H(1, 0; z)H(0; y) + 81H(1, 0, 1; z) - 81H(1, 1, 0; z) + 81H(2, 3, 2; y) - 27H(2, 0, 0; y) \\
& - 36H(3, 2; y) - 27H(0, 2, 0; y) + 81H(0, 3, 2; y) + 37H(0; y) - 27H(0, 0, 2; y) \\
& - 45H(0, 0; y) + 45H(0, 1, 0; y) + 30H(1, 0; y) + 36H(1, 0, 0; y) - 36H(1, 1, 0; y) \Big] \\
& + \frac{z}{18(1-y)} \Big[-9\pi^2H(0; z) - 9\pi^2H(1; z) + 9\pi^2H(2; y) - 36\pi^2H(0; y) + 36\pi^2H(1; y) \\
& + 54\zeta_3 + 62 - 54H(0; z)H(0, 0; y) + 54H(0, 0, 1; z) \\
& + 60H(0; z) - 144H(0; z)H(2; y) + 54H(0; z)H(2, 0; y) - 108H(0; z)H(0; y) \\
& - 18H(0, 1; z) - 54H(0, 1; z)H(2; y) - 54H(0, 1; z)H(0; y) - 54H(0, 1, 0; z) \\
& + 117H(1; z) - 54H(1; z)H(2, 3; y) - 162H(1; z)H(3; y) - 54H(1; z)H(0, 3; y) \\
& + 99H(1; z)H(0; y) + 162H(1; z)H(0, 0; y) - 18H(1, 0; z) \\
& + 54H(1, 0; z)H(2; y) - 54H(1, 0; z)H(0; y) + 54H(1, 0, 1; z) \\
& - 54H(1, 1, 0; z) + 54H(2, 3, 2; y) - 117H(2; y) - 99H(2, 0; y) - 162H(2, 0, 0; y) \\
& + 162H(3, 2; y) - 99H(0, 2; y) - 162H(0, 2, 0; y) + 54H(0, 3, 2; y) + 132H(0; y) \\
& - 162H(0, 0, 2; y) - 198H(0, 0; y) + 270H(0, 1, 0; y) + 18H(1, 0; y) \\
& + 216H(1, 0, 0; y) - 216H(1, 1, 0; y) \Big]
\end{aligned}$$

E. The $\gamma^* \rightarrow q\bar{q}g$ NNLO Matrix Element coefficients

$$\begin{aligned}
& +\frac{z}{(y+z)^3} [-2\pi^2 H(1; z) + 2\pi^2 H(2; y) + 12H(0; z)H(2, 0; y) + 12H(0, 1, 0; z) \\
& +12H(1, 0; z)H(2; y) - 12H(1, 0; z)H(0; y) - 12H(1, 1, 0; z) - 12H(2, 1, 0; y) \\
& +12H(1, 0; y) + 12H(1, 0; z) - 12H(0, 1, 0; y)] \\
& +\frac{z}{(y+z)^2} [2\pi^2 + \frac{4\pi^2}{3} H(1; z) - \frac{4\pi^2}{3} H(2; y) - 6H(0; z) \\
& -8H(0; z)H(2, 0; y) + 12H(0; z)H(0; y) - 8H(0, 1, 0; z) \\
& +4H(1, 0; z) - 8H(1, 0; z)H(2; y) + 8H(1, 0; z)H(0; y) \\
& +8H(1, 1, 0; z) + 8H(2, 1, 0; y) + 6H(0; y) + 8H(0, 1, 0; y) - 20H(1, 0; y)] \\
& +\frac{z}{y+z} [-\frac{\pi^2}{3} + 2H(0; z) - 2H(0; z)H(0; y) - 2H(1, 0; z) - 2H(0; y) + 2H(1, 0; y)] \\
& +\frac{z^2}{(1-y)^3} [+ \frac{2\pi^2}{3} H(0; z) + \frac{2\pi^2}{3} H(1; z) - \frac{2\pi^2}{3} H(2; y) - 12\zeta_3 - 4H(1, 0, 1; z) \\
& +4H(0; z)H(0, 2; y) - 4H(0, 0, 1; z) + 4H(0, 1; z)H(2; y) \\
& +4H(0, 1, 0; z) + 4H(1; z)H(2, 3; y) + 4H(1; z)H(0, 3; y) - 4H(1, 0; z)H(2; y) \\
& +4H(1, 1, 0; z) - 4H(2, 3, 2; y) - 4H(0, 3, 2; y)] + \frac{z^2}{(1-y)^2} [+4H(0; z)H(2; y) \\
& +4H(1; z)H(3; y) - 4H(3, 2; y)] + \frac{z^2}{1-y} [+2H(0; z)H(2; y) + 2H(1; z)H(3; y) \\
& -2H(3, 2; y)] + \frac{z^2}{(y+z)^4} [2\pi^2 H(1; z) - 2\pi^2 H(2; y) - 12H(0; z)H(2, 0; y) \\
& -12H(0, 1, 0; z) - 12H(1, 0; z)H(2; y) + 12H(1, 0; z)H(0; y) \\
& +12H(1, 1, 0; z) + 12H(2, 1, 0; y) + 12H(0, 1, 0; y)] \\
& +\frac{z^2}{(y+z)^3} [-2\pi^2 - \frac{4\pi^2}{3} H(1; z) + \frac{4\pi^2}{3} H(2; y) + 8H(0; z)H(2, 0; y) - 12H(0; z)H(0; y) \\
& +8H(0, 1, 0; z) - 12H(1, 0; z) + 8H(1, 0; z)H(2; y) - 8H(1, 0; z)H(0; y) - 8H(1, 1, 0; z) \\
& -8H(2, 1, 0; y) - 8H(0, 1, 0; y) + 12H(1, 0; y)] + \frac{z^2}{(y+z)^2} [-\frac{\pi^2}{3} + 2H(0; z)H(0; y) \\
& +2H(1, 0; z) - 2H(1, 0; y)] + \frac{1}{1-y-z} [\frac{\pi^2}{6} + H(0; z)H(0; y) + H(1, 0; z) - H(1, 0; y)] \\
& +\frac{1}{9(1-y)} [10\pi^2 + 12\pi^2 H(0; z) + 9\pi^2 H(1; z) - 9\pi^2 H(2; y) \\
& +12\pi^2 H(0; y) - 21\pi^2 H(1; y) - 234\zeta_3 + 54H(0; z)H(0, 2; y) \\
& +21H(0; z)H(0; y) + 18H(0; z)H(0, 0; y) - 18H(0; z)H(1, 0; y) - 90H(0, 0, 1; z) \\
& -63H(0, 1; z) + 63H(1, 0; z) + 18H(2, 0; y) + 54H(0, 1, 0; z) \\
& +90H(0, 1; z)H(2; y) + 36H(0, 1; z)H(0; y) + 90H(1; z)H(2, 3; y) \\
& -63H(1; z)H(3; y) + 90H(1; z)H(0, 3; y) - 18H(1; z)H(0; y) - 72H(1; z)H(0, 0; y)
\end{aligned}$$

E. The $\gamma^* \rightarrow q\bar{q}g$ NNLO Matrix Element coefficients

$$\begin{aligned}
& -54H(1, 0; z)H(2; y) - 90H(1, 0, 1; z) + 54H(1, 1, 0; z) - 90H(2, 3, 2; y) \\
& + 72H(2, 0, 0; y) - 36H(2, 1, 0; y) + 63H(3, 2; y) + 18H(0, 2; y) + 72H(0, 2, 0; y) \\
& - 90H(0, 3, 2; y) + 55H(0; y) + 72H(0, 0, 2; y) + 108H(0, 0; y) - 108H(0, 1, 0; y) + 3H(1, 0; y) \\
& - 90H(1, 0, 0; y) + 126H(1, 1, 0; y) \Big] + \frac{1}{9(y+z)^2} \Big[+ 18H(0; z)H(2, 2; y) + 27H(0; z)H(2; y) \\
& - 18H(0; z)H(3, 2; y) - 72H(0, 0, 1; z) + 39H(0, 1; z) + 36H(0, 1; z)H(2; y) \\
& - 90H(0, 1; z)H(3; y) + 18H(0, 1; z)H(0; y) + 18H(0, 1, 0; z) - 18H(0, 1, 1; z) + 230H(1; z) \\
& + 54H(1; z)H(2, 3; y) - 102H(1; z)H(2; y) - 18H(1; z)H(2, 0; y) + 36H(1; z)H(3, 2; y) \\
& - 108H(1; z)H(3, 3; y) + 66H(1; z)H(3; y) + 18H(1; z)H(3, 0; y) - 18H(1; z)H(0, 2; y) \\
& + 18H(1; z)H(0, 3; y) - 27H(1; z)H(0; y) - 27H(1, 0; z) - 18H(1, 0; z)H(2; y) \\
& - 36H(1, 0, 1; z) + 102H(1, 1; z) - 36H(1, 1; z)H(3; y) + 18H(1, 1; z)H(0; y) + 18H(1, 1, 0; z) \\
& + 102H(2, 2; y) + 18H(2, 2, 0; y) - 54H(2, 3, 2; y) - 230H(2; y) + 18H(1, 0; z)H(3; y) \\
& + 18H(2, 0, 2; y) + 27H(2, 0; y) - 36H(3, 2, 2; y) - 66H(3, 2; y) \\
& - 18H(3, 2, 0; y) + 108H(3, 3, 2; y) - 18H(3, 0, 2; y) + 18H(0, 2, 2; y) \\
& + 27H(0, 2; y) - 18H(0, 3, 2; y) \Big] + \frac{1}{9(y+z)} \Big[-\frac{3\pi^2}{2}H(1; z) + \frac{3\pi^2}{2}H(2; y) - 170 \\
& - 18H(0; z)H(2; y) + 9H(0; z)H(2, 0; y) - 72H(0, 1; z) + 9H(0, 1, 0; z) - 123H(1; z) \\
& - 90H(1; z)H(3; y) + 18H(1; z)H(0; y) + 18H(1, 0; z) + 9H(1, 0; z)H(2; y) \\
& - 9H(1, 1, 0; z) + 123H(2; y) - 18H(2, 0; y) - 9H(2, 1, 0; y) + 90H(3, 2; y) \\
& - 18H(0, 2; y) - 9H(0, 1, 0; y) - 9H(1, 0; z)H(0; y) \Big] \\
& + \frac{T\pi^2}{72} \Big[-115 - 24H(0; z)H(2; y) - 12H(0; z)H(1; y) - 12H(0, 1; z) + 12H(1, 1; z) \\
& + 7H(1; z) - 48H(1; z)H(2; y) + 36H(1; z)H(0; y) - 12H(1; z)H(1; y) - 12H(1, 0; z) \\
& + 48H(2, 2; y) + 19H(2; y) - 24H(2, 0; y) - 36H(0, 2; y) + 48H(0, 1; y) \\
& + 12H(1, 2; y) - 26H(1; y) + 36H(1, 0; y) - 48H(1, 1; y) \Big] + \frac{T}{54} \Big[-\frac{3\pi^4}{8} + \frac{15251}{12} - \frac{357}{2}\zeta_3 \\
& + 108\zeta_3H(1; z) - 270\zeta_3H(2; y) + 162\zeta_3H(1; y) - 360H(0; z) - 198H(0; z)H(2, 2; y) \\
& + 108H(0; z)H(2, 2, 0; y) + 108H(0; z)H(2, 3, 2; y) + 78H(0; z)H(2; y) \\
& + 54H(0; z)H(2, 0, 2; y) - 180H(0; z)H(2, 0; y) - 108H(0; z)H(2, 0, 0; y) \\
& + 54H(0; z)H(2, 1, 0; y) + 108H(0; z)H(3, 2, 2; y) + 297H(0; z)H(3, 2; y) \\
& - 108H(0; z)H(3, 3, 2; y) - 108H(0; z)H(0, 2, 2; y) - 180H(0; z)H(0, 2; y)
\end{aligned}$$

E. The $\gamma^* \rightarrow q\bar{q}g$ NNLO Matrix Element coefficients

$$\begin{aligned}
&+216H(0; z)H(0, 3, 2; y) - 216H(0; z)H(0; y) + 54H(0; z)H(0, 1, 0; y) \\
&-54H(0; z)H(1, 2, 0; y) - 378H(0, 0; z)H(2; y) + 216H(0, 0, 1; z)H(2; y) \\
&-108H(0; z)H(1, 0, 2; y) + 9H(0; z)H(1, 0; y) + 108H(0; z)H(1, 0, 0; y) \\
&-108H(0, 0; z)H(2, 0; y) - 108H(0, 0; z)H(0, 2; y) + 18H(0, 0, 1; z) \\
&-432H(0, 0, 1; z)H(3; y) - 108H(0, 0, 1; z)H(0; y) + 54H(0, 0, 1; z)H(1; y) \\
&+216H(0, 0, 1, 0; z) - 162H(0, 1; z)H(2, 0; y) - 117H(0, 1; z)H(0; y) \\
&+348H(0, 1; z) + 324H(0, 1; z)H(2, 3; y) - 279H(0, 1; z)H(2; y) \\
&+108H(0, 1; z)H(3, 2; y) - 540H(0, 1; z)H(3, 3; y) - 63H(0, 1; z)H(3; y) \\
&+108H(0, 1; z)H(3, 0; y) + 54H(0, 1; z)H(0, 2; y) - 108H(0, 1; z)H(0, 3; y) \\
&+108H(0, 1; z)H(0, 0; y) - 54H(0, 1; z)H(1, 2; y) + 54H(0, 1; z)H(1, 0; y) \\
&-54H(0, 1, 0; z)H(1; y) - 252H(0, 1, 0; z) - 78H(1; z)H(0; y) \\
&-216H(0, 1, 0; z)H(2; y) + 108H(0, 1, 0; z)H(3; y) - 54H(0, 1, 0; z)H(0; y) \\
&+198H(0, 1, 1; z) - 108H(0, 1, 1; z)H(3; y) + 108H(0, 1, 1, 0; z) + 17H(1; z) \\
&+432H(1; z)H(2, 3, 3; y) - 477H(1; z)H(2, 3; y) - 108H(1; z)H(2, 3, 0; y) \\
&+297H(1; z)H(2; y) - 108H(1; z)H(2, 0, 3; y) + 198H(1; z)H(2, 0; y) \\
&+162H(1; z)H(2, 1, 0; y) + 216H(1; z)H(3, 2, 3; y) - 396H(1; z)H(3, 2; y) \\
&-108H(1; z)H(3, 2, 0; y) + 216H(1; z)H(3, 3, 2; y) - 648H(1; z)H(3, 3, 3; y) \\
&+234H(1; z)H(3, 3; y) + 108H(1; z)H(3, 3, 0; y) + 426H(1; z)H(3; y) \\
&-108H(1; z)H(3, 0, 2; y) + 108H(1; z)H(3, 0, 3; y) - 297H(1; z)H(3, 0; y) \\
&-54H(1; z)H(0, 2, 3; y) + 198H(1; z)H(0, 2; y) - 108H(1; z)H(0, 3, 2; y) \\
&+108H(1; z)H(0, 3, 3; y) - 297H(1; z)H(0, 3; y) + 216H(1; z)H(0, 3, 0; y) \\
&+108H(1; z)H(0, 0, 3; y) + 378H(1; z)H(0, 0; y) - 54H(1; z)H(0, 1, 0; y) \\
&-54H(1; z)H(1, 0, 3; y) - 81H(1; z)H(1, 0; y) - 108H(1; z)H(1, 0, 0; y) \\
&+216H(1, 0; z)H(2, 2; y) - 108H(1, 0; z)H(2, 3; y) + 117H(1, 0; z)H(2; y) \\
&-162H(1, 0; z)H(2, 0; y) - 108H(1, 0; z)H(3, 2; y) + 108H(1, 0; z)H(3, 3; y) \\
&-297H(1, 0; z)H(3; y) - 216H(1, 0; z)H(0, 3; y) + 171H(1, 0; z)H(0; y) \\
&-54H(1; z)H(1, 2, 3; y) - 81H(1, 0; z)
\end{aligned}$$

E. The $\gamma^* \rightarrow q\bar{q}g$ NNLO Matrix Element coefficients

$$\begin{aligned}
&+108H(1, 0, z)H(0, 0; y) + 54H(1, 0, z)H(1, 2; y) + 54H(1, 0, z)H(1, 0; y) \\
&-108H(1, 0, 0; z)H(2; y) - 54H(1, 0, 0, 1; z) + 108H(1, 1; z)H(0, 3; y) \\
&+360H(1, 0, 1; z) - 162H(1, 0, 1; z)H(2; y) - 108H(1, 0, 1; z)H(3; y) \\
&+54H(1, 0, 1; z)H(0; y) + 54H(1, 0, 1; z)H(1; y) + 108H(1, 0, 1, 0; z) - 297H(1, 1; z) \\
&-216H(1, 1; z)H(3, 3; y) + 396H(1, 1; z)H(3; y) + 108H(1, 1; z)H(3, 0; y) \\
&-198H(1, 1; z)H(0; y) + 81H(1, 1, 0; z) - 378H(1, 1, 0; z)H(2; y) + 108H(1, 1, 0; z)H(3; y) \\
&+108H(1, 1, 0; z)H(0; y) - 54H(1, 1, 0; z)H(1; y) + 108H(1, 1, 0, 1; z) + 162H(1, 1, 1, 0; z) \\
&-297H(2, 2; y) - 198H(2, 2, 0; y) - 216H(2, 2, 1, 0; y) + 477H(2, 3, 2; y) \\
&+108H(2, 3, 2, 0; y) - 432H(2, 3, 3, 2; y) + 108H(2, 3, 0, 2; y) \\
&-17H(2; y) - 198H(2, 0, 2; y) + 108H(2, 0, 3, 2; y) + 78H(2, 0; y) \\
&-378H(2, 0, 0; y) + 108H(2, 0, 1, 0; y) - 162H(2, 1, 2, 0; y) - 162H(2, 1, 0, 2; y) \\
&+81H(2, 1, 0; y) + 108H(2, 1, 0, 0; y) + 396H(3, 2, 2; y) + 108H(3, 2, 2, 0; y) \\
&-216H(3, 2, 3, 2; y) - 426H(3, 2; y) + 108H(3, 2, 0, 2; y) + 297H(3, 2, 0; y) \\
&-216H(3, 3, 2, 2; y) - 234H(3, 3, 2; y) - 108H(3, 3, 2, 0; y) \\
&+648H(3, 3, 3, 2; y) - 108H(3, 3, 0, 2; y) + 108H(3, 0, 2, 2; y) \\
&+297H(3, 0, 2; y) - 108H(3, 0, 3, 2; y) - 198H(0, 2, 2; y) + 54H(0, 2, 3, 2; y) \\
&+78H(0, 2; y) - 378H(0, 2, 0; y) + 162H(0, 2, 1, 0; y) + 108H(0, 3, 2, 2; y) \\
&+297H(0, 3, 2; y) - 216H(0, 3, 2, 0; y) - 108H(0, 3, 3, 2; y) - 216H(0, 3, 0, 2; y) \\
&-360H(0; y) - 378H(0, 0, 2; y) - 108H(0, 0, 3, 2; y) + 108H(0, 0, 1, 0; y) \\
&+54H(0, 1, 0, 2; y) + 333H(0, 1, 0; y) - 216H(0, 1, 1, 0; y) + 54H(1, 2, 3, 2; y) \\
&+81H(1, 2, 0; y) + 108H(1, 2, 0, 0; y) + 81H(1, 0, 2; y) + 108H(1, 0, 2, 0; y) \\
&+54H(1, 0, 3, 2; y) + 3H(1, 0; y) + 108H(1, 0, 0, 2; y) + 378H(1, 0, 0; y) - 216H(1, 0, 1, 0; y) \\
&+117H(1, 1, 0; y) - 216H(1, 1, 0, 0; y) + 216H(1, 1, 1, 0; y) + 54H(0, 1, 2, 0; y)] \\
&+\frac{\pi^2}{18} [11 + 9H(0; z) - 24H(0; z)H(2; y) - 6H(0, 1; z) + 8H(1; z) \\
&-36H(1; z)H(2; y) + 24H(1; z)H(0; y) + 6H(1; z)H(1; y) + 24H(1, 1; z) \\
&+24H(2, 2; y) + 2H(2; y) - 24H(2, 0; y) + 12H(2, 1; y) - 6H(0, 2; y) + 9H(0; y) \\
&+12H(0, 1; y) - 6H(1, 2; y) - 10H(1; y) + 24H(1, 0; y) - 6H(1, 1; y)]
\end{aligned}$$

E. The $\gamma^* \rightarrow q\bar{q}g$ NNLO Matrix Element coefficients

$$\begin{aligned}
& +\frac{1}{18} [288\zeta_3 + 180\zeta_3 H(1; z) + 78H(0; z)H(0; y) \\
& -360\zeta_3 H(2; y) + 180\zeta_3 H(1; y) - 188H(0; z) - 150H(0; z)H(2, 2; y) \\
& +72H(0; z)H(2, 2, 0; y) + 72H(0; z)H(2, 3, 2; y) + 295H(0; z)H(2; y) \\
& -300H(0; z)H(2, 0; y) - 36H(0; z)H(2, 0, 0; y) + 72H(0; z)H(3, 2, 2; y) \\
& +216H(0; z)H(3, 2; y) - 72H(0; z)H(3, 3, 2; y) - 36H(0; z)H(0, 2, 2; y) \\
& -156H(0; z)H(0, 2; y) + 36H(0; z)H(0, 2, 0; y) + 144H(0; z)H(0, 3, 2; y) \\
& -72H(0; z)H(0, 0, 2; y) + 18H(0; z)H(0, 0; y) + 36H(0; z)H(0, 1, 0; y) \\
& -72H(0; z)H(1, 2, 0; y) - 36H(0; z)H(1, 0, 2; y) + 108H(0, 0, 1, 0; z) \\
& +132H(0; z)H(1, 0; y) + 36H(0; z)H(1, 0, 0; y) + 36H(0; z)H(1, 1, 0; y) \\
& +36H(0, 0; z) - 36H(0, 0; z)H(2, 2; y) - 108H(0, 0; z)H(2; y) - 36H(0, 0; z)H(2, 0; y) \\
& -36H(0, 0; z)H(0, 2; y) + 18H(0, 0; z)H(0; y) - 108H(0, 0, 0, 1; z) + 84H(0, 0, 1; z) \\
& +180H(0, 0, 1; z)H(2; y) - 288H(0, 0, 1; z)H(3; y) + 36H(0, 0, 1; z)H(1; y) \\
& -36H(0, 0, 1, 1; z) + 289H(0, 1; z) + 216H(0, 1; z)H(2, 3; y) - 222H(0, 1; z)H(2; y) \\
& -72H(0, 1; z)H(2, 0; y) + 72H(0, 1; z)H(3, 2; y) - 360H(0, 1; z)H(3, 3; y) \\
& +192H(0, 1; z)H(3; y) + 72H(0, 1; z)H(3, 0; y) - 72H(0, 1; z)H(0, 3; y) \\
& -60H(0, 1; z)H(0; y) + 36H(0, 1; z)H(0, 0; y) - 36H(0, 1; z)H(1, 2; y) \\
& -114H(0, 1, 0; z) - 144H(0, 1, 0; z)H(2; y) + 72H(0, 1, 0; z)H(3; y) \\
& -72H(0, 1, 0; z)H(0; y) + 36H(0, 1, 0; z)H(1; y) - 72H(0, 1, 0, 1; z) + 150H(0, 1, 1; z) \\
& -72H(0, 1, 1; z)H(3; y) + 36H(0, 1, 1; z)H(0; y) + 36H(0, 1, 1, 0; z) \\
& -376H(1; z) + 288H(1; z)H(2, 3, 3; y) - 372H(1; z)H(2, 3; y) - 72H(1; z)H(2, 3, 0; y) \\
& +204H(1; z)H(2; y) - 72H(1; z)H(2, 0, 3; y) + 150H(1; z)H(2, 0; y) \\
& +36H(1; z)H(2, 0, 0; y) + 36H(1; z)H(2, 1, 0; y) + 144H(1; z)H(3, 2, 3; y) \\
& -300H(1; z)H(3, 2; y) - 72H(1; z)H(3, 2, 0; y) + 144H(1; z)H(3, 3, 2; y) \\
& -432H(1; z)H(3, 3, 3; y) + 408H(1; z)H(3, 3; y) + 72H(1; z)H(3, 3, 0; y) \\
& +584H(1; z)H(3; y) - 72H(1; z)H(3, 0, 2; y) + 72H(1; z)H(3, 0, 3; y)
\end{aligned}$$

E. The $\gamma^* \rightarrow q\bar{q}g$ NNLO Matrix Element coefficients

$$\begin{aligned}
& -216H(1; z)H(3, 0; y) - 36H(1; z)H(0, 2, 3; y) + 150H(1; z)H(0, 2; y) \\
& + 36H(1; z)H(0, 2, 0; y) - 72H(1; z)H(0, 3, 2; y) + 72H(1; z)H(0, 3, 3; y) \\
& - 216H(1; z)H(0, 3; y) + 144H(1; z)H(0, 3, 0; y) - 295H(1; z)H(0; y) \\
& + 36H(1; z)H(0, 0, 2; y) - 36H(1; z)H(0, 0, 3; y) + 108H(1; z)H(0, 0; y) \\
& - 36H(1; z)H(1, 2, 3; y) - 36H(1; z)H(1, 0, 3; y) - 72H(1; z)H(1, 0, 0; y) \\
& + 15H(1, 0; z) + 108H(1, 0; z)H(2, 2; y) - 72H(1, 0; z)H(2, 3; y) + 6H(1, 0; z)H(2; y) \\
& - 72H(1, 0; z)H(2, 0; y) - 72H(1, 0; z)H(3, 2; y) + 72H(1, 0; z)H(3, 3; y) \\
& - 216H(1, 0; z)H(3; y) + 108H(1, 0; z)H(0, 2; y) - 144H(1, 0; z)H(0, 3; y) \\
& + 168H(1, 0; z)H(0; y) + 36H(1, 0; z)H(0, 0; y) - 36H(1, 0; z)H(1, 2; y) \\
& + 72H(1, 0; z)H(1, 0; y) + 18H(1, 0, 0; z) - 36H(1, 0, 0; z)H(2; y) \\
& - 72H(1, 0, 0, 1; z) + 222H(1, 0, 1; z) - 36H(1, 0, 1; z)H(2; y) - 72H(1, 0, 1; z)H(3; y) \\
& + 36H(1, 0, 1; z)H(0; y) + 36H(1, 0, 1; z)H(1; y) + 72H(1, 0, 1, 0; z) - 204H(1, 1; z) \\
& - 144H(1, 1; z)H(3, 3; y) + 300H(1, 1; z)H(3; y) + 72H(1, 1; z)H(3, 0; y) \\
& + 72H(1, 1; z)H(0, 3; y) - 150H(1, 1; z)H(0; y) - 36H(1, 1; z)H(0, 0; y) \\
& - 216H(1, 1, 0; z)H(2; y) + 72H(1, 1, 0; z)H(3; y) + 36H(1, 1, 0; z)H(0; y) \\
& + 108H(1, 1, 1, 0; z) - 204H(2, 2; y) - 150H(2, 2, 0; y) - 36H(2, 2, 0, 0; y) \\
& - 108H(2, 2, 1, 0; y) + 372H(2, 3, 2; y) + 72H(2, 3, 2, 0; y) + 36H(1, 1, 0; z)H(1; y) \\
& - 288H(2, 3, 3, 2; y) + 72H(2, 3, 0, 2; y) + 376H(2; y) - 150H(2, 0, 2; y) + 54H(1, 1, 0; z) \\
& - 36H(2, 0, 2, 0; y) + 72H(2, 0, 3, 2; y) + 295H(2, 0; y) - 36H(2, 0, 0, 2; y) \\
& - 108H(2, 0, 0; y) + 108H(2, 0, 1, 0; y) - 36H(2, 1, 2, 0; y) - 36H(2, 1, 0, 2; y) \\
& + 144H(2, 1, 0; y) + 72H(2, 1, 0, 0; y) - 72H(2, 1, 1, 0; y) + 300H(3, 2, 2; y) \\
& + 72H(3, 2, 2, 0; y) - 144H(3, 2, 3, 2; y) - 584H(3, 2; y) \\
& + 72H(3, 2, 0, 2; y) + 216H(3, 2, 0; y) - 144H(3, 3, 2, 2; y) \\
& - 408H(3, 3, 2; y) - 72H(3, 3, 2, 0; y) + 432H(3, 3, 3, 2; y) \\
& - 72H(3, 3, 0, 2; y) + 72H(3, 0, 2, 2; y) + 216H(3, 0, 2; y) \\
& - 72H(3, 0, 3, 2; y) - 150H(0, 2, 2; y) - 36H(0, 2, 2, 0; y)
\end{aligned}$$

E. The $\gamma^* \rightarrow q\bar{q}g$ NNLO Matrix Element coefficients

$$\begin{aligned} &+36H(0, 2, 3, 2; y) + 295H(0, 2; y) - 36H(0, 2, 0, 2; y) - 108H(0, 2, 0; y) \\ &+72H(0, 2, 1, 0; y) + 72H(0, 3, 2, 2; y) + 216H(0, 3, 2; y) - 144H(0, 3, 2, 0; y) \\ &-72H(0, 3, 3, 2; y) - 144H(0, 3, 0, 2; y) - 188H(0; y) - 36H(0, 0, 2, 2; y) \\ &-108H(0, 0, 2; y) + 36H(0, 0, 3, 2; y) + 36H(0, 0; y) + 108H(0, 0, 1, 0; y) + 6H(0, 1, 0; y) \\ &-72H(0, 1, 1, 0; y) + 36H(1, 2, 3, 2; y) + 72H(1, 2, 0, 0; y) + 72H(1, 2, 1, 0; y) \\ &+72H(1, 0, 2, 0; y) + 36H(1, 0, 3, 2; y) - 310H(1, 0; y) + 72H(1, 0, 0, 2; y) \\ &+90H(1, 0, 0; y) - 144H(1, 0, 1, 0; y) + 60H(1, 1, 0; y) - 108H(1, 1, 0, 0; y) \\ &+36H(1, 1, 1, 0; y) \end{aligned} \tag{E.4}$$

E. The $\gamma^* \rightarrow q\bar{q}g$ NNLO Matrix Element coefficients

$$\begin{aligned}
C_{20}(y, z) = & \\
& + \frac{z}{y^2} [6H(0; z)H(2; y) + 6H(1; z)H(3; y) - 6H(3, 2; y)] + \frac{z^2}{y^2} [-2H(0; z)H(2; y) \\
& - 2H(1; z)H(3; y) + 2H(3, 2; y)] + \frac{1}{y^2} [-4H(0; z)H(2; y) - 4H(1; z)H(3; y) \\
& + 4H(3, 2; y)] + \frac{z\pi^2}{6y} [-1 + 4H(0; z) + 10H(0; z)H(2; y) + H(1; z) + 6H(1; z)H(2; y) \\
& + 10H(1; z)H(3; y) - 16H(2, 2; y) + H(2; y) + 2H(2, 0; y) + 4H(2, 1; y) \\
& - 10H(3, 2; y)] + \frac{z}{4y} [-36\zeta_3 - 16\zeta_3 H(2; y) - 4H(0; z) + 6H(0; z)H(2, 2; y) \\
& - 40H(0; z)H(2, 2, 0; y) + 9H(0; z)H(2; y) - 8H(0; z)H(2, 0, 2; y) \\
& - 24H(0; z)H(2, 0; y) - 16H(0; z)H(3, 2, 2; y) + 46H(0; z)H(3, 2; y) \\
& - 40H(0; z)H(3, 2, 0; y) - 10H(0; z)H(0, 2; y) + 12H(0; z)H(1, 0; y) \\
& + 16H(0, 0; z)H(2, 2; y) + 40H(0, 0; z)H(2, 0; y) - 4H(0, 0, 1; z) + 17H(0, 1; z) \\
& + 24H(0, 1; z)H(2, 2; y) - 14H(0, 1; z)H(2; y) - 8H(0, 1; z)H(2, 0; y) \\
& - 8H(0, 1; z)H(3, 2; y) - 24H(0, 1; z)H(3, 3; y) + 14H(0, 1; z)H(3; y) - 8H(0, 1, 0; z) \\
& + 32H(0, 1, 0; z)H(2; y) - 40H(0, 1, 0; z)H(3; y) - 6H(0, 1, 1; z) + 8H(0, 1, 1; z)H(3; y) \\
& + 24H(1; z)H(2, 2, 3; y) - 8H(1; z)H(2, 3; y) - 16H(1; z)H(2, 0, 3; y) \\
& - 6H(1; z)H(2, 0; y) - 24H(1; z)H(3, 2, 3; y) + 12H(1; z)H(3, 2; y) \\
& + 8H(1; z)H(3, 2, 0; y) - 24H(1; z)H(3, 3, 2; y) - 24H(1; z)H(3, 3, 3; y) \\
& + 60H(1; z)H(3, 3; y) + 24H(1; z)H(3, 3, 0; y) + 26H(1; z)H(3; y) + 8H(1; z)H(3, 0, 2; y) \\
& + 18H(1; z)H(3, 0; y) - 6H(1; z)H(0, 2; y) - 10H(1; z)H(0, 3; y) - 17H(1; z)H(0; y) \\
& + 24H(1; z)H(1, 0; y) - 13H(1, 0; z) - 40H(1, 0; z)H(2, 2; y) + 4H(1, 0; z)H(2; y) \\
& - 24H(1, 0; z)H(3, 2; y) - 46H(1, 0; z)H(3; y) + 40H(1, 0; z)H(3, 0; y) + 40H(1, 0, 0; z)H(2; y) \\
& - 10H(1, 0, 1; z) - 16H(1, 0, 1; z)H(2; y) + 8H(1, 0, 1; z)H(3; y) + 24H(1, 1; z)H(3, 3; y) \\
& - 12H(1, 1; z)H(3; y) - 8H(1, 1; z)H(3, 0; y) + 6H(1, 1; z)H(0; y) - 20H(1, 1, 0; z) \\
& + 8H(1, 1, 0; z)H(2; y) + 24H(1, 1, 0; z)H(3; y) - 24H(2, 2, 3, 2; y) \\
& + 6H(2, 2, 0; y) + 48H(2, 2, 1, 0; y) + 8H(2, 3, 2; y) + 6H(2, 0, 2; y) \\
& + 16H(2, 0, 3, 2; y) + 17H(2, 0; y) - 48H(2, 0, 1, 0; y) + 18H(2, 1, 0; y) \\
& - 16H(2, 1, 1, 0; y) - 12H(3, 2, 2; y) - 8H(3, 2, 2, 0; y)
\end{aligned}$$

E. The $\gamma^* \rightarrow q\bar{q}g$ NNLO Matrix Element coefficients

$$\begin{aligned}
&+24H(3, 2, 3, 2; y) - 26H(3, 2; y) - 8H(3, 2, 0, 2; y) - 18H(3, 2, 0; y) \\
&+64H(3, 2, 1, 0; y) + 24H(3, 3, 2, 2; y) - 60H(3, 3, 2; y) \\
&-24H(3, 3, 2, 0; y) + 24H(3, 3, 3, 2; y) - 24H(3, 3, 0, 2; y) \\
&-8H(3, 0, 2, 2; y) - 18H(3, 0, 2; y) + 64H(3, 0, 1, 0; y) + 6H(0, 2, 2; y) \\
&+17H(0, 2; y) + 10H(0, 3, 2; y) + 18H(0, 1, 0; y) - 24H(1, 2, 0; y) - 24H(1, 0, 2; y) \\
&-30H(1, 0; y)] + \frac{z^2}{y} [-2H(0; z)H(2; y) - 2H(1; z)H(3; y) + 2H(3, 2; y)] \\
&+ \frac{1}{2y(y+z)} [-6H(0; z)H(2, 2; y) - 17H(0; z)H(2; y) + 18H(0; z)H(3, 2; y) \\
&-18H(0; z)H(0, 2; y) + 17H(0, 1; z) + 6H(0, 1; z)H(2; y) - 18H(0, 1; z)H(3; y) \\
&-6H(1; z)H(2, 0; y) + 18H(1; z)H(3, 0; y) - 6H(1; z)H(0, 2; y) - 18H(1; z)H(0, 3; y) \\
&-17H(1; z)H(0; y) - 17H(1, 0; z) + 24H(1, 0; z)H(2; y) - 18H(1, 0; z)H(3; y) \\
&+6H(1, 1; z)H(0; y) - 24H(1, 1, 0; z) + 6H(2, 2, 0; y) + 6H(2, 0, 2; y) + 17H(2, 0; y) \\
&+18H(2, 1, 0; y) - 18H(3, 2, 0; y) - 18H(3, 0, 2; y) + 6H(0, 2, 2; y) - 6H(0, 1, 1; z) \\
&+17H(0, 2; y) + 18H(0, 3, 2; y) + 18H(0, 1, 0; y) - 34H(1, 0; y) - 6H(1, 0, 1; z)] \\
&+ \frac{\pi^2}{3y} [-4H(0; z)H(2; y) + H(1; z) - 6H(1; z)H(2; y) - 4H(1; z)H(3; y) \\
&+10H(2, 2; y) - 6H(2; y) - 2H(2, 0; y) - 4H(2, 1; y) + 4H(3, 2; y) + H(1; y)] \\
&+ \frac{1}{4y} [-8\zeta_3 + 80\zeta_3 H(2; y) + 19 - 16H(0; z)H(1, 0; y) \\
&+8H(0; z) - 12H(0; z)H(2, 2; y) + 32H(0; z)H(2, 2, 0; y) + 26H(0; z)H(2; y) \\
&+16H(0; z)H(2, 0, 2; y) + 40H(0; z)H(2, 0; y) + 32H(0; z)H(3, 2, 2; y) \\
&-108H(0; z)H(3, 2; y) + 32H(0; z)H(3, 2, 0; y) + 68H(0; z)H(0, 2; y) \\
&-32H(0, 0; z)H(2, 2; y) - 32H(0, 0; z)H(2, 0; y) - 8H(0, 0, 1; z) - 26H(0, 1; z) \\
&-48H(0, 1; z)H(2, 2; y) + 36H(0, 1; z)H(2; y) + 16H(0, 1; z)H(2, 0; y) \\
&+16H(0, 1; z)H(3, 2; y) + 48H(0, 1; z)H(3, 3; y) - 28H(0, 1; z)H(3; y) + 16H(0, 1, 0; z) \\
&-16H(0, 1, 0; z)H(2; y) + 32H(0, 1, 0; z)H(3; y) - 16H(0, 1, 1; z)H(3; y) \\
&-2H(1; z) - 48H(1; z)H(2, 2, 3; y) + 24H(1; z)H(2, 3; y) + 32H(1; z)H(2, 0, 3; y) \\
&+12H(1; z)H(2, 0; y) + 48H(1; z)H(3, 2, 3; y) - 24H(1; z)H(3, 2; y) + 12H(0, 1, 1; z) \\
&-16H(1; z)H(3, 2, 0; y) + 48H(1; z)H(3, 3, 2; y) + 48H(1; z)H(3, 3, 3; y)
\end{aligned}$$

E. The $\gamma^* \rightarrow q\bar{q}g$ NNLO Matrix Element coefficients

$$\begin{aligned}
& -136H(1; z)H(3, 3; y) - 48H(1; z)H(3, 3, 0; y) - 16H(1; z)H(3, 0, 2; y) \\
& +12H(1; z)H(0, 2; y) + 68H(1; z)H(0, 3; y) + 30H(1; z)H(0; y) + 26H(1, 0; z) \\
& +32H(1, 0; z)H(2, 2; y) - 56H(1, 0; z)H(2; y) + 108H(1, 0; z)H(3; y) \\
& -32H(1, 0, 0; z)H(2; y) + 4H(1, 0, 1; z) + 32H(1, 0, 1; z)H(2; y) - 16H(1, 0, 1; z)H(3; y) \\
& -48H(1, 1; z)H(3, 3; y) + 24H(1, 1; z)H(3; y) + 16H(1, 1; z)H(3, 0; y) - 12H(1, 1; z)H(0; y) \\
& +56H(1, 1, 0; z) - 16H(1, 1, 0; z)H(2; y) + 48H(2, 2, 3, 2; y) - 12H(2, 2, 0; y) \\
& -48H(2, 2, 1, 0; y) - 24H(2, 3, 2; y) + 2H(2; y) - 12H(2, 0, 2; y) - 20H(1; z)H(3, 0; y) \\
& -32H(2, 0, 3, 2; y) - 30H(2, 0; y) + 48H(2, 0, 1, 0; y) - 36H(2, 1, 0; y) \\
& +32H(2, 1, 1, 0; y) + 24H(3, 2, 2; y) + 16H(3, 2, 2, 0; y) - 24H(1; z)H(1, 0; y) \\
& -48H(3, 2, 3, 2; y) + 16H(3, 2, 0, 2; y) + 20H(3, 2, 0; y) - 80H(3, 2, 1, 0; y) \\
& -48H(3, 3, 2, 2; y) + 136H(3, 3, 2; y) + 48H(3, 3, 2, 0; y) - 32H(1, 0; z)H(3, 0; y) \\
& -48H(3, 3, 3, 2; y) + 48H(3, 3, 0, 2; y) + 16H(3, 0, 2, 2; y) + 20H(3, 0, 2; y) \\
& -80H(3, 0, 1, 0; y) - 12H(0, 2, 2; y) - 30H(0, 2; y) - 68H(0, 3, 2; y) - 36H(0, 1, 0; y) \\
& +24H(1, 2, 0; y) + 24H(1, 0, 2; y) + 60H(1, 0; y) - 8H(1, 1, 0; y)] \\
& + \frac{z}{4(1-y)^2} [+5\pi^2 + 4H(0; z)H(0, 0; y) + 16H(1, 0; z) \\
& + \frac{14\pi^2}{3}H(0; z) + \frac{14\pi^2}{3}H(1; z) - \frac{14\pi^2}{3}H(2; y) + \frac{2\pi^2}{3}H(0; y) - \frac{4\pi^2}{3}H(1; y) - 92\zeta_3 \\
& +28H(0; z)H(0, 2; y) + 12H(0; z)H(0; y) - 32H(0, 0, 1; z) - 16H(0, 1; z) \\
& +32H(0, 1; z)H(2; y) + 4H(0, 1; z)H(0; y) + 28H(0, 1, 0; z) + 32H(1; z)H(2, 3; y) \\
& -16H(1; z)H(3; y) + 32H(1; z)H(0, 3; y) + 6H(1; z)H(0; y) - 4H(1; z)H(0, 0; y) \\
& -28H(1, 0; z)H(2; y) - 32H(1, 0, 1; z) + 28H(1, 1, 0; z) - 32H(2, 3, 2; y) - 6H(2, 0; y) \\
& +4H(2, 0, 0; y) - 4H(2, 1, 0; y) + 16H(3, 2; y) - 6H(0, 2; y) + 4H(0, 2, 0; y) \\
& -32H(0, 3, 2; y) + 23H(0; y) + 4H(0, 0, 2; y) - 10H(0, 0; y) - 8H(0, 1, 0; y) - 14H(1, 0; y) \\
& -8H(1, 0, 0; y) + 8H(1, 1, 0; y)] + \frac{z}{4(1-y)} [\frac{11\pi^2}{3} + 6\pi^2H(0; z) + 6\pi^2H(1; z) - 6\pi^2H(2; y) \\
& +2\pi^2H(0; y) - 4\pi^2H(1; y) - 132\zeta_3 + 17 + 28H(0; z)H(2; y) + 36H(0; z)H(0, 2; y) \\
& +12H(0; z)H(0, 0; y) - 48H(0, 0, 1; z) + 4H(0, 1; z) + 48H(0, 1; z)H(2; y) \\
& +36H(0, 1, 0; z) + 48H(1; z)H(2, 3; y) + 32H(1; z)H(3; y) + 48H(1; z)H(0, 3; y) \\
& -22H(1; z)H(0; y) - 12H(1; z)H(0, 0; y) - 36H(1, 0; z)H(2; y) + 4H(0; z) \\
& +12H(0, 1; z)H(0; y) - 48H(1, 0, 1; z) + 36H(1, 1, 0; z) - 2H(1; z)
\end{aligned}$$

E. The $\gamma^* \rightarrow q\bar{q}g$ NNLO Matrix Element coefficients

$$\begin{aligned}
& -48H(2, 3, 2; y) - 24H(0, 1, 0; y) + 22H(2, 0; y) + 12H(2, 0, 0; y) - 12H(2, 1, 0; y) \\
& + 12H(0, 0, 2; y) + 24H(1, 1, 0; y) + 12H(0, 2, 0; y) - 48H(0, 3, 2; y) - 24H(1, 0, 0; y) \\
& - 22H(0, 0; y) + 2H(2; y) - 26H(1, 0; y) + 39H(0; y) + 22H(0, 2; y) - 32H(3, 2; y)] \\
& + \frac{z}{(y+z)^3} [-6\pi^2 H(1; z) + 6\pi^2 H(2; y) + 36H(0, 1, 0; z) + 36H(1, 0; z) \\
& + 36H(1, 0; z)H(2; y) - 36H(1, 1, 0; z) - 36H(2, 1, 0; y) - 36H(0, 1, 0; y) \\
& + 36H(1, 0; y) + 36H(0; z)H(2, 0; y) - 36H(1, 0; z)H(0; y)] \\
& + \frac{z}{(y+z)^2} [+24H(1, 0; z)H(0; y) + 4\pi^2 H(1; z) - 4\pi^2 H(2; y) - 18H(0; z) - 24H(0, 1, 0; z) \\
& + 6\pi^2 + 36H(0; z)H(0; y) - 24H(0; z)H(2, 0; y) + 12H(1, 0; z) - 24H(1, 0; z)H(2; y) \\
& + 24H(1, 1, 0; z) + 24H(2, 1, 0; y) + 18H(0; y) + 24H(0, 1, 0; y) - 60H(1, 0; y)] \\
& + \frac{z}{y+z} [-\pi^2 + 6H(0; z) - 6H(0; z)H(0; y) - 6H(1, 0; z) - 6H(0; y) + 6H(1, 0; y)] \\
& + \frac{z^2}{(1-y)^3} [-\frac{2\pi^2}{3} H(0; z) - \frac{2\pi^2}{3} H(1; z) + \frac{2\pi^2}{3} H(2; y) + 12\zeta_3 - 4H(0; z)H(0, 2; y) \\
& - 4H(0, 1, 0; z) - 4H(1; z)H(2, 3; y) - 4H(1; z)H(0, 3; y) + 4H(1, 0; z)H(2; y) + 4H(1, 0, 1; z) \\
& - 4H(1, 1, 0; z) + 4H(2, 3, 2; y) + 4H(0, 3, 2; y) + 4H(0, 0, 1; z) - 4H(0, 1; z)H(2; y)] \\
& + \frac{z^2}{(1-y)^2} [-4H(0; z)H(2; y) - 4H(1; z)H(3; y) + 4H(3, 2; y)] \\
& + \frac{z^2}{1-y} [-2H(0; z)H(2; y) - 2H(1; z)H(3; y) + 2H(3, 2; y)] \\
& + \frac{z^2}{(y+z)^4} [+6\pi^2 H(1; z) + 36H(2, 1, 0; y) - 36H(0; z)H(2, 0; y) - 36H(0, 1, 0; z) \\
& - 36H(1, 0; z)H(2; y) + 36H(1, 0; z)H(0; y) - 6\pi^2 H(2; y) + 36H(1, 1, 0; z) + 36H(0, 1, 0; y)] \\
& + \frac{z^2}{(y+z)^3} [-6\pi^2 - 4\pi^2 H(1; z) + 4\pi^2 H(2; y) + 24H(0; z)H(2, 0; y) - 36H(0; z)H(0; y) \\
& + 24H(0, 1, 0; z) - 36H(1, 0; z) + 24H(1, 0; z)H(2; y) - 24H(1, 0; z)H(0; y) - 24H(1, 1, 0; z) \\
& - 24H(2, 1, 0; y) - 24H(0, 1, 0; y) + 36H(1, 0; y)] \\
& + \frac{z^2}{(y+z)^2} [\pi^2 + 6H(0; z)H(0; y) + 6H(1, 0; z) - 6H(1, 0; y)] \\
& + \frac{1}{1-y-z} [-\frac{\pi^2}{3} - 2H(0; z)H(0; y) - 2H(1, 0; z) + 2H(1, 0; y)] \\
& + \frac{1}{2(1-y)} [-2\pi^2 - 8H(0; z)H(2, 0; y) + 20H(0, 0, 1; z) + 12H(0, 1; z) \\
& - \frac{8\pi^2}{3} H(0; z) - \frac{4\pi^2}{3} H(1; z) + \frac{4\pi^2}{3} H(2; y) + \frac{2\pi^2}{3} H(0; y) + \frac{8\pi^2}{3} H(1; y) + 64\zeta_3 \\
& - 16H(0; z)H(0, 2; y) + 6H(0; z)H(0; y) + 4H(0; z)H(0, 0; y) + 8H(0; z)H(1, 0; y) \\
& - 20H(0, 1; z)H(2; y) - 4H(0, 1; z)H(0; y) - 8H(0, 1, 0; z) - 20H(1; z)H(2, 3; y)
\end{aligned}$$

E. The $\gamma^* \rightarrow q\bar{q}g$ NNLO Matrix Element coefficients

$$\begin{aligned}
& +12H(1; z)H(3; y) - 20H(1; z)H(0, 3; y) - 2H(1; z)H(0; y) + 4H(1; z)H(0, 0; y) \\
& + 8H(1, 0; z)H(2; y) + 8H(1, 0; z)H(0; y) + 20H(1, 0, 1; z) - 8H(1, 1, 0; z) + 20H(2, 3, 2; y) \\
& + 2H(2, 0; y) - 4H(2, 0, 0; y) + 12H(2, 1, 0; y) - 12H(3, 2; y) + 2H(0, 2; y) - 10H(1, 0; z) \\
& - 4H(0, 2, 0; y) + 20H(0, 3, 2; y) - 5H(0; y) - 4H(0, 0, 2; y) - 4H(0, 0; y) - 16H(1, 1, 0; y) \\
& + \frac{1}{2(y+z)^2} \left[\frac{22\pi^2}{3} H(1; z) - \frac{22\pi^2}{3} H(2; y) - 2H(0; z)H(2, 2; y) + 3H(0; z)H(2; y) \right. \\
& - 44H(0; z)H(2, 0; y) - 2H(0; z)H(3, 2; y) + 2H(0; z)H(0, 2; y) + 3H(0, 1; z) \\
& - 2H(0, 1; z)H(2; y) - 2H(0, 1; z)H(3; y) - 44H(0, 1, 0; z) + 2H(0, 1, 1; z) + 27H(1; z) \\
& - 4H(1; z)H(2, 3; y) + 6H(1; z)H(2; y) + 2H(1; z)H(2, 0; y) - 4H(1; z)H(3, 2; y) \\
& - 4H(1; z)H(3, 3; y) + 6H(1; z)H(3; y) + 2H(1; z)H(3, 0; y) + 2H(1; z)H(0, 2; y) \\
& + 2H(1; z)H(0, 3; y) - 3H(1; z)H(0; y) - 3H(1, 0; z) - 27H(2; y) + 2H(1, 0; z)H(3; y) \\
& + 44H(1, 0; z)H(0; y) + 2H(1, 0, 1; z) - 6H(1, 1; z) + 4H(1, 1; z)H(3; y) - 2H(1, 1; z)H(0; y) \\
& + 44H(1, 1, 0; z) - 6H(2, 2; y) - 2H(2, 2, 0; y) + 4H(2, 3, 2; y) - 44H(1, 0; z)H(2; y) \\
& - 2H(2, 0, 2; y) + 3H(2, 0; y) + 46H(2, 1, 0; y) + 4H(3, 2, 2; y) - 6H(3, 2; y) \\
& - 2H(3, 2, 0; y) + 4H(3, 3, 2; y) - 2H(3, 0, 2; y) - 2H(0, 2, 2; y) \\
& \left. + 3H(0, 2; y) - 2H(0, 3, 2; y) + 46H(0, 1, 0; y) \right] + \frac{1}{2(y+z)} \left[-\frac{22\pi^2}{3} - 2\pi^2 H(1; z) \right. \\
& + 2\pi^2 H(2; y) - 17 - 5H(0; z) - 4H(0; z)H(2; y) + 12H(0; z)H(2, 0; y) - 44H(0; z)H(0; y) \\
& - 4H(0, 1; z) + 12H(0, 1, 0; z) + 4H(1; z) - 4H(1; z)H(2; y) - 8H(1; z)H(3; y) \\
& - 42H(1, 0; z) + 12H(1, 0; z)H(2; y) - 12H(1, 0; z)H(0; y) + 4H(1, 1; z) - 12H(1, 1, 0; z) \\
& + 4H(2, 2; y) - 4H(2; y) - 4H(2, 0; y) - 12H(2, 1, 0; y) + 8H(3, 2; y) + 4H(1; z)H(0; y) \\
& \left. - 4H(0, 2; y) - 5H(0; y) - 12H(0, 1, 0; y) + 46H(1, 0; y) \right] + \frac{T\pi^2}{24} \left[+29 + 6H(1; z) \right. \\
& + 8H(1; z)H(2; y) - 16H(2, 2; y) + 12H(2; y) + 8H(2, 1; y) + 8H(0, 2; y) \\
& - 8H(0, 1; y) - 18H(1; y) + 8H(1, 1; y) \left. \right] + \frac{T}{8} \left[-\frac{22\pi^4}{45} + \frac{255}{4} - 60\zeta_3 - 16\zeta_3 H(1; z) \right. \\
& + 32\zeta_3 H(1; y) + 18H(0; z)H(2, 2; y) + 15H(0; z)H(2; y) - 8H(0; z)H(2, 0, 2; y) \\
& - 16H(0; z)H(3, 2, 2; y) + 42H(0; z)H(3, 2; y) - 16H(0; z)H(3, 3, 2; y) - 16\zeta_3 H(2; y) \\
& + 16H(0; z)H(3, 0, 2; y) - 42H(0; z)H(0, 2; y) + 16H(0; z)H(0, 3, 2; y) \\
& - 16H(0; z)H(0, 0, 2; y) + 16H(0, 0; z)H(2, 2; y) - 16H(0, 0, 1; z)H(2; y) \\
& + 8H(0, 0, 1; z)H(1; y) + 16H(0, 0, 1, 1; z) + 15H(0, 1; z) + 32H(0, 1; z)H(2, 2; y) \\
& \left. + 6H(0, 1; z)H(2; y) + 8H(0, 1; z)H(2, 0; y) - 16H(0, 1; z)H(3, 2; y) \right]
\end{aligned}$$

E. The $\gamma^* \rightarrow q\bar{q}g$ NNLO Matrix Element coefficients

$$\begin{aligned}
& -16H(0, 1; z)H(3, 3; y) + 42H(0, 1; z)H(3; y) + 8H(0, 1; z)H(0, 2; y) - 8H(0, 1; z)H(1, 2; y) \\
& -8H(0, 1; z)H(1, 0; y) - 8H(0, 1, 0; z)H(2; y) + 16H(0, 1, 0, 1; z) - 18H(0, 1, 1; z) \\
& + 16H(0, 1, 1; z)H(3; y) - 16H(0, 1, 1; z)H(0; y) + 16H(0, 1, 1, 0; z) - 52H(1; z) \\
& + 32H(1; z)H(2, 2, 3; y) + 24H(1; z)H(2, 3; y) - 18H(1; z)H(2; y) \\
& - 18H(1; z)H(2, 0; y) - 16H(1; z)H(2, 0, 0; y) - 8H(1; z)H(2, 1, 0; y) \\
& - 32H(1; z)H(3, 2, 3; y) + 36H(1; z)H(3, 2; y) + 16H(1; z)H(3, 2, 0; y) \\
& - 32H(1; z)H(3, 3, 2; y) - 32H(1; z)H(3, 3, 3; y) + 84H(1; z)H(3, 3; y) \\
& + 16H(1; z)H(3, 3, 0; y) + 30H(1; z)H(3; y) + 16H(1; z)H(3, 0, 2; y) \\
& + 16H(1; z)H(3, 0, 3; y) - 42H(1; z)H(3, 0; y) + 8H(1; z)H(0, 2, 3; y) \\
& - 18H(1; z)H(0, 2; y) - 16H(1; z)H(0, 2, 0; y) + 16H(1; z)H(0, 3, 2; y) \\
& + 16H(1; z)H(0, 3, 3; y) - 42H(1; z)H(0, 3; y) - 15H(1; z)H(0; y) \\
& - 8H(1; z)H(1, 0, 3; y) - 16H(1; z)H(0, 0, 2; y) + 16H(1, 1; z)H(0, 0; y) \\
& - 16H(1; z)H(0, 0, 3; y) + 8H(1; z)H(0, 1, 0; y) - 8H(1; z)H(1, 2, 3; y) \\
& + 16H(1; z)H(1, 0, 0; y) + 13H(1, 0; z) + 24H(1, 0; z)H(2; y) + 16H(1, 0; z)H(3, 3; y) \\
& - 42H(1, 0; z)H(3; y) + 16H(1, 0; z)H(0, 2; y) - 16H(1, 0; z)H(0, 3; y) + 8H(1, 0, 0, 1; z) \\
& - 6H(1, 0, 1; z) - 24H(1, 0, 1; z)H(2; y) + 16H(1, 0, 1; z)H(3; y) - 8H(1, 0, 1; z)H(0; y) \\
& + 8H(1, 0, 1; z)H(1; y) + 18H(1, 1; z) + 32H(1, 1; z)H(3, 3; y) - 36H(1, 1; z)H(3; y) \\
& - 16H(1, 1; z)H(3, 0; y) - 16H(1, 1; z)H(0, 3; y) + 18H(1, 1; z)H(0; y) \\
& + 12H(1, 1, 0; z) - 8H(1, 1, 0; z)H(2; y) + 16H(1, 1, 0, 1; z) + 16H(1, 1, 1, 0; z) \\
& - 32H(2, 2, 3, 2; y) + 18H(2, 2; y) + 18H(2, 2, 0; y) \\
& + 16H(2, 2, 0, 0; y) - 24H(2, 3, 2; y) + 52H(2; y) + 18H(2, 0, 2; y) \\
& + 16H(2, 0, 2, 0; y) + 15H(2, 0; y) + 16H(2, 0, 0, 2; y) - 8H(2, 0, 1, 0; y) \\
& + 8H(2, 1, 2, 0; y) + 8H(2, 1, 0, 2; y) - 42H(2, 1, 0; y) - 16H(2, 1, 0, 0; y) \\
& - 16H(2, 1, 1, 0; y) - 36H(3, 2, 2; y) - 16H(3, 2, 2, 0; y) \\
& + 32H(3, 2, 3, 2; y) - 30H(3, 2; y) - 16H(3, 2, 0, 2; y) + 42H(3, 2, 0; y) \\
& + 16H(3, 2, 1, 0; y) + 32H(3, 3, 2, 2; y) - 84H(3, 3, 2; y) \\
& - 16H(3, 3, 2, 0; y) + 32H(3, 3, 3, 2; y) - 16H(3, 3, 0, 2; y) \\
& - 16H(3, 0, 2, 2; y) + 42H(3, 0, 2; y) - 16H(3, 0, 3, 2; y) + 16H(3, 0, 1, 0; y)
\end{aligned}$$

E. The $\gamma^* \rightarrow q\bar{q}g$ NNLO Matrix Element coefficients

$$\begin{aligned}
& +18H(0, 2, 2; y) + 16H(0, 2, 2, 0; y) - 8H(0, 2, 3, 2; y) + 15H(0, 2; y) - 16H(1, 1, 1, 0; y) \\
& + 16H(0, 2, 0, 2; y) - 8H(0, 2, 1, 0; y) - 16H(0, 3, 2, 2; y) + 42H(0, 3, 2; y) \\
& - 16H(0, 3, 3, 2; y) + 16H(0, 0, 2, 2; y) + 16H(0, 0, 3, 2; y) - 8H(0, 1, 2, 0; y) \\
& - 8H(0, 1, 0, 2; y) - 42H(0, 1, 0; y) + 16H(0, 1, 1, 0; y) + 8H(1, 2, 3, 2; y) \\
& - 16H(1, 2, 0, 0; y) + 8H(1, 2, 1, 0; y) - 16H(1, 0, 2, 0; y) + 8H(1, 0, 3, 2; y) - 28H(1, 0; y) \\
& - 16H(1, 0, 0, 2; y) + 8H(1, 0, 1, 0; y) + 36H(1, 1, 0; y) + 16H(1, 1, 0, 0; y) \\
& + \frac{\pi^2}{6} [9 - 7H(0; z) + 6H(0; z)H(2; y) - 2H(0; z)H(1; y) + 4H(0, 1; z) - 24H(1; z) \\
& + 12H(1; z)H(2; y) + 8H(1; z)H(3; y) - 4H(1; z)H(0; y) - 6H(1; z)H(1; y) - 2H(1, 0; z) \\
& - 20H(2, 2; y) + 34H(2; y) + 6H(2, 0; y) + 8H(2, 1; y) - 8H(3, 2; y) - 6H(1, 1; z) \\
& + 8H(0, 2; y) - 7H(0; y) - 4H(0, 1; y) + 6H(1, 2; y) - 10H(1; y) - 4H(1, 0; y)] \\
& + \frac{1}{4} [40\zeta_3 + 40\zeta_3H(1; z) - 80\zeta_3H(2; y) + 40\zeta_3H(1; y) - 2 - 29H(0; z) + 20H(0; z)H(2, 2; y) \\
& - 32H(0; z)H(2, 2, 0; y) - 4H(0; z)H(2; y) + 32H(0; z)H(2, 0; y) \\
& + 16H(0; z)H(2, 0, 0; y) + 16H(0; z)H(2, 1, 0; y) - 24H(0; z)H(3, 2, 2; y) \\
& + 52H(0; z)H(3, 2; y) - 32H(0; z)H(3, 2, 0; y) - 24H(0; z)H(3, 3, 2; y) \\
& + 24H(0; z)H(3, 0, 2; y) + 8H(0; z)H(0, 2, 2; y) - 44H(0; z)H(0, 2; y) \\
& + 16H(0; z)H(0, 2, 0; y) + 24H(0; z)H(0, 3, 2; y) + 40H(0; z)H(0; y) - 24H(0; z)H(0, 0, 2; y) \\
& - 20H(0; z)H(0, 0; y) + 16H(0; z)H(1, 2, 0; y) - 8H(0; z)H(1, 0, 2; y) + 4H(0; z)H(1, 0; y) \\
& - 16H(0; z)H(1, 0, 0; y) - 16H(0; z)H(1, 1, 0; y) + 20H(0, 0; z) + 16H(0, 0; z)H(2, 2; y) \\
& - 4H(0, 0; z)H(2; y) + 16H(0, 0; z)H(2, 0; y) - 20H(0, 0; z)H(0; y) + 36H(0, 0, 1; z) \\
& - 16H(0, 0, 1; z)H(2; y) + 16H(0, 0, 1; z)H(1; y) - 16H(0, 0, 1, 0; z) + 16H(0, 0, 1, 1; z) \\
& + 48H(0, 1; z)H(2, 2; y) - 52H(0, 1; z)H(2; y) - 24H(0, 1; z)H(3, 2; y) \\
& - 24H(0, 1; z)H(3, 3; y) + 84H(0, 1; z)H(3; y) + 8H(0, 1; z)H(0, 2; y) - 8H(0, 1; z)H(0; y) \\
& - 16H(0, 1; z)H(1, 2; y) - 8H(0, 1; z)H(1, 0; y) - 28H(0, 1, 0; z) + 32H(0, 1, 0; z)H(2; y) \\
& - 32H(0, 1, 0; z)H(3; y) + 16H(0, 1, 0; z)H(0; y) - 24H(0, 1, 0; z)H(1; y) + 16H(0, 1, 0, 1; z) \\
& - 20H(0, 1, 1; z) + 24H(0, 1, 1; z)H(3; y) - 16H(0, 1, 1; z)H(0; y) + 32H(0, 1, 1, 0; z) \\
& + 48H(1; z)H(2, 2, 3; y) - 32H(1; z)H(2, 3; y) - 4H(1; z)H(2; y) - 58H(1; z) \\
& - 20H(1; z)H(2, 0; y) - 16H(1; z)H(2, 0, 0; y) - 8H(1; z)H(2, 1, 0; y)
\end{aligned}$$

E. The $\gamma^* \rightarrow q\bar{q}g$ NNLO Matrix Element coefficients

$$\begin{aligned}
& -48H(1; z)H(3, 2, 3; y) + 40H(1; z)H(3, 2; y) + 24H(1; z)H(3, 2, 0; y) \\
& -48H(1; z)H(3, 3, 2; y) - 48H(1; z)H(3, 3, 3; y) + 136H(1; z)H(3, 3; y) \\
& + 24H(1; z)H(3, 3, 0; y) - 4H(1; z)H(3; y) + 24H(1; z)H(3, 0, 2; y) + 24H(1; z)H(3, 0, 3; y) \\
& - 52H(1; z)H(3, 0; y) + 16H(1; z)H(0, 2, 3; y) - 20H(1; z)H(0, 2; y) \\
& - 16H(1; z)H(0, 2, 0; y) + 24H(1; z)H(0, 3, 2; y) + 24H(1; z)H(0, 3, 3; y) \\
& - 52H(1; z)H(0, 3; y) + 4H(1; z)H(0; y) - 16H(1; z)H(0, 0, 2; y) - 24H(1; z)H(0, 0, 3; y) \\
& + 4H(1; z)H(0, 0; y) + 8H(1; z)H(0, 1, 0; y) - 16H(1; z)H(1, 2, 3; y) \\
& + 24H(1; z)H(1, 0; y) + 16H(1; z)H(1, 0, 0; y) + 60H(1, 0; z) - 40H(1, 0; z)H(2, 2; y) \\
& + 80H(1, 0; z)H(2; y) + 16H(1, 0; z)H(2, 0; y) - 32H(1, 0; z)H(3, 2; y) \\
& + 24H(1, 0; z)H(3, 3; y) - 52H(1, 0; z)H(3; y) + 32H(1, 0; z)H(3, 0; y) \\
& - 24H(1, 0; z)H(0, 3; y) - 36H(1, 0; z)H(0; y) - 16H(1, 0; z)H(0, 0; y) \\
& - 16H(1, 0; z)H(1, 0; y) - 20H(1, 0, 0; z) + 16H(1, 0, 0; z)H(2; y) + 16H(1, 0, 0, 1; z) \\
& - 40H(1, 0, 1; z)H(2; y) + 24H(1, 0, 1; z)H(3; y) - 8H(1, 0, 1; z)H(0; y) \\
& - 24H(1, 0, 1, 0; z) + 4H(1, 1; z) + 48H(1, 1; z)H(3, 3; y) - 40H(1, 1; z)H(3; y) \\
& - 24H(1, 1; z)H(3, 0; y) - 24H(1, 1; z)H(0, 3; y) + 20H(1, 1; z)H(0; y) \\
& - 64H(1, 1, 0; z) + 16H(1, 1, 0; z)H(2; y) + 32H(1, 1, 0; z)H(3; y) - 16H(1, 1, 0; z)H(0; y) \\
& - 24H(1, 1, 0; z)H(1; y) + 24H(1, 1, 0, 1; z) - 8H(1, 1, 1, 0; z) - 48H(2, 2, 3, 2; y) \\
& + 4H(2, 2; y) + 20H(2, 2, 0; y) + 16H(2, 2, 0, 0; y) + 40H(2, 2, 1, 0; y) + 28H(1, 0, 1; z) \\
& + 32H(2, 3, 2; y) + 58H(2; y) + 20H(2, 0, 2; y) + 16H(2, 0, 2, 0; y) + 16H(1, 1; z)H(0, 0; y) \\
& - 4H(2, 0; y) + 16H(2, 0, 0, 2; y) - 4H(2, 0, 0; y) - 48H(2, 0, 1, 0; y) \\
& + 8H(2, 1, 2, 0; y) + 8H(2, 1, 0, 2; y) - 100H(2, 1, 0; y) - 32H(2, 1, 0, 0; y) \\
& - 32H(2, 1, 1, 0; y) - 40H(3, 2, 2; y) - 24H(3, 2, 2, 0; y) + 32H(1, 0; z)H(0, 2; y) \\
& + 48H(3, 2, 3, 2; y) + 4H(3, 2; y) - 24H(3, 2, 0, 2; y) - 16H(1; z)H(1, 0, 3; y) \\
& + 52H(3, 2, 0; y) + 56H(3, 2, 1, 0; y) + 48H(3, 3, 2, 2; y) + 24H(1, 0; z)H(1, 2; y) \\
& - 136H(3, 3, 2; y) - 24H(3, 3, 2, 0; y) + 48H(3, 3, 3, 2; y) + 16H(1, 0, 1; z)H(1; y) \\
& - 24H(3, 3, 0, 2; y) - 24H(3, 0, 2, 2; y) + 52H(3, 0, 2; y) - 24H(3, 0, 3, 2; y) \\
& + 56H(3, 0, 1, 0; y) + 20H(0, 2, 2; y) + 16H(0, 2, 2, 0; y) - 16H(0, 2, 3, 2; y)
\end{aligned}$$

E. The $\gamma^* \rightarrow q\bar{q}g$ NNLO Matrix Element coefficients

$$\begin{aligned}
& -4H(0, 2; y) + 16H(0, 2, 0, 2; y) - 4H(0, 2, 0; y) - 24H(0, 2, 1, 0; y) \\
& -24H(0, 3, 2, 2; y) + 52H(0, 3, 2; y) - 24H(0, 3, 3, 2; y) - 29H(0; y) \\
& + 16H(0, 0, 2, 2; y) - 4H(0, 0, 2; y) + 24H(0, 0, 3, 2; y) + 20H(0, 0; y) - 16H(0, 0, 1, 0; y) \\
& - 8H(0, 1, 2, 0; y) - 8H(0, 1, 0, 2; y) - 20H(0, 1, 0; y) + 16H(0, 1, 1, 0; y) \\
& + 16H(1, 2, 3, 2; y) - 24H(1, 2, 0; y) - 16H(1, 2, 0, 0; y) - 8H(1, 2, 1, 0; y) \\
& - 24H(1, 0, 2; y) - 16H(1, 0, 2, 0; y) + 16H(1, 0, 3, 2; y) - 56H(1, 0; y) - 16H(1, 0, 0, 2; y) \\
& + 24H(1, 0, 0; y) + 24H(1, 0, 1, 0; y) + 40H(1, 1, 0; y) + 32H(1, 1, 0, 0; y) \Big] ,
\end{aligned}
\tag{E.5}$$

$$\begin{aligned}
D_{20}(y, z) = & \frac{z}{3y} [-2H(0; z) - 3H(1, 0; z) - 3H(1, 0; y)] + \frac{1}{y(y+z)} [-2H(1, 0; z) - 2H(1, 0; y)] \\
& + \frac{1}{18y} [-74 + 15H(0; z) + 36H(1, 0; z) + 15H(0; y) + 36H(1, 0; y)] \\
& + \frac{z}{18(1-y)^2} [2\pi^2 - 3H(0; z)H(0; y) + 50H(0; y) - 18H(0, 0; y) - 12H(1, 0; y)] \\
& + \frac{z}{18(1-y)} [6\pi^2 + 38 - 3H(0; z) - 9H(0; z)H(0; y) + 87H(0; y) - 54H(0, 0; y) \\
& - 36H(1, 0; y)] + \frac{z}{(y+z)^3} [-2\pi^2H(1; z) + 2\pi^2H(2; y) + 12H(0; z)H(2, 0; y) \\
& + 12H(0, 1, 0; z) + 12H(1, 0; z) + 12H(1, 0; z)H(2; y) - 12H(1, 0; z)H(0; y) \\
& - 12H(2, 1, 0; y) - 12H(0, 1, 0; y) + 12H(1, 0; y) - 12H(1, 1, 0; z)] \\
& + \frac{z}{(y+z)^2} [2\pi^2 + \frac{4\pi^2}{3}H(1; z) - \frac{4\pi^2}{3}H(2; y) - 8H(1, 0; z)H(2; y) \\
& - 6H(0; z) - 8H(0; z)H(2, 0; y) + 12H(0; z)H(0; y) - 8H(0, 1, 0; z) + 4H(1, 0; z) \\
& + 8H(1, 0; z)H(0; y) + 8H(1, 1, 0; z) + 8H(2, 1, 0; y) + 6H(0; y) + 8H(0, 1, 0; y) \\
& - 20H(1, 0; y)] + \frac{z}{y+z} [-\frac{\pi^2}{3} + 2H(0; z) - 2H(0; z)H(0; y) - 2H(1, 0; z) - 2H(0; y) \\
& + 2H(1, 0; y)] + \frac{z^2}{(y+z)^4} [2\pi^2H(1; z) - 2\pi^2H(2; y) - 12H(0; z)H(2, 0; y) - 12H(0, 1, 0; z) \\
& - 12H(1, 0; z)H(2; y) + 12H(1, 0; z)H(0; y) + 12H(1, 1, 0; z) + 12H(2, 1, 0; y) \\
& + 12H(0, 1, 0; y)] + \frac{z^2}{(y+z)^3} [-2\pi^2 - \frac{4\pi^2}{3}H(1; z) + \frac{4\pi^2}{3}H(2; y) + 8H(0; z)H(2, 0; y) \\
& + 8H(0, 1, 0; z) - 12H(1, 0; z) + 8H(1, 0; z)H(2; y) - 8H(1, 0; z)H(0; y) - 8H(1, 1, 0; z) \\
& - 8H(2, 1, 0; y) - 8H(0, 1, 0; y) + 12H(1, 0; y) - 12H(0; z)H(0; y)] \\
& + \frac{z^2}{3(y+z)^2} [\pi^2 + 6H(0; z)H(0; y) + 6H(1, 0; z) - 6H(1, 0; y)] \\
& + \frac{1}{9(1-y)} [-4\pi^2 + 6H(0; z)H(0; y) - 70H(0; y) + 36H(0, 0; y) + 24H(1, 0; y)] \\
& + \frac{1}{(y+z)^2} [\frac{2\pi^2}{3}H(1; z) - \frac{2\pi^2}{3}H(2; y) - 4H(0; z)H(2, 0; y) - 4H(0, 1, 0; z) \\
& - 4H(1, 0; z)H(2; y) + 4H(1, 0; z)H(0; y) + 4H(1, 1, 0; z) + 4H(2, 1, 0; y) + 4H(0, 1, 0; y)] \\
& + \frac{1}{y+z} [-\frac{2\pi^2}{3} - \frac{\pi^2}{3}H(1; z) - 4H(1, 0; z) - H(0; y) \\
& + \frac{\pi^2}{3}H(2; y) + 2 - H(0; z) + 2H(0; z)H(2, 0; y) - 4H(0; z)H(0; y) + 2H(0, 1, 0; z) \\
& + 2H(1, 0; z)H(2; y) - 2H(1, 0; z)H(0; y) - 2H(1, 1, 0; z) - 2H(2, 1, 0; y) - 2H(0, 1, 0; y) \\
& + 4H(1, 0; y)] + \frac{T\pi^2}{216} [+431 - 12H(0; z) + 24H(2; y) - 12H(0; y) - 24H(1; y)]
\end{aligned}$$

E. The $\gamma^* \rightarrow q\bar{q}g$ NNLO Matrix Element coefficients

$$\begin{aligned}
& +\frac{T}{18} \left[\frac{4345}{36} - 38\zeta_3 + 3H(0; z)H(1, 0; y) - 18H(1, 0, 0; z) \right. \\
& + 31H(0; z) + 12H(0; z)H(2, 0; y) + 10H(0; z)H(0; y) - 18H(0; z)H(0, 0; y) \\
& - 41H(0, 0; z) - 18H(0, 0; z)H(0; y) - 3H(0, 1, 0; z) + 29H(1, 0; z) + 12H(1, 0; z)H(2; y) \\
& - 15H(1, 0; z)H(0; y) - 12H(2, 1, 0; y) + 31H(0; y) - 41H(0, 0; y) + 3H(0, 1, 0; y) \\
& \left. - 29H(1, 0; y) + 18H(1, 0, 0; y) + 12H(1, 1, 0; y) \right] \\
& + \frac{\pi^2}{3} + 2H(0; z)H(0; y) + 2H(1, 0; z) - 2H(1, 0; y) ,
\end{aligned} \tag{E.6}$$

E. The $\gamma^* \rightarrow q\bar{q}g$ NNLO Matrix Element coefficients

$$\begin{aligned}
E_{20}(y, z) = & \frac{z}{9y} [-2\pi^2 H(2; y) + 12H(0; z)H(2, 2; y) - 47H(0; z)H(2; y) + 3H(0; z)H(2, 0; y) \\
& -15H(0; z)H(3, 2; y) + 3H(0; z)H(0, 2; y) + 18H(0, 0; z)H(2; y) + 9H(0, 1; z) \\
& +3H(0, 1; z)H(3; y) + 12H(1; z)H(2, 3; y) + 12H(1; z)H(3, 2; y) - 12H(1; z)H(3, 3; y) \\
& -38H(1; z)H(3; y) + 3H(1; z)H(3, 0; y) + 3H(1; z)H(0, 3; y) - 9H(1; z)H(0; y) \\
& -12H(1, 0; z)H(2; y) + 15H(1, 0; z)H(3; y) - 12H(1, 1; z)H(3; y) - 12H(2, 3, 2; y) \\
& +9H(2, 0; y) - 12H(3, 2, 2; y) + 38H(3, 2; y) - 3H(3, 2, 0; y) + 9H(1, 0; z) \\
& +12H(3, 3, 2; y) - 3H(3, 0, 2; y) + 9H(0, 2; y) - 3H(0, 3, 2; y)] \\
& + \frac{1}{y(y+z)} [-2H(0; z)H(2; y) + 2H(0, 1; z) - 2H(1; z)H(0; y) + 2H(1, 0; z) + 2H(2, 0; y) \\
& +2H(0, 2; y)] + \frac{1}{18y} [8\pi^2 H(2; y) - 38 + 3H(0; z) - 48H(0; z)H(2, 2; y) \\
& +188H(0; z)H(2; y) - 12H(0; z)H(2, 0; y) + 60H(0; z)H(3, 2; y) - 12H(0; z)H(0, 2; y) \\
& -72H(0, 0; z)H(2; y) - 36H(0, 1; z) - 12H(0, 1; z)H(3; y) - 48H(1; z)H(2, 3; y) \\
& -48H(1; z)H(3, 2; y) + 48H(1; z)H(3, 3; y) + 152H(1; z)H(3; y) - 12H(1; z)H(3, 0; y) \\
& -12H(1; z)H(0, 3; y) + 36H(1; z)H(0; y) - 36H(1, 0; z) + 48H(1, 0; z)H(2; y) \\
& -60H(1, 0; z)H(3; y) + 48H(1, 1; z)H(3; y) + 48H(2, 3, 2; y) - 36H(2, 0; y) \\
& +48H(3, 2, 2; y) - 152H(3, 2; y) + 12H(3, 2, 0; y) - 48H(3, 3, 2; y) \\
& +12H(3, 0, 2; y) - 36H(0, 2; y) + 12H(0, 3, 2; y) + 15H(0; y)] + \frac{z}{18(1-y)^2} [-2\pi^2 \\
& +3H(0; z)H(0; y) - 50H(0; y) + 18H(0, 0; y) + 12H(1, 0; y)] \\
& + \frac{z}{18(1-y)} [-6\pi^2 - 38 + 3H(0; z) + 9H(0; z)H(0; y) - 87H(0; y) + 54H(0, 0; y) \\
& +36H(1, 0; y)] + \frac{1}{9(1-y)} [2\pi^2 - 3H(0; z)H(0; y) + 38H(0; y) - 18H(0, 0; y) - 12H(1, 0; y)] \\
& + \frac{1}{9(y+z)^2} [-9H(0; z)H(2; y) - 3H(0, 1; z) - 26H(1; z) + 12H(1; z)H(2; y) \\
& -12H(1; z)H(3; y) + 9H(1; z)H(0; y) + 9H(1, 0; z) - 12H(1, 1; z) \\
& -12H(2, 2; y) + 26H(2; y) - 9H(2, 0; y) + 12H(3, 2; y) - 9H(0, 2; y)] \\
& + \frac{1}{9(y+z)} [+38 - 9H(0; z) - 12H(1; z) + 12H(2; y) - 9H(0; y)] + \frac{T\pi^2}{36} [-7 + H(1; z) \\
& -5H(2; y) + 4H(1; y)] + \frac{T}{108} [-\frac{4085}{6} + 6\zeta_3 + 72H(0; z) + 72H(0; z)H(2, 2; y) \\
& -147H(0; z)H(2; y) + 36H(0; z)H(2, 0; y) - 108H(0; z)H(3, 2; y) + 36H(0; z)H(0, 2; y)
\end{aligned}$$

E. The $\gamma^* \rightarrow q\bar{q}g$ NNLO Matrix Element coefficients

$$\begin{aligned}
& -18H(0; z)H(1, 0; y) + 108H(0, 0; z)H(2; y) - 36H(0, 0, 1; z) - 201H(0, 1; z) \\
& + 72H(0, 1; z)H(2; y) - 36H(0, 1; z)H(3; y) + 72H(0, 1; z)H(0; y) + 18H(0, 1, 0; z) \\
& + 68H(1; z) + 144H(1; z)H(2, 3; y) - 108H(1; z)H(2; y) - 72H(1; z)H(2, 0; y) \\
& + 144H(1; z)H(3, 2; y) - 144H(1; z)H(3, 3; y) - 348H(1; z)H(3; y) + 108H(1; z)H(3, 0; y) \\
& - 72H(1; z)H(0, 2; y) + 108H(1; z)H(0, 3; y) + 147H(1; z)H(0; y) - 108H(1; z)H(0, 0; y) \\
& - 81H(1, 0; z) - 72H(1, 0; z)H(2; y) + 108H(1, 0; z)H(3; y) - 18H(1, 0; z)H(0; y) \\
& + 108H(1, 1; z) - 144H(1, 1; z)H(3; y) + 72H(1, 1; z)H(0; y) + 108H(2, 2; y) - 72H(1, 0, 1; z) \\
& + 72H(2, 2, 0; y) - 144H(2, 3, 2; y) - 68H(2; y) + 72H(2, 0, 2; y) - 72H(0, 1, 1; z) \\
& - 147H(2, 0; y) + 108H(2, 0, 0; y) - 144H(3, 2, 2; y) + 348H(3, 2; y) \\
& - 108H(3, 2, 0; y) + 144H(3, 3, 2; y) - 108H(3, 0, 2; y) + 72H(0, 2, 2; y) \\
& - 147H(0, 2; y) + 108H(0, 2, 0; y) - 108H(0, 3, 2; y) + 72H(0; y) + 108H(0, 0, 2; y) \\
& - 18H(0, 1, 0; y) + 228H(1, 0; y) - 108H(1, 0, 0; y) - 72H(1, 1, 0; y) \Big] + \frac{1}{9} [2\pi^2 + 2\pi^2 H(1; z) \\
& - 4\pi^2 H(2; y) + 2\pi^2 H(1; y) + 19H(0; z) + 12H(0; z)H(2, 2; y) - 29H(0; z)H(2; y) \\
& + 6H(0; z)H(2, 0; y) - 18H(0; z)H(3, 2; y) + 6H(0; z)H(0, 2; y) - 3H(0; z)H(0; y) \\
& - 3H(0; z)H(1, 0; y) - 9H(0, 0; z) + 18H(0, 0; z)H(2; y) - 6H(0, 0, 1; z) - 35H(0, 1; z) \\
& + 12H(0, 1; z)H(2; y) - 6H(0, 1; z)H(3; y) + 12H(0, 1; z)H(0; y) + 3H(0, 1, 0; z) \\
& + 38H(1; z) + 24H(1; z)H(2, 3; y) - 12H(1; z)H(2; y) - 12H(1; z)H(2, 0; y) - 12H(0, 1, 1; z) \\
& + 24H(1; z)H(3, 2; y) - 24H(1; z)H(3, 3; y) - 64H(1; z)H(3; y) + 18H(1; z)H(3, 0; y) \\
& - 12H(1; z)H(0, 2; y) + 18H(1; z)H(0, 3; y) + 29H(1; z)H(0; y) - 18H(1; z)H(0, 0; y) \\
& - 12H(1, 0; z)H(2; y) + 18H(1, 0; z)H(3; y) - 3H(1, 0; z)H(0; y) - 12H(1, 0, 1; z) \\
& - 24H(1, 1; z)H(3; y) + 12H(1, 1; z)H(0; y) + 12H(2, 2; y) + 12H(2, 2, 0; y) - 3H(1, 0; z) \\
& - 24H(2, 3, 2; y) - 38H(2; y) + 12H(2, 0, 2; y) - 29H(2, 0; y) + 12H(1, 1; z) \\
& + 18H(2, 0, 0; y) - 24H(3, 2, 2; y) + 64H(3, 2; y) - 18H(3, 2, 0; y) \\
& + 24H(3, 3, 2; y) - 18H(3, 0, 2; y) + 12H(0, 2, 2; y) - 29H(0, 2; y) \\
& + 18H(0, 2, 0; y) - 18H(0, 3, 2; y) + 19H(0; y) + 18H(0, 0, 2; y) - 9H(0, 0; y) \\
& - 3H(0, 1, 0; y) + 32H(1, 0; y) - 18H(1, 0, 0; y) - 12H(1, 1, 0; y) \Big] ,
\end{aligned}$$

(E.7)

E. The $\gamma^* \rightarrow q\bar{q}g$ NNLO Matrix Element coefficients

$$F_{20}(y, z) = \frac{T}{108} [-17\pi^2 - 20H(0; z) + 3H(0; z)H(0; y) + 15H(0, 0; z) - 20H(0; y) + 15H(0, 0; y)] , \quad (\text{E.8})$$

$$\begin{aligned} G_{20}(y, z) = & \frac{z}{y^2} [-9H(0; z)H(2; y) - 9H(1; z)H(3; y) + 9H(3, 2; y)] + \frac{z^2}{y^2} [3H(0; z)H(2; y) \\ & + 3H(1; z)H(3; y) - 3H(3, 2; y)] + \frac{1}{y^2} [6H(0; z)H(2; y) + 6H(1; z)H(3; y) - 6H(3, 2; y)] \\ & + \frac{z\pi^2}{9y} [12H(1; z)H(2; y) - 12H(2, 2; y) - 2H(2; y) + 12H(2, 0; y) - 2H(1; y)] \\ & + \frac{z}{3y} [-72\zeta_3 H(2; y) - 9H(0; z) + 12H(0; z)H(2, 2; y) - 18H(0; z)H(2; y) \\ & - 4H(0; z)H(2, 0; y) - 8H(0; z)H(3, 2; y) - 4H(0; z)H(1, 0; y) + 24H(0, 0, 1; z)H(2; y) \\ & + 24H(0, 1; z)H(2, 2; y) - 8H(0, 1; z)H(2; y) - 24H(0, 1; z)H(2, 0; y) \\ & - 24H(0, 1; z)H(3, 2; y) - 24H(0, 1; z)H(3, 3; y) + 4H(0, 1, 1; z) + 24H(0, 1, 1; z)H(3; y) \\ & + 24H(1; z)H(2, 2, 3; y) + 4H(1; z)H(2, 3; y) - 24H(1; z)H(2, 0, 3; y) \\ & + 4H(1; z)H(2, 0; y) - 24H(1; z)H(3, 2, 3; y) + 8H(1; z)H(3, 2; y) \\ & + 24H(1; z)H(3, 2, 0; y) - 24H(1; z)H(3, 3, 2; y) - 24H(1; z)H(3, 3, 3; y) \\ & - 8H(1; z)H(3, 3; y) + 24H(1; z)H(3, 3, 0; y) - 18H(1; z)H(3; y) + 24H(1; z)H(3, 0, 2; y) \\ & - 8H(1; z)H(3, 0; y) + 4H(1; z)H(0, 2; y) - 4H(1; z)H(1, 0; y) - 12H(1, 0; z)H(2; y) \\ & + 8H(1, 0; z)H(3; y) + 4H(1, 0, 1; z) - 24H(1, 0, 1; z)H(2; y) + 24H(1, 0, 1; z)H(3; y) \\ & + 24H(1, 1; z)H(3, 3; y) - 8H(1, 1; z)H(3; y) - 24H(1, 1; z)H(3, 0; y) \\ & + 4H(1, 1, 0; z) - 24H(2, 2, 3, 2; y) - 4H(2, 2, 0; y) + 24H(2, 2, 1, 0; y) \\ & - 4H(2, 3, 2; y) - 4H(2, 0, 2; y) + 24H(2, 0, 3, 2; y) - 24H(2, 0, 1, 0; y) \\ & - 8H(3, 2, 2; y) - 24H(3, 2, 2, 0; y) + 24H(3, 2, 3, 2; y) - 4H(1, 1; z)H(0; y) \\ & + 18H(3, 2; y) - 24H(3, 2, 0, 2; y) + 8H(3, 2, 0; y) + 24H(3, 2, 1, 0; y) \\ & + 24H(3, 3, 2, 2; y) + 8H(3, 3, 2; y) - 24H(3, 3, 2, 0; y) \\ & + 24H(3, 3, 3, 2; y) - 24H(3, 3, 0, 2; y) - 24H(3, 0, 2, 2; y) + 8H(3, 0, 2; y) \\ & + 24H(3, 0, 1, 0; y) - 4H(0, 2, 2; y) + 4H(1, 2, 0; y) + 4H(1, 0, 2; y) + 4H(1, 1, 0; y)] \\ & + \frac{z^2}{y} [3H(0; z)H(2; y) + 3H(1; z)H(3; y) - 3H(3, 2; y)] + \frac{1}{3y(1-y-z)} \left[\frac{2\pi^2}{3} H(1; y) \right] \end{aligned}$$

E. The $\gamma^* \rightarrow q\bar{q}g$ NNLO Matrix Element coefficients

$$\begin{aligned}
&+4H(0; z)H(3, 2; y) + 4H(0; z)H(1, 0; y) + 4H(1; z)H(3, 3; y) + 4H(1; z)H(3, 0; y) \\
&+4H(1; z)H(1, 0; y) - 4H(1, 0; z)H(3; y) - 4H(3, 2, 0; y) - 4H(3, 3, 2; y) \\
&-4H(3, 0, 2; y) - 4H(1, 2, 0; y) - 4H(1, 0, 2; y) - 4H(1, 1, 0; y)] + \frac{1}{3y(1-z)} \left[\frac{2\pi^2}{3} H(1; y) \right. \\
&+4H(0; z)H(3, 2; y) + 4H(0; z)H(1, 0; y) + 4H(1; z)H(3, 3; y) + 4H(1; z)H(3, 0; y) \\
&+4H(1; z)H(1, 0; y) - 4H(1, 0; z)H(3; y) - 4H(3, 2, 0; y) - 4H(3, 3, 2; y) \\
&-4H(3, 0, 2; y) - 4H(1, 2, 0; y) - 4H(1, 0, 2; y) - 4H(1, 1, 0; y)] \\
&+ \frac{1}{3y(y+z)} [8H(0; z)H(2, 2; y) - 8H(0, 1; z)H(2; y) + 8H(0, 1, 1; z) + 8H(1; z)H(2, 0; y) \\
&+8H(1; z)H(0, 2; y) - 8H(1, 0; z)H(2; y) + 8H(1, 0, 1; z) - 8H(1, 1; z)H(0; y) \\
&-8H(2, 2, 0; y) - 8H(2, 0, 2; y) - 8H(0, 2, 2; y) + 8H(1, 1, 0; z)] \\
&+ \frac{\pi^2}{9y} [-6H(1; z)H(2; y) + 6H(2, 2; y) + H(2; y) - 6H(2, 0; y) + H(1; y)] \\
&+ \frac{1}{3y} [36\zeta_3 H(2; y) + 18H(0; z) - 12H(0, 1; z)H(2, 2; y) + 9H(1; z) \\
&-12H(0; z)H(2, 2; y) + 11H(0; z)H(2; y) - 4H(0; z)H(2, 0; y) - 2H(0; z)H(3, 2; y) \\
&+6H(0; z)H(0, 2; y) + 2H(0; z)H(1, 0; y) - 12H(0, 0, 1; z)H(2; y) \\
&+4H(0, 1; z)H(2; y) + 12H(0, 1; z)H(2, 0; y) + 12H(0, 1; z)H(3, 2; y) \\
&+12H(0, 1; z)H(3, 3; y) + 6H(0, 1; z)H(3; y) - 8H(0, 1, 1; z) - 12H(0, 1, 1; z)H(3; y) \\
&-12H(1; z)H(2, 2, 3; y) - 8H(1; z)H(2, 3; y) + 12H(1; z)H(2, 0, 3; y) \\
&-8H(1; z)H(2, 0; y) + 12H(1; z)H(3, 2, 3; y) - 4H(1; z)H(3, 2; y) \\
&-12H(1; z)H(3, 2, 0; y) + 12H(1; z)H(3, 3, 2; y) + 12H(1; z)H(3, 3, 3; y) \\
&+4H(1; z)H(3, 3; y) - 12H(1; z)H(3, 3, 0; y) + 11H(1; z)H(3; y) - 12H(1; z)H(3, 0, 2; y) \\
&-2H(1; z)H(3, 0; y) - 8H(1; z)H(0, 2; y) + 6H(1; z)H(0, 3; y) + 2H(1; z)H(1, 0; y) \\
&+6H(1, 0; z)H(2; y) + 2H(1, 0; z)H(3; y) - 8H(1, 0, 1; z) + 12H(1, 0, 1; z)H(2; y) \\
&-12H(1, 0, 1; z)H(3; y) - 12H(1, 1; z)H(3, 3; y) + 4H(1, 1; z)H(3; y) \\
&+8H(1, 1; z)H(0; y) - 8H(1, 1, 0; z) + 12H(2, 2, 3, 2; y) + 8H(2, 2, 0; y) \\
&-12H(2, 2, 1, 0; y) + 8H(2, 3, 2; y) - 9H(2; y) + 8H(2, 0, 2; y) + 12H(1, 1; z)H(3, 0; y) \\
&-12H(2, 0, 3, 2; y) + 12H(2, 0, 1, 0; y) + 4H(3, 2, 2; y) \\
&+12H(3, 2, 2, 0; y) - 12H(3, 2, 3, 2; y) - 11H(3, 2; y) - 12H(3, 3, 3, 2; y) \\
&+12H(3, 2, 0, 2; y) + 2H(3, 2, 0; y) - 12H(3, 2, 1, 0; y) + 12H(3, 3, 0, 2; y) \\
&-12H(3, 3, 2, 2; y) - 4H(3, 3, 2; y) + 12H(3, 3, 2, 0; y) + 12H(3, 0, 2, 2; y)
\end{aligned}$$

E. The $\gamma^* \rightarrow q\bar{q}g$ NNLO Matrix Element coefficients

$$\begin{aligned}
& +2H(3, 0, 2; y) - 12H(3, 0, 1, 0; y) + 8H(0, 2, 2; y) - 6H(0, 3, 2; y) \\
& - 2H(1, 2, 0; y) - 2H(1, 0, 2; y) - 2H(1, 1, 0; y)] + \frac{z}{3(1-y-z)} \left[-\frac{2\pi^2}{3}H(1; z) - \frac{2\pi^2}{3}H(1; y) \right. \\
& - 8H(0; z)H(3, 2; y) + 4H(0; z)H(0, 2; y) - 4H(0; z)H(1, 0; y) + 8H(0, 0, 1; z) \\
& + 8H(0, 1; z)H(3; y) - 4H(0, 1; z)H(0; y) + 4H(0, 1, 0; z) - 8H(1; z)H(3, 0; y) + 8H(3, 2, 0; y) \\
& + 8H(1, 0; z)H(3; y) - 4H(1, 0; z)H(0; y) - 4H(1, 0, 1; z) - 8H(1, 1, 0; z) - 4H(1; z)H(1, 0; y) \\
& + 8H(3, 0, 2; y) - 4H(0, 1, 0; y) + 4H(1, 2, 0; y) + 4H(1, 0, 2; y) + 4H(1, 1, 0; y)] \\
& + \frac{z\pi^2}{3(1-y)^2} \left[-3 - H(0; z) - H(1; z) + H(2; y) \right] + \frac{z}{(1-y)^2} \left[6\zeta_3 - 2H(0; z)H(0, 2; y) \right. \\
& + 2H(0, 0, 1; z) + 6H(0, 1; z) - 2H(0, 1; z)H(2; y) - 2H(0, 1, 0; z) - 2H(1; z)H(2, 3; y) \\
& + 6H(1; z)H(3; y) - 2H(1; z)H(0, 3; y) - 6H(1, 0; z) + 2H(1, 0; z)H(2; y) + 2H(1, 0, 1; z) \\
& \left. - 2H(1, 1, 0; z) + 2H(2, 3, 2; y) - 6H(3, 2; y) + 2H(0, 3, 2; y) \right] \\
& + \frac{z}{1-y} \left[3H(0; z) - 2H(0; z)H(2; y) + 3H(1; z) - 2H(1; z)H(3; y) - 3H(2; y) + 2H(3, 2; y) \right] \\
& + \frac{z}{3(y+z)^3} \left[-8H(0; z)H(2, 2; y) - 24H(0; z)H(2; y) + 24H(0, 1; z) + 8H(0, 1; z)H(2; y) \right. \\
& - 8H(0, 1, 1; z) - 8H(1; z)H(2, 0; y) - 8H(1; z)H(0, 2; y) - 24H(1; z)H(0; y) + 24H(1, 0; z) \\
& + 8H(1, 0; z)H(2; y) - 8H(1, 0, 1; z) + 8H(1, 1; z)H(0; y) - 8H(1, 1, 0; z) + 8H(2, 2, 0; y) \\
& \left. + 8H(2, 0, 2; y) + 24H(2, 0; y) + 8H(0, 2, 2; y) + 24H(0, 2; y) \right] \\
& + \frac{z}{3(y+z)^2} \left[-24H(0; z) + 4H(0; z)H(2, 2; y) + 16H(0; z)H(2; y) - 16H(0, 1; z) \right. \\
& - 4H(0, 1; z)H(2; y) + 4H(0, 1, 1; z) + 4H(1; z)H(2, 0; y) + 4H(1; z)H(0, 2; y) \\
& + 16H(1; z)H(0; y) - 16H(1, 0; z) - 4H(1, 0; z)H(2; y) + 4H(1, 0, 1; z) - 4H(1, 1; z)H(0; y) \\
& + 4H(1, 1, 0; z) - 4H(2, 2, 0; y) - 4H(2, 0, 2; y) - 16H(2, 0; y) - 4H(0, 2, 2; y) \\
& \left. - 16H(0, 2; y) + 24H(0; y) \right] + \frac{z}{3(y+z)} \left[8H(0; z) - 8H(0; z)H(2, 2; y) + 8H(0, 1; z)H(2; y) \right. \\
& - 8H(0, 1, 1; z) - 8H(1; z)H(2, 0; y) - 8H(1; z)H(0, 2; y) + 8H(1, 0; z)H(2; y) - 8H(1, 0, 1; z) \\
& + 8H(1, 1; z)H(0; y) - 8H(1, 1, 0; z) + 8H(2, 2, 0; y) + 8H(2, 0, 2; y) + 8H(0, 2, 2; y) \\
& \left. - 8H(0; y) \right] + \frac{z^2}{(1-y)^3} \left[\pi^2H(0; z) + \pi^2H(1; z) - \pi^2H(2; y) - 18\zeta_3 + 6H(0; z)H(0, 2; y) \right. \\
& - 6H(0, 0, 1; z) + 6H(0, 1; z)H(2; y) + 6H(0, 1, 0; z) + 6H(1; z)H(2, 3; y) + 6H(1; z)H(0, 3; y) \\
& - 6H(1, 0; z)H(2; y) - 6H(1, 0, 1; z) + 6H(1, 1, 0; z) - 6H(2, 3, 2; y) - 6H(0, 3, 2; y)] \\
& \left. + \frac{z^2}{(1-y)^2} \left[6H(0; z)H(2; y) + 6H(1; z)H(3; y) - 6H(3, 2; y) \right] + \frac{z^2}{1-y} \left[3H(0; z)H(2; y) \right. \right.
\end{aligned}$$

$$\begin{aligned}
& +3H(1; z)H(3; y) - 3H(3, 2; y)] + \frac{1}{3(1-y-z)(1-y)} \left[-\frac{2\pi^2}{3}H(1; z) - 4H(0; z)H(3, 2; y) \right. \\
& +4H(0; z)H(0, 2; y) + 8H(0, 0, 1; z) + 8H(0, 1; z)H(3; y) - 4H(0, 1; z)H(0; y) \\
& +4H(0, 1, 0; z) + 4H(1; z)H(3, 3; y) - 4H(1; z)H(3, 0; y) + 4H(1, 0; z)H(3; y) \\
& -4H(1, 0; z)H(0; y) - 4H(1, 0, 1; z) - 8H(1, 1, 0; z) \\
& \left. +4H(3, 2, 0; y) - 4H(3, 3, 2; y) + 4H(3, 0, 2; y) - 4H(0, 1, 0; y) \right] \\
& + \frac{1}{3(1-y-z)} \left[\frac{2\pi^2}{3} + \frac{\pi^2}{2}H(1; z) - \frac{\pi^2}{2}H(1; y) - 3H(0; z)H(0, 2; y) + 4H(0; z)H(0; y) \right. \\
& -3H(0; z)H(1, 0; y) - 6H(0, 0, 1; z) - 6H(0, 1; z)H(3; y) + 3H(0, 1; z)H(0; y) \\
& -6H(1; z)H(3, 3; y) - 3H(1; z)H(1, 0; y) + 4H(1, 0; z) + 3H(1, 0; z)H(0; y) \\
& +6H(1, 1, 0; z) + 6H(3, 3, 2; y) + 3H(0, 1, 0; y) + 3H(1, 2, 0; y) + 3H(1, 0, 2; y) \\
& \left. -4H(1, 0; y) + 3H(1, 1, 0; y) - 3H(0, 1, 0; z) + 3H(1, 0, 1; z) \right] \\
& + \frac{1}{1-y} \left[-\frac{\pi^2}{2} + \frac{2\pi^2}{3}H(0; z) + \frac{2\pi^2}{3}H(1; z) - \frac{2\pi^2}{3}H(2; y) \right. \\
& +4H(0; z)H(0, 2; y) - H(0; z)H(0; y) - 4H(0, 0, 1; z) + H(0, 1; z) + 4H(0, 1; z)H(2; y) \\
& +4H(0, 1, 0; z) + 4H(1; z)H(2, 3; y) + H(1; z)H(3; y) + 4H(1; z)H(0, 3; y) - H(1; z)H(0; y) \\
& -H(1, 0; z) - 4H(1, 0; z)H(2; y) - 4H(1, 0, 1; z) + 4H(1, 1, 0; z) - 4H(2, 3, 2; y) - 12\zeta_3 \\
& \left. +H(2, 0; y) - H(3, 2; y) + H(0, 2; y) - 4H(0, 3, 2; y) + 3H(0; y) + 2H(1, 0; y) \right] \\
& + \frac{1}{3(y+z)^2} \left[-\pi^2H(1; z) + \pi^2H(2; y) - 6H(0; z)H(2, 2; y) - 6H(0; z)H(2; y) \right. \\
& +6H(0; z)H(2, 0; y) - 6H(0; z)H(3, 2; y) + 6H(0; z)H(0, 2; y) - 6H(0, 1; z) \\
& -6H(0, 1; z)H(2; y) - 6H(0, 1; z)H(3; y) + 6H(0, 1, 0; z) + 6H(0, 1, 1; z) + 24H(1; z) \\
& -12H(1; z)H(2, 3; y) - 8H(1; z)H(2; y) + 6H(1; z)H(2, 0; y) - 12H(1; z)H(3, 2; y) \\
& -12H(1; z)H(3, 3; y) - 12H(1; z)H(3; y) + 6H(1; z)H(3, 0; y) + 6H(1; z)H(0, 2; y) \\
& +6H(1; z)H(0, 3; y) + 6H(1; z)H(0; y) + 6H(1, 0; z) + 6H(1, 0; z)H(2; y) \\
& -6H(1, 0; z)H(0; y) + 6H(1, 0, 1; z) + 8H(1, 1; z) + 12H(1, 1; z)H(3; y) \\
& -6H(1, 1, 0; z) + 8H(2, 2; y) - 6H(2, 2, 0; y) + 12H(2, 3, 2; y) - 24H(2; y) \\
& -6H(2, 0, 2; y) - 6H(2, 0; y) + 12H(3, 2, 2; y) + 12H(3, 2; y) - 6H(1, 1; z)H(0; y) \\
& -6H(3, 2, 0; y) + 12H(3, 3, 2; y) - 6H(3, 0, 2; y) - 6H(0, 2, 2; y) + 6H(1, 0; z)H(3; y) \\
& \left. -6H(0, 2; y) - 6H(0, 3, 2; y) \right] + \frac{1}{3(y+z)} \left[\pi^2 + \frac{\pi^2}{2}H(1; z) - \frac{\pi^2}{2}H(2; y) - 12H(0; z) \right. \\
& -12H(0; z)H(2; y) - 3H(0; z)H(2, 0; y) + 6H(0; z)H(0; y) - 18H(0, 1; z) - 3H(0, 1, 0; z) \\
& \left. -32H(1; z) - 8H(1; z)H(2; y) - 30H(1; z)H(3; y) + 12H(1; z)H(0; y) + 12H(1, 0; z) \right]
\end{aligned}$$

E. The $\gamma^* \rightarrow q\bar{q}g$ NNLO Matrix Element coefficients

$$\begin{aligned}
& -3H(1, 0; z)H(2; y) + 3H(1, 0; z)H(0; y) + 8H(1, 1; z) + 3H(1, 1, 0; z) + 8H(2, 2; y) \\
& + 32H(2; y) - 12H(2, 0; y) + 3H(2, 1, 0; y) + 30H(3, 2; y) - 12H(0, 2; y) \\
& - 12H(0; y) + 3H(0, 1, 0; y) \Big] + \frac{T}{6} \Big[-\frac{2\pi^2}{3}H(2; y) + \frac{2\pi^2}{3}H(1; y) + 4H(0; z)H(2, 2; y) \\
& - 4H(0; z)H(2, 0; y) + 4H(0; z)H(1, 0; y) - 4H(0, 1, 1; z) - 9H(1; z) + 4H(1; z)H(2, 3; y) \\
& - 4H(1; z)H(2, 0; y) + 8H(1; z)H(3, 2; y) - 4H(1; z)H(0, 2; y) + 4H(1; z)H(1, 0; y) \\
& - 4H(1, 0; z)H(2; y) - 4H(1, 0, 1; z) - 8H(1, 1; z)H(3; y) + 4H(1, 1; z)H(0; y) \\
& + 4H(2, 2, 0; y) - 4H(2, 3, 2; y) + 9H(2; y) + 4H(2, 0, 2; y) - 4H(1, 1, 0; z) \\
& - 8H(3, 2, 2; y) + 4H(0, 2, 2; y) - 4H(1, 2, 0; y) - 4H(1, 0, 2; y) - 4H(1, 1, 0; y) \Big] \\
& + \frac{\pi^2}{18} \Big[25 - 12H(0; z) + 6H(0; z)H(2; y) - 6H(0; z)H(1; y) - 23H(1; z) + 12H(1; z)H(2; y) \\
& - 6H(1; z)H(1; y) - 6H(1, 0; z) - 6H(1, 1; z) - 12H(2, 2; y) + 22H(2; y) + 6H(2, 0; y) \\
& - 12H(0; y) + 6H(1, 2; y) + H(1; y) \Big] + \frac{1}{3} \Big[72\zeta_3 + 18\zeta_3H(1; z) - 36\zeta_3H(2; y) + 18\zeta_3H(1; y) \\
& - 5H(0; z) + 11H(0; z)H(2, 2; y) + 5H(0; z)H(2; y) + 6H(0; z)H(2, 0, 2; y) \\
& + 4H(0; z)H(2, 0; y) - 6H(0; z)H(3, 2, 2; y) + 9H(0; z)H(3, 2; y) \\
& - 6H(0; z)H(3, 3, 2; y) + 6H(0; z)H(3, 0, 2; y) + 6H(0; z)H(0, 2, 2; y) \\
& - 22H(0; z)H(0, 2; y) + 6H(0; z)H(0, 3, 2; y) + H(0; z)H(0; y) - 6H(0; z)H(0, 0, 2; y) \\
& - 6H(0; z)H(1, 0, 2; y) - 2H(0; z)H(1, 0; y) - 2H(0, 0, 1; z) + 6H(0, 0, 1; z)H(1; y) \\
& + 12H(0, 1; z)H(2, 2; y) - 9H(0, 1; z)H(2; y) - 6H(0, 1; z)H(2, 0; y) - 11H(0, 1; z) \\
& - 6H(0, 1; z)H(3, 2; y) - 6H(0, 1; z)H(3, 3; y) + 7H(0, 1; z)H(3; y) + 13H(0, 1; z)H(0; y) \\
& - 6H(0, 1; z)H(1, 2; y) - 10H(0, 1, 0; z) + 6H(0, 1, 0; z)H(2; y) - 6H(0, 1, 0; z)H(1; y) \\
& - 11H(0, 1, 1; z) + 6H(0, 1, 1; z)H(3; y) - 10H(1; z) + 12H(1; z)H(2, 2, 3; y) \\
& + 2H(1; z)H(2, 3; y) + 16H(1; z)H(2; y) - 11H(1; z)H(2, 0; y) \\
& - 12H(1; z)H(3, 2, 3; y) + 22H(1; z)H(3, 2; y) + 6H(1; z)H(3, 2, 0; y) \\
& - 12H(1; z)H(3, 3, 2; y) - 12H(1; z)H(3, 3, 3; y) + 16H(1; z)H(3, 3; y) \\
& + 6H(1; z)H(3, 3, 0; y) - 6H(1; z)H(3; y) + 6H(1; z)H(3, 0, 2; y) + 6H(1; z)H(3, 0, 3; y) \\
& - 9H(1; z)H(3, 0; y) + 6H(1; z)H(0, 2, 3; y) - 11H(1; z)H(0, 2; y) + 6H(1; z)H(0, 3, 2; y) \\
& + 6H(1; z)H(0, 3, 3; y) - 9H(1; z)H(0, 3; y) - 5H(1; z)H(0; y) - 6H(1; z)H(0, 0, 3; y)
\end{aligned}$$

E. The $\gamma^* \rightarrow q\bar{q}g$ NNLO Matrix Element coefficients

$$\begin{aligned}
& -6H(1; z)H(1, 2, 3; y) - 6H(1; z)H(1, 0, 3; y) - 2H(1; z)H(1, 0; y) + H(1, 0; z) \\
& -6H(1, 0; z)H(2, 2; y) + 13H(1, 0; z)H(2; y) + 6H(1, 0; z)H(3, 3; y) - 9H(1, 0; z)H(3; y) \\
& -6H(1, 0; z)H(0, 3; y) - 2H(1, 0; z)H(0; y) + 6H(1, 0; z)H(1, 2; y) + 6H(1, 0, 0, 1; z) \\
& -12H(1, 0, 1; z)H(2; y) + 6H(1, 0, 1; z)H(3; y) + 6H(1, 0, 1; z)H(1; y) - 6H(1, 0, 1, 0; z) \\
& -16H(1, 1; z) + 12H(1, 1; z)H(3, 3; y) - 22H(1, 1; z)H(3; y) - 6H(1, 1; z)H(3, 0; y) \\
& -6H(1, 1; z)H(0, 3; y) + 11H(1, 1; z)H(0; y) - 12H(1, 1, 0; z) + 6H(1, 1, 0; z)H(2; y) \\
& -6H(1, 1, 0; z)H(1; y) + 6H(1, 1, 0, 1; z) - 6H(1, 1, 1, 0; z) - 12H(2, 2, 3, 2; y) \\
& -16H(2, 2; y) + 11H(2, 2, 0; y) + 6H(2, 2, 1, 0; y) - 2H(2, 3, 2; y) + 11H(1, 0, 1; z) \\
& +10H(2; y) + 11H(2, 0, 2; y) + 5H(2, 0; y) - 6H(2, 0, 1, 0; y) - 24H(2, 1, 0; y) \\
& -22H(3, 2, 2; y) - 6H(3, 2, 2, 0; y) + 12H(3, 2, 3, 2; y) \\
& +6H(3, 2; y) - 6H(3, 2, 0, 2; y) + 9H(3, 2, 0; y) + 6H(3, 2, 1, 0; y) \\
& +12H(3, 3, 2, 2; y) - 16H(3, 3, 2; y) - 6H(3, 3, 2, 0; y) \\
& +12H(3, 3, 3, 2; y) - 6H(3, 3, 0, 2; y) - 6H(3, 0, 2, 2; y) \\
& +9H(3, 0, 2; y) - 6H(3, 0, 3, 2; y) + 6H(3, 0, 1, 0; y) + 11H(0, 2, 2; y) \\
& -6H(0, 2, 3, 2; y) + 5H(0, 2; y) - 6H(0, 3, 2, 2; y) + 9H(0, 3, 2; y) \\
& -6H(0, 3, 3, 2; y) - 5H(0; y) + 6H(0, 0, 3, 2; y) + H(0, 1, 0; y) + 6H(1, 2, 3, 2; y) \\
& +2H(1, 2, 0; y) + 2H(1, 0, 2; y) + 6H(1, 0, 3, 2; y) - 6H(1, 0; y) - H(1, 1, 0; y) \Big] . \quad (\text{E.9})
\end{aligned}$$

Appendix F

The $\mathcal{H} \rightarrow ggg$ NNLO Helicity Amplitude coefficients

In this appendix we give all one-loop coefficients $A_\Omega^{(1)}$, $B_\Omega^{(1)}$ and two-loop coefficients $A_\alpha^{(2)}$, $B_\alpha^{(2)}$, $C_\alpha^{(2)}$ and $D_\alpha^{(2)}$, defined in equations 8.32 and 8.33.

$$\begin{aligned}
 A_\alpha^{(1)} &= \frac{1}{6yzs_{123}(1-y-z)} \left\{ \right. \\
 & 2y - 2z^2 - 2yz - 6X_I + 6Y_I + 33i\pi - 2y^2 + 11W_I - 11Q_I + 2z - 6Z_I \left. \right\}, \\
 B_\alpha^{(1)} &= \frac{1}{6yzs_{123}(1-y-z)} \left\{ \right. \\
 & -2y + 2z^2 - 6i\pi + 2yz - 2W_I + 2Q_I + 2y^2 - 2z \left. \right\}, \\
 A_\beta^{(1)} &= \\
 & -X_I + Y_I - Z_I + \frac{11}{6}W_I - \frac{11}{6}Q_I + \frac{11}{2}i\pi - \frac{1}{3}\frac{z}{[1-y-z]} + \frac{-\frac{1}{3}z^2 + \frac{1}{3}z}{[1-y-z]^2}, \\
 B_\beta^{(1)} &= \\
 & -\frac{1}{3}W_I + \frac{1}{3}Q_I - i\pi + \frac{1}{3}\frac{z}{[1-y-z]} + \frac{-\frac{1}{3}z + \frac{1}{3}z^2}{[1-y-z]^2}, \tag{F.1}
 \end{aligned}$$

F. The $\mathcal{H} \rightarrow ggg$ NNLO Helicity Amplitude coefficients

$$\begin{aligned}
A_{\alpha}^{(2)} = & \frac{1}{y z s_{123}} \left\{ \frac{F^A}{(1-y-z)} \right. \\
& + \left(\frac{41}{36} W_I + \frac{1}{6} Y_I - \frac{1}{2} X_I - \frac{1}{6} Z_I + \frac{55}{36} i\pi + \frac{247}{54} - \frac{11}{12} Q_I + \frac{13}{9} H(0; z) \right) z + \\
& \left(\left(-\frac{5}{3} X_I + \frac{5}{3} W_I + \frac{5}{3} H(0; z) \right) z^2 + \left(\frac{25}{6} X_I - \frac{5}{3} W_I \right) z \right) y^{-1} \\
& + \frac{-\frac{5}{3} X_I z^3 + \frac{5}{3} X_I z^2}{y^2} + \left\{ \frac{1}{2} Y_I - \frac{1}{6} X_I - \frac{1}{6} Z_I + \frac{247}{54} + \frac{55}{36} i\pi \right. \\
& + \frac{41}{36} W_I + \frac{19}{36} Q_I - \frac{13}{9} H(0; z) + \left(-\frac{5}{3} W_I - \frac{25}{6} Y_I \right) z^{-1} \left. \right\} y + \\
& \left(\frac{\frac{5}{3} Y_I + \frac{5}{3} Q_I - \frac{5}{3} H(0; z) + \frac{5}{3} W_I - \frac{5}{3} \frac{Y_I}{z^2}}{z} y^2 - \frac{7}{2} W_I \right. \\
& - \frac{7}{2} H(0; z) + \frac{5}{3} \frac{Y_I y^3}{z^2} + \left\{ \left(\frac{10}{3} H(0; z) - \frac{5}{3} Q_I - \frac{5}{3} Z_I \right) z^2 \right. \\
& + \left(\frac{5}{3} Q_I - \frac{5}{3} H(0; z) + \frac{25}{6} Z_I \right) z \left. \right\} y (1-y-z)^{-2} \\
& + \frac{\left(-\frac{5}{3} Z_I z^3 + \frac{5}{3} Z_I z^2 \right) y}{(1-y-z)^3} + \left\{ \frac{5}{3} y H(0; z) z - \frac{41}{36} y z Q_I + \frac{11}{12} y z W_I \right. \\
& + \frac{247}{54} y z + \frac{1}{6} y z Y_I - \frac{1}{6} y z X_I - \frac{1}{2} y z Z_I + \frac{55}{36} i y z \pi - 7 H(0; z) y \\
& \left. + \frac{7}{2} y Q_I \right\} (1-y-z)^{-1} \left. \right\}, \tag{F.2}
\end{aligned}$$

F. The $\mathcal{H} \rightarrow ggg$ NNLO Helicity Amplitude coefficients

$$\begin{aligned}
B_{\alpha}^{(2)} = \frac{1}{y z s_{123}} & \left\{ \right. \\
& -\frac{1}{6} \frac{Y_1 y^3}{z^2} + \left(\frac{-\frac{1}{6} W_1 - \frac{1}{6} Q_1 + \frac{1}{6} H(0; z) - \frac{1}{6} Y_1 + \frac{1}{6} \frac{Y_1}{z^2}}{z} \right) y^2 \\
& + \left(\frac{\frac{1}{3} Y_1 - \frac{1}{12} Q_1 + \frac{1}{12} H(0; z) - \frac{1}{12} W_1 - \frac{1}{3} + \frac{-\frac{1}{3} Y_1 + \frac{1}{6} W_1}{z}}{z} \right) y \\
& + \left(-\frac{1}{3} X_1 - \frac{1}{12} H(0; z) - \frac{1}{3} - \frac{1}{12} W_1 \right) z - \frac{5}{12} W_1 + \frac{67}{24} + \frac{1}{2} i\pi - 2\zeta_3 \\
& + \frac{(-\frac{1}{6} W_1 + \frac{1}{6} X_1 - \frac{1}{6} H(0; z)) z^2 + (\frac{1}{3} X_1 + \frac{1}{6} W_1) z}{y} \\
& + \frac{\frac{1}{6} X_1 z^3 - \frac{1}{6} X_1 z^2}{y^2} + \left\{ \left(-\frac{1}{6} H(0; z) - \frac{1}{3} Z_1 + \frac{1}{12} Q_1 - \frac{1}{3} \right) z \right. \\
& + \frac{67}{24} + \frac{1}{2} i\pi + \frac{5}{12} Q_1 - \frac{5}{12} H(0; z) - 2\zeta_3 \left. \right\} y + \left\{ \frac{1}{2} i\pi + \frac{67}{24} - 2\zeta_3 \right. \\
& + \left. \frac{5}{12} H(0; z) \right\} z \left. \right\} [1-y-z]^{-1} \\
& + \frac{((-\frac{1}{3} H(0; z) + \frac{1}{6} Z_1 + \frac{1}{6} Q_1) z^2 + (-\frac{1}{6} Q_1 + \frac{1}{6} H(0; z) + \frac{1}{3} Z_1) z) y}{[1-y-z]^2} \\
& + \left. \frac{(\frac{1}{6} Z_1 z^3 - \frac{1}{6} Z_1 z^2) y}{[1-y-z]^3} \right\}, \tag{F.3}
\end{aligned}$$

F. The $\mathcal{H} \rightarrow ggg$ NNLO Helicity Amplitude coefficients

$$\begin{aligned}
C_\alpha^{(2)} &= \frac{1}{y z s_{123}} \left\{ \frac{F^C}{(1-y-z)} \right. \\
&+ \left(\left(-\frac{11}{6} Y_1 - \frac{11}{6} W_1 - \frac{11}{6} Q_1 + \frac{11}{6} H(0; z) \right) z^{-1} + \frac{11}{6} \frac{Y_1}{z^2} \right) y^2 + \frac{19}{12} W_1 \\
&+ \frac{19}{12} H(0; z) + \left(\frac{11}{6} Z_1 z^3 - \frac{11}{6} Z_1 z^2 \right) y [1-y-z]^{-3} \\
&+ \left(\left(\frac{11}{6} Q_1 - \frac{11}{3} H(0; z) + \frac{11}{6} Z_1 \right) z^2 + \left(-\frac{11}{6} Q_1 + \frac{11}{6} H(0; z) - \frac{7}{3} Z_1 \right) z \right) y [1-y-z]^{-2} \\
&- \frac{11}{6} \frac{Y_1 y^3}{z^2} + \left(\frac{11}{6} X_1 z^3 - \frac{11}{6} X_1 z^2 \right) y^{-2} + \left\{ -\frac{23}{18} W_1 + \frac{1}{6} Z_1 - \frac{59}{36} H(0; z) + \frac{13}{12} Q_1 \right. \\
&- \frac{275}{54} - \frac{1}{6} Y_1 + \frac{1}{6} X_1 - \frac{65}{36} i\pi \left. \right\} z + \left\{ -\frac{23}{18} W_1 - \frac{5}{9} Q_1 + \frac{59}{36} H(0; z) + \frac{1}{6} Z_1 \right. \\
&+ \frac{1}{6} X_1 - \frac{1}{6} Y_1 - \frac{275}{54} - \frac{65}{36} i\pi + \left(\frac{11}{6} W_1 + \frac{7}{3} Y_1 \right) z^{-1} \left. \right\} y + \\
&\left(\left(\frac{11}{6} X_1 - \frac{11}{6} W_1 - \frac{11}{6} H(0; z) \right) z^2 + \left(\frac{11}{6} W_1 - \frac{7}{3} X_1 \right) z \right) y^{-1} \\
&+ \left\{ \frac{19}{6} H(0; z) y - \frac{11}{6} y H(0; z) z + \frac{23}{18} y z Q_1 - \frac{13}{12} y z W_1 - \frac{65}{36} i y z \pi - \frac{19}{12} y Q_1 - \frac{275}{54} y z \right. \\
&- \left. \frac{1}{6} y z Y_1 + \frac{1}{6} y z X_1 + \frac{1}{6} y z Z_1 \right\} [1-y-z]^{-1} \left. \right\}, \\
D_\alpha^{(2)} &= \frac{1}{y z s_{123}} \left\{ \frac{F^D}{(1-y-z)} \right. \\
&+ \left(\frac{1}{9} H(0; z) + \frac{5}{27} + \frac{1}{18} W_1 + \frac{5}{18} i\pi - \frac{1}{18} Q_1 \right) y \\
&+ \left(\frac{1}{18} W_1 + \frac{5}{18} i\pi + \frac{1}{9} H(0; z) - \frac{1}{6} Q_1 + \frac{5}{27} \right) z \\
&+ \left(\frac{5}{18} i y z \pi + \frac{5}{27} y z + \frac{1}{6} y z W_1 - \frac{1}{18} y z Q_1 \right) [1-y-z]^{-1}, \tag{F.4}
\end{aligned}$$

F. The $\mathcal{H} \rightarrow ggg$ NNLO Helicity Amplitude coefficients

where:

$$\begin{aligned}
 Y_I &= H(2, 0; y) - H(3, 2; y) - H(1; z) H(3; y) \\
 &\quad - H(0, 1; z) + H(0, 2; y) - H(1, 0; y) + H(0; y) H(1; z) , \\
 Z_I &= H(1, 0; y) + H(1, 0; z) + H(0; y) H(0; z) + \frac{1}{6} \pi^2 , \\
 X_I &= H(3, 2; y) + H(1; z) H(3; y) - H(0; z) H(2; y) , \\
 W_I &= H(2; y) + H(1; z) , \\
 Q_I &= H(0; y) + H(0; z) , \tag{F.5}
 \end{aligned}$$

and:

$$\begin{aligned}
 F_A = & \\
 & -\frac{55}{6} i\pi H(1, 0; y) - \frac{55}{12} i\pi H(0, 1; z) - \frac{1}{4} \pi^2 H(0; y) H(1; z) - \frac{1}{6} \pi^2 H(1; z) H(3; y) \\
 & + \frac{49}{24} H(2, 0; y) - \frac{389}{72} H(0, 1; z) - \frac{605}{72} i\pi H(0; y) - \frac{55}{12} i\pi H(1, 0; z) - \frac{605}{72} i\pi H(0; z) \\
 & - \frac{55}{6} i\pi H(3, 2; y) - \frac{2}{3} \pi^2 H(1; z) H(2; y) - 2 H(0, 3, 0; y) H(1; z) \\
 & + 2 H(0, 1; z) H(3, 2; y) + \frac{1}{4} \pi^2 H(0; y) H(0; z) - \frac{1}{4} \pi^2 H(0; z) H(2; y) \\
 & + \frac{11}{3} H(0, 0; y) H(0; z) - 2 H(0, 3, 2; y) H(1; z) - 2 H(1, 0; z) H(2, 2; y) \\
 & - 2 H(1, 1, 0; z) H(3; y) - 2 H(1; z) H(3, 0, 2; y) + \frac{11}{3} H(1; z) H(3, 3; y) \\
 & - \frac{11}{3} H(0, 0; y) H(1; z) - \frac{55}{6} H(1; z) H(2, 3; y) + \frac{11}{3} H(0, 0; z) H(0; y) \\
 & + \frac{11}{12} H(0; y) H(1, 0; z) - \frac{11}{8} \zeta_3 - \frac{11}{3} H(0, 0; z) H(2; y) + \frac{11}{3} H(1; z) H(2, 0; y) \\
 & - \frac{22}{3} H(1, 1; z) H(3; y) + 4 \zeta_4 + 4 H(1; z) H(3, 3, 2; y) + \frac{11}{3} H(0; y) H(1, 1; z) \\
 & + \frac{11}{12} H(0; z) H(2, 0; y) + \frac{49}{24} H(0; y) H(1; z) - 2 H(1; z) H(2, 1, 0; y) \\
 & - \frac{22}{3} H(1; z) H(3, 2; y) + \frac{11}{12} H(0, 1; z) H(0; y) + \frac{11}{3} H(0; z) H(2, 2; y)
 \end{aligned}$$

F. The $\mathcal{H} \rightarrow ggg$ NNLO Helicity Amplitude coefficients

$$\begin{aligned}
& -2H(0, 1; z)H(2, 0; y) + \frac{49}{24}H(0; z)H(2; y) - H(0; y)H(1, 1, 0; z) \\
& -H(0; y)H(1, 0, 1; z) + H(0; y)H(1, 0, 0; z) - H(0, z)H(2, 0, 2; y) \\
& -H(0; z)H(2, 0, 0; y) + H(0; z)H(1, 2, 0; y) + H(0, z)H(1, 0, 2; y) \\
& +H(0, 0, 1; z)H(0; y) + H(0, 0; z)H(2, 2; y) - H(0, 0; z)H(2, 0; y) \\
& -H(0, 0; z)H(0, 2; y) + H(0, 0; y)H(1, 1; z) - H(0, 0; y)H(1, 0; z) \\
& -H(0, 0; y)H(0, 1; z) + H(0, 0; y)H(0, 0; z) - H(0, z)H(3, 2, 0; y) \\
& -H(0; z)H(3, 0, 2; y) - H(0; z)H(2, 3, 2; y) - H(0; z)H(2, 2, 0; y) \\
& -H(0; z)H(2, 1, 0; y) - 2H(1, 1; z)H(3, 0; y) + 4H(1, 1; z)H(3, 3; y) \\
& +\frac{13}{4}H(1; z) + \frac{13}{4}H(2; y) - \frac{67}{9}H(3, 2; y) + \frac{49}{24}H(0, 2; y) - \frac{13}{4}H(0; y) \\
& +\frac{1}{4}H(0; z) + \frac{22}{3}H(1, 0, 0; y) + \frac{185}{12}i\pi - \frac{55}{6}i\pi H(1; z)H(3; y) \\
& -\frac{55}{12}i\pi H(0; y)H(0; z) - \frac{389}{72}H(1, 0; z) + \frac{121}{24}H(2, 2; y) - \frac{67}{9}H(1, 0; y) \\
& -\frac{11}{2}H(1, 0, 1; z) + \frac{121}{24}H(1, 1; z) + \frac{55}{12}i\pi H(0; z)H(2; y) \\
& +\frac{55}{12}i\pi H(0; y)H(1; z) + \frac{3}{2}i\zeta_3\pi + \frac{55}{12}i\pi H(0, 2; y) + \frac{55}{12}i\pi H(2, 0; y) \\
& +\frac{605}{72}i\pi H(1; z) + \frac{605}{72}i\pi H(2; y) + \frac{121}{24}H(0, 0; y) + \frac{121}{24}H(0, 0; z) \\
& -\frac{11}{3}H(0, 0, 2; y) + \frac{55}{6}H(0, 1, 0; y) + \frac{11}{2}H(0, 1, 0; z) - \frac{11}{3}H(0, 1, 1; z) \\
& -\frac{11}{3}H(0, 2, 0; y) + \frac{11}{3}H(0, 2, 2; y) - \frac{11}{3}H(2, 0, 0; y) + \frac{11}{3}H(2, 0, 2; y) \\
& +\frac{11}{3}H(2, 2, 0; y) + \frac{11}{3}H(1, 0, 0; z) - \frac{11}{3}H(1, 1, 0; y) - \frac{55}{6}H(2, 3, 2; y) \\
& -\frac{22}{3}H(3, 2, 2; y) + \frac{11}{3}H(3, 3, 2; y) + 2H(0, 0, 1, 0; y) + H(0, 0, 1, 1; z) + H(0, 0, 2, 2; y) \\
& +H(0, 1, 0, 1; z) - 2H(0, 0, 3, 2; y) - 2H(0, 3, 0, 2; y) - 2H(0, 3, 2, 0; y) \\
& -2H(0, 3, 2, 2; y) - H(0, 1, 0, 2; y) + 4H(0, 1, 1, 0; y) + H(0, 1, 1, 0; z) \\
& -H(0, 1, 2, 0; y) + H(0, 2, 0, 2; y) - H(0, 2, 1, 0; y) + H(0, 2, 2, 0; y) \\
& -H(0, 2, 3, 2; y) + H(1, 0, 0, 1; z) - 2H(1, 0, 0, 2; y) + 4H(3, 3, 3, 2; y) \\
& +4H(1, 0, 1, 0; y) + H(1, 0, 1, 0; z) - 2H(1, 0, 2, 0; y) + 4H(1, 1, 0, 0; y) \\
& +H(1, 1, 0, 0; z) + 4H(1, 1, 1, 0; y) - 2H(1, 2, 0, 0; y) + H(2, 0, 0, 2; y)
\end{aligned}$$

F. The $\mathcal{H} \rightarrow ggg$ NNLO Helicity Amplitude coefficients

$$\begin{aligned}
& -\mathrm{H}(2, 0, 1, 0; y) + \mathrm{H}(2, 0, 2, 0; y) - \mathrm{H}(2, 0, 3, 2; y) - 2\mathrm{H}(2, 1, 0, 0; y) \\
& -2\mathrm{H}(2, 1, 0, 2; y) - 2\mathrm{H}(2, 1, 2, 0; y) + \mathrm{H}(2, 2, 0, 0; y) - 2\mathrm{H}(2, 2, 1, 0; y) \\
& + 2\mathrm{H}(2, 2, 3, 2; y) - \mathrm{H}(2, 3, 0, 2; y) - \mathrm{H}(2, 3, 2, 0; y) + 4\mathrm{H}(2, 3, 3, 2; y) \\
& - 2\mathrm{H}(3, 0, 2, 2; y) - 2\mathrm{H}(3, 2, 0, 2; y) - 2\mathrm{H}(3, 2, 2, 0; y) + 4\mathrm{H}(3, 2, 3, 2; y) \\
& + 4\mathrm{H}(3, 3, 2, 2; y) + \mathrm{H}(0, 0, 2; y) \mathrm{H}(0; z) + \mathrm{H}(0, 0, 2; y) \mathrm{H}(1; z) \\
& + \mathrm{H}(0, 1; z) \mathrm{H}(1, 0, y) - \mathrm{H}(0, 1; z) \mathrm{H}(3, 0; y) + \mathrm{H}(0, 1, 0; y) \mathrm{H}(0; z) \\
& - \mathrm{H}(0, 1, 0; y) \mathrm{H}(1; z) + \mathrm{H}(0, 1; z) \mathrm{H}(0, 3; y) + \mathrm{H}(0, 1, 0; z) \mathrm{H}(0; y) \\
& - \mathrm{H}(0, 1, 0; z) \mathrm{H}(2; y) - \mathrm{H}(0, 1, 1; z) \mathrm{H}(0; y) + \mathrm{H}(0, 2, 0; y) \mathrm{H}(0; z) \\
& + \mathrm{H}(0, 2, 0; y) \mathrm{H}(1; z) + \mathrm{H}(0, 2, 2; y) \mathrm{H}(0; z) - \mathrm{H}(0, 2, 3; y) \mathrm{H}(1; z) \\
& + \mathrm{H}(0, 3; y) \mathrm{H}(1, 0; z) + \mathrm{H}(0, 3, 2; y) \mathrm{H}(0; z) + \mathrm{H}(1; z) \mathrm{H}(2, 0, 0; y) \\
& - \mathrm{H}(1; z) \mathrm{H}(2, 0, 3; y) - \mathrm{H}(1; z) \mathrm{H}(2, 3, 0; y) + \mathrm{H}(1, 0; y) \mathrm{H}(1, 0; z) \\
& - \mathrm{H}(1, 0, z) \mathrm{H}(2, 3; y) - \mathrm{H}(1, 0, 0; z) \mathrm{H}(2, y) - \mathrm{H}(1, 0; z) \mathrm{H}(3, 0; y) \\
& + \frac{1}{2} \zeta_3 \mathrm{H}(1; z) + \frac{2}{3} \pi^2 \mathrm{H}(1, 1; y) + \frac{1}{2} \zeta_3 \mathrm{H}(2; y) - \frac{1}{6} \pi^2 \mathrm{H}(3, 2; y) \\
& - \frac{1}{4} \pi^2 \mathrm{H}(0, 2; y) - \frac{11}{18} \pi^2 \mathrm{H}(1; y) + \frac{55}{48} \pi^2 \mathrm{H}(2, y) - \frac{1}{2} \zeta_3 \mathrm{H}(0; y) - \frac{1}{2} \zeta_3 \mathrm{H}(0; z) \\
& + 2\mathrm{H}(0; z) \mathrm{H}(1, 0, 0; y) - \frac{1}{4} \pi^2 \mathrm{H}(2, 0; y) + \frac{1}{4} \pi^2 \mathrm{H}(0, 1; z) + \frac{1}{4} \pi^2 \mathrm{H}(1, 0; z) \\
& - 2\mathrm{H}(1, 0, 0; y) \mathrm{H}(1; z) + \frac{2}{3} \pi^2 \mathrm{H}(0, 1; y) - \frac{2}{3} \pi^2 \mathrm{H}(2, 2; y) + \frac{1}{2} \pi^2 \mathrm{H}(1, 0; y) \\
& + \frac{121}{24} \mathrm{H}(1; z) \mathrm{H}(2; y) + \frac{77}{144} \pi^2 \mathrm{H}(1; z) + \frac{55}{144} \pi^2 \mathrm{H}(0; z) + \frac{55}{144} \pi^2 \mathrm{H}(0; y) \\
& + 2\mathrm{H}(1, 0, 1; z) \mathrm{H}(3; y) - \frac{49}{24} \mathrm{H}(0; y) \mathrm{H}(0; z) - \frac{67}{9} \mathrm{H}(1; z) \mathrm{H}(3; y) \\
& + \frac{11}{3} \mathrm{H}(1, 0; z) \mathrm{H}(2; y) - 2\mathrm{H}(0, 3; y) \mathrm{H}(1, 1; z) - \frac{11}{2} \mathrm{H}(0, 1; z) \mathrm{H}(2; y) \\
& + \frac{11}{3} \mathrm{H}(0, 1; z) \mathrm{H}(3; y) + \frac{11}{12} \mathrm{H}(0, 2; y) \mathrm{H}(0; z) + \frac{11}{3} \mathrm{H}(0, 2; y) \mathrm{H}(1; z) \\
& - 2\mathrm{H}(0; z) \mathrm{H}(3, 2, 2; y) + 3\mathrm{H}(0, 0, 1; z) \mathrm{H}(2; y) + 4\mathrm{H}(0, 0, 1; z) \mathrm{H}(3; y) \\
& - 2\mathrm{H}(0, 0, 3; y) \mathrm{H}(1; z) + 2\mathrm{H}(0, 1; z) \mathrm{H}(2, 2, y) + 3\mathrm{H}(0, 1; z) \mathrm{H}(2, 3; y) \\
& + 4\mathrm{H}(0, 1; z) \mathrm{H}(3, 3; y) + 2\mathrm{H}(0, 1, 1; z) \mathrm{H}(3; y) + 2\mathrm{H}(1; z) \mathrm{H}(2, 2, 3, y) \\
& + 4\mathrm{H}(1; z) \mathrm{H}(2, 3, 3; y) - 2\mathrm{H}(1; z) \mathrm{H}(3, 2, 0; y) + 4\mathrm{H}(1; z) \mathrm{H}(3, 2, 3; y) \\
& + 4\mathrm{H}(1; z) \mathrm{H}(3, 3, 3; y) - 2\mathrm{H}(1, 0; z) \mathrm{H}(2, 0; y) - 2\mathrm{H}(1, 0; z) \mathrm{H}(3, 2; y) \\
& - 4\mathrm{H}(1, 1, 0; z) \mathrm{H}(2; y) - \frac{77}{144} i\pi^3 - \frac{1}{96} \pi^4 - \frac{5029}{432} \pi^2 + \frac{1321}{108}, \tag{F.6}
\end{aligned}$$

F. The $\mathcal{H} \rightarrow ggg$ NNLO Helicity Amplitude coefficients

$$\begin{aligned}
F_C = & \frac{1}{18} H(2, 0; y) + \frac{7}{6} H(0, 1; z) - \frac{2}{3} H(0, 0; y) H(0; z) - \frac{5}{6} i\pi H(0; z) H(2; y) \\
& - \frac{5}{6} i\pi H(0; y) H(1; z) + \frac{5}{3} i\pi H(1; z) H(3; y) + \frac{5}{6} i\pi H(0; y) H(0; z) \\
& - \frac{2}{3} H(1; z) H(3, 3; y) + \frac{2}{3} H(0, 0; y) H(1; z) + \frac{5}{3} H(1; z) H(2, 3, y) \\
& - \frac{2}{3} H(0, 0; z) H(0; y) - \frac{1}{6} H(0; y) H(1, 0; z) - \frac{7}{4} \zeta_3 + \frac{2}{3} H(0, 0; z) H(2; y) \\
& - \frac{2}{3} H(1; z) H(2, 0; y) + \frac{4}{3} H(1, 1; z) H(3; y) - \frac{2}{3} H(0; y) H(1, 1; z) \\
& - \frac{1}{6} H(0; z) H(2, 0; y) - \frac{1781}{216} + \frac{1}{18} H(0; y) H(1; z) + \frac{4}{3} H(1; z) H(3, 2; y) \\
& + \frac{7}{72} i\pi^3 - \frac{71}{9} i\pi - \frac{1}{6} H(0, 1; z) H(0; y) - \frac{2}{3} H(0; z) H(2, 2; y) \\
& + \frac{1}{18} H(0; z) H(2; y) - \frac{103}{54} H(1; z) - \frac{103}{54} H(2; y) + \frac{10}{9} H(3, 2; y) \\
& + \frac{1}{18} H(0, 2; y) + \frac{103}{54} H(0, y) + \frac{35}{108} H(0; z) - \frac{4}{3} H(1, 0, 0; y) + \frac{7}{6} H(1, 0; z) \\
& - \frac{11}{6} H(2, 2; y) + \frac{10}{9} H(1, 0; y) + H(1, 0, 1; z) - \frac{11}{6} H(1, 1; z) - \frac{11}{6} H(0, 0; y) \\
& - \frac{11}{6} H(0, 0; z) + \frac{2}{3} H(0, 0, 2; y) - \frac{5}{3} H(0, 1, 0; y) - H(0, 1, 0; z) + \frac{2}{3} H(0, 1, 1; z) \\
& + \frac{2}{3} H(0, 2, 0; y) - \frac{2}{3} H(0, 2, 2; y) + \frac{2}{3} H(2, 0, 0; y) - \frac{2}{3} H(2, 0, 2; y) \\
& - \frac{2}{3} H(2, 2, 0; y) - \frac{2}{3} H(1, 0, 0; z) + \frac{2}{3} H(1, 1, 0; y) + \frac{5}{3} H(2, 3, 2; y) \\
& + \frac{4}{3} H(3, 2, 2; y) - \frac{2}{3} H(3, 3, 2; y) + \frac{1}{9} \pi^2 H(1; y) - \frac{5}{24} \pi^2 H(2; y) \\
& - \frac{11}{6} H(1; z) H(2; y) - \frac{7}{72} \pi^2 H(1; z) - \frac{5}{72} \pi^2 H(0; z) - \frac{5}{72} \pi^2 H(0; y) \\
& - \frac{1}{18} H(0; y) H(0; z) + \frac{10}{9} H(1, z) H(3; y) - \frac{2}{3} H(1, 0; z) H(2; y) \\
& + H(0, 1; z) H(2; y) - \frac{2}{3} H(0, 1; z) H(3; y) - \frac{1}{6} H(0, 2; y) H(0; z) \\
& - \frac{2}{3} H(0, 2; y) H(1, z) + \frac{1879}{432} \pi^2 + \frac{55}{18} i\pi H(0; z) - \frac{5}{6} i\pi H(2, 0; y) \\
& + \frac{5}{6} i\pi H(1, 0; z) + \frac{5}{3} i\pi H(1, 0; y) - \frac{5}{6} i\pi H(0, 2; y) + \frac{5}{3} i\pi H(3, 2; y) \\
& + \frac{55}{18} i\pi H(0; y) - \frac{55}{18} i\pi H(1; z) + \frac{5}{6} i\pi H(0, 1; z) - \frac{55}{18} i\pi H(2; y) , \tag{F.7}
\end{aligned}$$

F. The $\mathcal{H} \rightarrow ggg$ NNLO Helicity Amplitude coefficients

$$\begin{aligned}
 F_D = & \\
 & \frac{5}{9} i\pi - \frac{5}{27} H(0; z) + \frac{1}{6} H(1, 1; z) - \frac{29}{72} \pi^2 - \frac{1}{18} H(0; z) H(2; y) \\
 & + \frac{5}{27} H(1; z) - \frac{5}{27} H(0; y) - \frac{1}{18} H(0, 2; y) + \frac{1}{6} H(2, 2; y) - \frac{5}{18} i\pi H(0; y) \\
 & + \frac{5}{27} H(2; y) + \frac{1}{6} H(1; z) H(2; y) - \frac{1}{18} H(0; y) H(1; z) - \frac{1}{18} H(0, 1; z) \\
 & + \frac{1}{6} H(0, 0; y) - \frac{1}{18} H(2, 0; y) + \frac{1}{18} H(0; y) H(0; z) + \frac{5}{18} i\pi H(2; y) \\
 & + \frac{5}{18} i\pi H(1; z) - \frac{1}{18} H(1, 0; z) + \frac{1}{6} H(0, 0; z) - \frac{5}{18} i\pi H(0; z) . \tag{F.8}
 \end{aligned}$$

Bibliography

- [1] R. P. Feynman, *QED: The Strange Theory of Light and Matter*, Princeton University Press, Princeton, New Jersey, 1985.
- [2] R. P. Feynman, A. R. Hibbs, *Quantum Mechanics and Path Integrals*, McGraw-Hill, New York, 1965.
- [3] M. E. Peskin and D. V. Schroeder, *An Introduction to Quantum Field Theory*, Reading, USA: Addison-Wesley (1995)
- [4] T. Muta, *Foundations of Quantum Chromodynamics*, World Scientific (2000)
- [5] R. K. Ellis, W. J. Stirling and B. R. Webber, *QCD and Collider Physics*, Cambridge, UK: CUP (1996).
- [6] J. C. Collins, *Renormalization*, Cambridge, UK:CUP (1989).
- [7] S. Weinberg, *The Quantum Theory Of Fields. Vol. 2: Modern Applications*, Cambridge, UK:CUP (1996).
- [8] G. 't Hooft and M. Veltman, Nucl. Phys. **B44** (1972) 189.
- [9] C.G. Bollini and J.J. Giambiagi, Nuovo Cim. **12B** (1972) 20.
- [10] G.M. Cicuta and E. Montaldi, Nuovo Cim. Lett. **4** (1972) 329.
- [11] S. Catani, M. H. Seymour and Z. Trocsanyi, Phys. Rev. D **55** (1997) 6819 [arXiv:hep-ph/9610553].
- [12] S. Catani, Phys. Lett. B **427** (1998) 161 [arXiv:hep-ph/9802439].

- [13] G. Leibbrandt, *Rev. Mod. Phys.* **47** (1975) 849.
- [14] J. F. Gunion, H. E. Haber, G. L. Kane and S. Dawson, *The Higgs Hunter's Guide*, (Addison-Wesley, Menlo Park, 1990).
- [15] See <http://lepewwg.web.cern.ch/LEPEWWG/> for updates.
- [16] M. A. Shifman, A. I. Vainshtein, M. B. Voloshin and V. I. Zakharov, *Sov. J. Nucl. Phys.* **30** (1979) 711 [*Yad. Fiz.* **30** (1979) 1368].
- [17] A. I. Vainshtein, V. I. Zakharov and M. A. Shifman, *Sov. Phys. Usp.* **23** (1980) 429 [*Usp. Fiz. Nauk* **131** (1980) 537].
- [18] M. B. Voloshin, *Sov. J. Nucl. Phys.* **44** (1986) 478 [*Yad. Fiz.* **44** (1986) 738].
- [19] K. G. Chetyrkin, B. A. Kniehl and M. Steinhauser, *Phys. Rev. Lett.* **79** (1997) 353 [arXiv:hep-ph/9705240].
- [20] K. G. Chetyrkin, B. A. Kniehl and M. Steinhauser, *Nucl. Phys. B* **510** (1998) 61 [arXiv:hep-ph/9708255].
- [21] M. Kramer, E. Laenen and M. Spira, *Nucl. Phys. B* **511** (1998) 523 [arXiv:hep-ph/9611272].
- [22] S. A. Larin, T. van Ritbergen and J. A. Vermaseren, *Nucl. Phys. B* **438** (1995) 278 [arXiv:hep-ph/9411260].
- [23] S. Dawson, *Nucl. Phys. B* **359** (1991) 283.
- [24] A. Djouadi, M. Spira and P. M. Zerwas, *Phys. Lett. B* **264** (1991) 440.
- [25] A. Nordsieck, *Phys. Rev.* **52** (1937) 59.
- [26] F. Bloch and A. Nordsieck, *Phys. Rev.* **52** (1937) 54.
- [27] T. Kinoshita, *J. Math. Phys.* **3** (1962) 650.
- [28] T. D. Lee and M. Nāuēnberg, *Phys. Rev.* **133B** (1964) 1549.

- [29] G. Sterman and M. E. Tejeda-Yeomans, Phys. Lett. B **552** (2003) 48 [arXiv:hep-ph/0210130].
- [30] E. W. N. Glover, arXiv:hep-ph/0211412.
- [31] W. Giele *et al.*, arXiv:hep-ph/0204316.
- [32] P. Nogueira, J. Comput. Phys. **105** (1993) 279.
- [33] *MAPLE V Release 7*, Copyright 2001 by Waterloo Maple Inc.
- [34] J.A.M. Vermaseren, arXiv:math-ph/0010025.
- [35] M. L. Mangano, Nucl. Phys. B **309** (1988) 461.
- [36] F. V. Tkachov, Phys. Lett. B **100** (1981) 65.
- [37] K. G. Chetyrkin and F. V. Tkachov, Nucl. Phys. B **192** (1981) 159.
- [38] S. Laporta, Int. J. Mod. Phys. A **15** (2000) 5087 [arXiv:hep-ph/0102033].
- [39] E. Remiddi and J. A. Vermaseren, Int. J. Mod. Phys. A **15** (2000) 725 [arXiv:hep-ph/9905237].
- [40] N. Nielsen, Nova Acta Leopoldiana (Halle) **90** (1909) 123.
- [41] K. S. Kölbig, J. A. Mignaco and E. Remiddi, BIT **10** (1970) 38.
- [42] T. Gehrmann and E. Remiddi, Nucl. Phys. B **580** (2000) 485 [arXiv:hep-ph/9912329].
- [43] T. Gehrmann and E. Remiddi, Nucl. Phys. **B601** (2001) 248 [arXiv:hep-ph/0008287]; **B601** (2001) 287 [arXiv:hep-ph/0101124].
- [44] W. T. Giele and E. W. N. Glover, Phys. Rev. D **46** (1992) 1980.
- [45] L. W. Garland, T. Gehrmann, E. W. N. Glover, A. Koukoutsakis and E. Remiddi, Nucl. Phys. B **627** (2002) 107 [arXiv:hep-ph/0112081].

- [46] L. W. Garland, T. Gehrmann, E. W. N. Glover, A. Koukoutsakis and E. Remiddi, Nucl. Phys. B **642** (2002) 227 [arXiv:hep-ph/0206067].
- [47] T. Binoth, E. W. N. Glover, P. Marquard and J. J. van der Bij, JHEP **0205** (2002) 060 [arXiv:hep-ph/0202266].
- [48] O. V. Tarasov, Phys. Rev. D **54** (1996) 6479 [arXiv:hep-th/9606018]. Nucl. Phys. B **502** (1997) 455 [arXiv:hep-ph/9703319].
- [49] V.A. Smirnov and O.L. Veretin, Nucl. Phys. **B566** (2000) 469 [arXiv:hep-ph/9907385].
- [50] C. Anastasiou, T. Gehrmann, C. Oleari, E. Remiddi and J.B. Tausk, Nucl. Phys. **B580** (2000) 577 [arXiv:hep-ph/0003261].
- [51] T. Gehrmann and E. Remiddi, Nucl. Phys. **B** (Proc. Suppl.) **89** (2000) 251 [arXiv:hep-ph/0005232].
- [52] C. Anastasiou, J.B. Tausk and M.E. Tejeda-Yeomans, Nucl. Phys. **B** (Proc. Suppl.) **89** (2000) 262 [arXiv:hep-ph/0005328].
- [53] C. Anastasiou, E. W. N. Glover and C. Oleari, Nucl. Phys. B **565** (2000) 445 [arXiv:hep-ph/9907523]. Nucl. Phys. B **572** (2000) 307 [arXiv:hep-ph/9907494].
- [54] V. A. Smirnov, Phys. Lett. B **460** (1999) 397 [arXiv:hep-ph/9905323].
- [55] J. B. Tausk, Phys. Lett. B **469** (1999) 225 [arXiv:hep-ph/9909506].
- [56] A. V. Kotikov, Phys. Lett. B **254** (1991) 158.
- [57] E. Remiddi, Nuovo Cim. A **110** (1997) 1435 [arXiv:hep-th/9711188].
- [58] M. Caffo, H. Czyz, S. Laporta and E. Remiddi, Acta Phys. Polon. B **29** (1998) 2627 [arXiv:hep-th/9807119].
- [59] M. Caffo, H. Czyz, S. Laporta and E. Remiddi, Nuovo Cim. A **111** (1998) 365 [arXiv:hep-th/9805118].

- [60] R. J. Gonsalves, *Phys. Rev. D* **28** (1983) 1542.
- [61] G. Kramer and B. Lampe, *J. Math. Phys.* **28** (1987) 945.
- [62] TASSO collaboration, D.P. Barber et al., *Phys. Rev. Lett.* **43** (1979) 830;
P. Söding, B. Wiik, G. Wolf and S.L. Wu, Talks given at Award Ceremony of
the 1995 EPS High Energy and Particle Physics Prize, Proceedings of the *EPS
High Energy Physics Conference*, Brussels, 1995, (World Scientific), p. 3.
- [63] J. Ellis, M.K. Gaillard and G.G. Ross, *Nucl. Phys.* **B111** (1976) 253; **B130**
(1977) 516(E).
- [64] S. Bethke, *J. Phys.* **G26** (2000) R27 [arXiv:hep-ex/0004021].
- [65] R.K. Ellis, D.A. Ross and A.E. Terrano, *Nucl. Phys.* **B178** (1981) 421.
- [66] K. Fabricius, I. Schmitt, G. Kramer and G. Schierholz, *Z. Phys.* **C11** (1981)
315.
- [67] Z. Kunszt and P. Nason, in *Z Physics at LEP 1*, CERN Yellow Report 89-08,
Vol. 1, p. 373.
- [68] S. Catani and M.H. Seymour, *Nucl. Phys.* **B485** (1997) 291; **B510** (1997)
503(E) [arXiv:hep-ph/9605323].
- [69] R.D. Heuer, D.J. Miller, F. Richard and P.M. Zerwas (Eds.), “TESLA Technical
Design Report Part III: Physics at an e^+e^- Linear Collider”, DESY-report
2001-011 [arXiv:hep-ph/0106315].
- [70] Z. Kunszt (ed.), Proceedings of the Workshop on “New Techniques for Calculating
Higher Order QCD Corrections”, Zürich, 1992, ETH-TH/93-01.
- [71] K. Hagiwara and D. Zeppenfeld, *Nucl. Phys.* **B313** (1989) 560.
- [72] F.A. Berends, W.T. Giele and H. Kuijf, *Nucl. Phys.* **B321** (1989) 39.
- [73] N.K. Falck, D. Graudenz and G. Kramer, *Nucl. Phys.* **B328** (1989) 317.

- [74] Z. Bern, L.J. Dixon, D.A. Kosower and S. Weinzierl, Nucl. Phys. **B489** (1997) 3 [arXiv:hep-ph/9610370].
- [75] Z. Bern, L.J. Dixon and D.A. Kosower, Nucl. Phys. **B513** (1998) 3 [arXiv:hep-ph/9708239].
- [76] E.W.N. Glover and D.J. Miller, Phys. Lett. **B396** (1997) 257 [arXiv:hep-ph/9609474].
- [77] J.M. Campbell, E.W.N. Glover and D.J. Miller, Phys. Lett. **B409** (1997) 503 [arXiv:hep-ph/9706297].
- [78] Z. Bern, L. Dixon and A. Ghinculov, Phys. Rev. **D63** (2001) 053007 [arXiv:hep-ph/0010075].
- [79] C. Anastasiou, E.W.N. Glover, C. Oleari and M.E. Tejeda-Yeomans, Nucl. Phys. **B601** (2001) 318 [arXiv:hep-ph/0010212]; **B601** (2001) 347 [arXiv:hep-ph/0011094].
- [80] C. Anastasiou, E.W.N. Glover, C. Oleari and M.E. Tejeda-Yeomans, Nucl. Phys. **B605** (2001) 486 [arXiv:hep-ph/0101304].
- [81] E.W.N. Glover, C. Oleari and M.E. Tejeda-Yeomans, Nucl. Phys. **B605** (2001) 467 [arXiv:hep-ph/0102201].
- [82] C. Anastasiou, E. W. N. Glover and M. E. Tejeda-Yeomans, Nucl. Phys. B **629** (2002) 255 [arXiv:hep-ph/0201274].
- [83] Z. Bern, A. De Freitas and L.J. Dixon, JHEP **0109** (2001) 037 [arXiv:hep-ph/0109078].
- [84] Z. Bern, A. De Freitas, L.J. Dixon, A. Ghinculov and H.L. Wong, JHEP **0111** (2001) 031 [arXiv:hep-ph/0109079].
- [85] T. Binoth and G. Heinrich, Nucl. Phys. **B585** (2000) 741 [arXiv:hep-ph/0004013].

- [86] V.A. Smirnov, Phys. Lett. **B491** (2000) 130 [arXiv:hep-ph/007032]; **B500** (2001) 330 [arXiv:hep-ph/0011056].
- [87] T. Gehrmann and E. Remiddi, Comput. Phys. Commun. **141** (2001) 296 [arXiv:hep-ph/0107173].
- [88] T. Gehrmann and E. Remiddi, CERN-TH/2001-326 [arXiv:hep-ph/0111255].
- [89] V.N. Baier, E.A. Kurayev and V.S. Fadin, Sov. J. Phys. **31** (1980) 364.
- [90] J.J. van der Bij and E.W.N. Glover, Nucl. Phys. B **313** (1989) 237.
- [91] G. Passarino and M.J. Veltman, Nucl. Phys. B **160** (1979) 151.
- [92] G. Kramer and B. Lampe, Z. Phys. **C34** (1987) 497; **C42** (1989) 504(E).
- [93] T. Matsuura and W.L. van Neerven, Z. Phys. **C38** (1988) 623.
- [94] T. Matsuura, S.C. van der Maarck and W.L. van Neerven, Nucl. Phys. **B319** (1989) 570.
- [95] Z. Bern, L.J. Dixon, D.C. Dunbar and D.A. Kosower, Nucl. Phys. **B425** (1994) 217 [arXiv:hep-ph/9403226].
- [96] D.A. Kosower, Nucl. Phys. **B552** (1999) 319 [arXiv:hep-ph/9901201].
- [97] D.A. Kosower and P. Uwer, Nucl. Phys. **B563** (1999) 477 [arXiv:hep-ph/9903515].
- [98] Z. Bern, V. Del Duca and C.R. Schmidt, Phys. Lett. **B445** (1998) 168 [arXiv:hep-ph/9810409].
- [99] Z. Bern, V. Del Duca, W.B. Kilgore and C.R. Schmidt, Phys. Rev. **D60** (1999) 116001 [arXiv:hep-ph/9903516].
- [100] S. Catani and M. Grazzini, Nucl. Phys. **B591** (2000) 435 [arXiv:hep-ph/0007142].

- [101] J.M. Campbell and E.W.N. Glover, Nucl. Phys. **B527** (1998) 264 [arXiv:hep-ph/9710255].
- [102] S. Catani and M. Grazzini, Phys. Lett. **B446** (1999) 143 [arXiv:hep-ph/9810389]; Nucl. Phys. **B570** (2000) 287 [arXiv:hep-ph/9908523].
- [103] F.A. Berends and W.T. Giele, Nucl. Phys. **B313** (1989) 595.
- [104] S. Catani, in [70].
- [105] A. Gehrmann-De Ridder, T. Gehrmann and E.W.N. Glover, Phys. Lett. B **414** (1997) 354 [arXiv:hep-ph/9705305].
- [106] A. Gehrmann-De Ridder and E.W.N. Glover, Nucl. Phys. **B517** (1998) 269 [arXiv:hep-ph/9707224].
- [107] L.J. Dixon and A. Signer, Phys. Rev. Lett. **78** (1997) 811 [arXiv:hep-ph/9609460]; Phys. Rev. D **56** (1997) 4031 [arXiv:hep-ph/9706285].
- [108] Z. Nagy and Z. Trocsanyi, Phys. Rev. Lett. **79** (1997) 3604 [arXiv:hep-ph/9707309].
- [109] J.M. Campbell, M.A. Cullen and E.W.N. Glover, Eur. Phys. J. C **9** (1999) 245 [arXiv:hep-ph/9809429].
- [110] S. Weinzierl and D.A. Kosower, Phys. Rev. D **60** (1999) 054028 [arXiv:hep-ph/9901277].
- [111] P. Igo-Kemenes, talk given at LEPC meeting, 3 November, 2000;
ALEPH Collaboration, R. Barate, *et al.*, Phys. Lett. **B 495** (2000) 1;
L3 Collaboration, M. Acciarri, *et al.*, Phys. Lett. **B 495** (2000) 18;
DELPHI Collaboration, P. Abreu, *et al.*, Phys. Lett. **B 499** (2001) 23;
OPAL Collaboration, G. Abbiendi, *et al.*, Phys. Lett. **B 499** (2001) 38.
- [112] A. Straessner, talk given at XXXVth Rencontres de Moriond, March 2000;
D. Strom, talk given at RADCOR-2000, September 2000.

- [113] M. Carena *et al.*, *Report of the Tevatron Higgs working group*, hep-ph/0010338.
- [114] M. Spira, A. Djouadi, D. Graudenz and P. M. Zerwas, Nucl. Phys. B **453** (1995) 17 [arXiv:hep-ph/9504378]; D. Graudenz, M. Spira and P. M. Zerwas, Phys. Rev. Lett. **70** (1993) 1372.
- [115] R. V. Harlander, Phys. Lett. B **492** (2000) 74 [arXiv:hep-ph/0007289].
- [116] R.K. Ellis, I. Hinchliffe, M. Soldate, and J.J. Van Der Bij, Nucl. Phys. **B297**, 221 (1988);
U. Baur and E. Glover, Nucl. Phys. **B339**, 38 (1990).
- [117] M. N. Dubinin, V. A. Ilyin and V. I. Savrin, arXiv:hep-ph/9712335.
- [118] Schmidt, Carl R., Phys. Lett. **B413** (1997) 391.
- [119] R. V. Harlander and W. B. Kilgore, Phys. Rev. D **64**, 013015 (2001) [arXiv:hep-ph/0102241].
- [120] L. W. Garland, E. W. N. Glover, A. Koukoutsakis, work in progress
- [121] Z. Xu, D. H. Zhang and L. Chang, Nucl. Phys. B **291** (1987) 392.
- [122] F. A. Berends *et. al.*, Nucl. Phys. B **206** (1982) 61; *ibid.* B **239** (1984) 362; *ibid.* B **239** (1984) 395; *ibid.* B **254** (1986) 265.
- [123] L. J. Dixon, arXiv:hep-ph/9601359.

